Titre: Title:	Elaboration of AL2O3-based graphite containing castables
Auteur: Author:	Ningsheng Zhou
Date:	2000
Type:	Mémoire ou thèse / Dissertation or Thesis
Référence: Citation:	Zhou, N. (2000). Elaboration of AL2O3-based graphite containing castables [Ph.D. thesis, École Polytechnique de Montréal]. PolyPublie. https://publications.polymtl.ca/8614/

UNIVERSITÉ DE MONTRÉAL

ELABORATION OF AL_2O_3-BASED GRAPHITE CONTAINING CASTABLES

Ningsheng ZHOU

DÉPARTEMENT DE GÉNIE PHYSIQUE ET DE GÉNIE DES MATÉRIAUX

ÉCOLE POLYTECHNIQUE DE MONTRÉAL

THÈSE PRÉSENTÉE EN VUE DE L'OBTENTION

DU DIPLÔME DE PHILOSOPHIAE DOCTOR (Ph.D.)

(GÉNIE MÉTALLURGIQUE)

AOÛT 2000

UNIVERSITÉ DE MONTRÉAL

ÉCOLE POLYTECHNIQUE DE MONTRÉAL

Cette thèse intitulée:

ELABORATION OF AL_2O_3-BASED GRAPHITE CONTAINING CASTABLES

Présentée par: ZHOU Ningsheng

En vue de l'obtention du diplôme de: Philosophiae Doctor

A été dûment acceptée par le jury d'examen constitué de:

Mr. ALLAIRE Claude, Ph.D., président

Mr. RIGAUD Michel, Ph.D., membre et directeur de recherche

Mr. CARREAU Pierre, Ph.D., membre

Mr. FRIEDRICHS James, Ph.D., membre

ACKNOWLEDGEMENTS

Recalling the passed days striving hard for my Ph. D. since March 1997, I acknowledge deeply to the golden opportunity, valuable guidance, helps, supports and encouragement from all sides, which I have received on the ragged path to glory. They are engraved on my heart.

First of all, I extend my heartiest thanks to my supervisor, Prof. Michel Rigaud at the Chair of Industrial Refractories, École Polytechnique (CIREP) and Prof. Xiangchong Zhong at Luoyang Institute of Refractories Research, China (LIRR), for their outstanding expertise, enlightening guidance, constant advice and support throughout this work.

I am very grateful to Prof. Jinxiang Wang, president of LIRR, for allowing me to study at CIREP while preserving my position at LIRR and for his encouragement.

It is hard to forget the nurturing time spent at CIREP. I am very thankful to my colleagues (in alphabet order of their surnames) Dr. S. Afshar, Dr. X. Cheng, Dr. K. Dehghani, E. Divry, Dr. C. L. Feng, Z. Q. Guo, H. Q. He, M. Kandel, V. Kovac, N. Ntakaburiumvo, Dr. S. Palco, Dr. E. Paransky, R. Pelletier and J. Sebbani for helpful discussions, assistance, valuable encouragement and friendship.

My particular thanks are due to J. P. Bouchard and H. Rioux at CIREP for their technical and secretarial helps, to F. B. Ye, Z. M. Wang, S. H. Zhang, Z. Y. Bi at LIRR for their useful discussions and helps with my experimental work, and to Z. W. Huang and X. H. Wei at LIRR for their assistance in SEM analysis.

Gratitude is the memory of the heart. Although it is impossible to list all the persons who have ever done any in favor of my Ph. D. work, directly or indirectly, mentally or materially, I bear them firmly in my mind forever.

At last but not least, I express my heartfelt gratitude to my wife and daughter, to whom I feel greatly indebted for their tolerance with the time they spent in China with my long absence, but their patience and encouragement did contribute a lot to my success. I owed also a great deal to my aged parents and parents-in-law for their encouragement.

RÉSUMÉ

Développer un béton réfractaire avec du graphite pour mieux résister à l'attaque par intrusion de scories, aux chocs thermiques et à l'écaillage structural, voilà le défi à relever. Le but de ce travail a été de trouver des méthodes efficaces et pratiques d'incorporer des paillettes de graphite naturel (FG, pour flake graphite dans le texte) dans des bétons à base d'alumine, en visant des applications sidérurgiques (fontes et aciers) en cherchant à minimiser les effets négatifs associés à l'hydrophobicité et à l'oxydabilité du graphite, tout en optimisant les propriétés d'ensemble de ces bétons.

Dans cette perspective, trois approches ont été développées en vue d'insérer des paillettes de graphite (FG) dans deux classes de bétons d'alumine, à base de Al_2O_3-SiC et Al_2O_3-MgO. Ces approches, dont les deux premières sont totalement originales, ont été intitulées : microboulettes de graphite (PG pour micro-pelletized graphite dans le texte), briquettes d'alumine-graphite broyées (BAG pour briquette alumina-graphite dans le texte) et revêtement de graphite (CFG pour coated flake graphite dans le texte). Ces approches ont été conceptualisées pour minimiser les problèmes associés à l'utilisation des paillettes de graphite, en vue : 1) de décroître la surface spécifique des paillettes (PG), 2) de réduire la différence de densité entre le graphite et les grains d'oxydes utilisées (BAG), 3) de modifier la surface du graphite pour la rendre plus hydrophile (CFG), 4) de contrôler la dispersabilité du graphite pour obtenir à froid, après

séchage, une adhésion suffisante du béton, et 5) d'utiliser les anti-oxydants appropriés pour inhiber l'oxydation des (FG).

L'ensemble du travail a été divisé en deux étapes. Dans la première, à partir de bétons Al_2O_3-SiC-C déjà connus, les quatre modes d'insertion du graphite (BG, BAG, CFG et FG) ont été comparés en se basant sur les mesures des propriétés de ces quatre types de bétons et ce, en fonction du contenu en carbone. Il a été clairement établi que les modes d'incorporation PG et BAG étaient supérieurs aux deux autres : CFG et FG.

Dans la deuxième étape, il a été décidé de travailler sur une nouvelle classe de bétons, les Al_2O_3-MgO. Une étude préalable du système Al_2O_3-MgO sans carbone s'est avérée nécessaire en vue de minimiser entre autre l'eau de gâchage requise et d'étendre la connaissance du système en poussant la proportion de magnésie utilisée jusqu'à 30 % de MgO.

Au total, au-delà de 50 séries d'essais ont été complétées sur 30 mélanges différents, en comptant les 2 classes de bétons Al_2O_3-SiC-C et Al_2O_3-MgO-C. Les mesures de caractérisation ont porté sur l'ouvrabilité et la demande en eau de gâchage, la densité et la porosité, les modules de rupture à froid, après séchage et différentes cuissons, les modules de rupture à chaud, la résistance aux chocs thermiques ; en plus, pour le système Al_2O_3-MgO-C, la résistance à l'oxydation et à la corrosion.

Les résultats obtenus ont permis de mettre en lumière les éléments suivants :

(1) Le mode d'incorporation du graphite dans les bétons est primordial. Les deux méthodes originales d'incorporation PG et BAG ont permis de minimiser les problèmes reconnus lorsqu'on cherche à utiliser directement les paillettes tel quel et ce, dans les deux classes de bétons Al_2O_3-SiC-C et Al_2O_3-MgO-C. Les avantages des PG et BAG sur les CFG et FG sont marqués en terme d'eau de gâchage pour une ouvrabilité donnée, porosité, résistances mécaniques, à froid et à chaud, résistance aux chocs thermiques, oxydation et corrosion.

(2) L'addition du graphite dans ces bétons, pour empêcher l'intrusion des scories et améliorer la résistance aux chocs thermiques a été, tel qu'escompté, très bénéfique. La résistance à la corrosion d'autre part est grandement influencée par la résistance à l'oxydation. En autant que le graphite demeure présent dans le béton, qu'il soit distribué de façon continue (grande dispersion) ou de façon discontinue (aggloméré), aucune pénétration de scorie en face chaude lors d'essais de corrosion n'a été observée.

(3) Le fait que même si les paillettes de graphite sont regroupées soit dans ces micro-boulettes, soit dans les petits agglomérats, la résistance vis-à-vis de la pénétration de la scorie demeure digne d'être soulignée de nouveau. Cela est tout à fait significatif pour tous les matériaux carbonés (briques et autres monolithiques) et aidera à promouvoir la poursuite des travaux dans cette direction.

(4) Pour prévenir la pénétration des scories, la quantité globale de carbone à utiliser est à limiter à 4 à 5 % poids (plus n'est pas mieux !). Pour les micro-boulettes, le

pourcentage en carbone peut aussi être ajusté à la baisse (encore une fois, plus de carbone n'est pas mieux !).

(5) L'addition d'Al rendue possible en utilisant des PG et BAG, ainsi que du Si, SiC et B_4C dans les bétons est favorable pour minimiser la perte du carbone par oxydation. Dans les bétons de Al_2O_3-MgO-C, le B_4C est particulièrement efficace jusqu'à 1200°C et le Si et SiC plus efficaces à températures plus élevées (T>1400°C). Le ZrB_2 a été moins efficace que les autres additifs dans tous les cas.

(6) À l'issue de ce travail, tous les objectifs fixés initialement ont été atteints. Il a été prouvé que par de nouvelles façons d'incorporer le graphite dans les bétons vibrés, il est possible d'élaborer des bétons contenant de 4 à 5 % de graphite.

L'apport majeur a été centré sur une sélection optimale du dispersant à partir de la détermination des caractéristiques rhéologiques des mélanges (partie matrice) à l'aide d'un viscosimètre à doubles cylindres coaxiaux. De plus, une étude sur la distribution granulométrique de la magnésie dans les mélanges a permis de réaliser des bétons de 18, 24 et même 30 % en magnésie avec un minimum d'eau de gâchage (4.7 %). C'est dans de tels mélanges « optimisés » que l'incorporation de graphite sous forme de micro-boulettes (PG) et d'agrégats d'alumine-graphite (BAG) a été effectuée, avec l'insertion directe de paillettes servant parfois de base de comparaison. C'est dans cette classe de bétons que l'étude de l'influence des additions d'anti-oxydants a été poussée. Les anti-oxydants utilisés dans les PG et BAG ou directement dans le béton ont été l'aluminium,

le silicium, le carbure de silicium, le carbure de bore et le diborure de zirconium. La détermination des caractéristiques de résistance à l'oxydation et à la corrosion de ces bétons a constitué la dernière partie du travail de cette thèse. L'objectif a été d'optimiser ces résistances et ces caractéristiques essentielles. Une analyse microstructurale a été réalisée sur les compositions ayant les caractéristiques suivantes : moins que 6.5 % d'eau de gâchage requis ; ouvrabilité ASTM de 170 mm. ; MDR à froid, après séchage > 4 MPa ; MDR à chaud, à 1400°C ou 1450°C > 2 MPa ; un retrait linéaire après cuisson dans l'intervalle 1000-1500°C de ± 0.5 % pour les bétons de Al_2O_3-SiC-C et < 2.5 % pour les bétons de Al_2O_3-MgO-C et enfin une relativement bonne résistance à l'oxydation et à la corrosion. Il faut toutefois souligner que seulement le MDR à froid des bétons après cuisson à 1000°C demeure faible, de l'ordre de 3 MPa et que la résistance à l'oxydation devra être améliorée entre 900 et 1200°C.

ABSTRACT

Developing oxide-graphite composite refractory castables is a big challenge to the improvement of the resistance to slag intrusion, thermal shock resistance and structural spalling resistance. The aim of this work was set to develop effective and practicable new methods to incorporate natural flake graphite (FG) into the Al_2O_3 based castables for iron and steel making applications, which can minimise the negative effects associated with the hydrophobicity and oxidation of FG, and to optimise overall properties of the graphite containing castables.

For this purpose, three approaches, viz. micro-pelletized graphite (PG), crushed briquette of Al_2O_3-graphite (BAG) and TiO_2 coated graphite (CFG), have been developed to insert flake graphite into Al_2O_3 rich Al_2O_3-SiC based and Al_2O_3-MgO based castables. These approaches were put into effect as countermeasures against the problems caused by FG in order: 1) to agglomerate the FG powders so as to decrease the specific surface area; 2) to diminish the density difference by using crushed carbon bonded compact of oxide-FG mixture; 3) to modify the surface of the flake graphite by forming hydrophilic coating; 4) to control the dispersion state of the graphite in the castable to maintain enough bonding strength; and 5) to use appropriate antioxidants to inhibit the oxidation of FG.

The whole work was divided into two stages. In stage one, Al_2O_3-SiC-C castables were

dealt with to compare 4 modes of inserting graphite, i.e., by PG, BAG, CFG and FG. Overall properties were measured, all in correlation with graphite amount and incorporating mode, which revealed that PG and BAG methods were superior to CFG and FG ones. In stage two, before graphite addition, efforts were made to reduce water demand in the Al_2O_3-MgO castables system. For this purpose, the matrix portion of the castable mixes was extracted and a coaxial double cylinder viscometer was adopted to investigate rheological characteristics of the matrix slurries vs. 4 kinds of deflocculants, through which the best deflocculant and its appropriate amount were found in order to reduce water addition at its minimum. Efforts were then made to add up to 30% MgO into the castables, by controlling size of the magnesia, using a limited amount of powders (< 0.3 mm), the rest being increased in size gradually up to the top size of 4.76 mm. Into the optimized Al_3O_2–MgO castables, graphite was incorporated by PG and BAG, suggested by stage one, and 4 kinds of antioxidants, Si, SiC, B_4C and ZrB_2, were added respectively or in combination to compare their effect on oxidation resistance. Overall properties of the castables, with oxidation resistance and slag resistance as the focus, were investigated in correlation with MgO amount and graphite and antioxidant packages. Optimization work on oxidation and slag resistance was pursued. Finally, microstructure analysis on the samples after oxidation and slag tests was conducted.

Totally, about 50 experiments on nearly 30 different designed mixes of the two types of castables have been made and characterized in terms of flowability, water demand, bulk density, apparent porosity, cold modulus of rupture and hot modulus of rupture, thermal

shock resistance, oxidation, static and dynamic slag tests, and microscopic analysis by SEM and EDAX.

The achieved results bring to light the following findings:

(1) The mode of incorporating graphite plays a big role in minimizing the problems caused by FG and has pronounced influence on overall properties of the graphitic castables. In both Al_2O_3-SiC-C and Al_2O_3-MgO-C castables, incorporating graphite via PG or BAG have shown net advantages over straight addition of FG and TiO_2 coated flake graphite (CFG), in terms of water addition, flowability, porosity, cold and hot strengths, thermal shock resistance, oxidation resistance and slag resistance. CFG doesn't show positive effects on strength and slag resistance of the Al_2O_3-SiC-C castables, though it imparts lower water demand and better oxidation resistance than FG.

(2) The role of the inserted graphite in precluding slag intrusion and also improving thermal shock resistance reveals itself dramatically. Slag resistance is strongly dependent on oxidation resistance. The key to maintain a good slag resistance is to protect the carbon from oxidation at elevated temperatures. So long as the incorporated graphite is retained in the castable, regardless of whether continuous or discontinuous distribution, no penetration, even micro-structurally, has been observed.

(3) At a microscopic scale, a discontinuous distribution of graphite in the castables does not harm slag penetration resistance. Only 1% amorphous graphite as dispersed carbon

has been used in this work, not like it tends to believe that the ability of preventing slag penetration is strongly depending on the uniform distribution of graphite in the matrix.

(4) For the purpose of inhibiting slag penetration, the amount of carbon in the castables is not necessarily to be the higher, the better, 4-5% being sufficient. Even in the graphite based micropellets, graphite can also be replaced to a considerable extent by alumina to reach an equal resistance to slag attack.

(5) Incorporating Al, Si and SiC as antioxidants both in PG or BAG and in the castables plays a big role in minimizing carbon oxidation. The oxidation resistance is attributed to liquid phase protection. For the Al_2O_3-MgO-C castable, boron carbide additive helps improve the oxidation resistance at intermediate temperature (1200°C), while silicon and silicon carbide are more effective in enhancing oxidation resistance at higher temperatures (above 1400°C). Zirconium diboride additive does not show a positive effect on anti-oxidation at both 1200°C and 1400°C. For this particular Al_2O_3-MgO-C castable system, boron bearing compounds are not recommended to be used as dominant antioxidants.

(6) This work has met the predetermined objectives to pave a new way to incorporate natural flake graphite into castables, which can minimize the problems encountered with straight addition of flake graphite and to develop Al_2O_3-SiC-C and Al_2O_3-MgO-C castables containing 4-5% flake graphite with such targeted properties as: water addition: < 6.5%; flow value: >170mm; CMOR (after drying): >4MPa; HMOR(at 1400

or 1450°C): >2MPa; PLC (after 1000-1500°C): ± 0.5% for Al_2O_3-SiC-C castables and <+2.5% for Al_2O_3-MgO-C castables; good oxidation resistance and slag resistance. Nevertheless, the CMOR of the Al_2O_3-MgO-C castables after 1000°C heating is not high enough, only around 3 MPa at present. Oxidation resistance of the Al_2O_3-MgO-C castables under 1200°C needs also to be further improved.

CONDENSÉ

Ce travail de thèse s'inscrit dans la lignée des travaux de recherche qui sont entamés depuis cinq ans sur le développement de bétons basiques avec et sans ciment alumineux, avec ou sans addition de carbone, principalement le graphite naturel. Ces travaux constituent l'axe majeur des travaux qui sont financés par le Conseil de Recherche en Sciences Naturelles et en Génie du Canada (CRSNG) et les partenaires industriels de la Chaire Industrielle des Réfractaires de l'École Polytechnique (CIREP).

Ce travail porte cette fois sur l'élaboration de bétons réfractaires graphités à base d'alumine plutôt qu'à base de magnésie. Ceci se démarque nettement des travaux antérieurs de N. Wang et de X. Cheng (Optimization of Magnesia-Based, Cement-Free, Spinel-Bonded Castables, Ph. D., U. de M., Novembre 1999). Les aspects originaux de ce travail, au départ, sont d'une part la recherche de nouveaux modes d'incorporation du graphite dans les bétons, suivant en cela les travaux précurseurs de M. Kandel et, d'autre part, la mise au point de bétons d'alumine à haute teneur en magnésie avec graphite. Le but ultime est de mettre au point un béton réfractaire susceptible d'être utilisé dans la zone de laitier des poches de coulée d'aciers, pouvant résister à l'action corrosive des scories des fours poches, au moins de façon équivalente aux briques de magnésie-carbone couramment utilisées. Ceci est primordial pour que l'utilisation des bétons vibrés, ou mieux, projetés puisse se propager dans les aciéries. En effet, ce n'est que lorsque toute la paroi de travail des poches de coulée pourra être réalisée

économiquement en monolithique, et pas seulement la partie virole, que la substitution briques-bétons sera effectuée. Les enjeux sont majeurs pour les aciéristes et les fabricants de réfractaires et justifient pleinement l'orientation de ces travaux de recherches.

L'incorporation de graphite dans les bétons est en soi une « solution » qui a été envisagée depuis plusieurs années, mais les premiers résultats ont été peu satisfaisants. De grandes différences subsistent entre briques et bétons, la principale dans notre contexte est la porosité intrinsèque qui, par définition, est et demeurera vraisemblablement toujours supérieure pour les bétons par rapport aux briques et ce, en dépit des améliorations apportées aux distributions granulométriques. En effet, pour contrôler les propriétés rhéologiques requises pour assurer une mise en place adéquate (par vibration ou par gunitage humide), il faut toujours une certaine quantité minimale d'eau de gâchage qui, après séchage, conduit à une porosité importante, supérieure à 14-15 %. C'est là que l'utilisation du graphite naturel vient compliquer les choses : d'une part, le graphite est hydrophobe, d'autre part, le facteur de forme des paillettes est très néfaste en vue d'obtenir une compacité maximale. Ceci n'est pas un facteur aussi insurmontable dans le cas des briques, étant donné la nature des liants carbonés (résines, brais) plutôt qu'hydrauliques (ciment alumineux ou sols) et l'utilisation du formage par pression pour les briques. Cette porosité initiale supérieure entraîne en conséquence des inconvénients au niveau oxydation du graphite, principalement au moment de la mise en chauffe initiale et au niveau corrosion-intrusion dans les zones décarburées. Cette problématique a été clairement énoncée récemment par M. Rigaud [6].

Dans cette perspective, trois approches d'insertion du graphite ont été développées et évaluées, les deux premières étant des « innovations-maison ». Ces approches ont été conceptualisées pour minimiser les problèmes associés à l'utilisation des paillettes de graphite en vue 1) de décroître la surface spécifique des paillettes, 2) de réduire la différence de densité entre le graphite et les agrégats utilisés dans les bétons, 3) de modifier la surface du graphite pour la rendre plus hydrophile, donc de minimiser la quantité d'eau de gâchage requise, 4) de contrôler la dispersabilité du graphite pour obtenir à froid, après séchage, une cohésion suffisante du béton, 5) d'utiliser les anti-oxydants appropriés pour inhiber l'oxydation du graphite. Ces modes d'insertion ont été établis à partir de la fabrication 1) de micro-boulettes de graphite (PG pour « micro-pelletized graphite », dans le corps de la thèse), 2) de briquettes d'alumine-graphite broyées (BAG pour briquette alumine-graphite) et 3) de revêtement de graphite (CFG pour « coated flake graphite »).

L'ensemble de la thèse comporte huit chapitres. Après un chapitre d'introduction pour situer le contexte, une revue des principaux travaux antérieurs sur les bétons contenant du carbone est réalisée au chapitre 2. Les limites propres à l'utilisation du graphite sont précisées. Dans le troisième chapitre, les stratégies mises en place pour amorcer et compléter ce travail sont décrites et les procédés de fabrication visant à modifier la nature des paillettes de graphite en vue de leur insertion dans les bétons sont définis. Au chapitre quatre, les plans d'expérience et les procédures expérimentales tant au niveau élaboration que caractérisation sont soigneusement définis ; les propriétés essentielles

des matières premières sont indiquées et toutes les méthodes de mesure sont détaillées, ceci inclut les mesures de coulabilité des bétons vibrés, les densités et porosités, la résistance mécanique à froid et à chaud, en flexion trois points, la résistance aux chocs thermiques, à l'oxydation et à la corrosion, la dilatation sans charge et bien sûr, tous les aspects concernant la caractérisation microscopique. Les trois chapitres suivants traitent des résultats expérimentaux, l'un sur les bétons Al_2O_3-SiC-C, le suivant sur les bétons Al_2O_3-MgO sans carbone et le dernier sur les bétons Al_2O_3-MgO-C. Au dernier chapitre se retrouvent les conclusions, une discussion sur l'importance relative des résultats et des recommandations. C'est ce qui va être repris dans les paragraphes suivants, selon les termes du résumé.

Les résultats obtenus ont permis de mettre en lumière les éléments suivants :

(1) Le mode d'incorporation du graphite dans les bétons est primordial. Les deux méthodes originales d'incorporation PG et BAG ont permis de minimiser les problèmes reconnus lorsqu'on cherche à utiliser directement les paillettes tel quel et ce, dans les deux classes de bétons Al_2O_3-SiC-C et Al_2O_3-MgO-C. Les avantages des PG et BAG sur les CFG et FG sont marqués en terme d'eau de gâchage pour une ouvrabilité donnée, porosité, résistances mécaniques, à froid et à chaud, résistance aux chocs thermiques, oxydation et corrosion.

(2) L'addition du graphite dans ces bétons, pour empêcher l'intrusion des scories et améliorer la résistance aux chocs thermiques a été, tel qu'escompté, très bénéfique. La résistance à la corrosion d'autre part est grandement influencée par la résistance à

l'oxydation. En autant que le graphite demeure présent dans le béton, qu'il soit distribué de façon continue (grande dispersion) ou de façon discontinue (aggloméré), aucune pénétration de scorie en face chaude lors d'essais de corrosion n'a été observée.

(3) Le fait que même si les paillettes de graphite sont regroupées soit dans des micro-boulettes, soit dans les petits agglomérats, la résistance vis-à-vis de la pénétration de la scorie demeure digne d'être soulignée de nouveau. Cela est tout à fait significatif pour tous les matériaux carbonés (briques et autres monolithiques) et aidera à promouvoir la poursuite des travaux dans cette direction.

(4) Pour prévenir la pénétration des scories, la quantité globale de carbone à utiliser est à limiter à 4 à 5 % poids (plus n'est pas mieux !). Pour les micro-boulettes, le pourcentage en carbone peut aussi être ajusté à la baisse (encore une fois, plus de carbone n'est pas mieux !).

(5) L'addition d'Al rendue possible en utilisant des PG et BAG, ainsi que du Si, SiC et B_4C dans les bétons est favorable pour minimiser la perte du carbone par oxydation. Dans les bétons de Al_2O_3-MgO-C, le B_4C est particulièrement efficace jusqu'à 1200°C et le Si et SiC plus efficaces à températures plus élevées (T>1400°C). Le ZrB_2 a été moins efficace que les autres additifs dans tous les cas.

(6) À l'issue de ce travail, tous les objectifs fixés initialement ont été atteints. Il a été prouvé que par de nouvelles façons d'incorporer le graphite dans les bétons vibrés, il est possible d'élaborer des bétons contenant de 4 à 5 % de graphite.

L'apport majeur a été centré sur une sélection optimale du dispersant à partir de la détermination des caractéristiques rhéologiques des mélanges (partie matrice) à l'aide d'un viscosimètre à doubles cylindres coaxiaux. De plus, une étude sur la distribution granulométrique de la magnésie dans les mélanges a permis de réaliser des bétons de 18, 24 et même 30 % en magnésie avec un minimum d'eau de gâchage (4.7 %). C'est dans de tels mélanges « optimisés » que l'incorporation de graphite sous forme de micro-boulettes (PG) et d'agrégats d'alumine-graphite (BAG) a été effectuée, avec l'insertion directe de paillettes servant parfois de base de comparaison. C'est dans cette classe de bétons que l'étude de l'influence des additions d'anti-oxydants a été poussée. Les anti-oxydants utilisés dans les PG et BAG ou directement dans le béton ont été l'aluminium, le silicium, le carbure de silicium, le carbure de bore et le diborure de zirconium. La détermination des caractéristiques de résistance à l'oxydation et à la corrosion de ces bétons a constitué la dernière partie du travail de cette thèse. L'objectif a été d'optimiser ces résistances et ces caractéristiques essentielles. Une analyse microstructurale a été réalisée sur les compositions ayant les caractéristiques suivantes : moins que 6.5 % d'eau de gâchage requis ; ouvrabilité ASTM de 170 mm. ; MDR à froid, après séchage > 4 MPa ; MDR à chaud, à 1400°C ou 1450°C > 2 MPa ; un retrait linéaire après cuisson jusqu'à 1500°C de ± 0.5 % pour les bétons de Al_2O_3-SiC-C, et < +2.5% pour les bétons de Al_2O_3-SiC-C, et enfin une relativement bonne résistance à l'oxydation et à la corrosion. Il faut toutefois souligner que seulement le MDR à froid des bétons après

cuisson à 1000°C demeure faible, de l'ordre de 3 MPa et que la résistance à l'oxydation devra être améliorée entre 900 et 1200°C.

Suite à ce travail, nous pouvons affirmer que la mise au point de bétons contenant du graphite est certainement sur la bonne voie. D'une part, il nous apparaît certain de pouvoir à brève échéance améliorer la production des micro-boulettes de graphite. Les travaux en cours menés dans le cadre d'une autre thèse sont, à ce point, très encourageants. D'autre part, l'optimisation des mélanges suite au présent travail est maintenant ouverte à de nouvelles orientations, notamment en utilisant du spinelle synthétique et de nouveaux liants.

Notre analyse micrographique a démontré que de nombreux mécanismes sont mis à contribution lors de l'oxydation directe des bétons graphités et que l'optimisation des anti-oxydants à utiliser est à parfaire. Néanmoins, il est recommandé d'ores et déjà de se lancer dans une série d'essais-pilotes, en usine, pour mesurer les progrès qui ont été accomplis lors de cette thèse, dont la contribution majeure aura été de démontrer qu'il y a moyen d'incorporer du graphite dans des bétons sans dépasser une limite de 6.5 % d'eau de gâchage, ce qu'aucune équipe de recherche n'a réussi jusqu'à présent, avec un niveau de 5 % de graphite ajouté. Comme il est mentionné dans le chapitre d'introduction, en page un de cette thèse, « Rien n'aboutit sans le concevoir d'abord en rêve ». Ce rêve d'incorporer du graphite dans les bétons est maintenant devenu une réalité concrète susceptible d'être parfaite et donc riche en potentialités futures.

TABLE OF CONTENTS

LIST OF TABLES

LIST OF FIGURES

LIST OF SYMBOLS AND NOMENCLATURE

AES	Auger Electron Spectroscope
AM	Al_2O_3-MgO Spinel
AP	Apparent Porosity
BAG	Briquetted Alumina-Graphite
BD	Bulk Density
BSE	Back Scatter Electron
CAC	Calcium Aluminate Cement
CCS	Cold Crushing Strength
CFG	TiO_2 Coated Flake Graphite
CMOR	Cold Modulus of Rupture
EDAX	Energy Distribution Analysis by X-ray
FG	Flake Graphite
HMOR	Hot Modulus of Rupture
MP	Melamine Polymer
PG	Micro-Pelletized Graphite
PEG	Polyethyleneglycol
PLC	Permanent Linear Change
PSD	Particle Size Distribution
SEM	Scanning Electron Microscope
SHP	Sodium Hexametaphosphate
SPA	Sodium Polyacrylate
SSA	Specific Surface Area
TSR	Thermal Shock Resistance

CHAPTER 1. INTRODUCTION

Looking back on the evolution of refractories technology, we come to the consensus that introducing carbon into oxide based refractories is an epochmaking milestone in the past two or three decades. Since the late 1970's, carbon containing refractories have been developed rapidly and have dominated many important application areas in metallurgy. Their widespread has led to remarkable increase in service lives and reduction in specific consumption and specific cost of refractories[1-4,22].

To compete with and to challenge the oxide-carbon composite bricks, with oxides conferring high strength, refractoriness and oxidation resistance while carbons providing increased thermal conductivity, low thermal expansion, non-wetting, good resistance to thermal shock, structural spalling and slag attack, the same critical prerequisites are to be met by any high performance refractory castables. For this purpose, incorporating some non-oxide ingredients like carbon and carbides (a successful practice in bricks like MgO-C, Al_2O_3-C, Al_2O_3-SiC-C, Al_2O_3-ZrO_2-C and Al_2O_3-MgO-C), into castables is a wise concept deserving efforts.

Nothing happens unless first a dream. Incorporating carbon into castables for iron and steel making applications has become in recent years an active deed more than a dream. This is especially meaningful for hot metal pre-treatment and continuous casting and secondary steel making processes, where aggressive slag attack becomes the main

concern to refractory linings. To improve slag resistance, especially penetration resistance, has become nowadays a focus of R & D work on monolithic refractories for iron and steel making applications, because structural spalling caused by slag intrusion is, in many cases, the main wear mechanism. Several recent articles have pointed out the imperative of minimizing structural spalling and the meaningfulness and potential of carbon containing castables[5-13].

Natural flake graphite, due to its availability and superiority in anti-oxidation and corrosion resistance, deserves the first choice as the carbon source. However, not like in bricks, its incorporation into castables remains to be a hot potato, when taking a series of problems into consideration, such as poor wettability with water, much lower density than the oxide materials, lack of bonding with the oxides and oxidation at elevated temperatures. Elaboration work by taking effective countermeasures to minimize these negative effects is very necessary to make a breakthrough in truly graphite containing castables.

This work is set to tackle such big challenges. As an initial stage of such an endeavour, the aim and scope of the present work include:

(1) To develop effective and practicable new methods to incorporate flake graphite into the Al_2O_3 based castables, which can minimise the negative effects associated with the hydrophobicity of the graphite;

(2) To compare and evaluate the different incorporating methods by measurable parameters of the castables covering workability, physical, mechanical and thermal properties, slag resistance and oxidation resistance.

(3) To figure out the relationships between composition, microstructure and properties as well as graphite incorporating way, and to elucidate related mechanisms;

(4) To optimise properties of the chosen alumina based graphite containing castables.

To meet stringent requirements of more durable monolithic linings in advanced iron and steel making processes, two systems of Al_2O_3 based castables have been chosen in this work. One is the Al_2O_3-SiC-C system, aimed for iron-making applications like blast furnace trough, torpedo and hot metal ladle linings; and the other is the Al_2O_3-MgO-C system, aimed for steel ladle linings. The former, both as bricks and monolithics, has been applied to the above mentioned applications. As commercialized castables, however, the carbon source has been a combination of pitch, coke and petro-coke, instead of flake graphite[14-16]. The latter, as castables, is not yet available so far, but a new idea to be fulfilled by this work. As well known, Al_2O_3-Spinel(MgO) castables and Al_2O_3–MgO–C bricks have already successfully found their application in steel ladles[17-22]. The to-be-developed Al_2O_3-MgO-C castable is thus aimed to be the alternative that combines the advantages achieved both in Al_2O_3–MgO–C bricks and in the Al_2O_3-Spinel(MgO) castables.

Countering the problems caused by flake graphite, three new approaches, viz. micro-pelletized graphite, crushed briquette of Al_2O_3-graphite and TiO_2 coated graphite, have been developed to insert natural flake graphite into the two types of castables.

This work is divided into two steps, or two parts. For comparison and evaluation purpose, Al_2O_3-SiC-C castables were firstly dealt with. The results of four modes of incorporating graphite did help recognize and understand the role and potential of the incorporating method to minimize the problems caused by graphite and the way to optimize properties of the graphite containing castables. Considering Al_2O_3-SiC-C castables are relatively mature and due to time limitation, no microscopic analysis has been pursued on this system. Emphasis of this work is actually laid on Al_2O_3-MgO-C castables, the second part.

So far Al_2O_3-Spinel(MgO) castables are the most successful monolithic linings in steel ladles[5,17-20], but only for barrel and bottom zones and not yet for slag line zone where they need to challenge, performance-wise, the MgO-C bricks. Many published works [18-20,45,50] have revealed that the MgO content in this system, by using either preformed MA spinel or directly adding magnesia to form in-situ spinel, is a dilemma concerning slag corrosion and penetration. This work is thus to incorporate graphite into the alumina rich corner Al_2O_3-MgO castables, so as to improve firstly the slag penetration resistance, and then to make higher MgO level possible to enhance corrosion resistance.

Hints and know-hows obtained from the first part of this work as a reference have been applied to the second part. After using the above mentioned two advantageous methods to insert flake graphite, i.e., micro-pelletized graphite and crushed Al_2O_3-graphite briquette, overall properties of the Al_2O_3-MgO-C castables, including water demand, flowability, porosity, cold and hot strengths, slag resistance and anti-oxidation have been investigated in correlation with the methods of incorporating graphite, MgO amount, carbon level and antioxidants. Based on this, optimization work focusing on oxidation and slag resistance of the castables has been pursued with encouraging results.

In total, about 50 experiments with different designed mixes of the two types of castables have been made and characterized in terms of flowability, water demand, apparent porosity, bulk density, cold and hot modulus of rupture, thermal shock resistance, oxidation, static and dynamic slag tests, and microscopic analysis by SEM and EDAX. At the end of this work, the following new findings are believed contributive to the development of graphitic castables:

(1) A discontinuous distribution of graphite in castables, at least at a microstructural scale, does not do harm to the penetration resistance. Only 1% amorphous graphite as dispersed carbon was used in this work, not like it tends to believe that the ability of preventing slag penetration is strongly depending on the uniform distribution of graphite in the matrix[8]. If this picture is accepted, it should be realized that graphite encapsulated structure, micro-structurally disuniform but macro-structurally uniform,

could be the tomorrow of graphitic castables, when all properties must be compromised.

(2) The anti-oxidation behavior of some antioxidants acts differently in castables than in bricks. This is believed to relate to the more porous structure and lower levels of carbon and MgO, compared with carbon bonded basic bricks. Thus, whether some good experiences and mechanisms of anti-oxidation with graphitic bricks are applicable to graphitic castables is questionable.

(3) Slag corrosion is strongly influenced by retained carbon in the castables. So long as the incorporated graphite is retained in the castable, regardless of whether continuous or discontinuous distribution, no penetration, even micro-structurally, is observed. Anti-oxidation becomes thus especially critical to slag resistance, in such a low level graphite containing system, compared with graphitic bricks.

(4) From inhibiting penetration point of view, the amount of carbon in castables is not necessarily to be the higher, the better, against the previously accepted "belief". Even in the graphite based micropellets, the graphite can be replaced to a considerable extent by oxide to show a negligible difference in corrosion. This enlightens how to economically and efficiently make full use of the graphite in castables.

This thesis consists of eight chapters, reporting the following:

The background and current description of the developments of carbon containing

refractory castables are provided in Chapter 2. To help perceive the necessity and meaningfulness of developing alumina based graphite containing castables, a brief review on the prosperity of monolithic refractories and on the existing Al_2O_3-SiC-C and Al_2O_3-Spinel(MgO) castables has been presented firstly, covering their developments and drawbacks, then the progress and remaining problems in graphite containing castables are underlined.

In Chapter 3, the strategy adopted to tackle the problems caused by flake graphite is put forward, following three approaches (micro-pelletized graphite, crushed Al_2O_3-graphite briquette and TiO_2 coated graphite) to incorporate natural graphite, instead of straight addition of flakes.

Experimental procedure is dealt with in Chapter 4, where experimental design, raw materials, compositions for different castable mixes and test methods for flowability, density, porosity, cold and hot strengths, permanent linear change, thermal shock resistance, oxidation, slag resistance, thermal expansion under load and microstructure analysis are detailed.

In Chapter 5 are shown the results related to the Al_2O_3-SiC-C castables. By comparing overall properties and correlating them with graphite incorporating methods, it has been verified that graphite-incorporating modes play a big role in minimizing the problems caused by straight addition of graphite. Among the four modes of inserting graphite, the micropellets of graphite and the crushed Al_2O_3-graphite briquette have shown a series of

advantages over straight addition of graphite and TiO_2 coated graphite.

Chapter 6 documents the optimization work on Al_2O_3-MgO castables. Before graphite issue, work was centered on flowability and volume-stability issues to optimize physical, mechanical and thermal properties of the Al_2O_3-MgO castables, into which graphite was then inserted. A rheological approach, using a double cylindrical viscometer, was adopted to investigate the rheological characteristics of the matrix slurries vs. 4 kinds of deflocculants, through which the best deflocculant and its appropriate amount were found and good flowability at 4.7% water addition was achieved. By controlling grain size, magnesia was added up to 30%.

Then, graphite was inserted into the optimised Al_2O_3-MgO castables and overall properties of the Al_2O_3-MgO-C castables were characterised in correlation with graphite, magnesia and antioxidant packages. Focus was laid on slag resistance and oxidation issues. Their interdependence is underlined. The elaborated Al_2O_3-MgO-C castables demonstrated encouraging results. These are documented in Chapter 7.

Finally, after interpretation of the experimental results and comprehensive discussions, summary and conclusions are made in Chapter 8. Considerations and suggestions for further improvement and study in-depth on alumina based graphite containing castables are also presented in this chapter.

This work has been achieved to meet the following set of objectives:

(1) To pave a new way to incorporate natural flake graphite into castables, to minimize the problems encountered with straight addition of flake graphite.

(2) To develop Al_2O_3-SiC-C and Al_2O_3-MgO-C castables containing at least 4-5% flake graphite with such targeted properties matching carbon-free castables as: water addition: <6.5%; flow value: >170mm; CMOR (after drying): >4MPa; HMOR (at 1400/1450°C): >2 MPa; PLC (after 1000-1500°C): ± 0.5% for Al_2O_3-SiC-C castables and <+2.5% for Al_2O_3-MgO-C castables; good oxidation resistance and slag resistance.

(3) To enhance slag penetration resistance and hence thermal shock and structural spalling resistance, especially for Al_2O_3-MgO castables, by graphite insertion to overcome the inherent poor resistance of magnesia to slag penetration.

(4) To increase the MgO content in Al_2O_3-MgO castable without loosing the slag penetration resistance, at present 12% is possible. The Al_2O_3-MgO-Graphite castables developed based on this work should be able to be used in not only the barrel zone but also in the slag zone of steel ladles, depending on MgO and C contents, which can be adjusted when specific working conditions are concerned.

Nevertheless, the cold strength of the Al_2O_3-MgO-C castables after intermediate temperature (1000°C) heating seems to be not quite acceptable, CMOR being only around 3 MPa at present. Oxidation resistance of the Al_2O_3-MgO-C castables under1200°C needs also to be improved.

CHAPTER 2. LITERATURE REVIEW

2.1 On the Prosperity of Monolithic Refarctories

Monolithic refractories, also called unshaped refractories, are mixtures that contain aggregates, fines, binders and admixtures, prepared ready-for-use either directly as they are supplied or after addition of suitable liquid. The word "monolithic" here means joint-free, in distinction from bricklaying where multiple joints are unavoidable.

Monolithic refractories, in a broad sense have existed from the very beginning of the refractories, that is several hundreds years ago[23,24], but it is not until the early 20th century that their use has gained general acceptance in refractories family. The basis of modern monolithic refractories is believed to be established since Sain-Claire Deville's discovery in 1850s of the hydraulic properties of calcium aluminate cement [24]. In 1856, he reported on a fired mixture of alumina and lime, which, when mixed with alumina aggregates and water, could be used to produce crucibles for high temperature application. The first plastic monolithics in the USA were made by Schaefer before 1914, they were installed in chunks with a hammer[24]. In 1914, Schaefer established the Pliable Firebrick Company to manufacture and install this new product. Initially, they were used in boilers, but, by 1930, they had been used in forge furnaces, gas generators, coke ovens and heat-treatment furnaces[25]. Since then, monolithic refractories, as extensive conscious practice, have substantially developed along with the

development of binders (in particular CA cement), powder dispersion and deflocculation technology, raw materials and installation method, as review in Ref. 4, pp. 1389-1392. Some highlights in the last 85 years are shown in Figure 2.1[26].

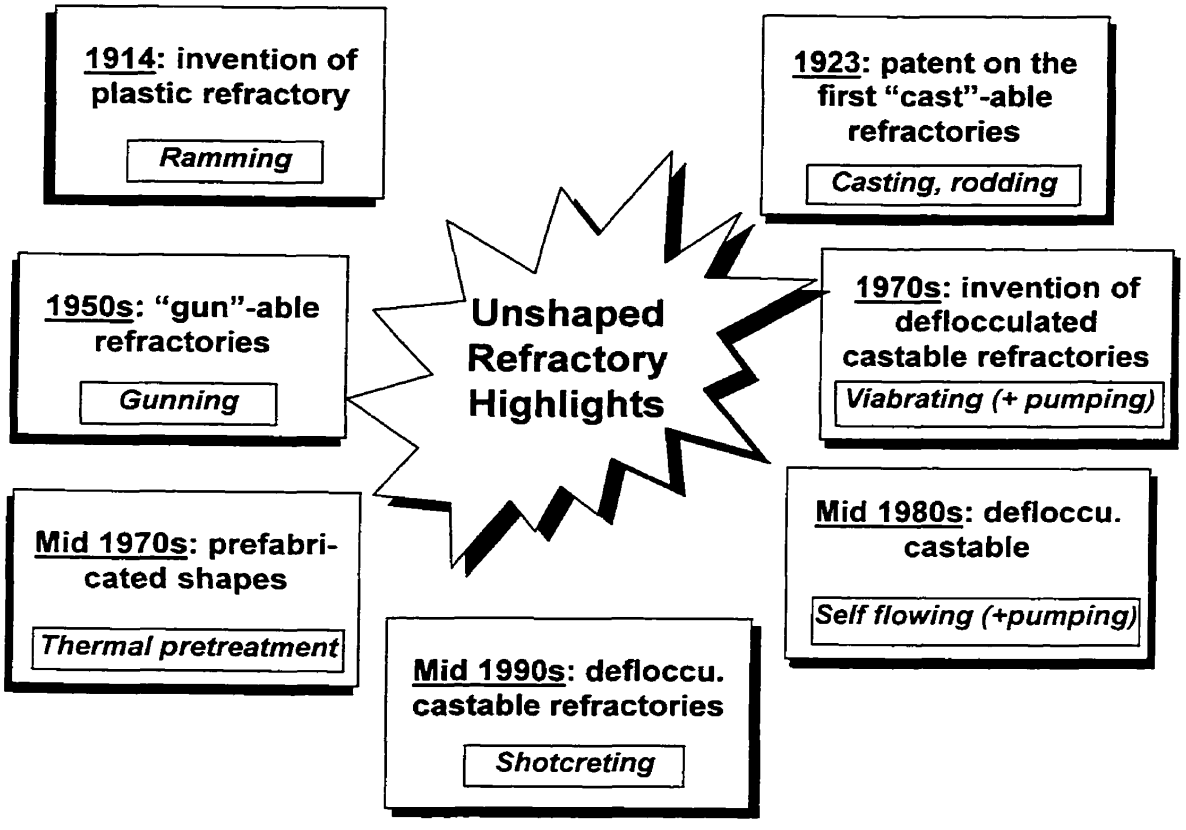

Figure 2.1 Highlights of monolithic refractories historical evolution (from Ref. 26).

There seems no argument that the greatest event in the history of modern monolithic refractories was the advent of low cement castables (LCC's) or deflocculated castables since late 1960s[23, 26,27]. This basic development had led to all further developments in regard to ultra-low cement castables (ULCC's) and none-cement castables (NCC's),

as reviewed by William E. Lee and Robert E. Moore in Ref. 4, p. 1391-1392. Before then, monolithics were used mostly for atmospheric furnaces. The advent of LCC enabled monolithic refractories to acquire lower porosity, higher strength and corrosion resistance, due to reduced low melting phases like gehlenite (C_2AS) and anorthite (CAS_2), as products of the reactions between the associated CaO in the cement and aluminosilicate materials. As a result, monolithic refractories have been able to replace more shaped refractories in a variety of applications, not only atmospheric furnaces but also places in direct contacting with molten iron and steel as well as slag at high temperatures.

As pointed out by B. Clavaud et al[27]: "Low cement castables are now used in large quantities by the steel industry to solve problems where service conditions are particularly difficult or exacting. The selected applications in steel making which are presented include porous plugs, injection and bubbling lances, sliding gate repairs, degassing units and tundish linings. In all these cases, low cement castables are giving results superior to many other types of refractory, yet there is still a large potential for research work in this field... ". This explains the fact that the quantity of monolithic refractories for iron and steel making has kept increasing worldwide in the last 15-20 years. In Japan in 1989, the consumption of monolithic refractories for steel industry for the first time became higher than that of shaped refractories[28]. Currently the proportion of monolithic refractories accounts for about 60% of the total refractory consumption in Japanese iron and steel industry[29]. Since 1992 also in Japan, the share

of monolithic refractories in total refractory production has exceeded 50% and reached 59.8% in 1998[30]. The same upward trend occurs also in USA, European countries and China. For example, the proportion of monolithics produced in the UK has increased from 20% in 1983 to over 35% in 1997[31]. In China, the percentage of monolithics in total refractory production is nearly 40% currently, compared with 20% in 1995[32].

To reflect the prosperity of monolithic refractories, the remarkable technical evolution and challenge in the last two or three decades, in terms of raw materials, bonding system, installation, performance and application, are briefly summarized below, citing only a few of the major papers published on the subject[4,23,24,26-29,33-39].

Raw Materials[28,35,39]

Formerly the raw materials for monolithics were mainly from natural resource, like chamotte and bauxite. In recent years, however, more synthesized high purity and performing materials, such as mullite, tabular alumina, fused alumina, sea-water magnesia, spinel, MgO-CaO clinker etc., have been used, shifting from semi-acid based to neutral and semi-basic, bringing about higher service temperature and performance. On the other hand, some non-oxide ingredients like SiC, carbon, Si_3N_4, have been also used in monolithics. New and high duty raw materials have made the variety of monolithics nowadays surpass that of shaped ones, and their performances match those of bricks.

Binders and Additives[4,23,35,37,38]

All efforts made in this aspect are to get maximum particle packing and reduce impurity components from binders. The striking progress in binding system for castables is believed to be the adoption of ultrafine oxides and the conversion from hydraulic towards coagulating binding. The reduction of cement content has been a key trend in the last 20-30 years. Since 1970s, R & D work on monolithic refractories has been centered around LCC's, ULC's and NCC's, by using high purity CA cement, fine clay, ultra-fine oxides, hydratable alumina, oxide sols together with advanced dispersing technologies to reduce cement addition from more than 15-30% for conventional castables to 4-8% for LCC's and 1-4% for ULC's.

Pure binding system has made it possible to adjust the chemical and mineralogical components of the matrix to be very close to those of the host materials, or to react with the host raw materials to produce new favorable phases, which, as bonding phases at elevated temperatures, are compatible with the host materials and favorable to the performance of the whole material. Typical examples are mullite-bonded castables using microsilica and small amount of CA cement as binder and spinel bonded MgO-Al_2O_3 castables using hydratable alumina as binder.

All these achieved merits have been made possible using appropriate admixtures, such as dispersants, accelerators, retarders, plasticizers, explosion inhibitors, etc. Upgraded and new additives are still coming on-stream, contributing greatly to the advancement in

the state-of-the-art on monolithics.

Installation Process[33,35,36]

The workability of monolithics, especially castables, has been improved and adapted to new installation processes by using ultra-fine powders, controlling particle distribution and admixtures. Ramming mixes and plastic mixes have been greatly replaced by castables, installed on-site by vibrating or self-flowing. To adjust labor costs, and to satisfy the needs for friendly environmental conditions, self-flowing and shotcreting monolithics have been booming. For a quick installation and a short heating-up time, precast blocks have also been adopted, in heating or soaking furnaces, BF troughs, EAF roofs, steel ladle bottoms and side walls etc.

Performance and Application[27-29,33-35]

Due to comprehensive advantages and improved properties, monolithics are challenging more and more shaped refractories. Monolithic linings have distinct advantages as compared with brick linings, such as shorter manufacturing cycle, energy and manpower saving, higher installation efficiency, flexibility for complex configuration, joint free and local repair or re-lining possible. Consequently, monolithic refractories, with castables as the mainstay, have increasingly been used, in place of shaped refractories, especially in iron and steel industry. Al_2O_3-SiC-C castables for BF troughs and hot iron ladles since late 1970s and Al_2O_3-spinel (MgO) castables for steel ladles since mid 1980s are typical examples[29,33]. They correspond to the continuous increase of castables, see Figure

2.2[33]. Some high performance castables can serve also as functional components, for example, lances, purging plugs, well blocks, impact pads, weirs, dams, etc.

By reviewing the past and looking into the future, we still see challenges. For example, as mentioned by M. Rigaud[6], the use of monolithics in ladles will be well accepted with much less resistance, once a solution to avoid using MgO-C bricks in the slag line zone will be found; yet there are still too few reports available on in-plant trails, with carbon containing castables.

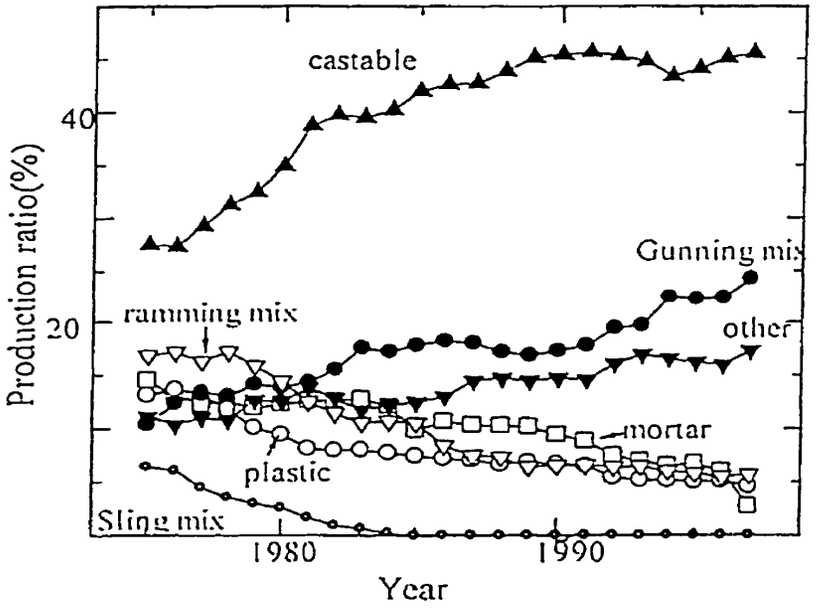

Figure 2.2 Production ratio of monolithic refractories in Japan (from Ref. 33).

In summary, the most striking advances in refractories industry worldwide in the last two or three decades are coming from new monolithic refractories, more varieties, higher performance and extended applications. No doubt, the switch from bricks to monolithics will continue, and innovations and new breakthroughs are still expected.

2.2 On Al_2O_3-SiC-C and Al_2O_3-Spinel(MgO) Castables

2.2.1 Al_2O_3-SiC-C Castables

Al_2O_3-SiC-C low cement castables emerged in mid 1970s, initially for blast furnace troughs to replace ramming mixes[14,33,39], later also for hot metal ladles[15,28]. The role of the main three components can be illustrated by Figure 2.3.[28], though it was for Al_2O_3-SiC-C brick.

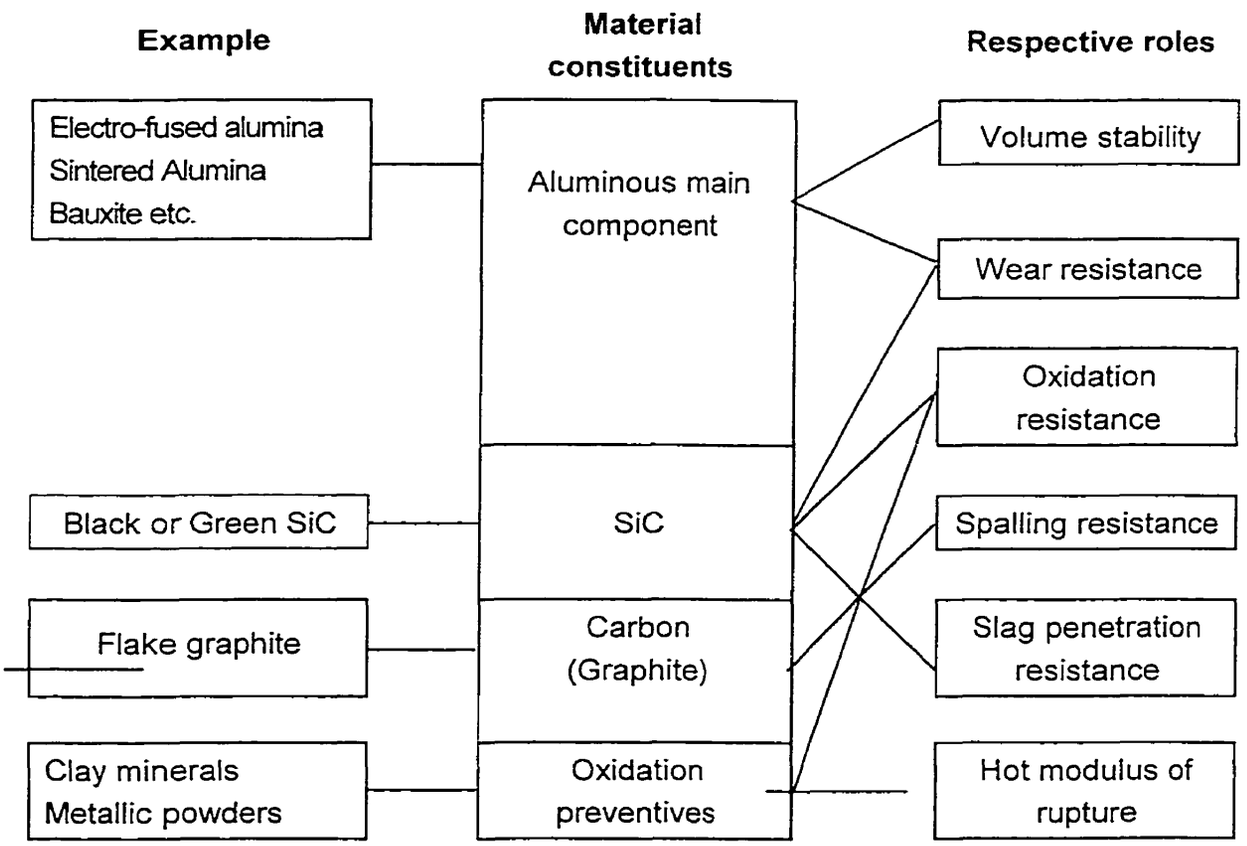

Figure 2.3 Raw material components and respective role of Al_2O_3-SiC-C bricks (from Ref. 28).

Carbon can be added in various forms such as coke, pitch, resin, carbon black, amorphous graphite or flake graphite. The purpose is to prevent the wetting of the lining surface by slag and to reduce temperature gradient by increasing thermal conductivity. Carbon is susceptible to oxidation, especially on the back face of the trough where is it has a long term exposure to the atmosphere. Oxidation is also prevalent at the air/slag interface. A partial solution is to use metallic antioxidants like Al and Si powders.

SiC is added to increase thermal conductivity and also to improve the oxidation and slag resistance. The oxidation reaction of SiC is:

$$SiC + O_2 \rightarrow SiO_2 + C, \text{ and } 2C + O_2 \rightarrow 2CO$$

The reaction products are silica and carbon monoxide, with the silica forming a protective film against deeper oxidation.

Customer process technology changes have been a principal driver for improvements in refractory technology. To improve the productivity of BOF and steel quality, hot metal pretreatment, consisting of desiliconization in the runner of BF, desulphurization and dephosphorization in torpedo ladle, has since early 1980s been increasing. Fluxes are stirred into the iron and oxygen is injected while the iron is maintained at a certain temperature. The fluxes commonly used are mill scale (iron oxide), lime plus fluorite or soda ash, all of them have extremely corrosive attack on the refractory lining. As a result, the torpedo ladle has become a reaction vessel subjected to very severe service conditions, rather than a mere transport vehicle. By comparing various refractories

[28,41], the most effective lining for the torpedo ladle was found to be Al_2O_3-SiC-C bricks (with 10-15% graphite), see Figure 2.4[28] for example.

Attempts have also been made to use castables in iron pretreatment ladles. Drawing lessons from brick practice, castables were made also of Al_2O_3-SiC-C to satisfy 3 requirements[15]: 1) high resistance against repeated thermal shocks; 2) high volume stability against cracks; and 3) high erosion resistance against desulphurization/ dephosphorization flux. This may have sparked off the Al_2O_3-SiC-C castables with higher carbon content on one hand, and on the other, containing flake graphite.

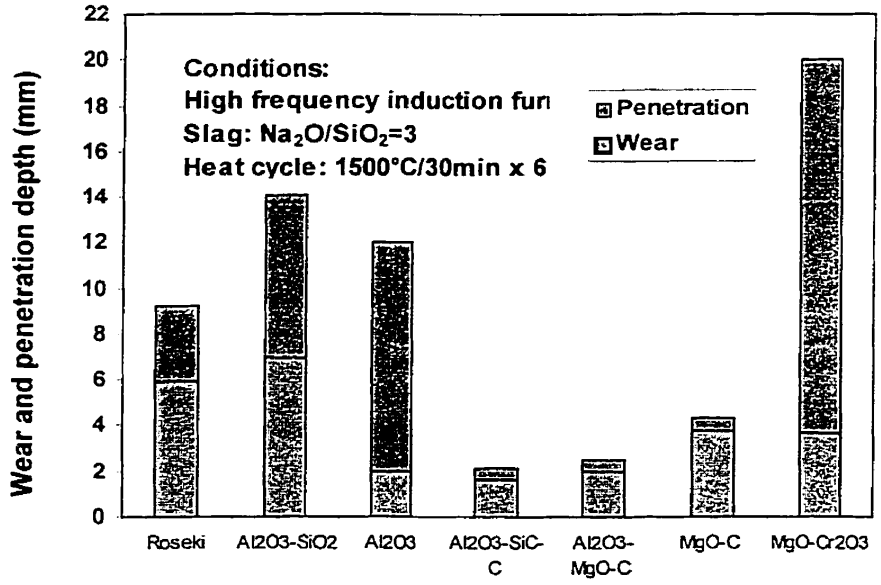

Figure 2.4 Comparison of corrosion resistance in various refractories (from Ref. 28).

Table 2.1, according to T. Miwa et al[15], shows the Al_2O_3-SiC-C castables developed

for hot metal pre-treatment ladle. In-plant trials turned out that the metal zone castable was capable of providing a life equal to the brick, while the slag zone castable performed less well as the brick, with large range of wear rate varying from 0.27 to 0.49

Table 2.1 Properties of Al_2O_3-SiC-C castables for metal zone and slag zone of hot metal ladle (from Ref. 15)

		Metal zone		Slag zone	
		Castable	Brick	Castable	Brick
Chemical Comp. (%)	Al_2O_3	36	50	74	68
	SiO_2	37	28	2	9
	SiC	15	5	15	8
	C	8	10	7	9
Linear change (%) After heating	105°C, 24h	-0.03		-0.03	
	1000°C, 3h	+0.72		-0.09	
	1500°C, 3h	+1.51		-0.03	
C.M.O.R. (kg/cm^2) After heating	105°C, 24h	20		50	
	1000°C, 3h	15	(130)	80	(200)
	1500°C, 3h	15		60	
C.C.S. (kg/cm^2) After heating	105°C, 24h	90		180	
	1000°C, 3h	140	(500)	300	(645)
	1500°C, 3h	130		270	
Apparent porosity (%) After heating	105°C, 24h	15.8		17.7	
	1000°C, 3h	19.7	(10.0)	21.4	(9.0)
	1500°C, 3h	20.4		21.5	
Bulk density (g/cm^3) After heating	105°C, 24h	2.43		2.78	
	1000°C, 3h	2.34	(2.65)	2.73	(2.87)
	1500°C, 3h	2.27		2.75	
Water demand (%)	(in addition)	6.8		6.8	

( ) : As received

mm/charge, due to peeling. For both castables, the carbon, at a relative high level, was however from non-graphite source, a combination of pitch, coke and other carbons. As can be seen, at 7 or 8% of the carbon, the strength of the castables is rather low.

Not until recently graphite has been used as the carbon source in Al_2O_3-SiC-C castables. An early work reported[40], however, graphite bearing such castable exhibited poor slag erosion resistance and was easily penetrated by slag, whereas pitch and resin bearing such castables exhibited good placement and erosion resistance. S. Sakamoto et al [7], developed a truly flake graphite containing Al_2O_3-SiC-C castable, using SiC coated graphite by high speed impact method. The SiC, 5 microns in size, was stuck on the surface of flake graphite with a size of 100-150 microns by impact processing. This approach led to an improved dispersibility of the graphite, and consequently flowability of the castable. The main concern, however, is the firmness of the coating, as a longer mixing time lowered the flow of the castable was observed, due to decoating effect.

Typical properties of the developed castables containing 5% surface treated graphite vs. 5% amorphous graphite and a brick used in slag zone of iron pre-treatment ladle are shown in Table 2.2[7]. Their resistance to corrosion and oxidation are compared in Table 2.3[7]. The performance of A and D was compared by in-plant test in slag zone of a 200t de-phosphorization pre-treatment ladle. After 255 charges of the service, the erosion rate was 0.31 mm/ch. for A vs. 0.29 mm/ch. for D, quite equivalent. By using A in place of C as a tap hole trough lining of a 100t EAF, a pronged life was obtained, 160-

210 charges vs. 130 charges, erosion rate 0.75-0.94 vs. 1.15 mm/ch..

Table 2.2 Properties of Al_2O_3-SiC-C castables and unburned brick (from Ref. 7)

		Castables A	Castables B	Castables C	Brick D
Raw materials	Fused alumina	↑		↑	
	Bauxite		↑		↑
	Flake graphite				↑
	Amorphous graphite			↑	
	Treated graphite	↑	↑		
Chemical comp. (%)	Al_2O_3	81.0	75.5	80.2	72.4
	SiO_2	3.8	7.5	3.7	7.1
	SiC	6.7	6.7	6.7	4.9
	F.C.	5.0	5.0	5.0	9.2
Bulk density (g/cm^3)	After drying	2.92	2.70	2.91	2.88
	1400°C, 2h	2.93	2.60	2.88	2.82
Apparent porosity (%)	After drying	15.0	17.0	15.0	7.0
	1400°C, 2h	15.2	20.0	15.0	14.5
C.M.O.R. (MPA)	After drying	3.9	3.9	3.9	-
	1400°C, 2h	9.8	7.8	11.8	-
C.C.S. (MPA)	After drying	14.7	14.7	14.7	58.8
	1400°C, 2h	39.2	34.3	44.1	44.1
P.L.C. (%)	1400°C, 2 h	+0.1	+0.3	0.0	+0.2
Water addition (%)		6.2	7.5	6.0	

Table 2.3 Results of corrosion and oxidation tests (from Ref. 7)

	A	B	C	D
Max. corrosion depth (mm)*	15.2	17.5	16.8	17.0
Oxidation layer (mm)**	1.0	3.0	3.0	2.0

* 1500°C, 5h by induction furnace, de-P slag; ** 1500°C, 5h in air, sample size: 50×50×50mm

All the results mentioned above reveal the meaningfulness of flake graphite in Al_2O_3-SiC-C castable, without impairing other properties. More recently, hot metal pre-treatment tends to be performed in the BF trough, measures against FeO, basic flux and higher tapping temperature become the challenges to monolithic BF trough linings. Further efforts in improving Al_2O_3-SiC-C castables are of great necessity.

2.2.2 Al_2O_3-Spinel(MgO) Castables

There are numerous published papers on Al_2O_3-Spinel and Al_2O_3-MgO castables, as they have become the mainstay of monolithic lining materials in steel ladles. Important issues involved in this area include spinel or magnesia content in relation to penetration and corrosion resistance, stoichiometric spinel or Al_2O_3 enriched spinel? the mechanism of slag resistance, pre-formed spinel or in-situ forming spinel?

Before dealing with these issues, it is necessary to go over some fundamentals on spinel. In refractories, the term "spinel" refers to a crystal structure comprising a 1:2 ratio of +2 and +3 cations in a cubic lattice with oxygen. For refractory castables, the word "spinel" is habitually confined to the MgO-Al_2O_3 compound $MgAl_2O_4$ (or also written as $MgO{\cdot}Al_2O_3$). It has special properties that make it useful as a refractory material, e.g., high melting point around 2105°C, with a wide range of solid solution from 50 to 85 mol% of Al_2O_3, isotropic, lower thermal expansion than Al_2O_3 and MgO, good ability to absorb some other cations like Fe^{+2}, Mn^{+2} and Fe^{+3} in solid solution with little reduction in melting point and structural destroy. Spinel does not occur in nature, but can be

synthesized trough the reaction between magnesia and alumina, which starts usually around 1100°C or lower if more active powders of MgO and/or Al_2O_3 are used. Theoretically, spinel formation accompanies a 7.8% volume expansion, calculated based on density change. A distinction needs to be made between spinel containing and spinel forming castables. The former contains preformed spinel aggregates or fines rather than the free constituent oxides. Spinel containing castables are easier to be handled since the preformed spinel can be inert to water. The latter contains free MgO and free Al_2O_3 in the composition prior to use. During use they react to form spinel. Customarily, Al_2O_3-Spinel or Al_2O_3-MA represents spinel containing system, while Al_2O_3-MgO represents spinel forming system, though chemically both belong to the Al_2O_3-MgO system. For both castables, CA cement is used as the binder, which impart good hot strength to the castable by interlocked platy $CaO{\cdot}6Al_2O_3$ crystals, as one of the bonding phases, the other being spinel.

Al_2O_3-Spinel castables emerged firstly in Japan in mid 1980s, due to the shortage of zircon raw material and the demand on quality steel, and the use of them has been reported by several Japanese authors since the late 1980s[17-19]. The key point leading to the evolution and optimization of such castables is the reduction of penetration by slag. Before shaping up to Al_2O_3-Spinel system, it underwent a transition from magnesia-alumina to spinel-alumina and finally to Al_2O_3-Spinel, to overcome cracking and slag penetration, hence the ladle life was drastically increased, as reported by K. Furuta et al[19].

Several papers have discussed the addition of preformed spinel in Al_2O_3-spinel castable, and found the most appropriate addition should be around 20%[42-47], when penetration and corrosion are compromised. Figure2.5 represents one of the similar results.

K. Fujii et al[48], Yamamura et al[49] and H. Sumimura[50] demonstrated that the castables added alumina-rich spinel was better in resistance to slag penetration than stoichiometric spinel or magnesia-rich spinel added castables. The reason is that the Al_2O_3–rich spinel, due to lattice defects of cation vacancy, has a stronger capability to capture Fe^{+2}, Mn^{+2} and Fe^{+3} cations from slag, to form (Mg, Fe, Mn)(Al, Fe)$_2O_4$ solid solution, and therefore, further prevents slag penetration. Figure 2.6[49] shows the slag penetration as a function of spinel compositionby a slag test performed in a horizontal rotary drum furnace, at 1650°C for 4h, using a converter slag (CaO/SiO_2 =3.6, Fe_2O_3 = 33.7%).

The slag penetration mechanism of Al_2O_3-Spinel castable was studied by B. Nagai[45], Y. Oguchi et al[46] and H. Sumimura et al[50]. B. Nagai[45] and Y. Oguchi et al[46] concluded, as schematically represented in Figure 2.7, as follows: CaO reacts with Al_2O_3 to form $CaO.6Al_2O_3$ or $CaO.2Al_2O_3$. FeO in the slag reacts with spinel to form (Mg, Fe, Mn)$O{\cdot}Al_2O_3$ solid solution. On account of these reactions, the viscosity of the slag gets higher because the slag changes to a SiO_2-rich composition.

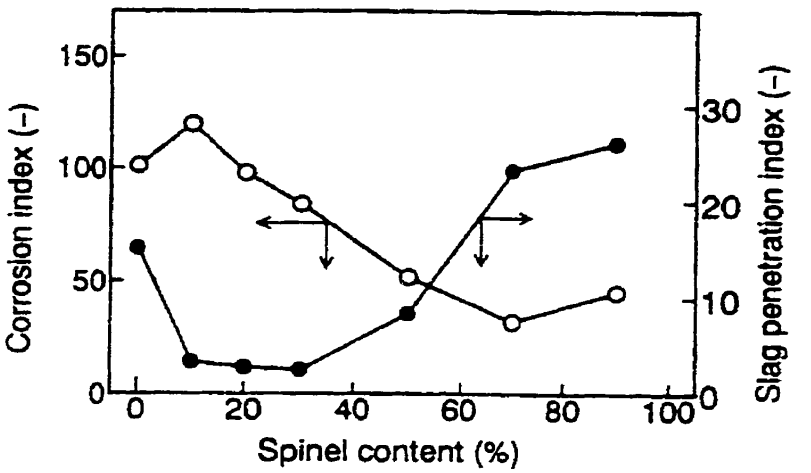

Figure 2.5 Effect of added spinel on slag resistance of Al_2O_3-MA castable (from Ref. 47).

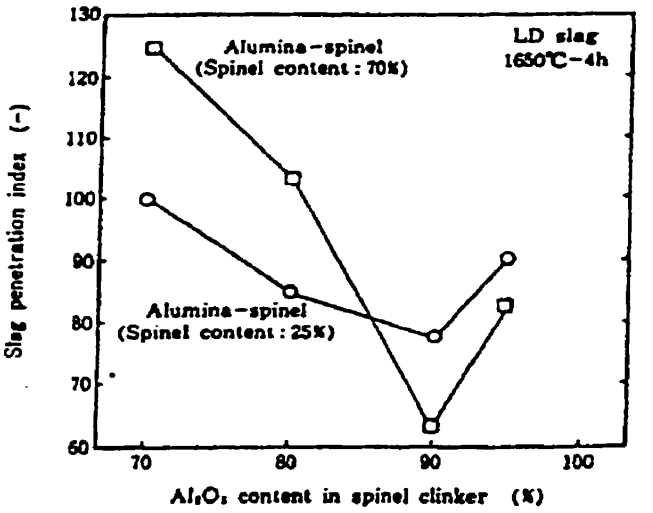

Figure 2.6 Relationship between slag penetration and Al_2O_3 content in spinel (from Ref. 49).

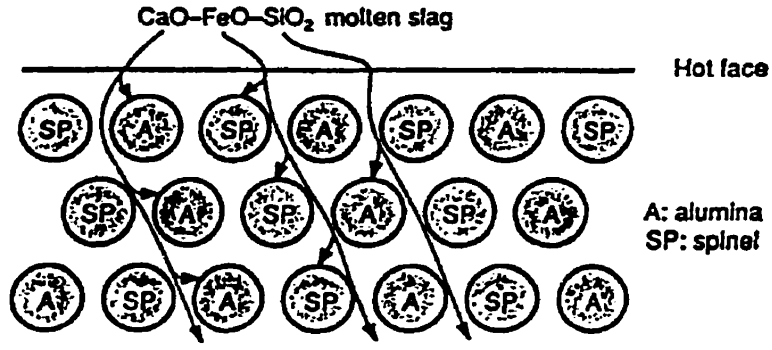

Figure 2.7 Schematic representation of slag penetration in Al_2O_3-Spinel castable (from Ref. 46).

Arguing with this explanation, H. Sumimura et al[50] put forward a new presumption, based on their experimental results, of the slag penetration mechanism, as described in the following:

1) Spinel reacts with alumina in the castable and forms solid solution having lattice defect with cation vacancy by the alumina-rich composition;
2) SiO_2 and FeO in the slag accelerated this reaction;
3) FeO in the slag is trapped in the cation vacancy of the Al_2O_3-rich spinel;
4) CaO reacts with alumina and forms $CaO{\cdot}6\ Al_2O_3$;
5) The crystal growth of $CaO{\cdot}6\ Al_2O_3$ leads to the densification of the texture. The penetrated SiO_2 facilitates this growth; and
6) These reactions restrain the slag penetration.

The viewpoint stated above supports the fact that the castables containing alumina-rich spinel showed better slag penetration resistance than those containing stoichiometric spinel.

Recently, Al_2O_3-MgO castables, added fine magnesia instead of previous pre-formed spinel, are being viewed with keenest interest. Some reports [47,51,52] have indicated a superior slag resistance of such castables to that of Al_2O_3-Spinel castables, as compared in Figure 2.8[52], by rotary slag test at 1650°C for 4h, using two kinds of synthetic slag (C/S=3.7 and 1.3 respectively, Fe_2O_3=10%). As seen, from the point of view of penetration resistance, appropriate magnesia addition should be set around 7%. In-plant trials have also confirmed a better performance of Al_2O_3-MgO castables than Al_2O_3-Spinel castables[47].

I. Ohishi[18] considered that spinel in Al_2O_3-Spinel castable should be as fine and homogeneous as possible to limit the penetration by slag. F. W. Henry et al [5] pointed out, however, that adding even very finely ground pre-reacted spinel, it will still be much larger than spinel formed by in-situ reaction. Spinel containing castables are thus not nearly as effective in preventing penetration of the matrix by slag because the slag simply goes around the grains. This explains the superiority in preventing slag penetration of spinel forming castable. The expansion of in-situ spinel formation, when appropriately controlled, will densify the texture of the castable, which contributes also to suppressing slag penetration[20].

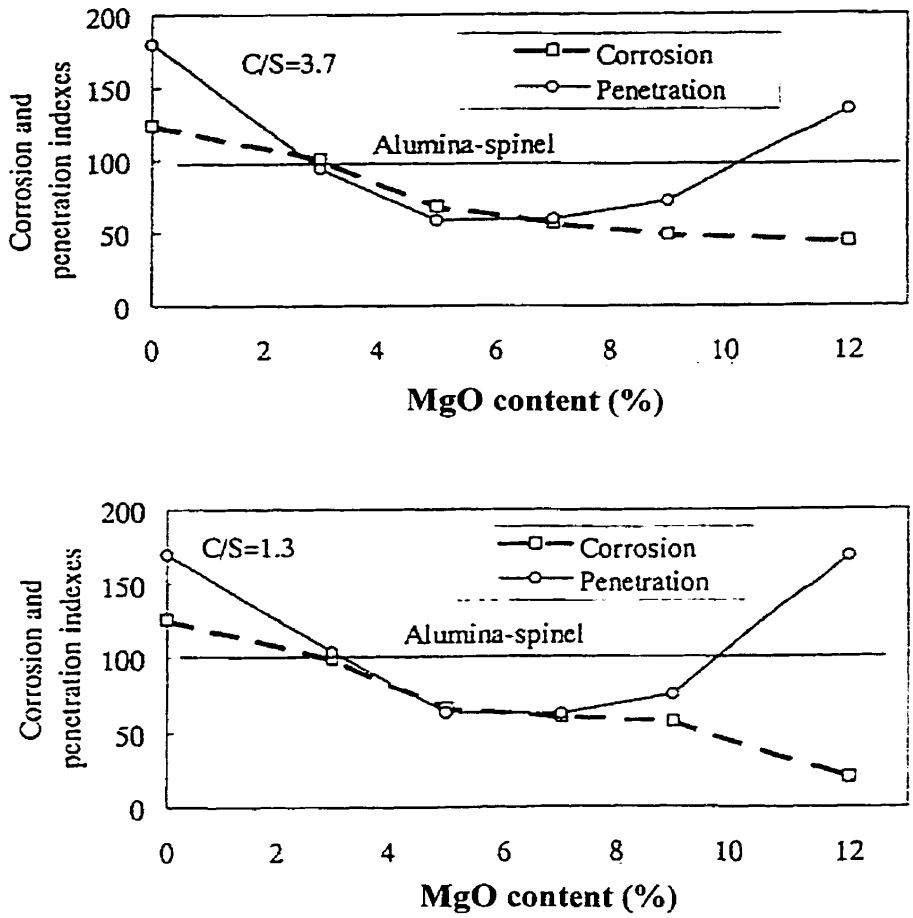

Figure 2.8 Corrosion and penetration indexes vs. magnesia content (from Ref. 52).

However, for a reliable application of the Al_2O_3-MgO castables, with free MgO presenting in the composition, three inter-linked challenges have to be tackled with.

1) Impact of magnesia upon castable rheology, which leads to short working time and rapid setting [53].

2) Risk of magnesia hydration and subsequent destruction of the castable.

3) Large volume expansion from the reaction of spinel formation, it may be detrimental by cracks, high porosity and low strength.

Adjusting the magnesia size, adding a small amount of silica fume (around 0.5%) and using suitable admixture have been proven effective in solving these problems.

By thermal expansion under load (0.2MPa) test on Al_2O_3-MgO castables, M. Kobayashi et al[20] suggested an appropriate magnesia addition of 7.5%, while according to the slag test in a high frequency induction furnace at 1650°C using a slag with C/S=3, they suggested an optimum MgO content of 7.5-10.0 %. They carried out expansion under load tests further on Al_2O_3-MgO castables containing 7.5% MgO and 0.2, 0.5 and 1% silica fume respectively. The thermal expansion with silica content >0.5% is larger than that when silica content <0.5% around 1300°C. The lowest maximum thermal expansion is at 0.5% silica. They concluded that SiO_2 in Al_2O_3-MgO castable accelerated the in-situ spinel formation rate. From the fracture resistance point of view, S. Itose et al. [52] confirmed that for a maximum fracture resistance, the optimum MgO content in Al_2O_3-MgO castable is indeed around 7.0 % and the optimum silica fume addition is 0.5%, quite in accordance with the results by Kobayashi et al[20].

The results of field trials showed a significant difference in the ladle lining lives, 180-200 heats for the Al_2O_3-MgO castable(7.5 % MgO and 0.5% silica) vs. 140-160 heats for the Al_2O_3-Spinel castables[20].

It has been found[20,47], by testing thermal expansion under load of Al_2O_3-Spinel and Al_2O_3-MgO castables, that Al_2O_3-MgO castable deforms easier and heavier at high temperatures, and the additional expansion by spinel formation even does not appear under the load, when MgO content is controlled under 10%. The deformation creates an ability of relaxing the thermal stress. By adjusting the magnesia size and content and silica fume amount, not only the slag resistance, but also the expansion and relaxing thermal stress can be controlled.

Reviewing the so far undergone researches on both Al_2O_3-Spinel and Al_2O_3-MgO castables, we can see that the MgO content in the castables, irrespective of using preformed spinel or directly adding fine magnesia, is at dilemma concerning slag corrosion and penetration aspects, viz. increased MgO level tends to increase corrosion resistance, while decrease penetration resistance. Efforts have been centered on the improvement of the resistance to penetration, which, however, is more or less at a sacrifice in corrosion resistance. The reality of the situation is, on the one hand, penetration resistance is always emphasized, being critical in preventing peeling-off and impact wear and thought of more important than hot strength[5,54], and on the other hand, the resistance to high basicity slag is not promising, hence such castables are not able to be used at slag line of steel ladles to challenge, performance-wise, MgO-C bricks, nor are magnesia-based basic castables, due to poor penetration resistance and spalling problem[19,38,55].

2.3 On Carbon Containing Castables

2.3.1 Carbon Source Materials and Features of Natural Flake Graphite[2, 56-61]

For carbon bearing refractories, there are several carbon sources, such as natural graphite, synthetic graphite, coal coke, petroleum coke, pitch, metallurgical-tar, pitch-tar, carbon black, etc., while graphite takes the lead. Graphite can be divided into natural graphite and synthetic graphite. The former can be subdivided into 3 sub groups, known as amorphous, flake and high crystalline graphite.

Amorphous graphite is generally mined directly from the ground and does not require any processing. "Amorphous", meaning without crystal structure, is customarily used, but not in fact the real case. A more appropriate name would be microcrystalline graphite, with a low degree of structural order. The carbon content generally falls in the range of 80 to 85% and true density around 2.3 g/cm^3. Flake graphite is different from the other natural graphite in that it has to be processed once retrieved from the ground, as it only occurs in concentrations from 3 to 28%, in order to rise the carbon to higher levels. The big increase in application of this kind has fallen within refractory industry mainly for MgO-C and Al_2O_3-C refractories. Flake graphite for refractories are classified according to the flake size and fixed carbon. Usually, the greater the flake size, the higher the purity and better the quality. Industrial purity varies between 90 and 98% of fixed carbon. Natural flake graphite occurs all over the world, with the major producers being China, Brazil, Germany, South Africa and Canada. High crystalline

graphite is the only one that appears to have a needle-type structure, in addition to having materials which appear to have sublimed and left nothing but a graphitic structure. It is considered 100% graphitic and the true density is 2.26 g/cm^3. It comes only from one place in the world and is somewhat limited in supply.

Synthetic graphite is classified into two groups, called primary artificial graphite and secondary artificial graphite. The former is manufactured from calcined petroleum coke and simply goes through a high temperature heat treating process. The latter is a combination of coal tar pitch, along with calcined petroleum coke which has been formed into the shape of electrodes. Besides these, other forms are called pyrolitic graphite and graphite fibers.

The uniqueness of graphite is outlined below.

(1) Planar structure with no reactivity and wettability

The perfect graphite structure indicates a planar structure, with an infinite two-dimensional array of C atoms arranged in a hexagonal network in the form of a giant aromatic molecule. The C-C bond in the plane is much stronger than the bond between the planes, as indicated by the interatomic distance of 1.420 Å vs. the interplanar space of 3.354 Å. The carbon atoms in a planar are in Sp^2 bonding with no bonding directed out of the layer. Thus each layer is bond to its neighbor by Van der Waal's or some other form of weak binding energy. Simplistically, there is no propensity to bond or react in

the direction at right angles to the plane. Any reactivity must be seen as deriving from the crystal edges. Any penetration of the crystal surface through the layers, any attempt to bond, must destroy the structure. It must be realized that it should be difficult to bond to a basal surface other than through some physical mechanism. Further more, the basal surface has no ready wetting ability. When using binders, they cannot be made to distribute freely amongst the graphite flakes and the use of wetting agents is of doubtful value. In its physical form, natural graphite mirrors its crystal structure and presents itself as a plate or flake, usually with high aspect ratio, diameter to thickness.

(2) Strong anisotropy

The planar structure results in marked anisotropic properties, e.g., thermal expansion perpendicular to the planes is much greater than parallel to the planes, the expansion coefficient being 30-33 $\times 10^{-6}$ $°C^{-1}$ in the "c" direction vs. about 1 $\times 10^{-6}$ $°C^{-1}$ in the "a" direction; thermal conductivity parallel to the planes is 200 times that perpendicular to the planes; compressibility is 104-105 times greater in direction perpendicular to the plane. However, the anisotropy degree decreases for a graphitic component produced from a random array of graphite and properties of such a body can not readily be inferred from orientation factors in the random structure.

(3) High thermal stability

Graphite has a very high melting temperature, over 3500°C, and does not melt at normal

pressure. Thus the atom mobility is limited and sintering is not possible under practicable conditions. As a result graphite either in its own right or as an admixture in a refractory needs to be "glued' together by a second phase.

(4) High thermal conductivity and flexibility

As well known, the thermal conductivity of graphite (55 Kcal/m·h·°C at 1000°C) is about 10 times higher than some refractory oxides. 5.8 Kcal/m·h·°C at 1000°C for MgO, 5 Kcal/m·h·°C at 1000°C for Al_2O_3, for example.

As consequence of the cleavage on the basal plane and the lack of any directional bonding in the plane, graphite is extremely flexible. This makes graphite a very tough material and fracture across the flake is very difficult.

Flake graphite has been widely used in refractories designed to withstand molten metal and slag and thermal shock. The role of graphite in improvement of thermal shock resistance is attributed to the following, as analyzed by C. F. Cooper et al[59], based on the thermal shock resistance parameter R_{st}, defined by Hasselman as $R_{st} = (\gamma_{wof} / E\alpha^2)^{1/2}$, where γ_{wof} is the work of fracture, E is the modulus of elasticity, and α is the thermal expansion coefficient.

1) Lower thermal expansion. C. F. Cooper et al[59] pointed out that the contribution of the graphite itself to thermal expansion of a composite refractory is almost

negligible, due to the presence of "Mrozowski" cracks, which introduce porosity into which the graphite moves on expansion. Many graphitic refractories with significant level of flake graphite have a thermal expansion in the region of half that might be expected from the oxide phases.

2) Lower modulus of elasticity. The Young's modulus of graphitic refractories is lower than those of non graphitic alumino-silicate refractories, being between 1/2 and 1/5, a reflection of an inability to create a true chemical bond between the low surface energy surfaces of the graphite and the matrix, and also the presence of widely distributed "Mrozowski" cracks.

3) Higher work of fracture. Higher work of fracture endowed with graphite has been observed. The graphite can give tortuous crack path and cause crack branching, which has the ability to absorb energy through basal plane slip. It may act also as a plate-reinforcement, absorbing energy either through pullout effect or actual plate fracture.

4) Higher strain to failure. The mean failure strain of graphitic materials is in the range of 0.15 to 0.2%, compared to only 0.03% for alumino-silicate refractories. With high failure strain, materials can withstand high failure stress.

5) Higher thermal conductivity. Thermal conductivity is often introduced as a multiplier in thermal shock resistance parameters, such as $R'_{st} = R_{st} \times k$, where k is

the conductivity. Graphitic refractories are amongst the most thermally conducting available.

The carbon phase serves to impart thermal shock resistance and, by virtue of its inability to be wetted by molten slag, it inhibits the slag penetration and protects the oxide phase against corrosion. However, the main drawback of such refractories is the oxidation of graphite, once it is removed, the corrosion protection is lost. Despite its highly refractory nature and its mechanical and thermal interesting properties, graphite cannot operate along in a large number of hostile environments. This is due to the relative ease of oxidation and also because of its ready solution in carbon-unsaturated iron. Hence it needs to be compounded with other refractories.

2.3.2 Current Status of Carbon Containing Castables

Carbon containing refractories have been known for at least 200 years. By 1769 a patent had been granted for "improvements" in black lead crucibles[62]. Anstey is claimed to be the first to use coke in admixture with Stourbridge clay to make crucibles and received a silver medal from the Society of Arts in 1925[63]. A. Ure[64] in his dictionary in 1842 gave details of the mining of graphite in Borrowdale. J. Precy[63] in 1875 gave details on graphite containing crucibles showing that they were commonly manufactured. It is thus clear that graphite was widely exploited as a refractory by mid to late 1800s.

But a revolutionary evolution happened in 1970s, since then graphite containing refractories have been developed so vigorously that today "black refractories" can be found almost everywhere in metallurgical industry, taking those for iron and steel making processes for example, BF troughs, torpedo cars, iron ladles, BOF linings, EAF linings, steel ladles, ladle-tundish system including sliding gate, long nozzles, stoppers, submerged nozzles, etc. However, making carbon containing castables is a new dream, not yet fully fulfilled, due to some technical restrictions.

So far, carbon containing castables may be divided into two groups: castables containing non-flake graphite carbon and castables containing flake graphite. Adding flake graphite is highly desirable with respect to corrosion and oxidation resistance, but it reaches a point where the increased water addition, consequently porosity, limits the benefit expected from flake graphite in comparison to other carbon sources. The former, due to less dispersion and wetting problems, is easier to use up to relatively high carbon content (8% as reported by T. Miwa et al[15]), while for the latter, it is hard to reach such a high level, unless special approach is applied[7,11].

H. Teranishi et al [10] reported that the water demand of the MgO-C castable at 5% carbon level can vary from more than 18% with flake graphite down to 10% with amorphous graphite and 7-6% with other sources of carbons, as compared in Figure 2.9, indicating the difficulty to introduce flake graphite. For a dense structure and avoiding cracking after drying, a combination of pitch and carbon black was used to make a

MgO-C castable with the properties shown in Table 2.4. Such a MgO-C castable was used in the extension repair of slag line of a LF ladle, the durability was twice that obtained by the conventional Al_2O_3-MgO castable, very encouraging for carbon containing basic castables.

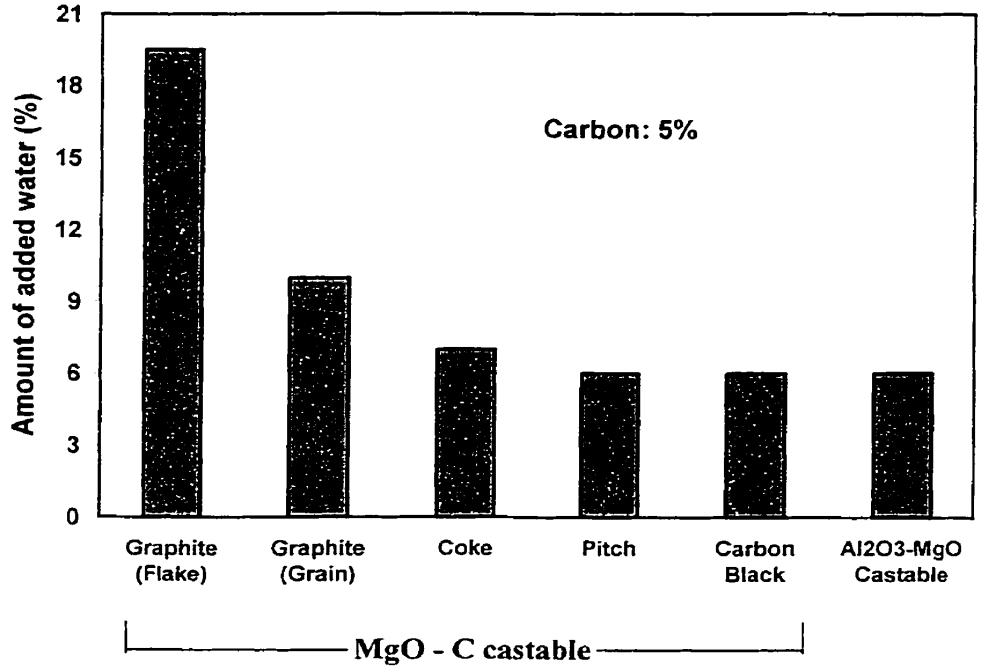

Figure 2.9 Relation between carbon and added water in MgO-C castable (from Ref. 10).

Other encouraging results were reported by S. Sakamoto et al [7] and K. Isomura et al[11] on Al_2O_3-SiC-C castable and Al_2O_3-Spinel-C castable respectively. By using SiC coated flake graphite, made by newly developed "high speed impact method", the developed Al_2O_3-SiC-C castable, with 5% flake graphite, showed good flowability at

Table 2.4 Properties of MgO-C castable (from Ref. 10)

Chemical composition (%)	MgO C	90 5
Apparent porosity (%)	110°, 24h 1500°C, 3h	15.3 18.2
Bulk density (g/cm^3)	110°, 24h 1500°C, 3h	2.71 2.65
Cold crushing strength (Mpa)	110°, 24h 1500°C, 3h	28.3 25.4
Permanent linear change (%)	1500°C, 3h	+ 0.64
Water addition (%)		6

6.2% water addition, and was used in the slag zone of a 200t iron pretreatment ladle. A service life of 255 heats was achieved, equivalent to resin bonded unburned Al_2O_3-SiC-C brick containing 9% graphite, indicating that such castable is competitive with brick lining. It was also used in tap hole trough of a 100t EAF. 30% increase in service life was achieved, compared with the Al_2O_3-SiC-C castable containing 5% amorphous graphite. In Ref. 11, a new type of graphite containing castable Al_2O_3-Spinel-C for metal line of BF trough was reported, containing 10% graphite at 6% water addition by using special dispersant developed by the authors. But actually, the used graphite is not natural flake graphite, instead, amorphous graphite and artificial graphite. Nevertheless, such a 10% graphite containing castable gives very encouraging results: corrosion resistance to BF slag, evaluated at lab, is above 1.5 times that of conventional

Al_2O_3-Spinel-SiC castable (spinel 39%, SiC 15%); applied to BF trough, the life is about twice as long as the conventional castable at low flow speed of molten iron, but only 1.1 times at high speed, due to insufficient bonding strength at high temperature.

As seen, not so many achievements have been made, despite some encouraging results so far achieved. Owing to the hydrophobicity of flake graphite, to make successful, commercially meaningful and truly flake graphite containing castables remains a big challenge.

2.3.3 Countermeasures So Far Taken to Tackle Key Problems in Using Graphite

Problems caused by graphite can be summarized as:

- Poor wettability with water, leading to dispersion, flowability and higher water demand problems
- Big density difference between graphite and refractory raw materials, resulting in segregation
- Lack of bonding between graphite and refractory oxides, engendering strength problem
- Oxidation at elevated temperatures, causing a degradation of the texture

Countering the hydrophobicity problems, the approaches so far, according to accessible literatures, are in two avenues: using surface active agent and doing surface modification of graphite.

(1) Surface active agent

Commercially available wetting agents or dispersants especially suitable for graphite seem not yet readily available. H. Kawasaki et al[65] used two agents, one layer of water soluble polymer (cationic cellulose) and a deposition of a second layer of sodium metasilicate (Na_2SiO_3) adsorbed on graphite surface, to make the graphite hydrophilic, and the dispersion is improved. However, excess adsorption of anions removes the polymeric adsorption layer.

K. Isomura et al [11] claimed a self developed dispersant superior to other dispersants, e.g. polycarboxylic acid, polyacrylic acid and naphthalenesulfone acid, irrespective of amorphous, artificial or flake graphite. But no detail on the dispersant is given in their paper.

(2) Surface coating

Metal precursor method

H. Yoshimatsu et al [66] investigated the improvement in water wettability and oxidation resistance of Al_2O_3-coated graphite. In their work, flake graphite powders were coated with a chelate compound of aluminium $Al(OC_3H_7)_2(C_6H_9O_3)$ in a high speed mixer, then the mixture was heated at 500°C for 2h in air to get Al_2O_3-coated graphite. The wettability and oxidation resistance were improved by the Al_2O_3 coating, but the flowability was not satisfactory.

Later, using a similar method, J. Yu et al [67] coated flake graphite with TiO_2 formed by heating the absorbed tetra-n-butoxy titanium $Ti(OCH_2CH_2CH_2CH_3)_4$ at 120°C in air for 12h. Their study reveals that the wettability with water and flowability of the graphite are greatly improved when the coated TiO_2 amount reached 0.5% or more, and the oxidation resistance increases with the amount of TiO_2 coated.

However, the application of such coated graphite, whichever Al_2O_3, SiO_2, ZrO_2 or TiO_2 by metal precursor method, in castables has not been found reported, maybe due to availability and cost reasons.

SiC coating by high speed impact method

The basic idea of this method is to stick hydrophilic constituent onto graphite surface. oxides or carbides can serve as the coating as they possess better dispersion and wettability than graphite. S. Sakamoto et al [7] developed a high speed impact method to do the surface modification. Flake graphite (under 150 microns) and SiC powder (5 microns), at a ratio of 10:3, were put into a high speed impact machine. Through repeated mechanical work such as impact force, compressive force, friction force and shearing force, SiC fines can be stuck on the surface of graphite. SEM observation found that after the treatment, the surface of graphite was covered with very fine SiC powders. In addition, the shape of the graphite after impact treatment becomes a little spherical, which can be expected favorable to the improvement of flowability. Indeed the

dispersion of such SiC coated graphite and flowability of the castable containing such coated graphite are improved, confirmed by Zeta-potential and flow value measurements.

The advantage of this method is that it facilitates a mass production at low treatment cost. The shortcoming is the decoating effect that may happen under long time and intensive mixing. because the binding between SiC and graphite is physical and is easily destroyed by severe abrasion during mixing.

Reviewing overall, graphite, as a singular mineral with unique properties, has become a very important material for modern refractories. For good reasons, developing graphitic castables is meaningful, but a tough task. So far, research efforts seem to be concentrated around surface modification of graphite. It is well accepted that carbon improves thermal shock resistance and corrosion resistance of bricks, eliminating the damage by spalling to a minimum. However, straight addition of carbon in particular flake graphite into castables has not yet yielded the wished same benefits.

CHAPTER 3. THREE APPROACHES TO INCORPORATE GRAPHITE

In dealing with graphite in castables, the following problems have to be addressed:

- Poor wettability with water, leading to problems of dispersion, flowability and higher water demand
- Big density difference between graphite and refractory raw materials, resulting in segregation
- Lack of bonding between graphite and refractory oxides, engendering strength problem
- Oxidation at elevated temperatures, causing the degradation of the texture

In view of these problems, the strategy in this work is dictated in order to:

1) agglomerate the flake graphite powders so as to decrease the specific surface area;
2) diminish the density difference by using crushed carbon-bonded mixture of refractory oxide and graphite;
3) modify the surface of the flake graphite by forming hydrophilic coating;
4) control distribution state of the graphite in the castable to maintain enough bonding strength; and finally
5) use suitable anti-oxidants.

In compliance with the above, three approaches, viz. micro-pelletized graphite, briquetted Al_2O_3-Graphite and TiO_2 coated graphite, have then been developed and used

to bring flake graphite into the two types of castables.

3.1 Micro-pelletized Graphite

The so called micro-pelletized graphite (denoted as PG hereafter) are agglomerates of natural flake graphite powders with or without other additives, typically "hairs" with a chosen diameter of 0.5 mm and length up to 5 mm, as shown in Figure 3.1. Since the dimension of the pellets is much smaller than the size of the coarse aggregates in the castables, a prefix of "micro" is thus used. They are made by an extrusion-shaping technique, as described below.

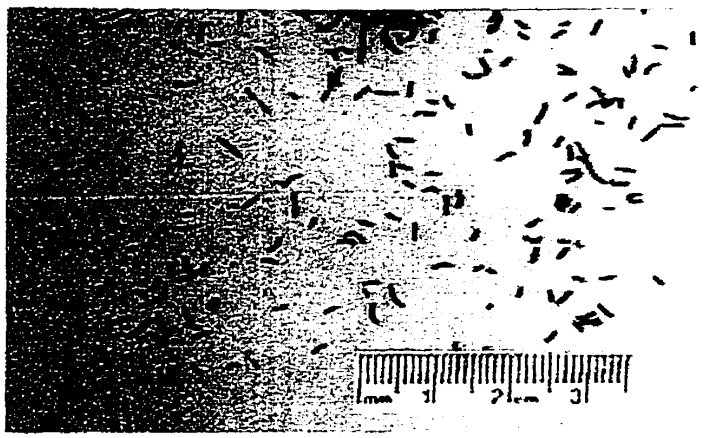

Fig. 3.1 Outlook of the micro-pelletized graphite.

3.1.1 Fabrication of PG

The principle of making the micropellets is to use a suitable organic binder to bind the graphite powders with or without the addition of other constituents, then to force the

homogenized plastic mix to go through a shaping orifice as a continuous body. After curing and heat treatment, the binder is pyrolized to form carbon bonding. Incorporating various additives in the micropellets is to bring the antioxidants where they are needed, close to the graphite, also to favor density and bonding in the matrix.

The raw materials for the pellets include flake graphite, antioxidant, alumina and liquid binder. Two kinds of metallic powders, i.e., aluminium (Al) and silicon (Si), and two kinds of boron bearing powders, i.e., boron carbide (B_4C) and zirconium diboride (ZrB_2), both as antioxidants, are incorporated as per the designed combination into the graphite-based micropellets. To adjust the graphite content and to increase the density of the pellets, fine alumina powders are added in replacement of graphite in some pellets. Three liquid organic binders, i.e., polyviny alcohol, molasses and phenolic resin have been evaluated. As viewed from wettability, workability, shelf-life, ease in use, health risk, availability and price, molasses has finally been chosen as the binder in this work. Table 3.1 shows the specification and source of the materials.

The process of fabricating PG comprises 4 steps, as described below.

1) Mixing

Put all the material powders into Horbart N50 mixer, dry mix for 3 minutes, add proper amount of the binder during mixing, and then wet mix for 5 minutes after the binder addition. The homogenised wet mass should be used up within one hour.

Table 3.1 Raw materials for making graphite based micropellets

Material	Specification	Commercial Brand	Source
Flake graphite	Fixed C ≥ 97%, -200 mesh	Stratmin 20097	Stratmin Graphite Co., Canada
Al	Al>99%, -200 mesh	Al-101	Reade Manufacturing Co., USA
Si	Si>99%, - 200 mesh	J-99	Elkem ASA Materaials
B_4C	B_4C>90%, B_2O_3 < 7%, - 325 mesh	Tetrabor®	ESK GmbH, Germany
ZrB_2	Purity 99%, -325 mesh		CERAC™, Inc., USA
Alumina	Al_2O_3 ≥ 99, -325 mesh	T-64	Alcoa, USA
Molasses	100% pure	Grandma®	Grandma Food Products Co., Canada

2) Extruding

Feed the plastic wet mix continuously to the belly of the extruder that is a commercial screw-press extruder, as an attached part to the Horbart N50 mixer. The extrusion mould-plate has been made changeable with different diameters of orifice, which makes it possible to produce pellets with different diameters. In this work, a diameter of 0.5 mm is adopted. The flowing-out green micropellets are on a glass or steel board.

3) Drying

The green pellets are cured at ambient temperature for 6-8h, then heated to remove the

volatile in a dry oven at a rate of 1°C/min to 200°C and soaked at this temperature for at least 16h. For this purpose, Cole-Parmer Oven, 52000-80 type, made by Cole-Parmar Instrument Co., USA, is used in this work.

4) Breaking up

By using a disc grinder, UA53 BICO Pulverizer, made by BICO, Inc., USA, with carefully controlled gap between the discs, the sticking between the dried pellets can be removed. On the other hand, the long pellets can be broken up and length range of the pellets can be controlled by adjusting the gap between the discs.

3.1.2 Characterization of the Micropellets

Three groups of micropellets have been produced by the above described process. Their composition and density after the heat treatment are shown in Table 3.2. In Group I, pure graphite micropellets are made as a reference in comparison with those containing 3 levels of Al and Si additives, the (Al : Si) ratio being 1 : 1. In Group II, boron bearing additives B_4C and ZrB_2 are respectively incorporated into the pellets, where Si is eliminated. These two kinds of pellets are made for the use in Al_2O_3-MgO-C castables. In Group III, when the dry basis of PG3, before adding the binder, is substituted by certain amount of alumina, while the ratio of (Al + Si) to graphite remaining unchanged, three kinds of micropellets containing 7-26% Al_2O_3 are made, to be used to compare with the PG3 in Al_2O_3-MgO-C castables.

Table 3.2 Composition and density of the different micropellets

	Code	Fixed carbon* (%)	Al_2O_3 content (%)	Antioxidant type and content (%)	Bulk density (g/cm^3)
Group I	PG1	98	0	(Al + Si) = 0	1.31
	PG2	91	0	(Al + Si) = 6.5	1.33
	PG3	85	0	(Al + Si) = 13.0	1.35
	PG4	79	0	(Al + Si) = 19.5	1.37
Group II	PG5	81	0	Al = 6.6; B_4C=10	1.37
	PG6	81	0	Al = 6.6; ZrB_2=10	1.39
Group III	PG3	85	0	(Al + Si) = 13.0	1.35
	PG3/a	79	7	(Al + Si) = 12.0	1.43
	PG3/b	71	17	(Al + Si) = 10.6	1.50
	PG3/c	63	26	(Al + Si) = 9.5	1.57

* Flake graphite plus the pyrolized carbon from the binder.

The microphotographs of some micropellets observed by SEM back scatter electronic (BSE) image are shown in Figure 3.2-3.4. It can be seen that they are uniform in diameter, the inclusions are uniformly distributed, and the flakes and the inclusions are well bonded by the binder. Microstructurally, they look porous, probably due to the uncontrolled particle size distribution. By optimizing particle size distribution of the flakes and the inclusions, the density of the pellets is expected to be higher.

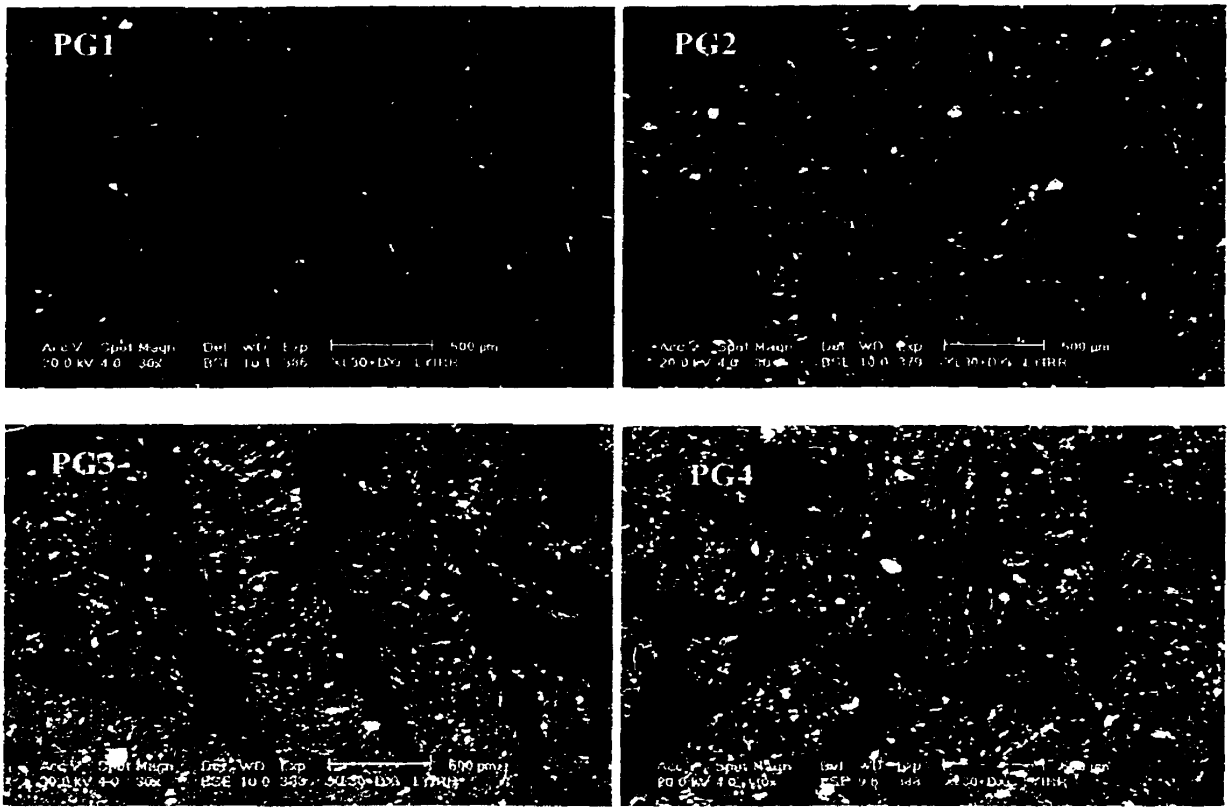

Figure 3.2 Microstructure of PG1-PG4, by BSE image of SEM

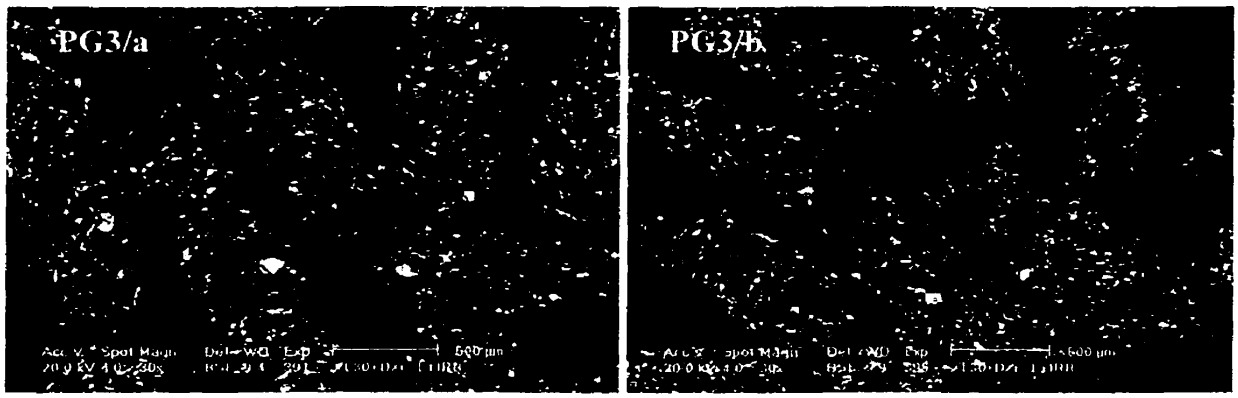

Figure 3.3 Microstructure of PG3/a and PG3/b, by BSE image of SEM.

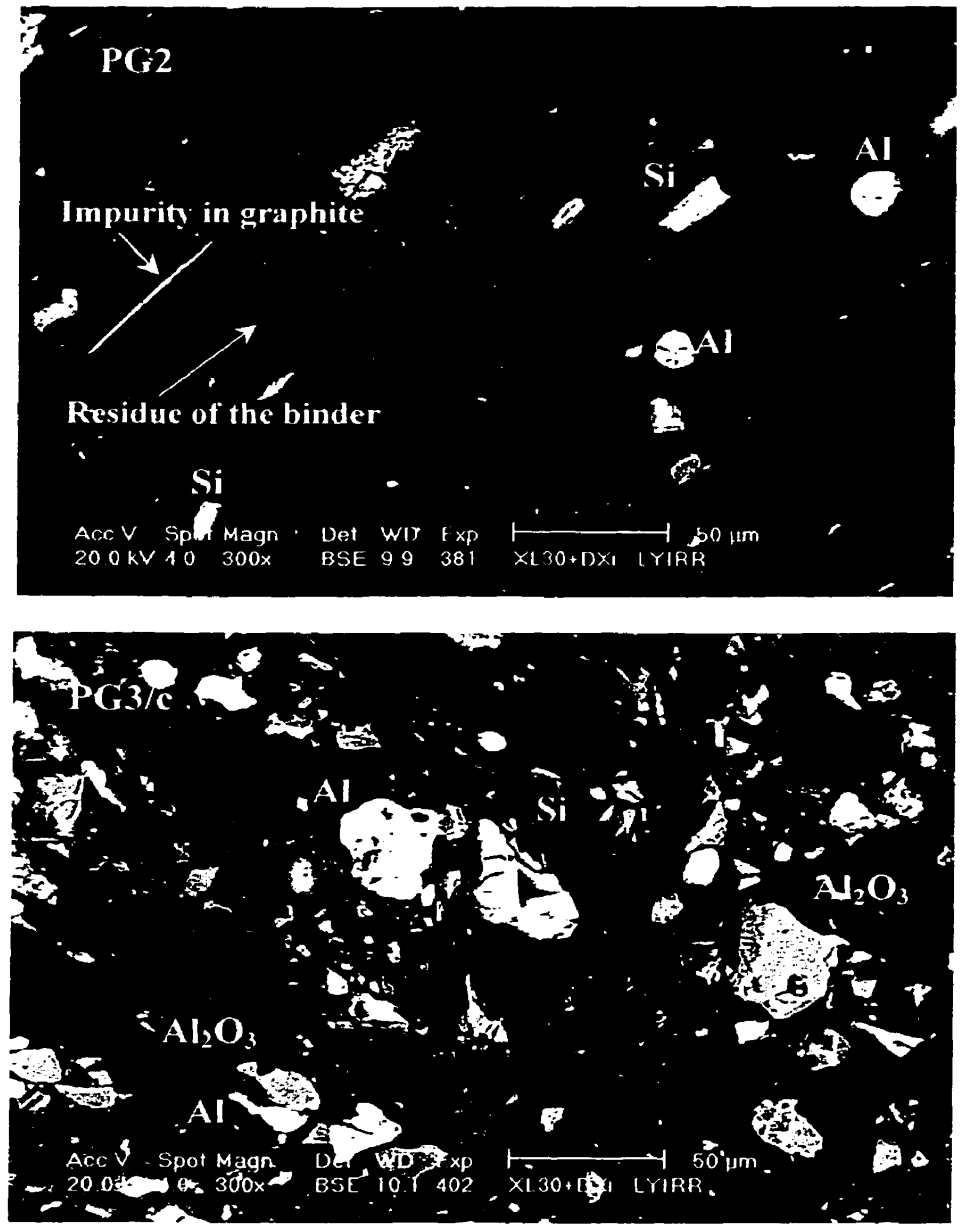

Figure 3.3 The inclusions in the micropellets observed by BSE image of SEM.

3.2 Briquetted Alumina-Graphite (BAG)

It is a pressed compact of resin bonded mixture of alumina and graphite, containing 30-

32% graphite. Graphite can be brought into the castables by adding the crushed BAG grains. It has a considerably higher density than that of graphite and a high strength to hold the graphite in it.

Two types of BAG are made according to the formulation shown in Table 3.3. Type 1 is for Al_2O_3-SiC-C castables, while Type 2 for Al_2O_3-MgO-C castables. The starting materials are mixed and blended homogeneously in an Eirich RV02 mixer, and liquid phenolic resin was used as the binder. The blended mixes are hydraulically pressed under a pressure of 70 MPa into 204 × 52 × 62 mm prisms. then heat-treated at 180°C for 24h and finally crushed into different size fractions between 0.074 and 3.36 mm.

Table 3.3 The formulations of two kinds of BAG

Material	Size (mm)	Percentage (%)	
		Type1	Type 2
Tabular alumina	2.38 –1.19	22	22
	1.19 –0.59	12	12
	0.59 – 0.30	9	9
	0.30 – 0.074	5	5
	- 0.044	7	9
	- 0.020	5	5
Antioxidants Al	- 0.044	3	3
Si	- 0.075	3	3
SiC	- 0.044	4	0
Flake graphite	- 0.15	30	32
Phenolic resin	(in addition)	6.2	6.2

Bulk density of the both types of BAG after the heat treatment is 2.6 g/cm^3, apparent porosity 8% and cold modulus of rupture 13.2 and 13.7 MPa for Type 1 and Type 2 respectively.

3.3 TiO_2 Coated Flake Graphite (CFG)

Surface treatment on flake graphite by metal precursors to form Al_2O_3 or TiO_2 coating to get improved water wettability and resistance to oxidation has been reported[66,67] and it was found that TiO_2 coating is more effective than Al_2O_3[67]. This work adopts the same TiO_2 precursor as used in Ref. 67 to prepare TiO_2 coated graphite, but not simply by solution immersion and drying at 120°C as done in Ref. 67, instead, a sol-gel process is adopted to get rid of the volatilization of the TiO_2 precursor.

3.3.1 Preparation of TiO_2 Coating by Sol-Gel Method

By TG (Cahn TG-171, Cahn Instruments, Inc., USA) analysis on, titanium (IV) butoxide and aluminium sec-butoxide, heating up at 5°C/min in oxygen atmosphere to 300°C and 500°C respectively, a big difference between expected and collected remained mass exists, the collected data are under the expected range, see Table 3.4. It is put in evidence that a big amount of the metal precursor volatilizes by heating.

A good way to avoid metal precursor vaporization is to make the coating via sol-gel method[68].

Table 3.4 The residue of two metal precursors measured by TG

Metal precursor	Expected if		TG results
	Oxide (wt%)	Metal (wt%)	Remained mass (wt%)
$Ti(C_4H_9O)_4$	23.50	14.00	10.26 (by 300°C)
$Al(C_4H_9O)_3$	20.70	10.95	13.65 (by 500°C)

In order to obtain a proper gel (so called Alcogel because the gelification occurs before the drying step), a metal alkoxide must be associated with a complexant agent (acetic acid or acetyl acetone) and water to perform the hydrolyzing reaction. The solvent will also have a great importance, and propanol is chosen because of its ability to form long chains. Three reactions will occur at room temperature when the components are introduced at proper ratios[68,69].

1) Hydrolysis of the metal precursor:

$M–[O–(Rad)]_4 + H_2O \rightarrow HO–M–[O–(Rad)]_3 + (Rad)–OH$

Condensation simultaneously by:

2) Oxolation

$HO–M–[O–(Rad)]_3 + HO–M–[O–(Rad)]_3 \rightarrow [(Rad)_3–O]–M–O–M–[O–(Rad)]_3 + H_2O$

3) Alcoxolation

$M–[O–(Rad)]_4 + HO–M–[O–(Rad)]_3 \rightarrow [(Rad)]_3–M–O–M–[O–(Rad)]_3 + (Rad)–OH$

Where "M" is the metal ion and "Rad" is the alkyl radical.

In general, hydrolysis and condensation are simultaneous and in competition. The pH of

the sol will influence the kinetic of the reaction. A low pH value will lead to a high speed of hydrolysis, whereas a high pH value will lead to a high speed of condensation.

The synthesis of a gel should satisfy two criteria: at first, this method should assure the formation of a homogeneous coating. (Indeed, the gel prevents particles from sediment by gravity and form agglomeration). After gelification, particles are in suspension well around by the metal precursor. The other interesting aspect is the formation of the M-O-M lattice, which is almost completed at room temperature, thus, the metal oxide evaporation is prevented at low temperature.

The starting materials used in the sol-gel process are given in Table 3.5. Propanol was chosen because of its ability to exchange alkyl radicals. Acetic acid can lower the pH and postpone the condensation reaction so that the hydrolysis is well completed before the gelification.

Table 3.5 Starting materials used in the sol-gel process

Compounds	Specific gravity (H_2O=1)	Molar weight (g/mol.)	Concentration (mol/L)
Titanium (IV) butoxide [$Ti(C_4H_9O)_4$]	0.95	340.4	2.79
Propanol ($CH_3CH_2CH_2OH$)	0.784	60.1	13.04
Acetic acid (CH_3COOH)	0.975	60.05	16.22
Pure water (H_2O)	1	18	55.56

According to Ref. 68, the following variables are needed to control the right proportion of the different materials in order to get a good kinetic of reaction and to obtain a proper gelification.

C = [concentration of metal precursor in the sol] = 0.5, mol/L

W = [concentration of water] / C = 3.5

R = [concentration of acid acetic]/ C = 0.7

By using the above mentioned starting materials and under the properly chosen parameters (see Annex 3.3.1 A), -200 mesh FG powders, at a batch of 500g, were treated by the sol-gel process, following the layout as illustrated in Figure 3.5.

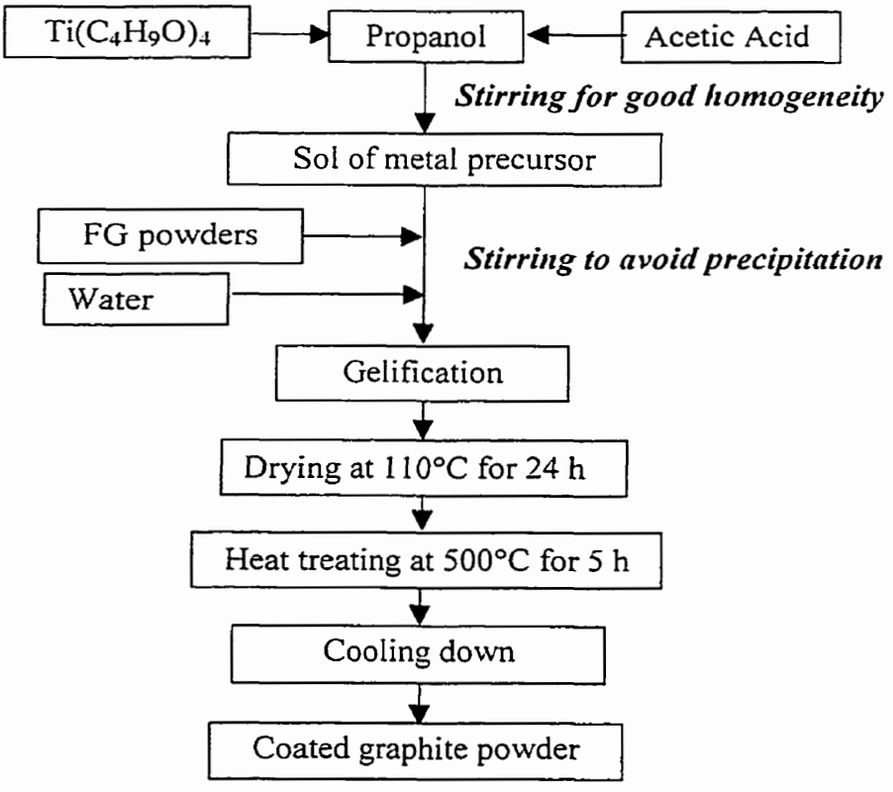

Fig. 3.5 Main steps to obtain TiO_2 coated flake graphite.

TG analysis was pursued on the as-dried gel. Good agreement between the obtained and the theoretical data was reached. Hence, almost no vaporization was detected according to the very close experiment and theoretical percentage mass obtained at the end of the heat treatment, 21% practically vs. 23.5 % theoretically. The TG analysis result is attached in Annex 3.3.1 B.

According to the mass gain measured after the treatment at 500°C, the TiO_2 coating accounts for about 6 % of the graphite, see Annex 3.3.1 A.

3.3.2 Identification of the TiO_2 Coating

3.3.2.1 By SEM and EDAX

Because of the extreme thinness of the coating layer, SEM was unable to provide a visible manifestation of the TiO_2 presence on surfaces of the graphite particles, except for on some individual particles, where the coating is rather thick, up to 0.5 μm, as shown in Figure 3.6, but scarcely to be found. Nevertheless, EDAX spot analysis has revealed the existence of the very thin TiO_2 film. For example, at each of the three spots on the surface of a graphite particle as marked in Figure 3.7, the EDAX spectrum contains the titanium peak, though rather weak, see Figure 3.8. Some TiO_2 drops are also observed by SEM.

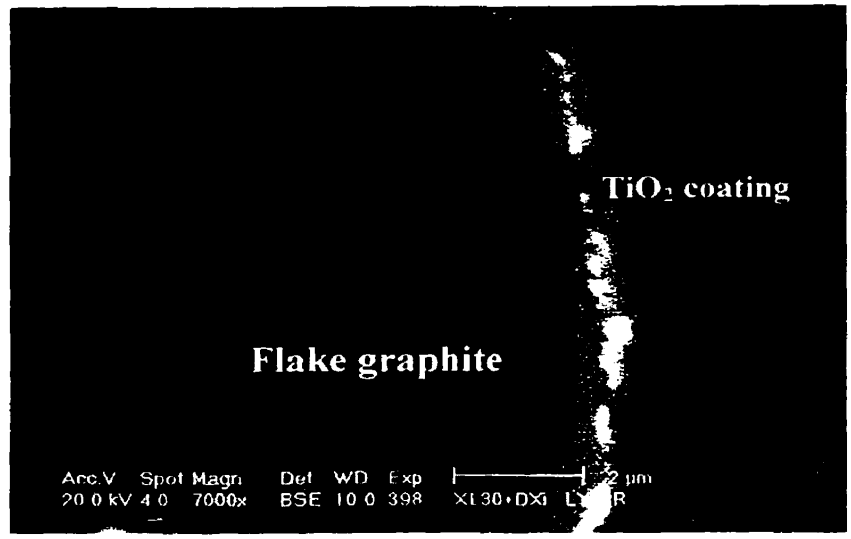

Figure 3.6 TiO_2 coating on a graphite particle, observed by BSE image of SEM.

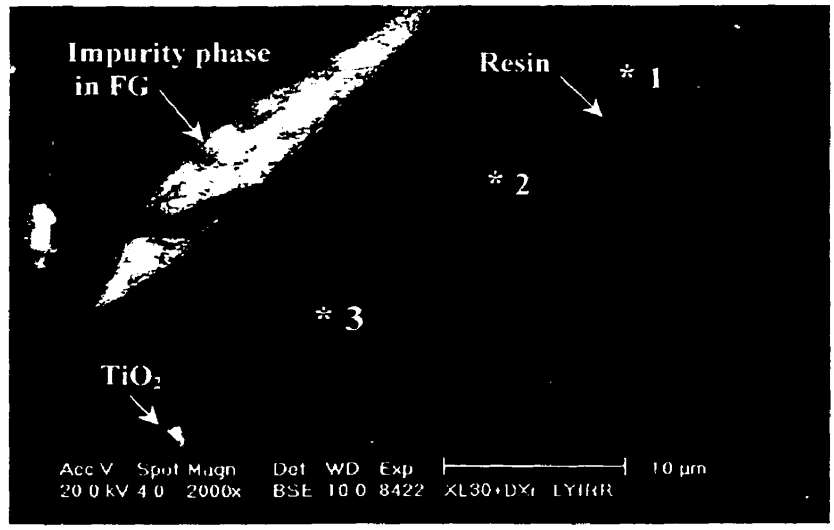

Figure 3.7 The location for EDAX spot analysis on the surface of a graphite particle.

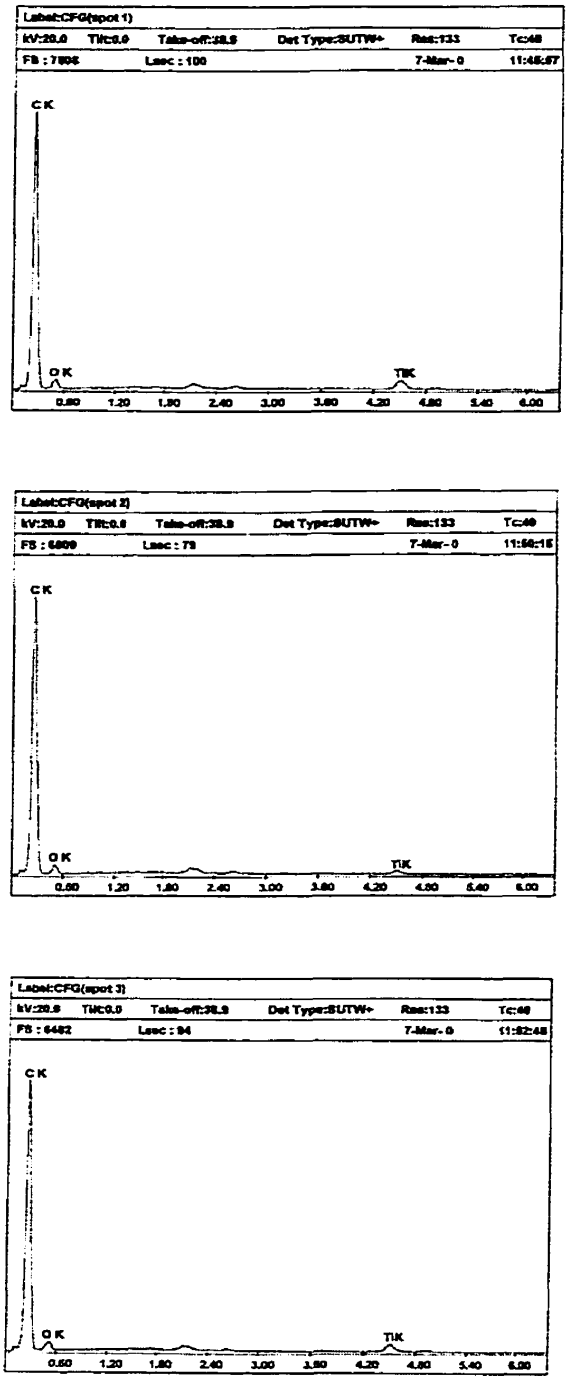

Figure 3.8 EDAX analysis at the spots marked in Figure 3.7.

3.3.2.2 By Auger Electron Spectroscopy (AES)

The AES technique for chemical analysis of surfaces is based on the Auger radiationless process. When a core level of a surface atom is ionized by an impinging electron beam, the atom may decay to a lower energy state through an electronic rearrangement, which leaves the atom in a doubly ionized state. The energy difference between these two states is given to the ejected Auger electron which will have a kinetic energy characteristic of the parent atom. When the Auger transitions occur within a few angstroms of the surface, the Auger electrons may be ejected from the surface without loss of energy and give rise to peaks in the secondary electron energy distribution function. The energy and shape of these Auger features can be used to identify the composition of the solid surface.

AES survey spectra are used to identify surface constituents. The analyzer is stepped through a selected energy range and the electron signal level at each step is measured and stored. It puts clearly in evidence, as seen in Figure 3.9, of the presence of titanium and oxygen, and of cause also the carbon on the surface of the coated graphite.

With Auger thin film analysis, the surface is sputter-etched by argon ion bombardment, and Auger analysis is performed on each sputtered layer step by step. The result is a composition versus depth profile. The thickness of the layer is estimated according to the fact that a 50 nm layer can be torn in one minute. This experiment was repeated on different particles and the collected data put in evidence of the repeatability of the test.

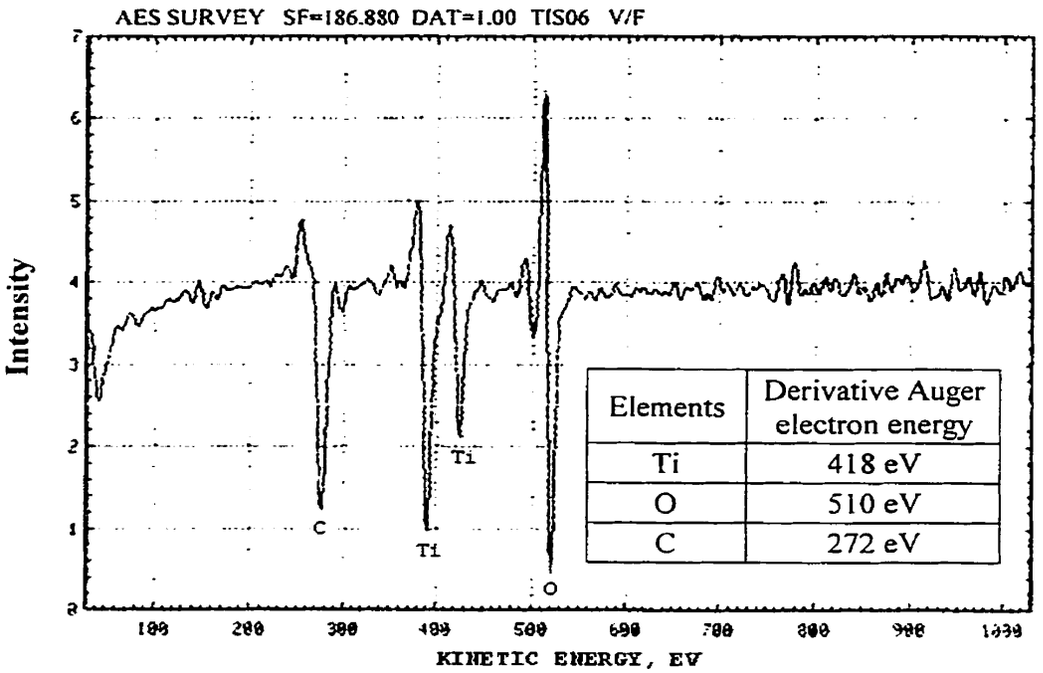

Figure 3.9 AES spectrum of the coated flake graphite surface.

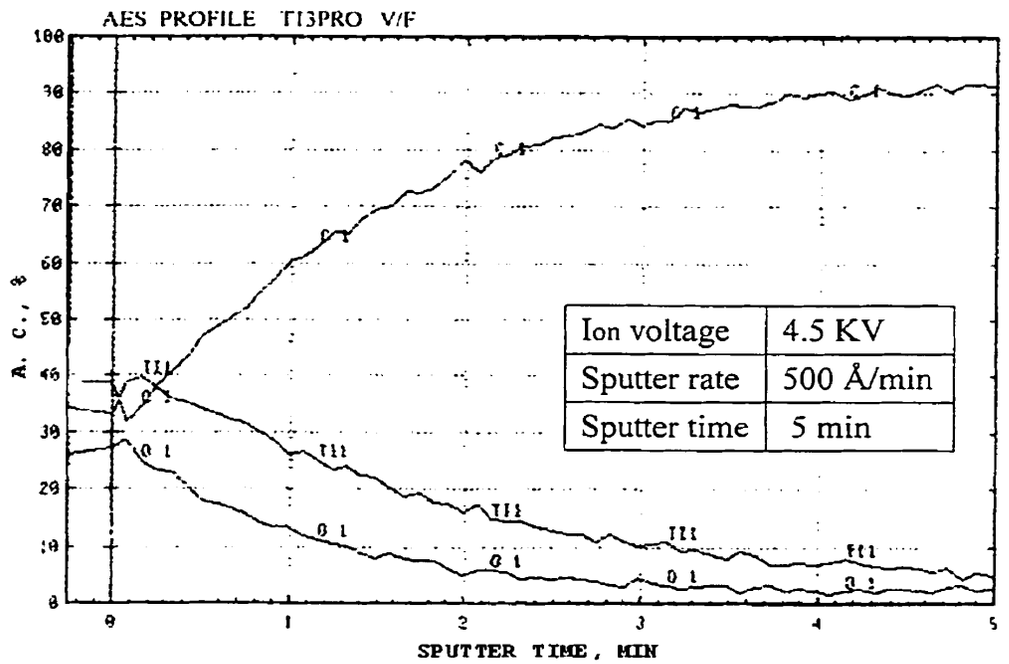

Figure 3.10 AES depth profile of Ti, O and C atomic concentration vs. sputtering time.

As seen in Figure 3.10, the levels of titanium and oxygen decrease while carbon increases remarkably as sputtering goes until 2 or 3 minutes, indicating that the coated TiO_2 layer is 100-150 nm in depth.

3.4 Evidence of Improved Hydrophilicity of the Treated Graphite

For the purpose of showing evidence of the improvement in hydrophilicity of the TiO_2 coated graphite and the micro-pelletized graphite, two simple ways have been used. One is to measure the wetting angle of a water drop on the pressed tablet of FG and CFG respectively. The other is to observe the sedimentation of FG, CFG and PG3 in water to see the difference in water wettability.

To get a smooth and densified surface, ϕ15x 3 mm pellets were pressed under a pressure of 50 MPa, using 1 g of the –200 mesh sieved graphite powders. Then, by using a glass dropper, a drop of water was laid on the surface of the as-pressed pellets. After 5 seconds, the picture was taken, and the wetting angle was measured on each sample, as shown in Figure 3.11, 74° for FG vs. 48° for CFG.

As for the sedimentation test, the pictures themselves, as shown in Figure 3.12, show clearly the difference. The contribution of the improved water wettability and reduced specific surface area of PG, BAG and CFG to lowering water demand and bettering flowability of the castables will be seen later in Chapter 5 and Chapter 7.

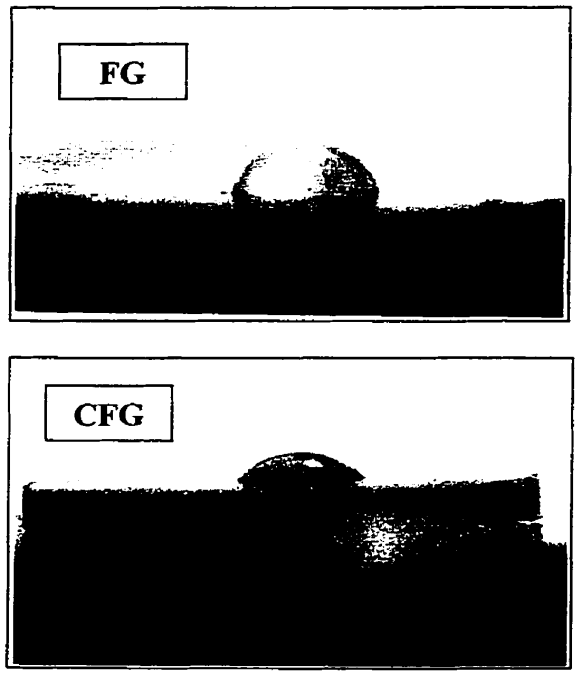

Figure 3.11 Wetting angle of the dropped water on pressed pellet of FG and CFG respectively.

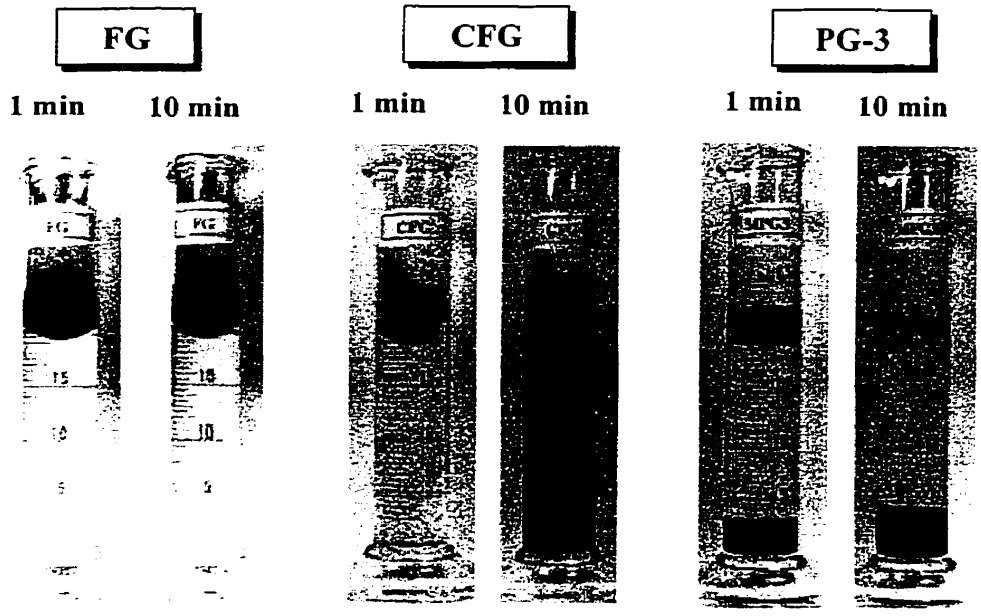

Figure 3.12 Water affinity comparison among FG, CFG and PG3 (the time elapse was counted after placing 2 g of each sample onto the water).

CHAPTER 4. EXPERIMENTAL PROCUDURE

This chapter will introduce the experimental program, raw materials, composition of the to be investigated castables, sample preparation and test methods to characterize the developed Al_2O_3-SiC-C and Al_2O_3-MgO-C castables.

4.1 Experimental Program

The whole work is carried on in two stages. In stage I, Al_2O_3-SiC-C castables are dealt with to compare 4 modes of inserting graphite, i.e., by PG, BAG, CFG and FG. The experimental items include water demand, flowability, bulk density, apparent porosity, cold modulus of rupture, hot modulus of rupture, oxidation, slag resistance and thermal shock resistance, all in correlation with graphite amount and incorporating method. Based on these, two advantageous methods of incorporating graphite should stand out and will be applied to Al_2O_3-MgO-C castables to be dealt with in stage II.

According to some published data[10,51,70,71] and CIREP's involvement in some commercial Al_3O_2–spinel(MgO) castables, water addition of such castables is usually in a range of 5.5 - 6.5%. This amount has to be reduced to make it possible that a water addition of the graphite containing Al_3O_2–MgO-C castables can still match this level. So, in stage II, before graphite addition, efforts are dictated to reduce water demand of the Al_2O_3-MgO castable, via selecting the most effective deflocculant among 4 kinds. For this purpose, the matrix portion of the castable is extracted to be investigated on the

rheological behavior as a function of deflocculant type and addition.

As reviewed on Al_3O_2–Spinel(MgO) castables in section 2.2.2 of Chapter 2, self-forming spinel is better than pre-formed spinel, but to increase MgO in Al_3O_2–MgO castables is tricky. In this work, only seawater magnesia is used as MgO source. Efforts are then made to add up to 30% MgO into the castables, by controlling the size distribution of the magnesia, using a limited amount of powders (< 0.3 mm), the rest being increased in size gradually up to the top size of 4.76 mm.

Using the acceptable Al_3O_2–MgO castables as starting castables, graphite is incorporated by the two favorable methods suggested by stage I, and four kinds of antioxidants are added respectively or in combination to the castables with optimized MgO and carbon contents to compare their effect on oxidation resistance. Overall properties of the castables, with oxidation resistance and slag resistance as the focus, are investigated in correlation with MgO amount and graphite and antioxidant packages. Optimization work on oxidation and slag resistance is pursued. Finally, microstructure analysis on the samples after slag and oxidation tests is conducted.

The main steps and experimental items for the whole work are illustrated in Figure 4.1.

4.2 Raw Materials

The raw materials involved in the two systems include alumina, silica carbide, graphite, magnesia, silica fume, calcium aluminate cement and anti-oxidation additives.

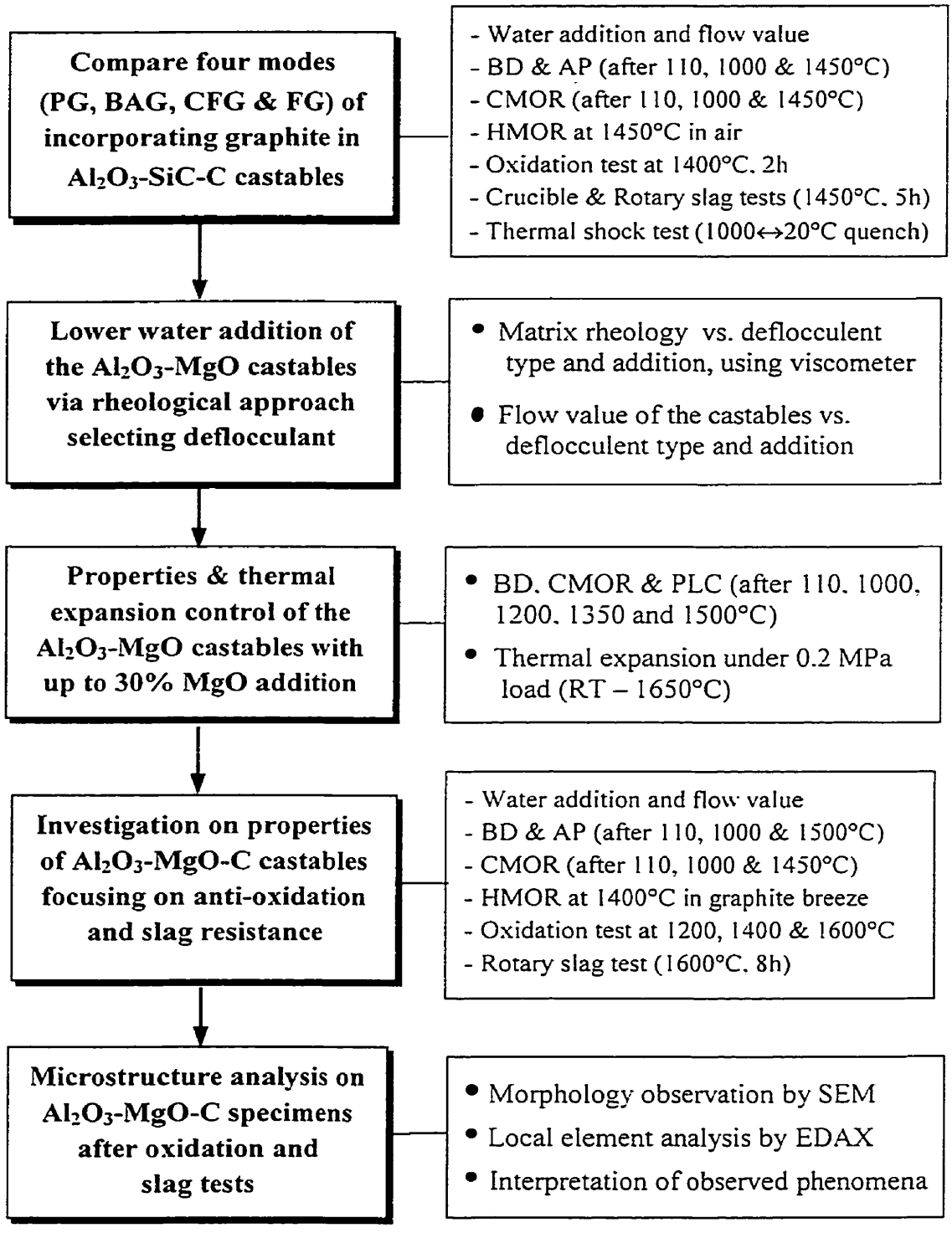

Figure 4.1 Experimental program.

4.2.1 Alumina

Two sorts of alumina have been used. As aggregates and fine powders, T-64 Tabular Alumina, from Alcoa Industrial Chemicals, has been used. The size fractions used in this work are: ¼"-8, 6-10, 8-14, 14-28, 28-48,48-200, -100, -325 mesh and –20 μm. Calcined alumina A12 and A3000FL from Alcoa, and RMA325 and XA-45B from Alcan have been optioned as ultrafines (from 10 microns down to submicrons). Their typical properties are shown in Table 4.1[72-74].

Table 4.1 Properties data of the alumina materials (from Ref. 72-74)

		Tabular Al_2O_3	Calcined alumina			
		T-64	RMA325	A12	A3000FL	XA-45B
Chem. analysis (%)	Al_2O_3	99.7	99.7	99.7	99.8	99.8
	Na_2O	≤0.19	0.02	0.17	0.03	0.05
	SiO_2	≤0.10	0.05	0.02	0.04	0.002
	Fe_2O_3	≤0.05	0.02	0.01	0.01	0.03
	CaO	≤0.05	0.01	0.04	0.03	0.01
	MgO	≤0.003	-	≤0.001	≤0.001	0.05
	B_2O_3	≤0.001	0.05	0.001	0.03	-
Density (g/cm^3)	Green	-	N. A.	2.17	2.48	2.05
	Fired	3.6-3.7	N. A.	2.56[1]	3.79[2]	3.93[3]
SSA (m^2/g)		-	0.3	1.0	2.6	8
Median particle size[4] (μm)			14	4.8	3.0	0.45

(1) at 1620°C; (2) at 1750°C; (3) at 1650°C ; (4) by sedigraph particle size analyzer

Alcoa Tabular Alumina is a pure, sintered alumina that has been converted to corundum

form by heating to a temperature slightly below the fusion point of aluminium oxide (2035°C). The word "tabular" is applied because it is composed of hexagonal tablet-shaped crystal with a median range of 40 to 200 microns. The excellent thermal volume stability and thermal shock characteristics are attributed to these large crystals with closed spherical pores that were entrapped upon recrystallization of the alumina crystals during rapid sintering[72].

Calcined alumina is produced by calcining Bayer process aluminium trihydroxide in rotary kilns. During calcination, the combined water is driven off and the oxide formed passes through several intermediate phases until the stable α-alumina structure is reached. By controlling the temperature and time of calcination, soda content, and processing parameters, a long list of calcined aluminas are available for selection, in terms of crystal size, particle size and distribution, soda level, reactivity, etc.[74].

4.2.2 Silicon Carbide

Silicon carbide powders, black, –200 mesh and –325 mesh size fractions, made by Exolon-ESK Co., USA, are used. Their quality is shown in Table 4.2[75].

Table 4.2 Data of the silicon carbide [from Ref. 75]

Chemical composition (%)						Bulk density
SiC	SiO_2	Si	Fe	Al	Free C	(g/cm^3)
97.7	0.75	0.65	0.15	0.15	0.6	3.20

4.2.3 Graphite

As a main carbon source for straight addition, natural flake graphite (denoted as FG hereafter), M10097 (-100 mesh, C ≥ 97%) and M20097 (-200 mesh, C ≥ 97%) from Stratmin Graphite Co., Canada, is chosen. As a supplementary carbon source, amorphous graphite (denoted as AG hereafter), Grade # 9985 Grafunex, -30 mesh, 78.65% carbon, provided by Cummings-Moore Graphite Co., USA, is also used. Their sieve analysis results are given in Table 4.3.

Table 4.3 Sieve analysis of the flake graphite and amorphous graphite

Mesh size	+100	100 -200	200 -325	- 325
FG M10097	9.0	56.2	20.1	14.7
FG M20097	11.6	34.6	27.6	26.2
Mesh size	20 -30	30 -50	50 - 140	- 140
AG #9985	0.3	28.6	34.9	36.2

4.2.4 Magnesia

Dead-burned brine extracted magnesia, LUD98, provided by Marelan Plant, Resco Products Co., is chosen to add into Al_2O_3-MgO and Al_2O_3-MgO-C castables. Four size fractions, i.e., BMF50, -28, 10-28, and 4-10 mesh are used as both fines and aggregates, their chemical analysis being shown in Table 4.4 and sieve analysis in Table 4.5.

Table 4.4 Chemical analysis of LUD98 magnesia (%)

MgO	CaO	SiO_2	Fe_2O_3	Al_2O_3	TiO_2	K_2O	Na_2O
98.8	0.89	0.85	0.19	0.1	0.01	0.005	0.11

Table 4.5 Sieve analysis of LUD98 magnesia (%)

Mesh size	4 - 6	6 - 14	14 - 28	28 - 48	48 - 200	- 200
BMF50	0	0	0	0	30	70
- 28 mesh	0	0	15.4	40.0	37.1	7.5
10 – 28 mesh	0	18.5	68.4	8.2	3.5	1.4
4 – 10 mesh	18.3	79.6	2.1	0	0	0

4.2.5 Fumed Silica

As submicron ultrafines and an indispensable constituent of binder system, Microsilica 971U from Elkem Materials, Norway has been used in the ultra-low cement Al_2O_3-SiC-C castables. Such fumed silica is amorphous, very fine in size (submicrons), very high in specific surface area (>20 m^2/g), spherical in shape, and reactive with cement and water to form S-C-H bond in LCC's or ULCC's. Table 4.6 provides its chemical analysis [76].

Table 4.6 Chemical analysis of Microsilica 971U (%) (from Ref. 76)

SiO_2	Fe_2O_3	CaO	MgO	K_2O	Na_2O	C	L.O.I.@975°C
98.9	0.02	0.17	0.05	0.17	0.01	0.66	0.58

4.2.6 Calcium Aluminate Cement

In both castables, Secar 80 CA cement, supplied by Lafarge Cement, Canada, has been used as a hydraulically setting binder. Monocalcium aluminate ($CaO \cdot Al_2O_3$ or CA) is the main active ingredient that reacts with water to form hydrates responsible for developing strength. The data of the cement are given in Table 4.7[77].

Table 4.7 Data of Secar 80 CA cement (from Ref. 77)

Al_2O_3, %	CaO, %	SiO_2, %	Fe_2O_3, %	R_2O, %	BD, g/cm^3	SSA (Blaine)
79.5-82.5	16.2-17.8	< 0.4	< 0.3	< 0.7	3.2-3.3	> 8000 cm^2/g

4.2.7 Antioxidant

The antioxidants to be added in the castables include: (A) silicon powders (Si ≥ 97%, -200 mesh) from Elkem Materials; (B) silicon carbide (SiC ≥ 97%, -325 mesh), from Exolon-ESK Co., USA; (C) boron carbide (B_4C ≥ 90%, -325 mesh), from Elektroschmelzwerk Kempten GmbH, Germany; and (D) zirconium diboride (ZrB_2 ≥ 98%, - 325 mesh), from CERAC™ Inc., USA.

4.3 Composition of the Castables

4.3.1 Composition of the Al_2O_3-SiC-C Castables

Like commercial Al_2O_3-SiC-C castables, the Al_2O_3-SiC-C castables in this work are also

designed as a ULCC, using 4% Microsilica 971 U and 3% Secar 80 cement as the binder system. The maximum size is 6.35 mm and the particle size distribution (PSD) from 1 micron up is adjusted by approaching to the well known Andreassen's PSD equation, $CPFT = (d/D)^q \times 100$, where the exponent q is set at 0.29, which is suitable for LCC or UCC vibratable castables[78,79]. CPFT means Cumulative Percent Finer Than (in vol.%), d particle size and D the maximum particle size.

The composition and the notation for the Al_2O_3-SiC-C castables are listed in Table 4.8. Starting from zero graphite addition, 2, 4 and 6 wt% of PG3 is added, respectively, and at about 4% graphite, the three approaches are compared with straight FG. PG1 and PG3 are compared to reveal the role of anti-oxidants inside the micropellets. In commercial Al_2O_3-SiC-C castables, non-flake graphite carbons as high as a few percents are usually added. In this work, however, only 1% AG is used as a supplementary carbon source and dispersed carbon in the samples.

In view of that Al and Si powders in Al_2O_3-SiC-C castables have pronounced influence on strength and anti-oxidation, the Si content in all the samples, directly added plus that incorporated in PG3 or in BAG, is controlled as (1.00±0.15)%, so the difference can be neglected. In regarding to Al, however, as it is so reactive that as low as 0.1% straight addition can also lead to swelling and effloresce due to the violent reaction of Al with H_2O. For this reason, PG-0, FG-4, CFG-4 and PG1-4 samples contain zero Al, while the others contain 0.12 to 0.4% Al coming from either PG3 or BAG.

Table 4.8 Composition (wt%) and notation of the Al_2O_3-SiC-C castables

Notation	**PG-0**	**PG3-2**	**PG3-4(5)**	**PG3-6**	**PG1-4**	**FG-4**	**CFG-4**	**BAG-13**
Al_2O_3	87	84	82(81)	80	82	83	83	82
SiC	7	7	7	7	7	7	7	7
SiO_2	4	4	4	4	4	4	4	4
CaO	0.5	0.5	0.5	0.5	0.5	0.5	0.5	0.5
Si	1	~1	~1	~1	1	1	1	~1
MPG3	**0**	**2**	**4(5)**	**6**	0	0	0	0
MPG1	**0**	0	0	0	**4**	0	0	0
FG	**0**	0	0	0	0	**4**	0	0
CFG	**0**	0	0	0	0	0	**4**	0
ACB	**0**	0	0	0	0	0	0	**13.3**
AG	**0**	1	1	1	1	0	0	1

4.3.2 Composition of the Al_2O_3-MgO and Al_2O_3-MgO-C Castables

In commercial Al_2O_3-MA(MgO) castables, CA cement has been used as the binder. The outstanding advantage of this kind of hydraulic bonding is that it brings about high hot strength due the interlocked CA_6 phase derived from the cement[70,80]. Nevertheless, the cement addition should be controlled under 8% for good slag resistance[52]. To promote sintering and control the thermal expansion, tiny quantity (0.5% or so) of silica fume is added, which must be carefully controlled to avoid some detrimental effects like increased expansion, bigger shrinkage at high temperature, decreased HMOR and cracking[20,81,82].

In this work, 6% Secar 80 cement is adopted as binder, but no silica is added to eliminate a less controllable variable. The PSD from 1 micron up to the top size of 6.35 mm is also made to approximately conform to the above mentioned Andreassen's equation with q-value also 0.29.

Before inserting graphite, work is centered on making acceptable Al_2O_3-MgO castables containing up to 30% MgO at an interval of 6%. The designed composition of such castables and their notation are given in Table 4.9.

Table 4.9 Composition (wt%) and denotation of the Al_2O_3-MgO castables

Material	Size (mesh)	**M0**	**M6**	**M12**	**M18**	**M24**	**M30**
T64 Al_2O_3	¼''-325	77	71	65	59	53	47
T64 + Calcined Al_2O_3	< 325	17	17	17	17	17	17
LUD98 MgO	BMF50	0	6	5	5	5	5
	-28	0	0	7	7	7	9
	10-28	0	0	0	6	6	8
	4-10	0	0	0	0	6	8
Secar 80 CAC	-200	6	6	6	6	6	6

After graphite insertion and with or without antioxidant addition, the composition of the castables will be indicated by the used notations, Table 4.10 shows some of them to help get the composition related information implicated in the notations, e.g., M×× tells the

MgO addition; following which either PGx-xx, BAG-xx or FG-xx tells the carbon source and amount; and the coded antioxidant and its amount added in the castable stand at the end. The balance consists of Al_2O_3 and about 1.1% CaO corresponding to 6% CA cement in each case. Those unlisted in this table will be clarified where they appear.

Table 4.10 Composition (wt%) and notation of some of the castable mixes

	M6-FG-1(~4)	**M6-PG1-2(~6)**	**M6(~24)-PG3-6**	**M12-BAG-15**	**M12-PG3-6-C_1B_3**
Al_2O_3	89 ~ 92	87 ~ 91	69 ~ 87	81	77
MgO	6	6	6 ~ 24	12	12
C	1 ~ 4	2 ~ 6	5	5	5
CaO	1.1	1.1	1.1	1.1	1.1
FG	1 ~ 4	0	0	0	0
PG	0	PG1: 2 ~ 6	PG3 : 6	0	PG3: 6
BAG	0	0	0	15	0
Anti-oxidant	0	0	0	0	C: 1 B: 3

4.4 Sample Preparation

All the samples are cast, using a vibration table working at 0.4 mm of amplitude and 60 Hz of frequency. The mixes are dry mixed for 3 min and wet mixed for further 3 min after adding water, using Hobart mixer, model N50 or D340, depending on the quantity. After casting, the samples are cured for 24h in mould at room temperature (20-22°C) and for another 24h after demoulding also at the room temperature, then dried at 110°C for 24h.

Prisms of 160×40×40 mm and 25×25×150 mm (for Al_2O_3-MgO and Al_2O_3-MgO-C castables only) are made for the determination of bulk density (BD), apparent porosity (AP), permanent linear change (PLC), cold modulus of rupture (CMOR), hot modulus of rupture (HMOR) and thermal shock resistance (TSR). ϕ50×50 mm cynlidrical samples of Al_2O_3-SiC-C castables are prepared for oxidation test. Al_2O_3-MgO castable cylinders of ϕ50×50 mm with a hole of ϕ12×50 mm are cast for testing thermal expansion under load. Conical crucibles of ϕ(100-90)×100 mm with a hole of ϕ(50-44)×60 mm are made for static slag test and trapezoidal prisms with a 229×38 mm area exposed to slag and 38 mm in thickness, are prepared for rotary slag test.

4.5 Test Methods

4.5.1 Flowability and Water Demand

Flowability is represented by flow value, which is measured by the flow cone [ϕ(70-100) ×50 mm] conforming to ASTM C860-91[83] method, as described hereinafter. The castable mass is prepared by first dry mixing for 3 min, using Hobart N50 mixer at low speed, then on addition of a specific amount of tap water, wet mixing for further 3 min also at low speed. Excess amount of the castable is filled into the cone and then pre-vibrated for up to 25 seconds while holding firmly on a Sinex vibrating table (600 × 600 mm). After leveling the surface to the top of the cone, the cone is carefully removed, and then vibrated for a further 15 seconds, operating at 60 Hz in frequency and 0.8 mm in amplitude. The diameter of the spread mass is measured every 30° angle at 6 impartial

corners. The flow value is the resulted increase in average base diameter of the castable mass, over the original base diameter of 100 mm.

Water demand is counted extra based on the dry mix of the castable. It is so controlled as to enable the castable to reach a flow value between 170 and 200 mm.

4.5.2 BD, AP and PLC

BD and AP are measured in conformance with standardized testing method by ASTM C830-93[84]. PLC is determined according to ASTM C1407-98[85]. Each value of BD, AP or PLC is of the average of three parallel samples.

4.5.3 CMOR and HMOR

CMOR and HMOR are determined by the conventional three-point bending method conforming to ASTM C133-97[86], using universal testing machine (model TTCML, Instron Engineering Co., USA) and HMOR testing apparatus (model HMOR-II, LIRR, China) respectively. For Al_2O_3-SiC-C specimens, HMOR is tested at 1450°C in air atmosphere, as a self-formed film on the surface of the specimens can prevent the carbon inside from oxidation. Whereas, the Al_2O_3-MgO-C specimens for HMOR testing are embedded in graphite breeze in a Si_3N_4 bonded SiC sager to prevent oxidation, as illustrated in Figure 4.2. All the specimens for HMOR testing are dried at 110°C, without pre-firing. The heating rate for HMOR testing is 5°C/min before 1000°C and 3°C/min thereafter. The loading rate for both CMOR and HMOR is 0.15 MPa/sec..

The MOR value is calculated by the following formula:

$$\mathbf{MOR = 3LF/(2bh^2)},$$

where L is the span between the lower supporting points (100 mm for all the tests in this work); F is the maximum load when the specimen is broken (N); b is the breadth and h is the height of the specimen. Each value is the average of three parallel specimens.

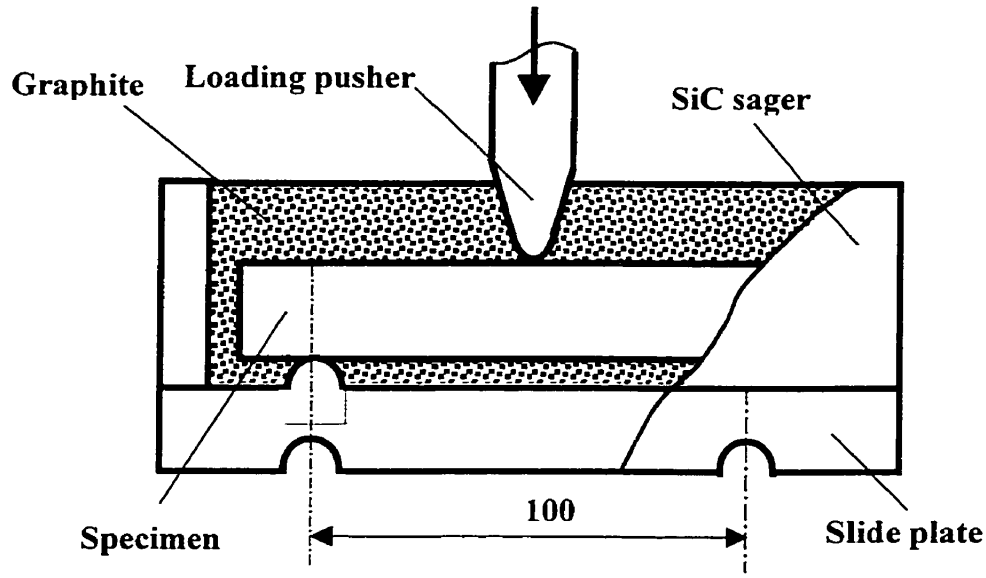

Figure 4.2 Specimen embedded in graphite breeze for HMOR testing.

4.5.4 Oxidation Resistance

Oxidation resistance is evaluated by the depth of decarbonized layer of the specimens heated at a certain temperature in air atmosphere, though the procedure is a little different for both types of castables at different temperatures. It is reported that oxidation test on MgO-C brick in stilled air in a electrical box furnace may have an

unavoidable error as high as 30% in weight loss, due to the unevenness of oxygen distribution[87]. To minimize such possible error, the furnace chamber is swept with compressed air to make the atmosphere constantly refreshed and homogenized.

For Al_2O_3-SiC-C castables, the test is performed by heating the ϕ50×50 mm specimens in a vertical tube furnace with a chamber of ϕ260×230 mm, at 5°C/min to 1400°C and holding for 2h. The furnace chamber is swept with compressed air at a flow of 1.8L/min (under normal temperature and pressure). The furnace is then cooled down also at 5°C/min and the specimens are longitudinally sectioned. In total, 12 decarbonized depths on both sections of the specimen are measured and averaged, as illustrated by Figure 4.3.

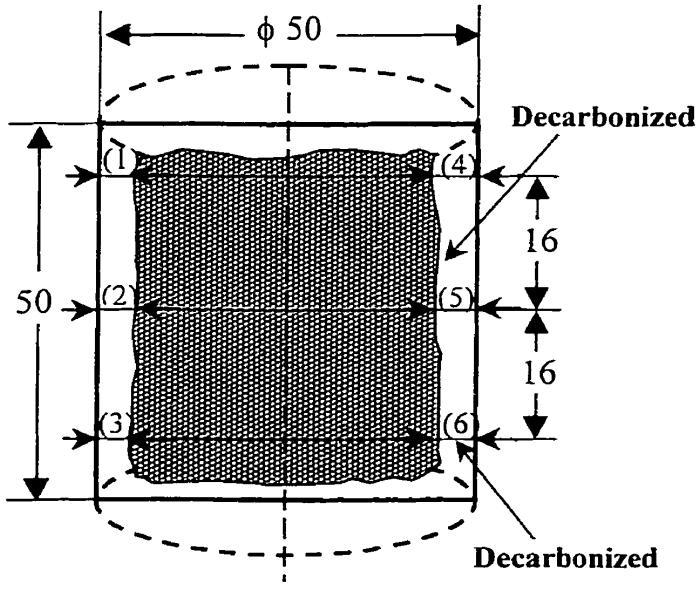

Figure 4.3 Section of the Al_2O_3-SiC-C specimen after oxidation test (unit: mm).

Oxidation test on the Al_2O_3-MgO-C castables is performed by imposing unidirectional oxidation with the top surface of a specimen being exposed to hot air in an electrical box

furnace. Cubic specimens of 40×40×40 mm cut from the 40×40×160 mm prisms are used to be embedded in graphite powders except for the top surface in a SiC sager, see Figure 4.4, then heated to 1200°C and 1400°C and held for 3h respectively. The heating rate is 5°C/min to 1200°C, and then 3°C/min to 1400°C. The furnace is swept with compressed air at a flow of 2-2.5 L/min (under normal temperature and pressure) during soaking. After cooled down, the samples are sectioned and the average depth of the fully decarbonized layer is taken as the measurement of the oxidation resistance. At 1600°C, however, due to the unadaptability of the SiC sager, oxidation is pursued by dynamic rotary furnace. The experimental set-up, specimen sizes and configuration are similar to those for rotary slag test described in 4.5.6 of this chapter. Six specimens are simultaneously tested, at rotating speed of 2 rpm, heated up to 1600°C in about 1.5h and held for 5h. They are then, when cooled down, sectioned perpendicularly to hot surface and evaluated by average decarbonized depth.

4.5.5 TSR

TSR test is carried out only on the Al_2O_3-SiC-C specimens. It is represented by strength loss on thermal cycling from 1000°C soaking for 20 min to water at 20°C, by percentage of remained CMOR after quenching for 1, 3 and 10 cycles respectively. The CMOR value fired at 1450°C for 5h in air is used as the reference. This method is of course limited by the propensity of graphite to oxidize. Fortunately, the investigated castables are not carbon-bonded, otherwise the carbon bond itself would be oxidized to some extent. On the other hand, the oxidation during thermal cycling is not serious.

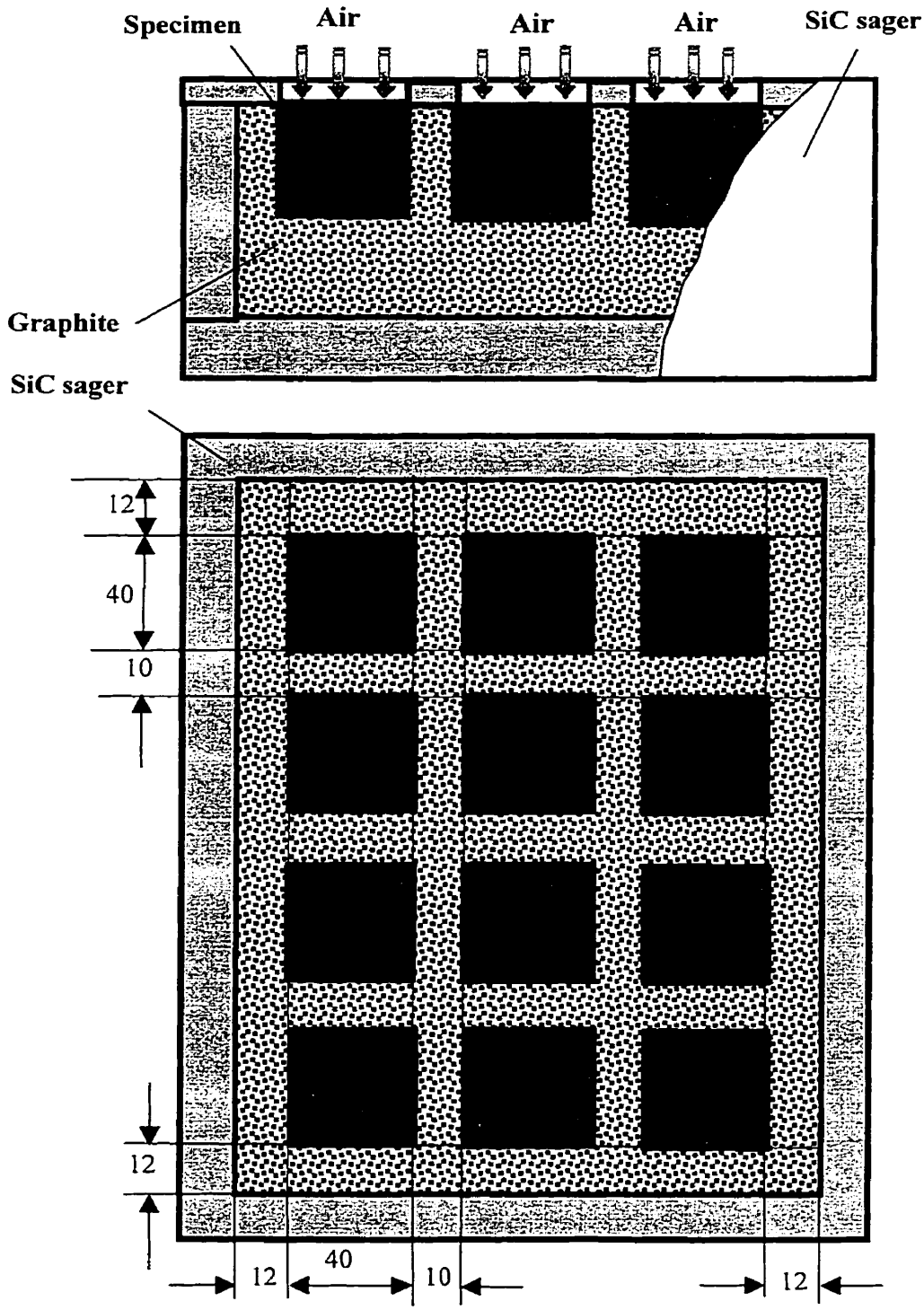

Figure 4.4 Illustration of oxidation test on Al_2O_3-MgO-C castables at 1200 and 1400°C respectively (unit in the figure: mm).

4.5.6 Slag Resistance

Static slag test by crucible method is made on Al_2O_3-SiC-C castables. Each of the crucibles (dried at 110°C) is charged with 100g slag, then heated to 1450°C in air and soaked for 5h. The sections after slag attack are visually compared.

Dynamic slag test by rotary furnace method is made on the both kinds of castables. The experimental set-up (furnace configuration and specimen geometry) is shown in Figure 4.5. Six samples in a hexagonal configuration are installed in the furnace. The furnace, rotating at 2 rpm, is heated to the set temperature (1450°C and 1600°C respectively for Al_2O_3-SiC-C and Al_2O_3–MgO-(C) samples), then soaked at the temperature for 5h or 8h, during which the slag was fed, firstly 3 times at a rate of 200g per 15 min., then at a rate of 200g per 30 min. The temperature of the hot face is measured by an optical infrared radiation pyrometer (Minolta/Land Cyclops 152). The furnace is then cooled naturally down. The slag-attacked specimens are sectioned longitudinally, see the dotted area of the lower part in Figure 4.5. Visual examination and measurements of the eroded depth are pursued on the sectioned specimens.

The eroded area is estimated by the equation given below, based on a trapezoid approximation, as schematically illustrated by Figure 4.6.

$$\mathbf{A = \sum[(H - h_i) + (H - h_{i+1})] \times L/2,\ mm^2} \quad (i=1\sim19),$$

where A is the total eroded area, H is the original height of the specimen, h is the remained unattacked height and L is the measuring step.

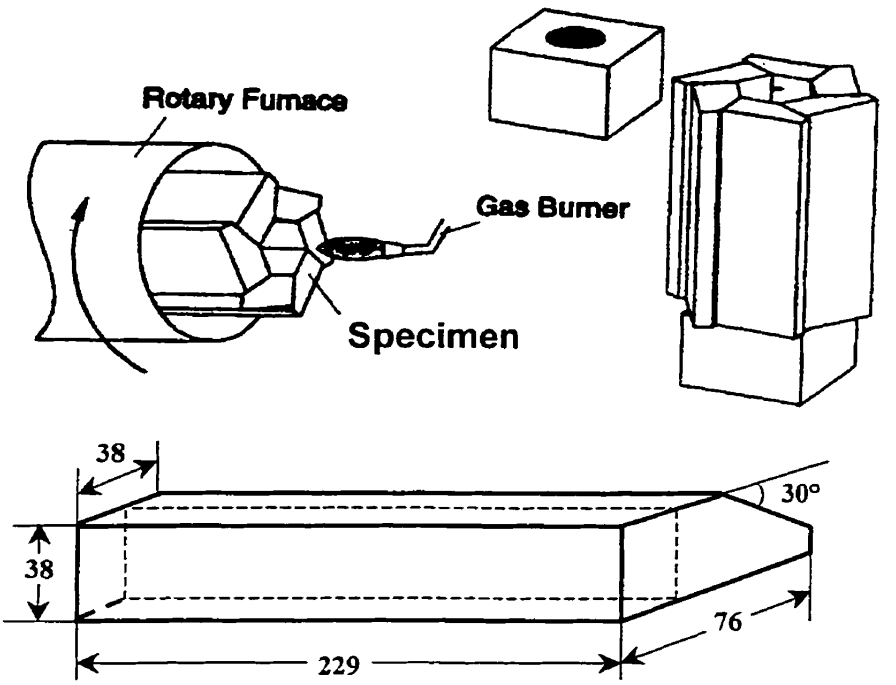

Figure 4.5 Experimental set-up for rotary slag test (unit: mm).

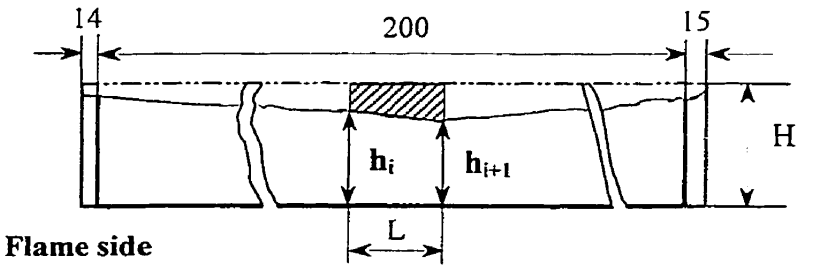

Figure 4.6 A schematic view of the approximation of real eroded area (unit: mm).

4.5.7 Thermal Expansion Under Load

Thermal expansion behavior under 0.2 MPa load are measured on M6, M12, M24 and M30 specimens, using the device and following the procedure described in ISO R 1893-

70[88] for testing refractoriness under load of refractories. The heating speed is 5°C/min from room temperature to 1650°C.

4.5.8 Microstructure Analysis

Microstructure analysis on chosen Al_2O_3-MgO and Al_2O_3-MgO-C castable specimens after oxidation test and slag test is conducted by means of SEM and EDAX, using Philips XL30-DXi SEM-EDAX instrument.

CHAPTER 5. INVESTIGATION ON THE Al_2O_3-SiC-C CASTABLES

This chapter presents the results of the investigation on Al_2O_3-SiC-C castables, being incorporated graphite by the four modes: PG, BAG, CFG and FG. Overall properties of the castables, in terms of water demand, flowability, bulk density (BD), apparent porosity (AP), cold and hot modulus of rupture (CMOR and HMOR), permanent linear change (PLC), slag resistance, oxidation resistance and thermal shock resistance, have been measured and compared in correlation with the methods of incorporating graphite.

5.1 Water Demand and Flowability

According to our practice, good workability for casting a castable under vibration requires a flow value, as defined in section 4.5.1 of Chapter 4, of more than 160 up to 200 mm. The criterion for good flowability is thus set as a flow value between 170 and 200 mm in this work.

When the flow value is controlled in this range, the water demand in weight percentage (on the dry basis of the castable mix) is compared in Figure 5.1. With straight addition of FG, the castable requires the highest water level, but lowest flow value, compared with addition of PG, CFG or BAG, at an equivalent level of graphite (4-5%). The water demands in weight and in volume percentage respectively are shown in Table 5.1. It can be seen that inserting graphite by PG and by BAG can significantly reduce the water demand other than by CFG, not to mention by FG.

The effectiveness of these three approaches in improving hydrophilicity and reducing specific surface of FG has been demonstrated by Figure 3.12 in Chapter 3. Here again, the expected effects in lowering water addition and bettering flow of the castables have been confirmed.

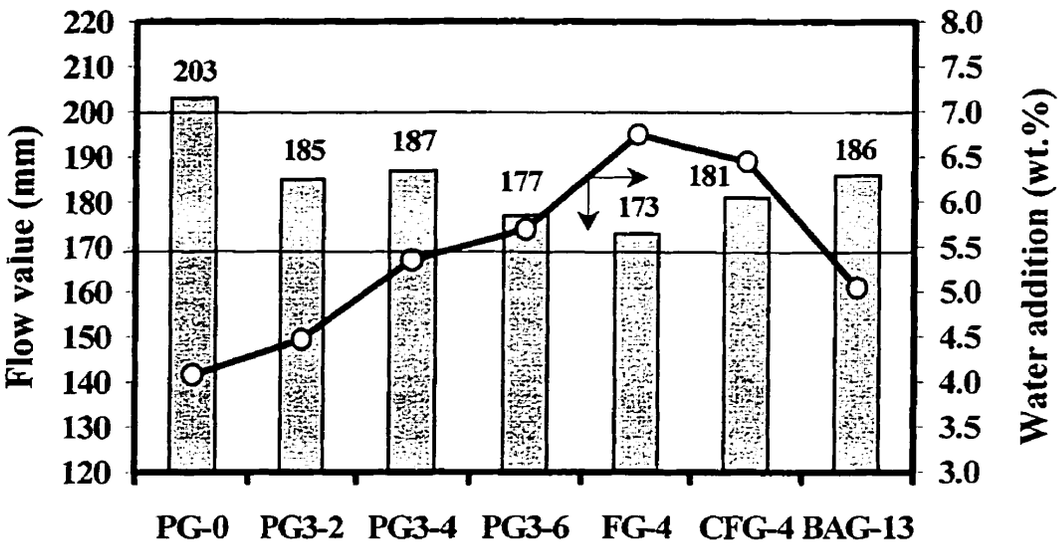

Figure 5.1 Water demand and flow value vs. graphite content and inserting method.

Table 5.1 Water demand of Al_2O_3-SiC-C castables to achieve a flow value of 170-200 mm

	PG-0	PG3-2	PG3-4	PG3-6	FG-4	CFG-4	BAG-13
Wt.%	4.08	4.48	5.36	5.70	6.75	6.45	5.05
Index	100	110	131	140	165	158	124
Vol.%	12.6	13.2	15.0	15.4	18.8	18.0	14.4
Index	100	105	119	122	149	143	114

5.2 BD and AP

Figure 5.2 presents a very good linear relationship of BD and AP with PG3 addition in the castables treated at three temperatures in air atmosphere, which corresponds well to the linear increase in water addition as PG3 addition increases, see Figure 5.3. Understandably, more water at casting stage engenders higher porosity at heating stage.

Figure 5.4 compares AP data of the castables after drying, heating at 1000°C for 5h and 1450°C for 5h in air respectively. As expected, at an equivalent graphite content, inserting graphite by PG or BAG brings about significantly reduced AP than by CFG or FG. In regard to the role in reducing AP, CFG is slightly better than FG.

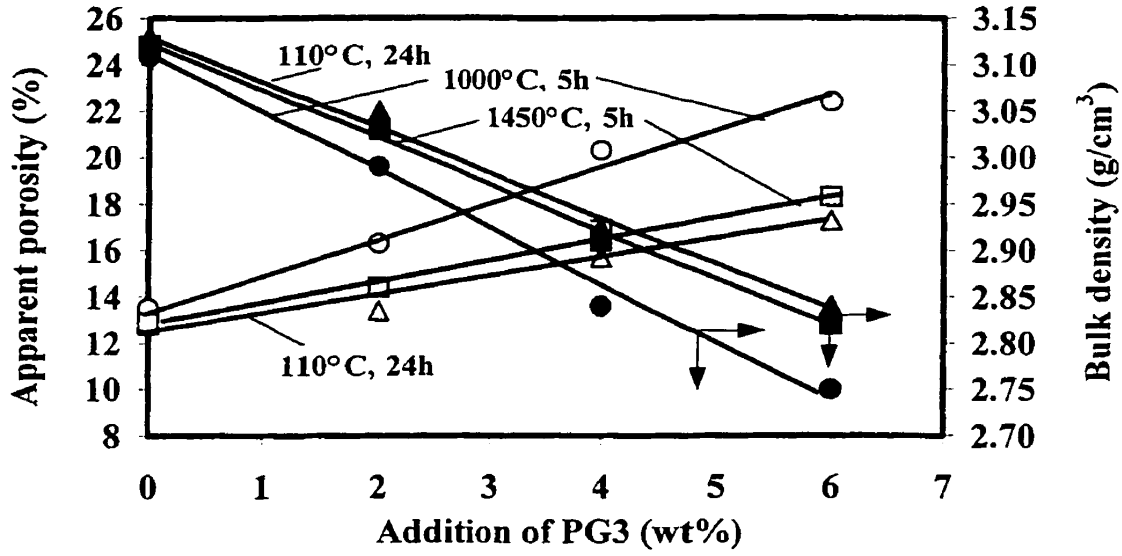

Figure 5.2 BD and AP of the castables as a function of PG3 addition.

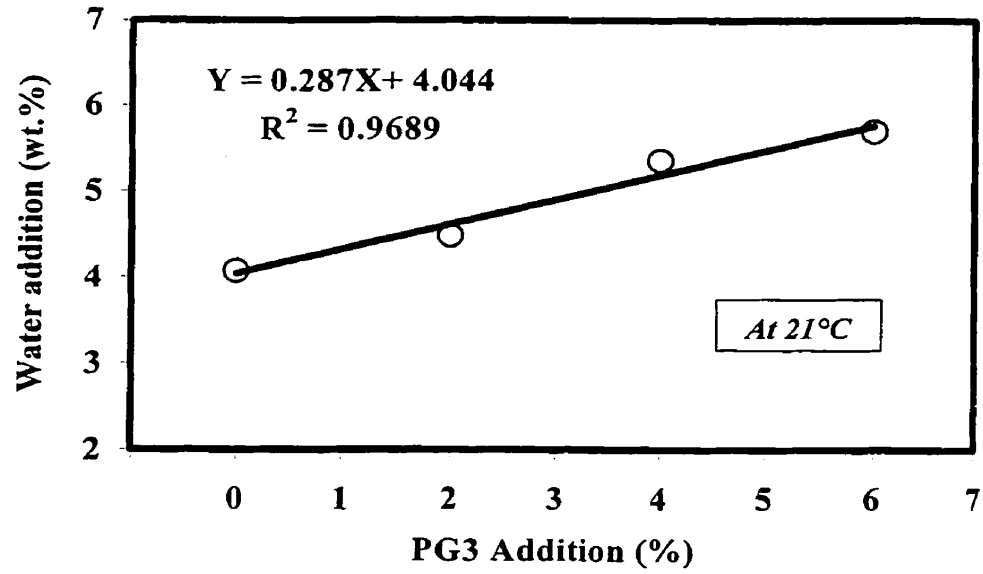

Figure 5.3 Water addition to reach a target flow value as a function of PG3 amount.

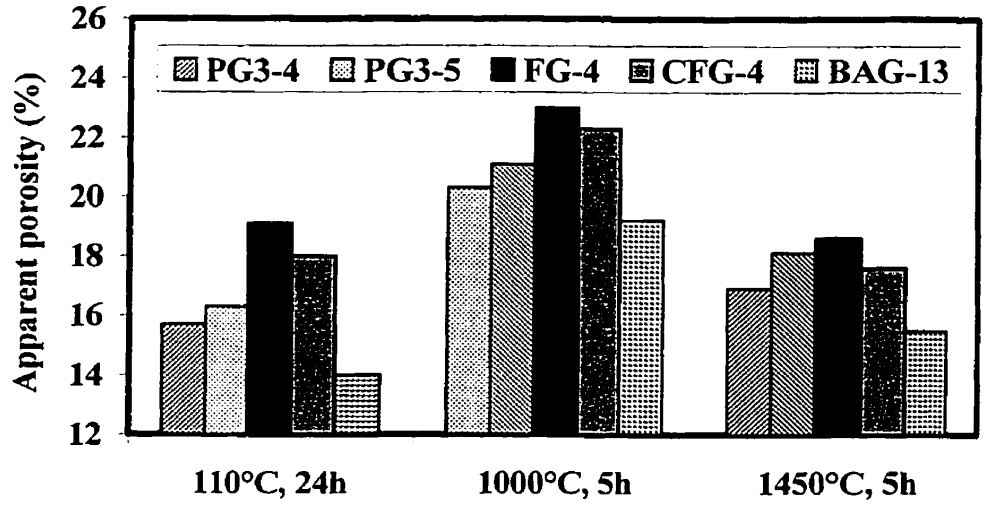

Figure 5.4 AP of the castables in relation to the method of incorporating graphite.

5.3 CMOR and HMOR

CMOR of the castables as a function of PG3 addition is shown in Figure 5.5. Clearly, as PG3 addition increases, CMOR tends to decrease, which means that graphite in the castable disturbs the bonding, but the strength even at 6% of PG3 addition retains still appreciably high, due to the relatively reduced dispersion of the graphite in the castable. After firing, the slight gain in CMOR at 6% PG3 is deemed to be attributed to the higher level of Al and Si additives in PG3.

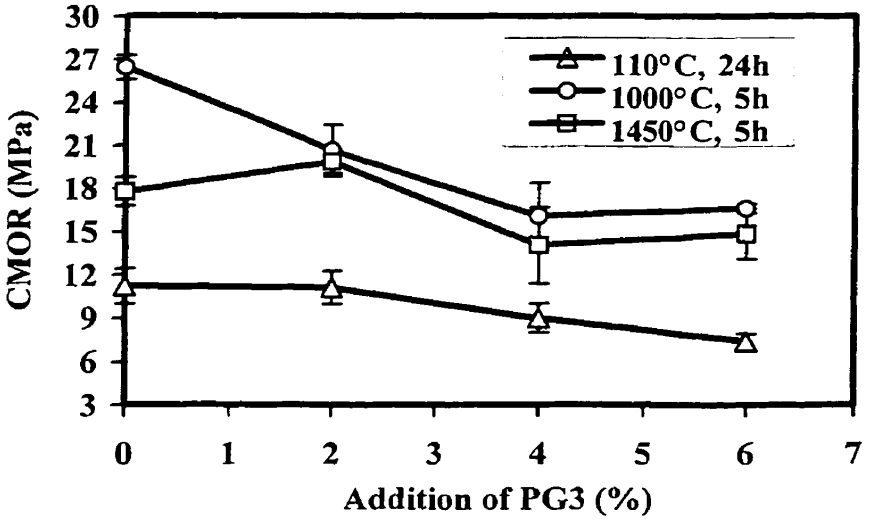

Figure 5.5 CMOR as a function of PG3 addition.

Figure 5.6 and Figure 5.7 compare CMOR and HMOR of the castables respectively among the different graphite inserting methods. It can be seen that straight addition of FG yields the lowest strength, just half or one third of those by PG or BAG. Inserting Al and Si additives in PG contributes to enhancing both cold and hot bending strengths, but

not so strikingly in CMOR, comparing PG3 with PG1 in Figures 5.6 and 5.7. CFG appears to make almost no contribution to the cold and hot strengths, the CMOR after drying and HMOR being only very slightly higher than those of FG-4's. Here, once again, the influence of dispersing state of graphite on strength is put well in evidence.

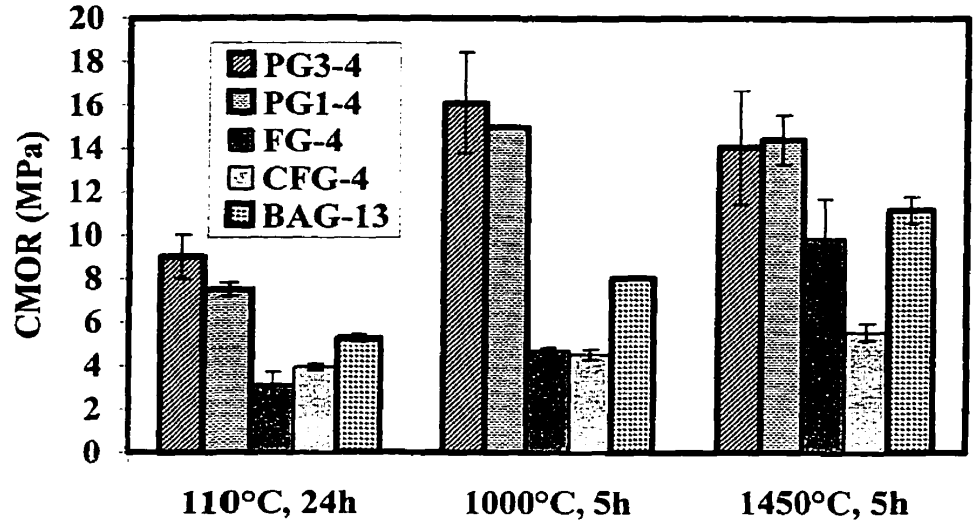

Figure 5.6 CMOR in relationship with the method of incorporating graphite.

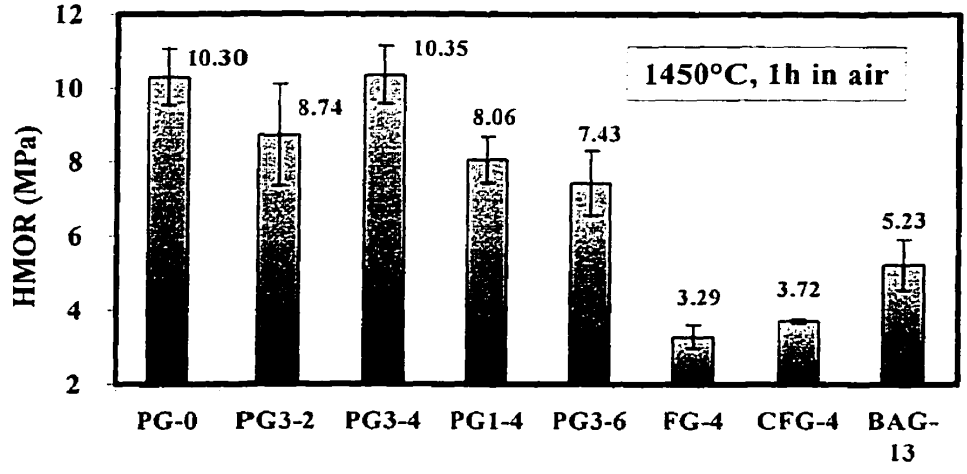

Figure 5.7 HMOR in relationship with the method of incorporating graphite.

Observed at a microstructural scale, Figure 5.8 shows a typical undispersed distribution of the graphite as micropellets in the castable, putting it in evidence that the micropellets are not damaged during the mixing process, what was of course a concern at first, but now can be released. Such a graphite-encapsulated structure is believed beneficial to maintain the bonding strength.

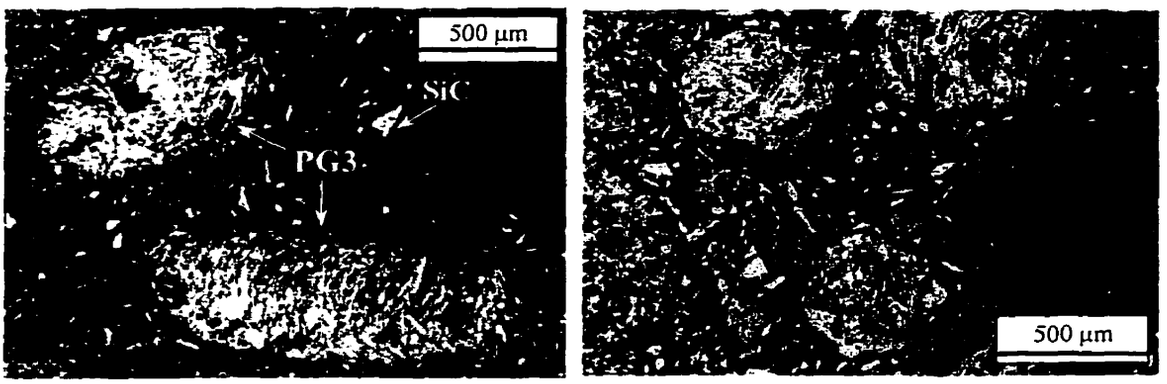

Figure 5.8 Micro-pelletized graphite in the PG3-4 castable after drying, observed by reflecting optical microscopy.

5.4 PLC

PLC data of the castables heat-treated in air at different temperatures are given in Table 5.2, from which no evidence can be found that PLC of the castables has been perceptibly influenced by the graphite content and the incorporating method. In each case, the PLC changes itself very little, suggesting that such Al_2O_3-SiC-C castables have very good volume stability.

Table 5.2 PLC data of the Al_2O_3-SiC-C castables

Castable	110°C, 24h	1000°C, 5h	1450°C, 5h
PG-0	- 0.03	- 0.09	- 0.07
PG-2	- 0.02	- 0.07	- 0.04
PG-4	- 0.04	- 0.09	- 0.03
PG-6	- 0.06	- 0.11	± 0.00
BAG-13	- 0.01	- 0.06	- 0.09
CFG-4	- 0.04	- 0.05	+ 0.05
FG-4	- 0.02	- 0.05	- 0.05

5.5 Oxidation Resistance

The sections of the samples after oxidation test are shown in Figure 5.9. Taking the average decarbonized depth of FG-4 specimen as a reference, index 100, the oxidation resistance is compared in Figure 5.10, the less the index value, the better the oxidation resistance.

As shown in Figures 5.9 and 5.10, inserting graphite by CFG, PG or BAG shows a much better anti-oxidation effect than by FG. The highest porosity of FG-4 should account for its worst oxidation resistance. Incorporating Al and Si in PG helps improve the resistance to oxidation, comparing PG3-4 with PG1-4.

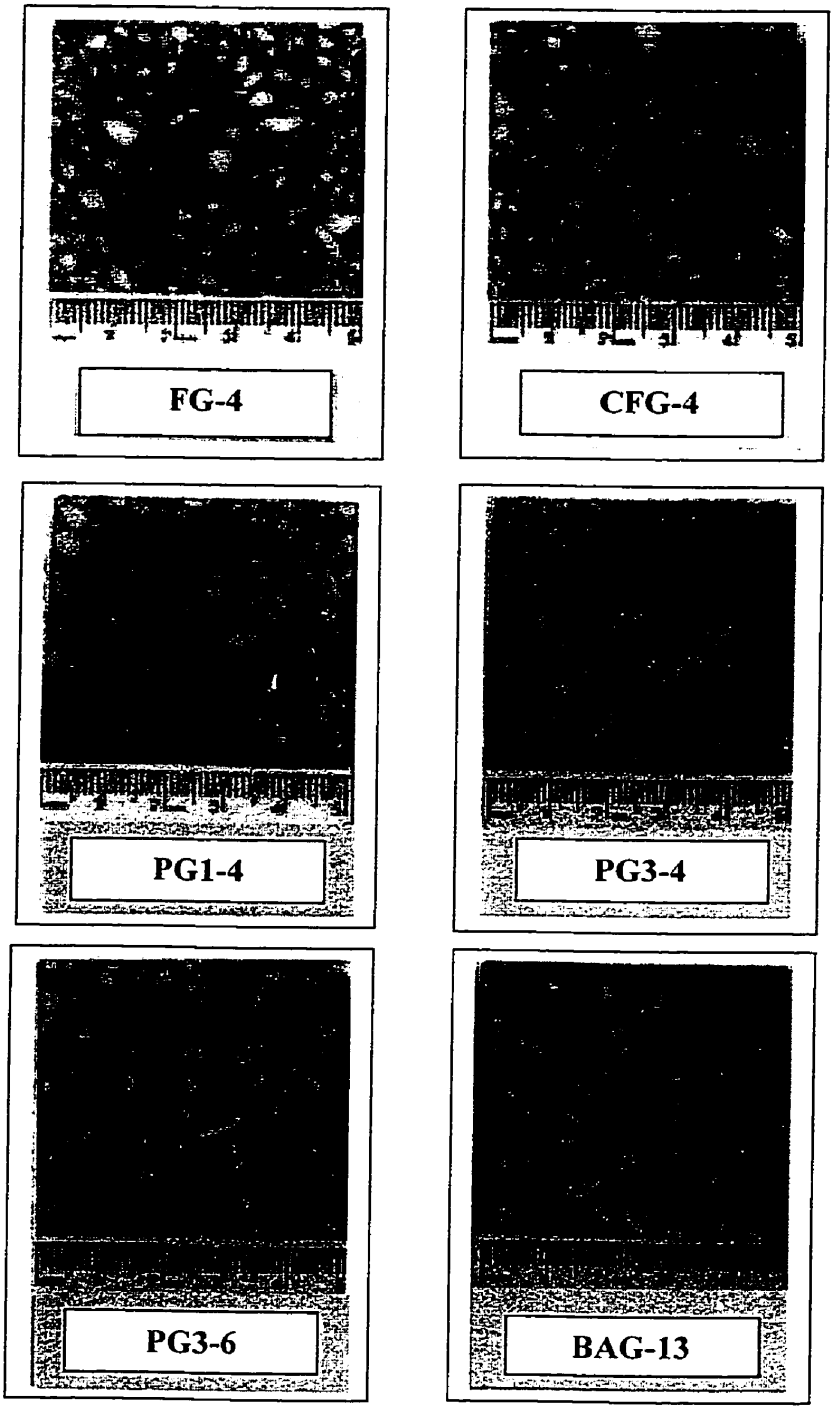

Figure 5.9 The sections of the Al_2O_3-SiC-C specimens after oxidation test.

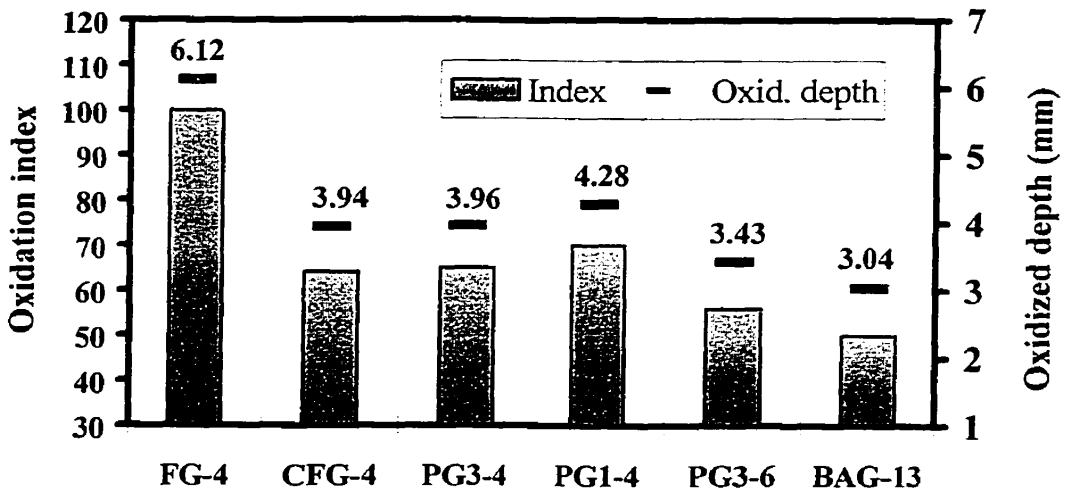

Figure 5.10 Oxidation resistance vs. the method of incorporating graphite.

5.6 Slag Resistance

An iron-making slag in hot metal pretreatment process is used for the slag tests, its chemical analysis and basicity are given in Table 5.3.

Table 5.3 Chemical composition (%) and basicity of the iron-making slag

CaO	SiO_2	Al_2O_3	MgO	Fe_2O_3	TiO_2	MnO	Na_2O	K_2O	CaO/SiO_2
42.80	36.00	9.90	9.78	0.38	1.02	0.53	0.57	0.60	1.19 (wt.)

The sections of the specimens after crucible slag test and rotary slag test are respectively shown in Figure 5.11 and Figure 5.12 respectively.

The static slag test result, see Figure 5.11, indicates that slag corrosion and penetration

can be dramatically inhibited by incorporating graphite, in whatever the four ways, yet PG3-6 and CFG-4 perform better than the others. The inhibition of slag penetration by graphite can be simply observed from the residual slag amount in the crucible, comparing PG-0 with the others. With the presence of graphite, almost no trace of penetration is visible to the naked eye.

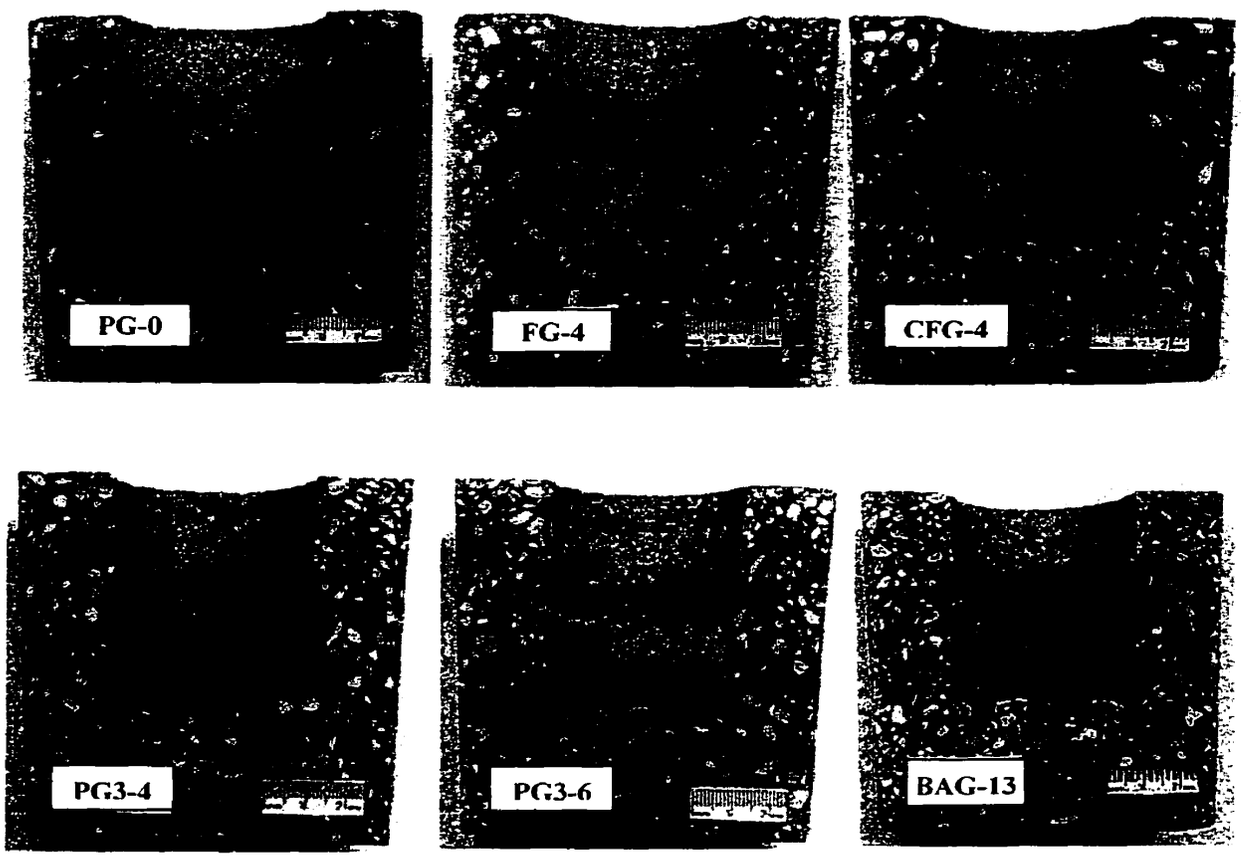

Figure 5.11 Sections of the crucible samples after static slag test at 1450°C for 5h.

The erosion is compared by eroded area index and maximum eroded depth after rotary slag test, as shown in Figure 5.12, the less the index value, the better the slag resistance.

Incorporating graphite by PG and BAG shows better slag resistance than by FG, with PG3-6 being the best, while CFG shows no improvement in slag resistance.

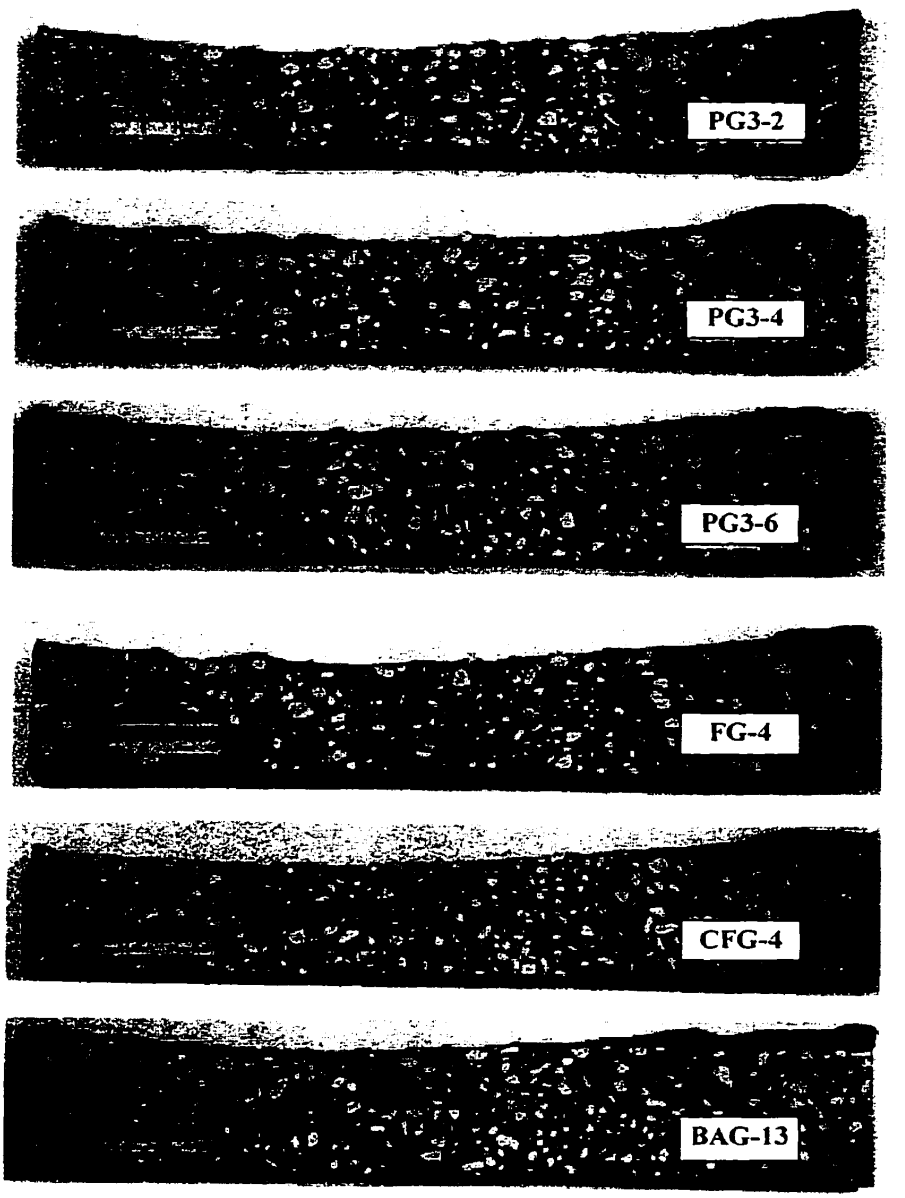

Figure 5.12 Sections of the Al_2O_3-SiC-C samples after rotary slag test at 1450°C for 5h.

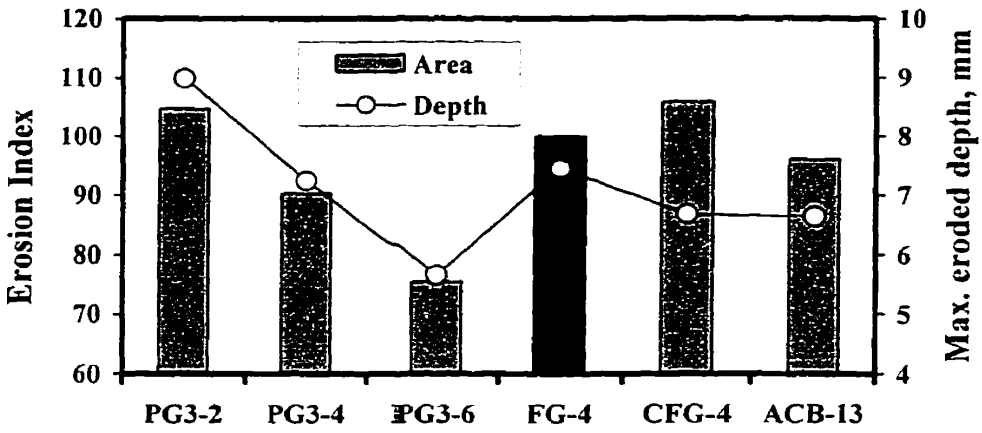

Figure 5.13 Erosion index and maximum eroded depth after rotary slag test.

5.7 Thermal Shock Resistance

The residual CMOR ratios of the castables vs. thermal shock cycle are shown in Figure 5.14. They decline exponentially with the quenching cycle, as indicated by a log-log plot shown in Figure 5.15, using the same data as in Figure 5.14.

Improvement in TSR has been achieved by incorporating graphite, especially via BAG and PG. It should be noted that original strength has an impact on TSR. From this point of view, too high strength after firing is not necessarily needed. The strength can however be adjusted by graphite amount, dispersing state and incorporating method as well as the level of the metallic additives.

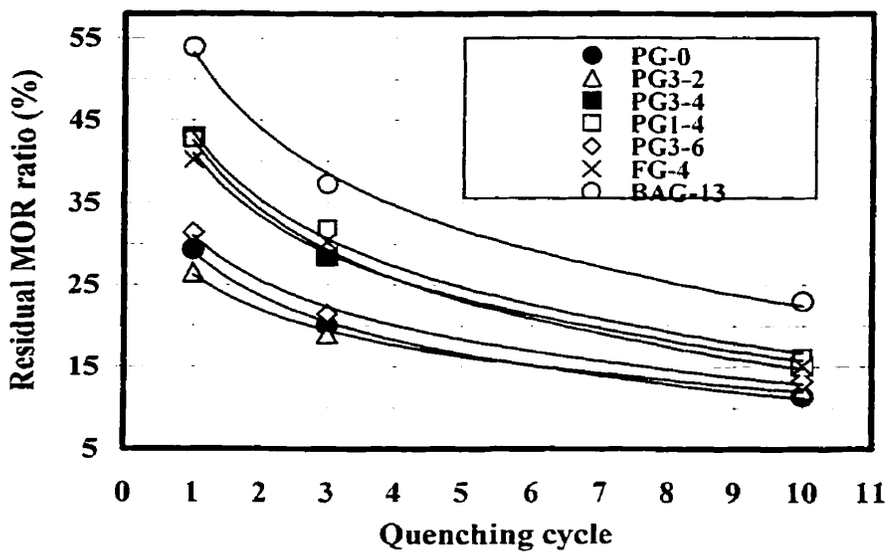

Figure 5.14 Residual CMOR ratio of the Al_2O_3-SiC-C castables after thermal shock by 1000°C ↔ 20°C water quenching.

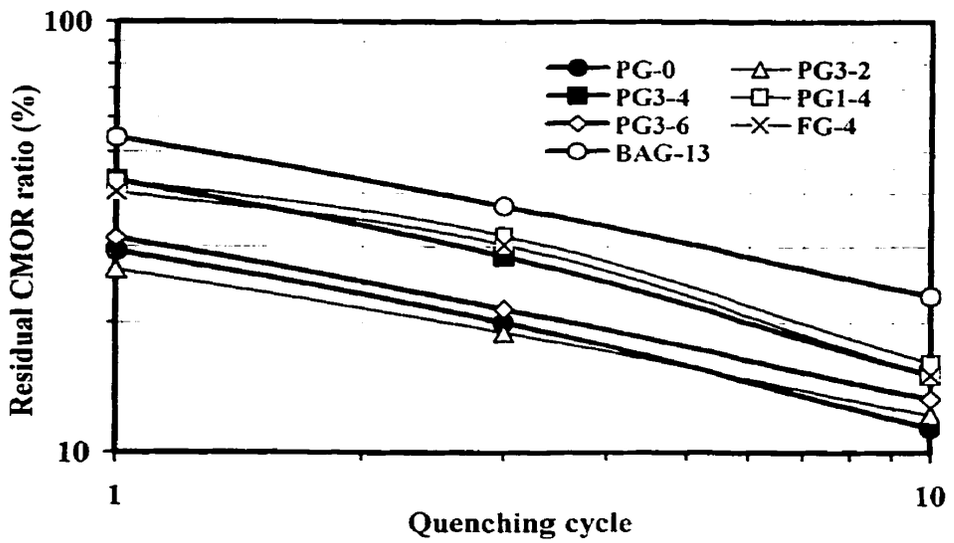

Figure 5.15 Residual CMOR ratio vs. quenching cycle in log-log plot.

5.8 Conclusions of This Chapter

Based on the achieved results, the following conclusions are reached.

(1) Al_2O_3-SiC-C castables incorporated with flake graphite via micro-pelletized graphite (PG) or crushed briquette Al_2O_3-graphite (BAG) have shown net advantages over straight addition of flake graphite (FG), in terms of water addition, flowability, porosity, cold and hot bending strengths, oxidation resistance, slag resistance and thermal shock resistance. The role of the incorporated graphite in precluding slag penetration and improving thermal shock resistance reveals itself dramatically.

(2) These advantages are ascribed to the reduced specific surface area and dispersion of the graphite in the castables. In a non-carbon bonded castable system, such a discontinuous and heterogeneous distribution of graphite is not undesirable for compromising properties, strength in particular.

(3) Incorporating Al and Si metallic powders as antioxidants in the vicinity of graphite entrapped in the micropellets or the briquette grains, hence in the castables, contributes to the improved oxidation resistance and hot strength, but a dense texture of the castable itself is also crucial to oxidation resistance.

(4) TiO_2 coated graphite (CFG) doesn't show positive effects on strength and slag resistance of the investigated Al_2O_3-SiC-C castables, though it imparts lower water demand and better oxidation resistance than natural flake graphite.

(5) The following properties as listed in Table 5.4 of the Al_2O_3-SiC-C castables developed by this work have been achieved, which are found superior to those published in the so far accessible literature.

Table 5.4 The achieved properties of the Al_2O_3-SiC-C castables developed by this work

		PG3-6	BAG-13
Chemical composition (%)	Al_2O_3	81	82
	SiO_2	4	4
	SiC	7	7
	F.C.	6	5
Bulk density (g/cm^3)	110°C, 24h	2.84	2.94
	1000°C, 5h	2.75	2.86
	1450°C, 5h	2.82	2.92
Apparent porosity (%)	110°C, 24h	17.3	14.0
	1000°C, 5h	22.4	19.2
	1450°C, 5h	18.3	15.4
C.M.O.R. (MPa)	110°C, 24h	7.40	5.28
	1000°C, 5h	16.60	8.04
	1450°C, 5h	14.85	11.17
H.M.O.R. (MPa)	1450°C, 1h	7.43	5.23
P.L.C. (%)	1000°C, 5h	- 0.11	- 0.06
	1450°C, 5h	0.00	- 0.09
Water addition (%)		5.70	5.05

(6) Incorporating graphite method plays a big role in minimizing the problems caused by flake graphite and has pronounced influence on overall properties of graphitic castables. Micro-pelletized graphite and crushed briquette of alumina-graphite, as compared with straight natural flake graphite or TiO_2 coated flake graphite, hold good potential for practical application and are worth of adoption in Al_2O_3-MgO-C castables.

CHAPTER 6. OPTIMIZATION OF Al_2O_3-MgO CASTABLES

In this chapter, optimization work on Al_2O_3-MgO castables is documented. Before graphite incorporation in Chapter 7, work is centered on flowability and volume stability issues to optimize the Al_2O_3-MgO castables. A rheological approach, using a coaxial double cylinder viscometer, is adopted to investigate on the rheological characteristics of the matrix slurries vs. 4 kinds of deflocculants, through which the best deflocculant and its appropriate amount have been found in order to reduce water addition at its minimum. By controlling magnesia size, the linear expansion of the castables is controlled under 1,5% in the temperature range of 1000-1500°C when MgO addition varies from 6 to 30%.

6.1 Flowability Investigation of the Al_2O_3-MgO castables

For a thixotropic castable, good flow by vibration and ease of placement are important prerequisites. Ideally, a well designed castable will have good flow at as low as possible water addition and form a well consolidated and homogeneous dense body. Flow properties can be influenced by a number of factors. The most important are: (1) particle size distribution (PSD), (2) the chemical, surface and shape characteristics of the ultrafine powders used and (3) admixtures added to disperse the oxide fine and ultrafines and cement and to control setting.

Intensive study has been conducted on PSD and flowability of castables by J. E. Funk et

al [89] and B. Myhre et al[90-92]. They stressed the role of superfine particles in reducing water addition and improving flowability. The use of superfines is based on the concept that in a castable, the density is limited by interparticle voids that are filled with excess water. These voids can however be filled by successively finer particles, thus replacing the water. However, consideration must also be given to the rheology response to a dense PSD. As the solids loading increases, the rheological property called dilatancy becomes more severe, which can be disastrous to flow. The required flow can be obtained by keeping the coarse particles apart by a suspension of well-dispersed fine particles. The rheology of the matrix suspension must be suitable, which is determined by the PSD and the state of flocculation.

For good hot strength and slag resistance, fumed silica as superfines source is not suitable for the bonding system in this work, to avoid the formation of liquid phases in the Al_2O_3-CaO-SiO_2 system[81]. Instead, ultrafine alumina has to be used. B. Mhyre et al[91,92] reported that use of ultrafine reactive alumina in castables is likely to bring about dilatancy and quick setting problems. T. A. Bier et al[53] reported that adding MgO fine powders into cement bonded Al_2O_3-MgO castables will shorten the flowable time. Facing these challenges, efforts are therefore exerted to optimize the rheology of the matrix suspension by using the most suitable and effective deflocculant.

Flowability investigation and optimization have been made into two steps. Firstly, the matrix portion and its key components are extracted to investigate their rheological

characteristics (shear stress-shear rate relationship), when in suspensions. Four kinds of deflocculants are compared in three suspension systems respectively. After using the appropriate deflocculant and optimized addition suggested by step one, the flow values of the Al_2O_3-MgO castables are then examined by the flow cone method described in 4.5.1 of Chapter 4, as the second step.

6.1.1 Matrix Rheology vs. Four Kinds of Deflocculants

6.1.1.1 Fundamentals and Experimental Procedure

Rheological characteristics can be expressed by the relationships between shear stress (σ) and shear rate (D), apparent viscosity and shear rate, or viscosity (η) and time under a constant shear rate. Commonly, flow behavior of a fluid can be characterized using flow curves (σ–D or η–D curves). As shown in Figure 6.1[93], there are 6 flow patterns under a narrow range of shear rates, as described below.

(1) *Newtonian flow* is characterized by a straight line from the origin, which slopes upwards, when shear stress is plotted vs. shear rate. The apparent viscosity is constant at constant temperature.

(2) *Bingham flow* is characterized also by a straight line, not from the origin but from a specific yield stress, σ_y. The apparent viscosity (plastic viscosity) approaches a constant value with increasing shear rate.

(3) *Pseudo-plastic flow* is characterized by a convex curve from the origin when σ is plotted against D. The apparent viscosity decreases with increasing shear rate (shear thinning).

(4) *Plastic flow* is essentially the same as pseudo-plastic flow except that it starts at a specific yield stress, σ_y.

(5) *Dilatant flow* is characterized also by a concave σ–D curve from the origin. The apparent viscosity increases with increasing shear rate (shear thickening).

(6) *Dilatant flow with a yield value* is essentially the same as dilatant flow except for the yield stress. The apparent viscosity decreases with increasing shear rate up to a certain value, thereafter increases with increasing shear rate.

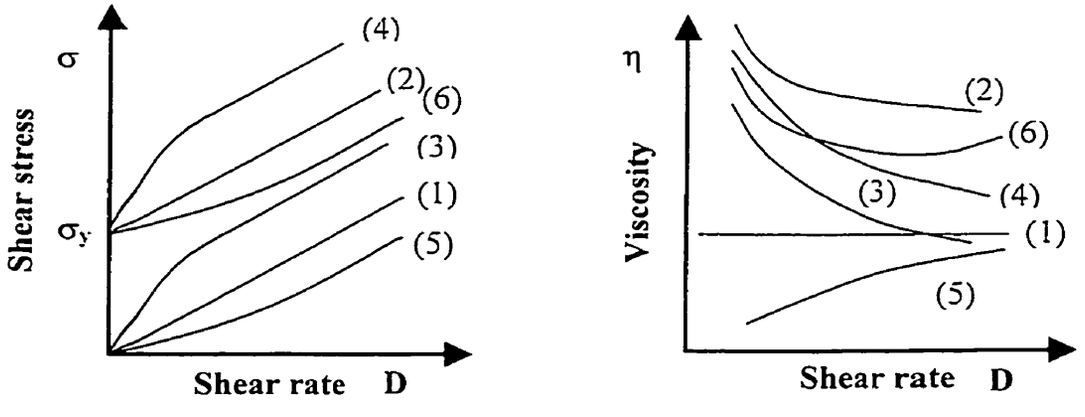

Figure 6.1 Flow patterns under a narrow range of shear rate.

Vibration type castables follow a Bingham flow or plastic flow rheological behavior.

Both have a yield stress σ_y. When the applied stress $\sigma \leq \sigma_y$, no flow occurs; when $\sigma > \sigma_y$, plastic flow occurs. The rheological equation is

$$\sigma = \sigma_y + \eta_p D ,$$

where η_p is called plastic viscosity. For plastic flow, the equation applies to the linear part. Such a flow pattern has shear-thinning effect, what is needed for the casting by vibration. By and during the vibration, castables should easily flow to fill everywhere in the configuration, during which the wrapped air should escape to avoid leaving big pores. This flowability comes from thixotropy, instead of too much water, otherwise the porosity of the placed body would be too high and segregation may happen. After casting when the vibration stops, the internal structure should soon recover to avoid segregation of the coarse aggregates.

Using a rotational coaxial double cylinder viscometer (in this work, NXS-11A model, made by Chendu Instruments Co., China), as schematically shown in Figure 6.2, the shear stress at different shear rate by varying the rotation speed can be measured. Plot σ vs. D, and a flow curve can be obtained. The working principle is as follows. The sample is placed into the annular gap between the outer cylinder and the rotor. A motor drives the inner cylinder. A viscosity related torque, caused by the resistance of the sample to shearing, act on the inner cylinder. This torque deflects a measuring spring placed between the motor and the inner cylinder. The size of the spring twist correlates linearly with the torque. The spring deflection shows up as an angle indication on the scale.

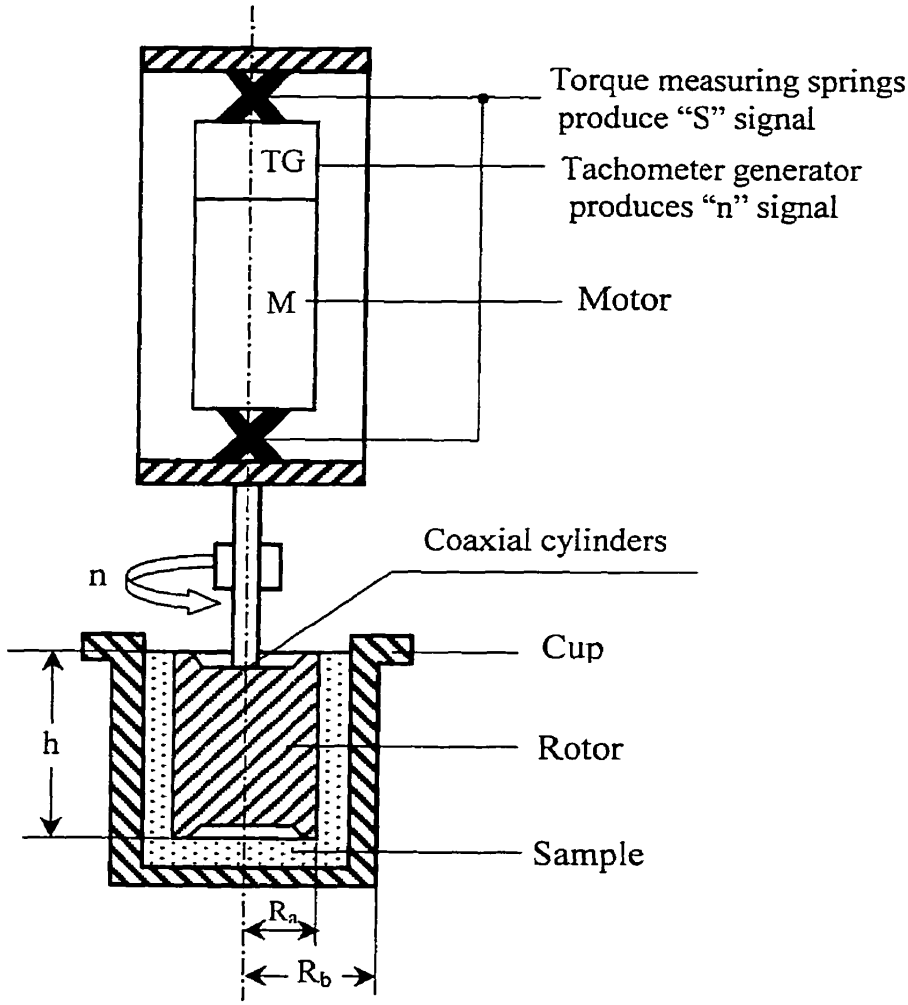

Figure 6.2 A schematic set-up of the rotary coaxial double cylinder viscometer used.

For such a viscometer, some parameters can be deduced and calculated by the following formulas:

$$\eta = \sigma / D$$

$$\sigma = T / 2\pi R_a^2 h$$

$$D = 2\omega R_b^2 / (R_b^2 - R_a^2)$$

$$= [(\pi/15) \cdot R_b^2 / (R_b^2 - R_a^2)] \cdot n = K \cdot n$$

where η = viscosity (Pa.s), σ = shear stress (Pa), D = shear rate (sec.$^{-1}$), R_a = radius of the inner cylinder-rotor (m), h = height of the inner cylinder (m), R_b = radius of the outer cylinder-rotor (m), T = torque (N·m), $\omega = 2\pi \cdot n/60$, angular velocity (radians/sec.), n = rotor speed (min^{-1}) and $K = [(\pi/15) \cdot R_b^2 / (R_b^2 - R_a^2)]$, shear rate factor that depends only on the radii of the cup and the rotor.

There are 5 measuring systems consisting of 5 sets of inner and outer cylinders respectively for a wide measuring range from 0.28 $\times 10^{-2}$ to 18,000 Pa.s. Each has 15 velocity gears, yielding 15 varying D-values. Increasing the velocity of the rotor, per se D, from the lowest to the highest, taking down each reading (α) on the scale at each D, and the shear stress can be obtained by

$$\sigma = Z \times \alpha,$$

where Z is a cylinder geometry dependent constant, available with the instrument, and α is the scale reading. By the σ-D curve, flow pattern is assessed.

For a typical plastic flow curve, as shown by Figure 6.3, the yield stress σ_y corresponds to the intercept of the extended straight line to σ-axis and the slope of the linear part corresponds to the plastic viscosity η_p, both can be calculated using the measured data by the formulas as shown at the right top of the next page.

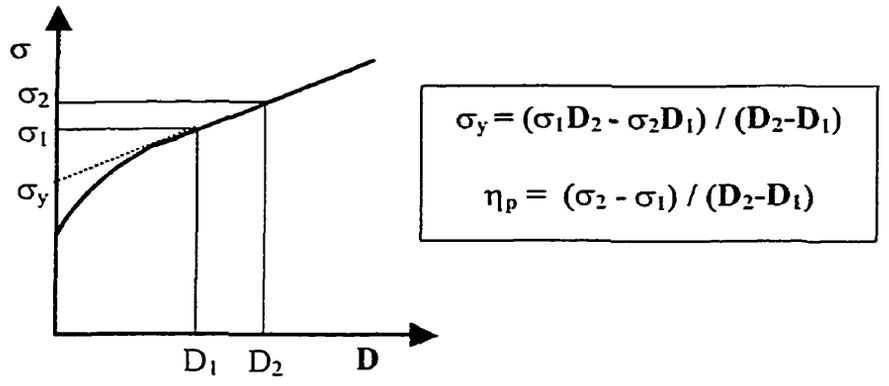

Figure 6.3 Yield stress and plastic viscosity for a plastic flow pattern.

From flowability point of view, both σ_y and η_p should be low. For a castable, they should never be too low, when water addition is adjusted to reach a minimum. For a high packing fraction suspension at a certain consistency, various deflocculants will have an impact on these two parameters. When other things being equal, the lower they are, the better the flowability is expected.

In this work, four types of deflocculants denoted in Table 6.1 are compared in three suspension systems as shown in Table 6.2, by measuring σ_y and η_p parameters.

Table 6.1 Four deflocculants and their denotation

Chemical name	Denotation
Sodium hexametaphosphate	SHP
Sodium polyacrylate	SPA
Polyethyleneglycol	PEG
Melamine polymer	MP

Table 6.2 Composition (%) of the three suspension systems

	(1) Al_2O_3-H_2O	(2) Al_2O_3-CAC-H_2O	(3) Al_2O_3-MgO-CAC-H_2O
A3000FL calc. Al_2O_3	100	20	20
White fused Al_2O_3 (-325 mesh)	0	60	40
MgO (BMF50)	0	0	20
Secar 80 CA Cement	0	20	20
Water (in addition)	30 (45*)	28	28

* The water addition when no deflocculant is added.

6.1.1.2 Test Results

(1) Al_2O_3-H_2O System

The shear stress-shear rate curves of Al_2O_3-H_2O system as a function of the deflocculant type and addition are presented in Figures 6.4~6.8, and the calculated rheological parameters are summed up in Table 6.3.

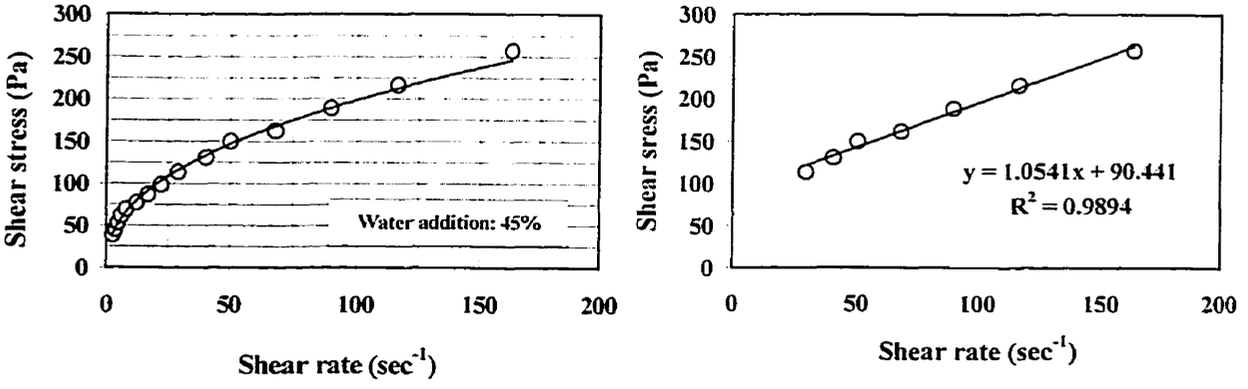

Figure 6.4 Flow curve of Al_2O_3-H_2O system without adding deflocculant.

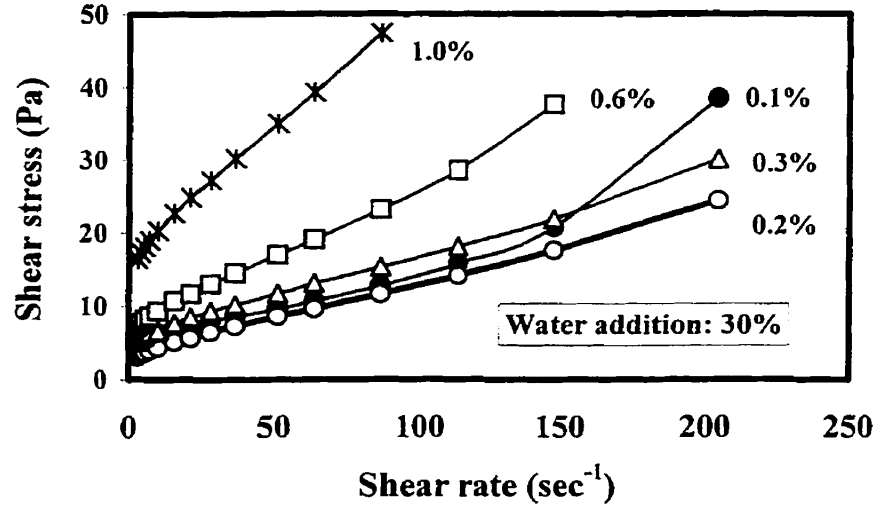

Figure 6.5 Flow curve of Al_2O_3-H_2O system with addition of SHP.

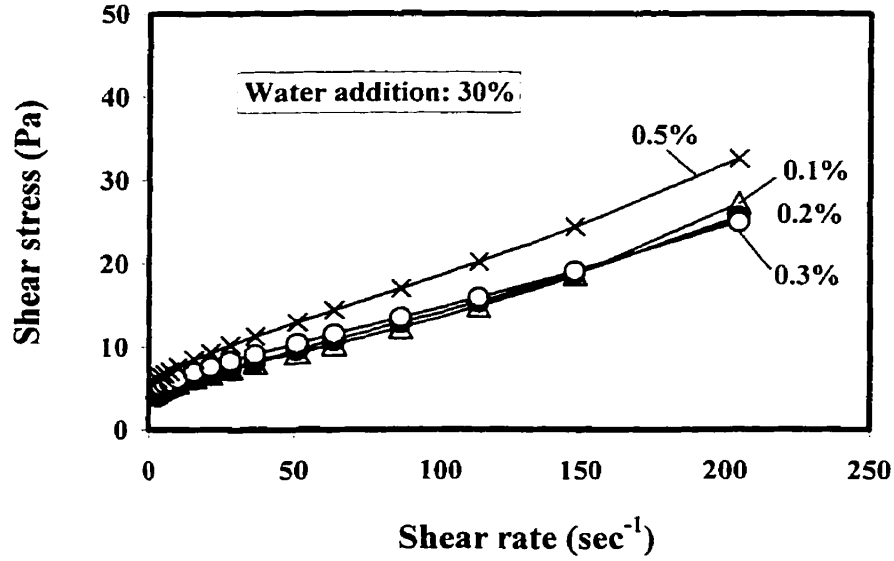

Figure 6.6 Flow curve of Al_2O_3-H_2O system with addition of SPA.

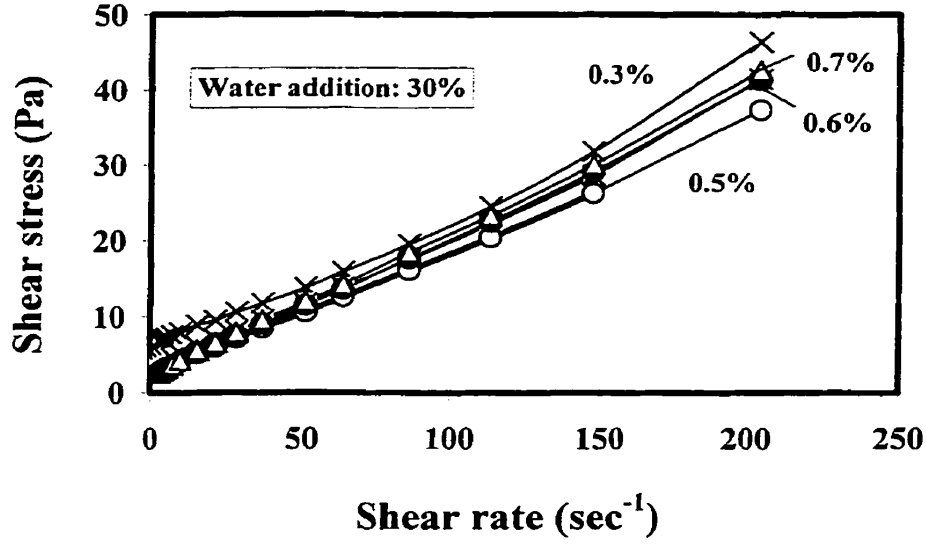

Figure 6.7 Flow curve of Al_2O_3-H_2O system with addition of PEG.

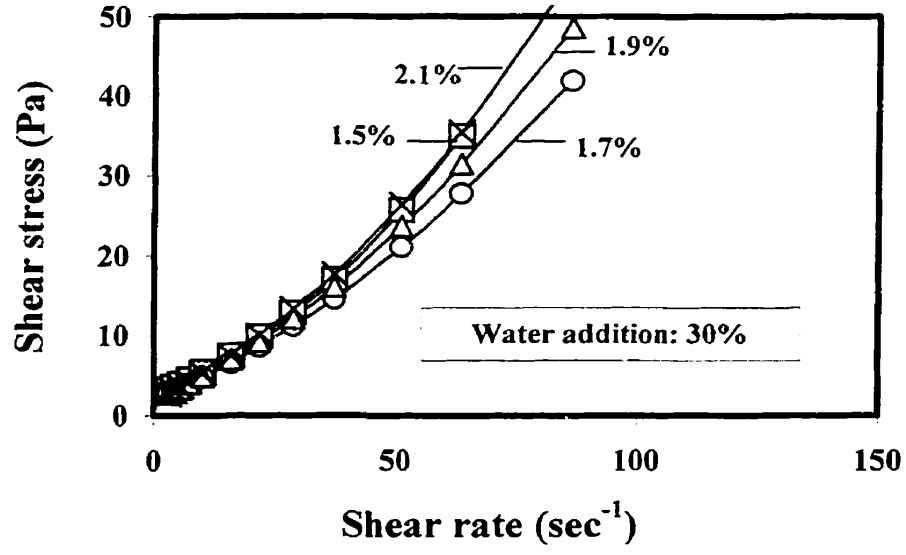

Figure 6.8 Flow curve of Al_2O_3-H_2O system with addition of MP.

Table 6.3 Rheological parameters of the Al_2O_3-H_2O system

Deflocculant	Amount (%)	Plastic viscosity (mPa.s)	Yield stress (Pa)
SHP	0.1	Dilatant	Dilatant
	0.2	**99.8**	**4.408**
	0.4	115.9	5.598
	0.6	198.2	7.035
SPA	**0.1**	**104.5**	**4.172**
	0.2	**100.5**	**4.414**
	0.3	94.6	5.413
	0.5	126.5	6.230
PEG	0.4	182.9	2.563
	0.5	**168.4**	**2.045**
	0.6	188.9	**1.811**
	0.7	193.9	2.065
MP	0.3 –2.1	Dilatant flow	

By comparing Figure 6.4 with Figures 6.5-6.8 and noticing their yield stress values in Table 6.3, it can be seen that without using any deflocculant, the yield stress is 90.4 Pa, over 20 times higher than those with any one of the four deflocculants, even at higher water addition! This means that deflocculant do help to disperse the ultrafine Al_2O_3 powders and reduce the internal friction. SHP and SPA show an equivalent effect at 0.1 or 0.2% addition, but both show a doubled yield stress, in comparison with PEG's at 0.5 or 0.6% addition. MP, in wide range of addition, results in dilatancy. In Figure 6.8, only four additions have been shown, below 1.5%, the dilatancy is severer. In short, from yield stress point of view, PEG among the four, at 0.5-0.6% addition, works the best.

(2) Al_2O_3-CAC-H_2O System

The flow curves of Al_2O_3-CAC-H_2O system vs. the deflocculant type and addition are presented in Figures 6.9~6.12, and the rheological parameters are listed in Table 6.4.

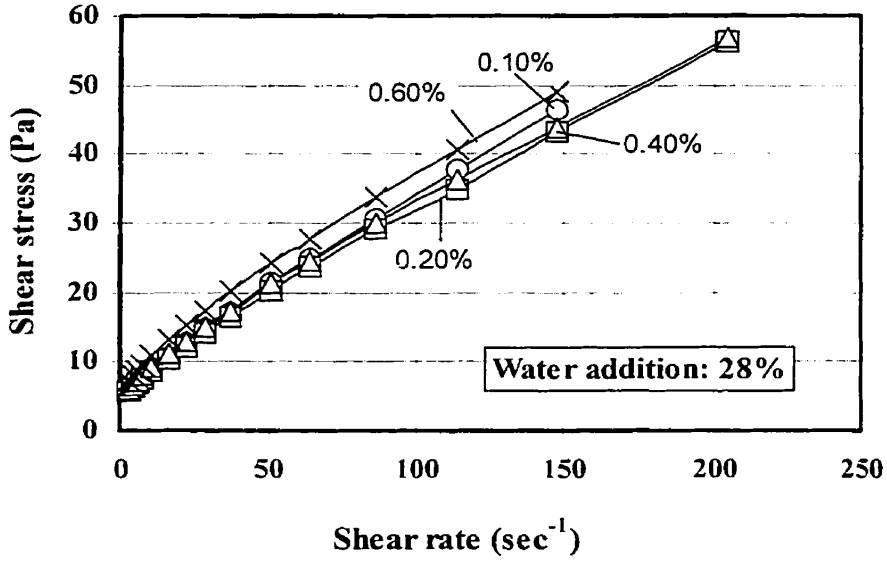

Figure 6.9 Flow curves of Al_2O_3-CAC-H_2O system with addition of SHP.

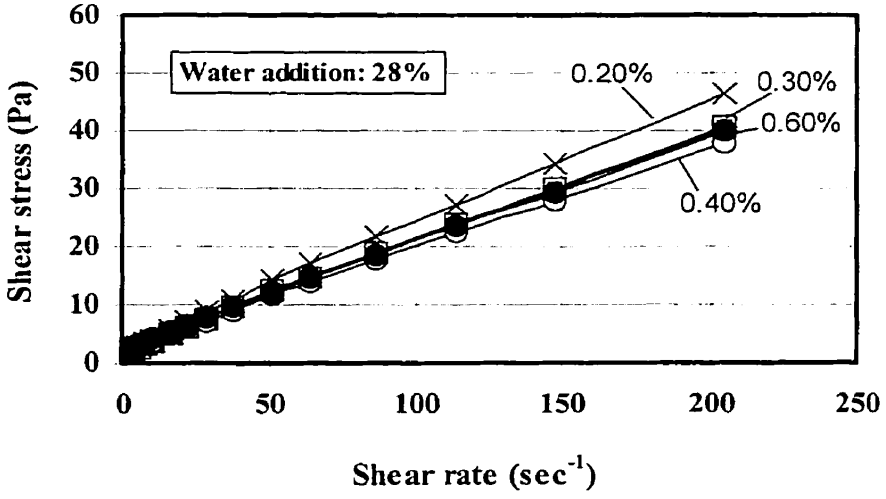

Figure 6.10 Flow curves of Al_2O_3-CAC-H_2O system with addition of SPA.

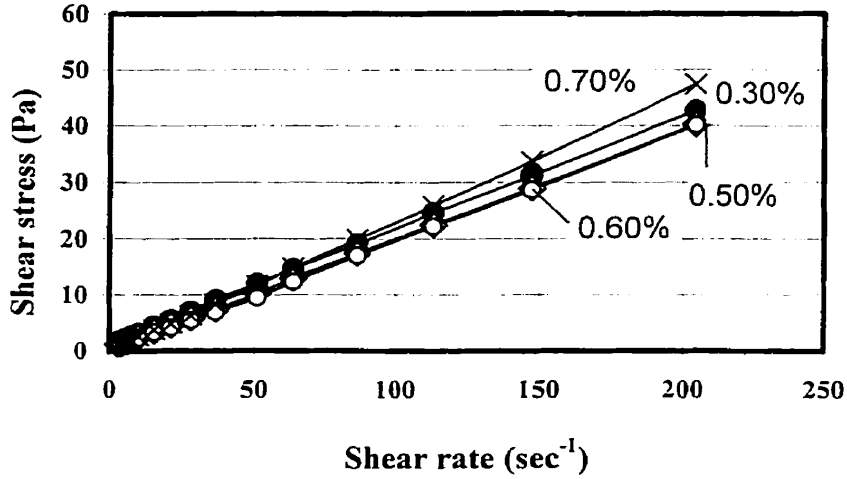

Figure 6.11 Flow curves of Al_2O_3-CAC-H_2O system with addition of PEG.

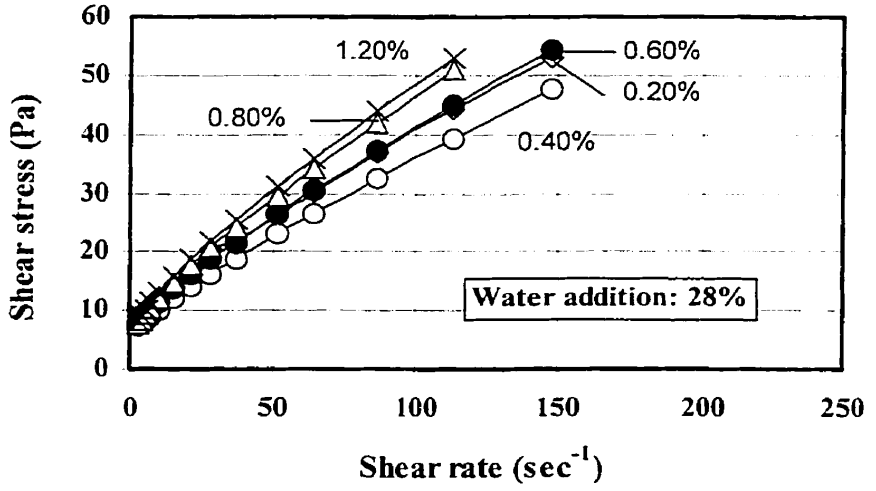

Figure 6.12 Flow curves of Al_2O_3-CAC-H_2O system with addition of MP.

Table 6.4 Rheological parameters of the Al_2O_3-CAC-H_2O system

Deflocculant	Amount (%)	Plastic viscosity (mPa.s)	Yield stress (Pa)
SHP	0.1	279.3	6.14
	0.2	**251.3**	**6.31**
	0.4	251.6	7.01
	0.6	288.7	8.16
SPA	0.2	213.8	2.96
	0.3	**188.0**	**2.52**
	0.4	**173.6**	**2.55**
	0.5	186.5	2.67
	0.6	184.3	2.79
PEG	0.3	202.2	1.52
	0.4	202.3	0.47
	0.5	**195.6**	**0.28**
	0.6	**194.3**	**0.15**
	0.7	228.9	0.17
MP	0.2	306.2	9.58
	0.4	**282.9**	**7.42**
	0.6	323.2	8.43
	0.8	393.8	8.14
	1.2	407.6	8.86

In system (2), each at its optimum addition, PEG is ranked as the best in deflocculation, followed by SPA > SHP >MP. This is similar to the result in system (1), implying that ultrafine alumina is the key component dominating the rheological behavior of the matrix. MP, being not any more dilatant as in the system (1), still results in too high yield values, and plastic viscosity, compared to the others.

(3) Al_2O_3-MgO-CAC-H_2O System

Figure 6.13 and Figure 6.14 show the flow curves of Al_2O_3-MgO-CAC-H_2O system vs. SPA and PEG respectively. SHP and MP, due to poor performance in system (1) and system (2), have been eliminated in this system.

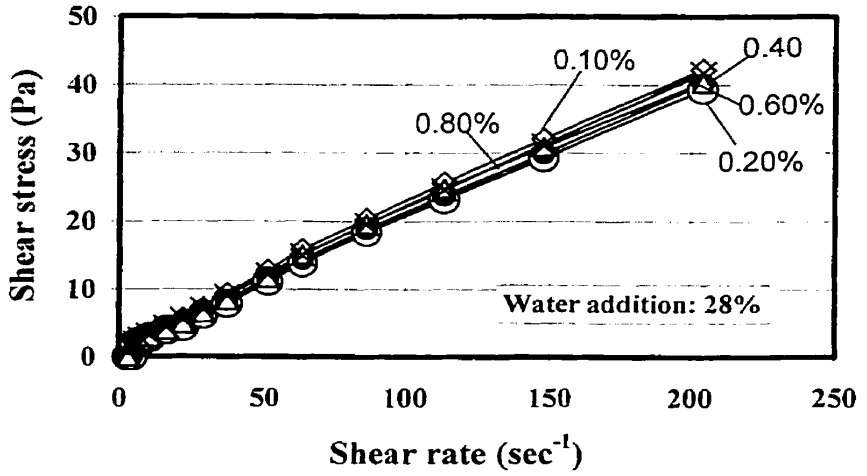

Figure 6.13 Flow curves of Al_2O_3-MgO-CAC-H_2O system with addition of SPA.

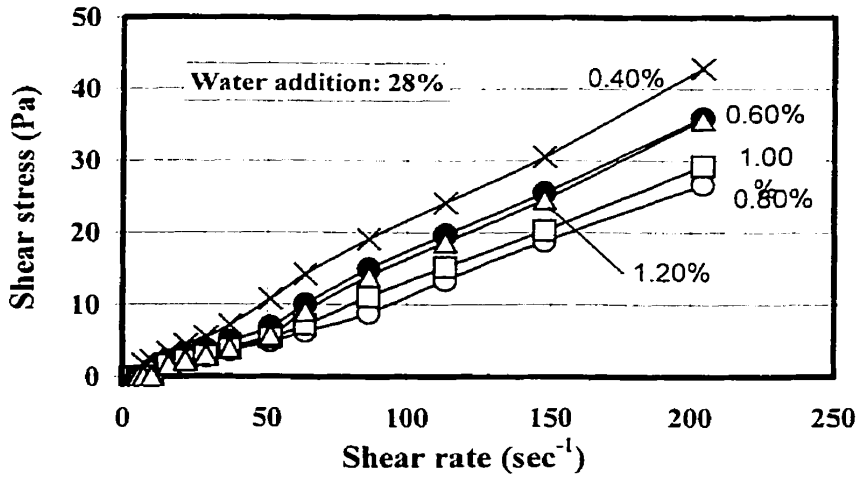

Figure 6.14 Flow curves of Al_2O_3-MgO-CAC-H_2O system with addition of PEG.

It is seen in Figure 6.13 that the difference between various levels of SPA is not significant, with 0.2% addition as the best. This means that system (3) is not sensitive to SPA addition varying from 0.2 to 0.8%.

There appears an abnormal phenomenon in Figure 6.14, as a negative intercept appears, when PEG addition being at and beyond 0.6%. Theoretically it is not possible for a yield value to be negative. This is believed to be due to a measuring error, as PEG imparts the best flow among the four deflocculants, which makes the system at the same water addition of 28% a little too dilute; the α values also appear in a low scale range, especially at lower D, with thus bigger systematic error. The same thing happened also in system (2), see Figure 6.11. Nevertheless, it can be seen that an addition of 0.6 to 1.0% of PEG is better than 0.4%.

6.1.2 Flowability of the Al_2O_3-MgO Castables

From above, the two deflocculants, SPA and PEG, seem the most effective. They are thus being used in a true castable mix, containing at first 6% weight of magnesia, as defined in Table 4.9, p.75, with the same matrix composition as system (3) in Table 6.2.

As seen in Figure 6.15, at the same water addition of 4.7%, PEG confers significantly better flow. To achieve a flow value between 170 and 200 mm, SPA deflocculated M6 castable requires 5,3% water, 12% higher than that of PEG deflocculated. Figure 6.16 shows the flow value vs SHP addition of M6 castable at 5.3% water addition, which is

not as good as when using PEG as deflocculant at 4,8% water addition.

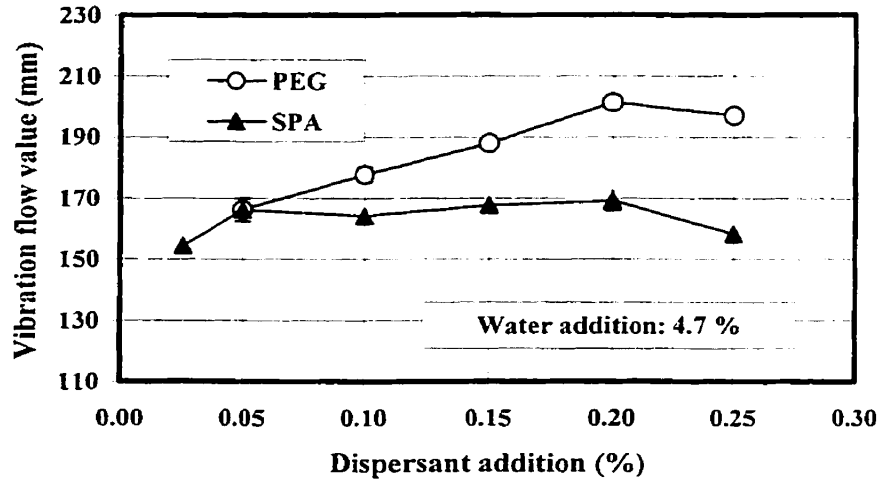

Figure 6.15 Flow value of M6 castable as a function of deflocculant type and addition.

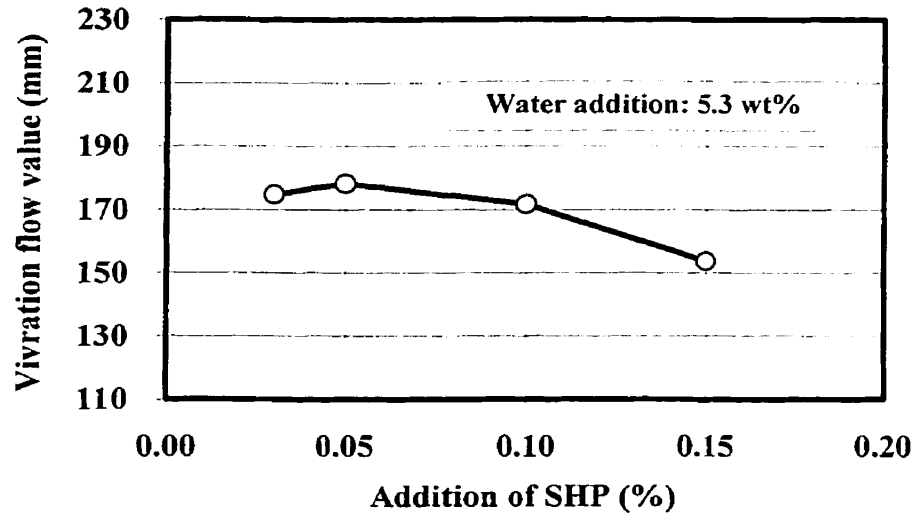

Figure 6.16 Flow value of M6 castable as a function of SHP addition.

Table 6.5 correlates the used deflocculant, at an optimum addition set from flowability point of view, with the properties of M6 castable. Clearly, deflocculant type has a

considerable influence on properties of the castable.

Table 6.5 Correlation of the used deflocculant and properties of M6 castables

	SHP	SPA	PEG
Dosage (%)	0.05	0.05	0.2
Water addition (%)	5.3	5.3	4.7
Flow value (mm)	177	194	201
Bulk density (g/cm^3)	3.12	3.15	3.20
Apparent porosity (%)	15.2	14.2	12.8
CMOR (MPa)	5.46	6.85	8.57

Although good flow by now have been achieved, measurements on the flow decay, as shown in Figure 6.17, indicate that such castables set rather fast. After 30 min or so the flow value drops below 170 mm. Such a workable time could be insufficient, from in-plant installation point of view. To prolong the workable time, citric acid has been used as a retarder. Adding only 0.03% of citric acid, the flow value can be sustained above 170mm for 50-60 min or more when using PEG, as shown also in Figure 6.17.

Interestingly, these results in the castable mixes correspond well to those in the matrix suspensions, in terms of the deflocculant type and dosage. The matrix portion accounts for about 30% for the total castable mix. The castable-based appropriate addition of each deflocculant, turns to be almost exactly the matrix–based optimum addition, determined by the rheological parameters. This means that extracting the matrix and its key

component(s) and making rheological measurement is very worthwhile and useful for optimizing the flow behavior of the castable, in other words, flow ability is predictable from the extracted matrix.

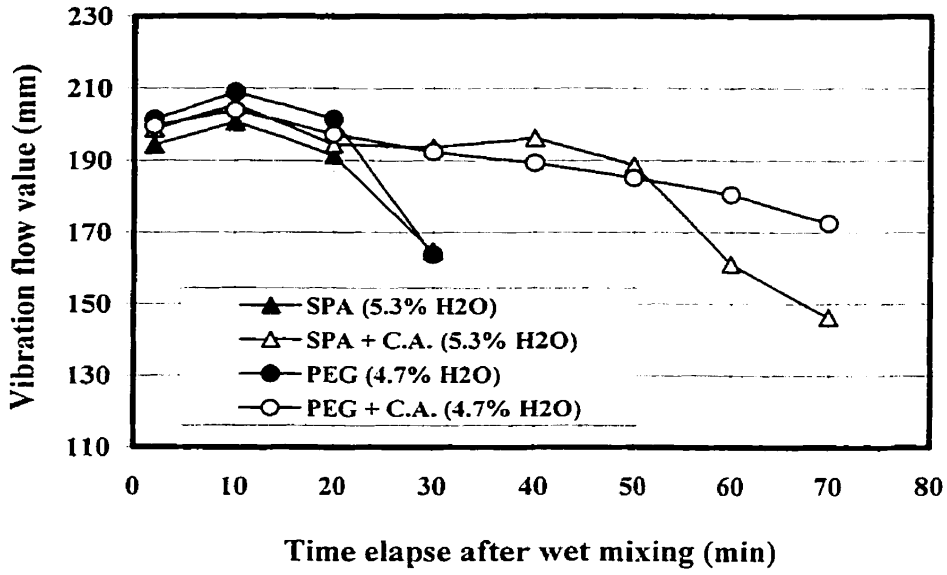

Figure 6.17 Flow decay of M6 castables with or without retarder, comparing SPA with PEG.

The effective deflocculants, SPA and PEG, are organic compounds with long molecules, and a steric hindrance is believed to result in the improvement of flowability. The dispersing mechanism of deflocculant is highly related to the particle interactions, which is interpreted using DLVO theory in Annex 6.1.

6.2 Properties of the Al_2O_3-MgO castables

6.2.1 Thermal Expansion Behavior

Thermodynamically, more MgO addition means more spinel formation, which could result in more significant volume expansion (7.8% in volume and 2.6% linearly, based on molar volume calculation). It is reported[97-99] that if the MgO and Al_2O_3 reactants are powders rather than bulk solid materials, then the solid state reaction often yields linear expansion much larger than the predicted value simply from the molar volumes.

To avoid excessive expansion, the size of MgO in fine portion (<0.3 mm) is strictly controlled to be no more than 8-9%, equivalent to 5-10% (<0.074 mm) suggested by M. Kobayashi et al[20], R. Nakamura et al[47] and S. Itose et al[52], the rest being increased in size gradually until the top size of 4.76 mm. The actual size distribution of the MgO at different additions is shown in Figure 6.18. Actually some coarse MgO grains will not convert to spinel even at high temperatures (>1500°C), due to dynamic restriction. This is confirmed by microscopic analysis on the fired Al_2O_3-MgO samples.

The thermal expansion under load of the castables with 6-30% MgO is shown in Figure 6.19. They behave quite similarly, though the absolute value is of course a function of MgO amount. Under this particular condition, spinel starts to form around 1050°C, reaches maximum between 1240 and 1285°C, depending on the MgO addition, but the difference being not big. Without load, however, the temperature for the maximum

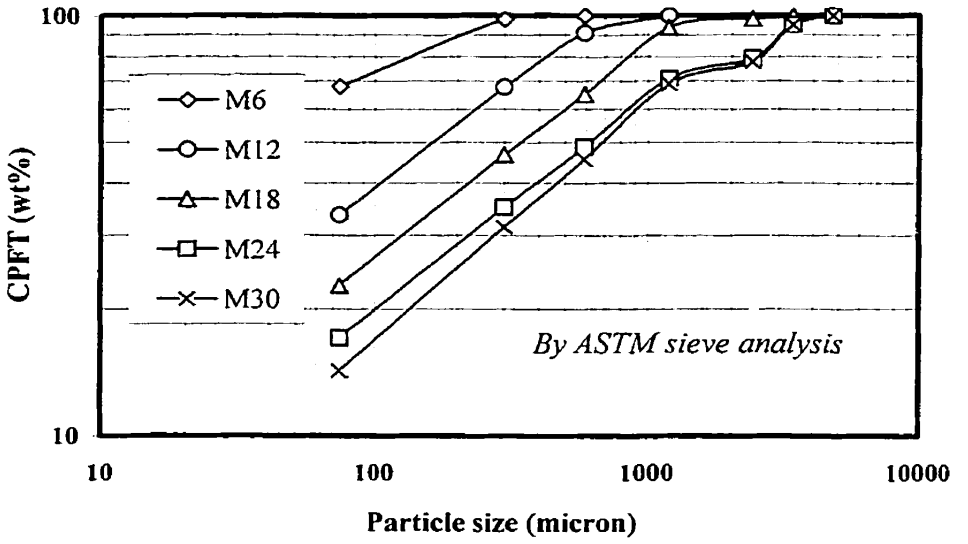

Figure 6.18 Particle size distribution of the added magnesia in the castables.

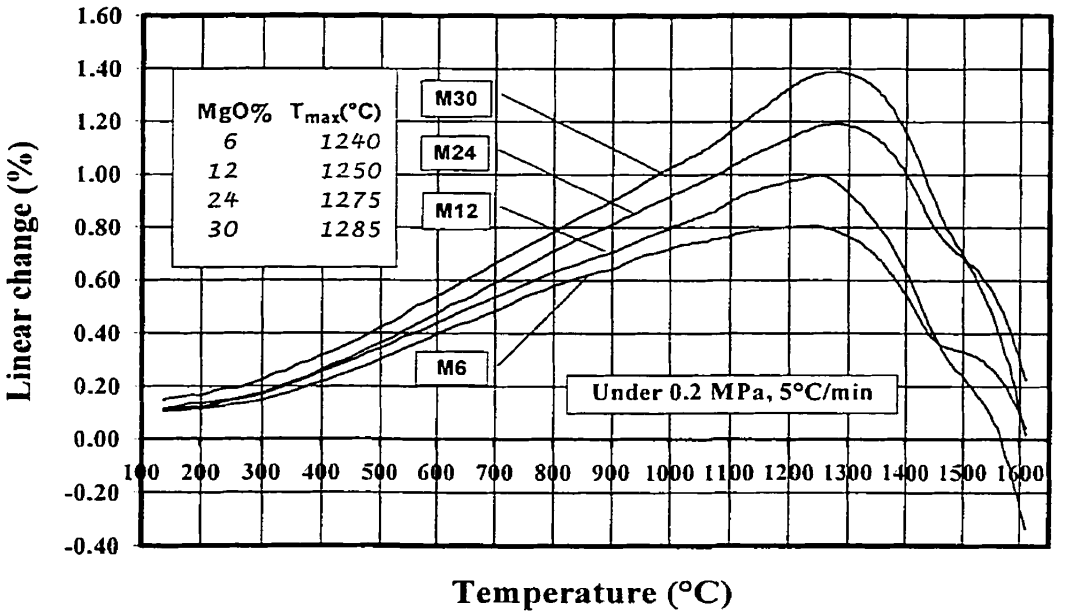

Figure 6.19 Thermal expansion under load of M6-M30 Al_2O_3-MgO castables.

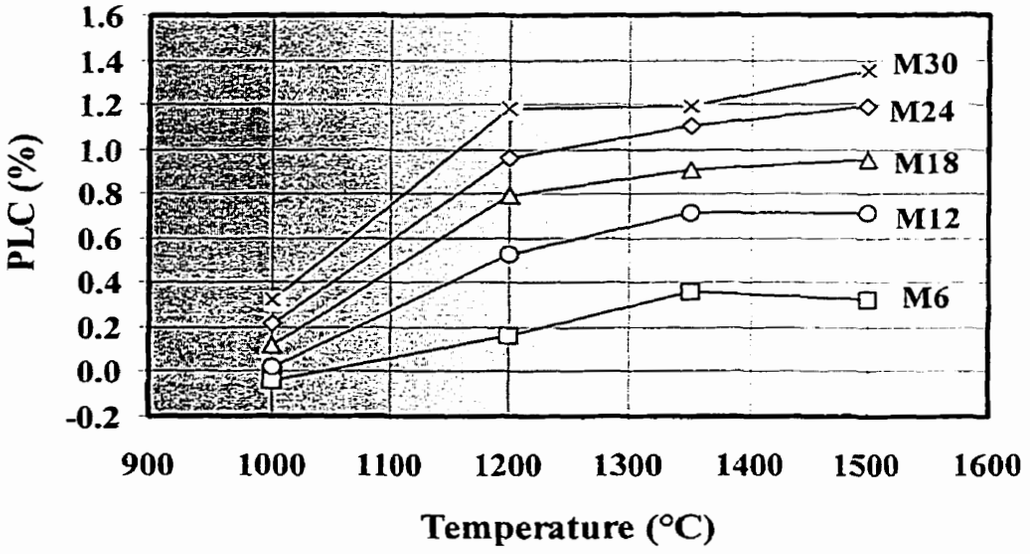

Figure 6.20 Permanent linear change as a function of temperature and MgO addition.

expansion to appear extends to a higher temperature, 1350-1500°C, as seen in Figure 6.20. Even at 30% MgO addition, the maximum PLC is under 1.5%, acceptable for spinel forming castable system.

6.2.2 Cold Modulus of Rupture

The CMOR of the castables decreases linearly with increasing magnesia, and the higher the fired temperature, the sharper this tendency is, as shown in Figure 6.21. This correlates well with the increase of expansion as MgO increases. The mismatch in thermal expansion between alumina and magnesia induces micro-gaps or cracks in the matrix, as it will be shown later in Figure 7.20 (c) for M12 mix, as an example. This

accounts for the strength decrease, but these defects are known to improve the thermal shock resistance[100].

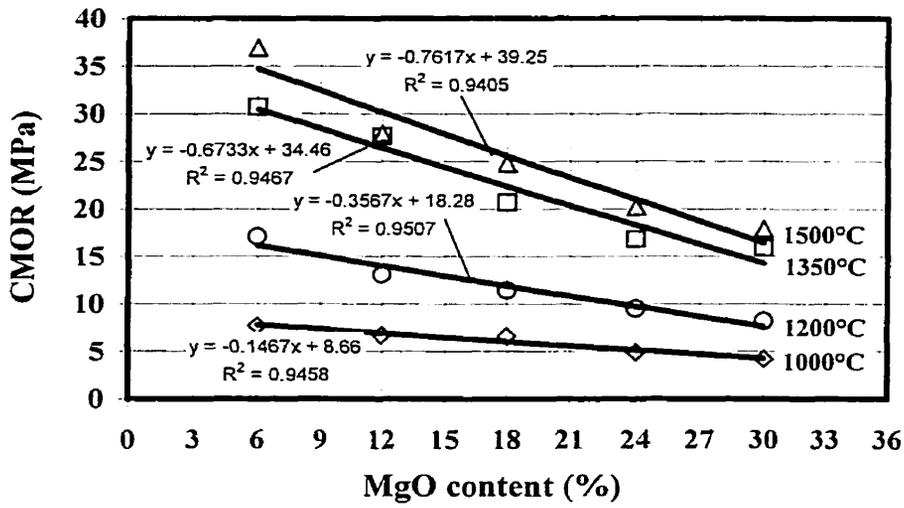

Figure 6.21 Cold modulus of rupture of the Al_2O_3-MgO castables as a function of MgO addition.

6.2.3 Slag Resistance

By rotary slag test at 1600°C for 8h, using a basic steelmaking slag whose chemical composition is given in Table 7.5 in Chapter 7, slag resistance of the castables containing 0-30% MgO is compared, as shown by their photographed sections after slag attack in Figure 6.22. By numeral values, their erosion and penetration are compared in Figure 6.23, the depth of erosion being counted from the original hot surface and the penetration depth being the thickness of the residual reacted layer, excluding the eroded

layer. To estimate penetration degree, both the depth and the area should be taken into account. Clearly, the favorable role of an appropriate amount of magnesia has been

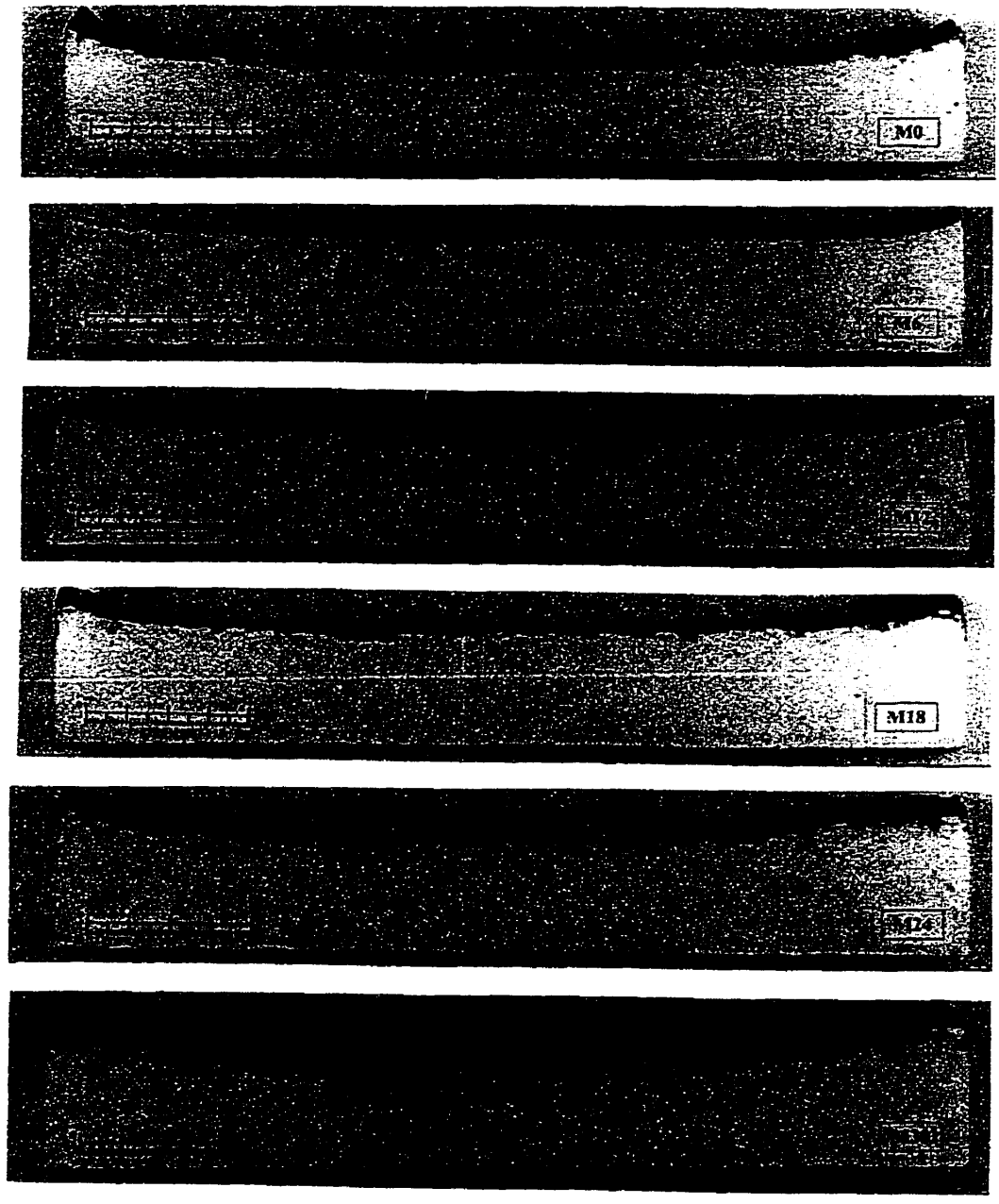

Figure 6.22 Sections of the M0-M30 samples after rotary slag test at 1600°c for 8h.

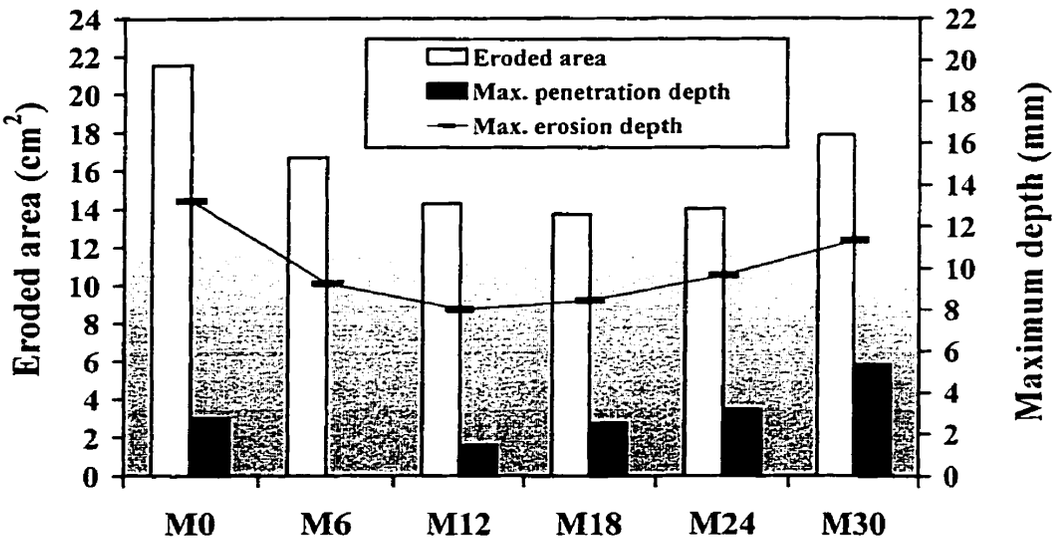

Figure 6.23 Slag resistance comparison among M0 ~ M30 samples after rotary slag test at 1600°c for 8h.

presented, comparing M0 with M6~18. As MgO addition increases, slag penetration increases, a well known fact confirmed by many publications. Under the circumstances in this work, when MgO addition goes more than 6%, visible residual penetration appears, more pronounced when MgO reaches 12% and more. From chemical point of view, higher MgO content should enable a better resistance to basic slag corrosion, but the penetration may make the matrix soft at such a high temperature and the matrix can easily be eroded under dynamic action. This is why where the penetration is severe, the erosion is also high, probably not like the situation of static slag test.

Table 6.6 sums up the data of physical and chemical properties of the Al_2O_3-MgO castables. The next step will be graphite incorporation, into M6, M12 and M24 mixes.

Table 6.6 Properties of the Al_2O_3-MgO castables

		M6	M12	M18	M24	M30
Chemical composition (%)	Al_2O_3	92	86	80	74	68
	MgO	6	12	18	24	30
	CaO	1.1	1.1	1.1	1.1	1.1
Bulk density (g/cm^3)	110°C, 24h	3.20	3.19	3.15	3.15	3.14
	1000°C, 5h	3.15	3.12	3.09	3.07	3.06
	1500°C, 5h	3.11	3.05	2.98	2.97	2.94
CMOR (MPa)	110°C, 24h	8.6	8.7	8.2	7.9	7.8
	1000°C, 5h	7.7	6.7	6.6	4.9	4.2
	1200°C, 5h	17.1	13.1	11.4	9.5	8.2
	1350°C, 5h	30.7	27.6	20.4	16.8	15.9
	1500°C, 5h	36.9	27.9	24.8	20.2	17.9
PLC (%)	1000°C, 5h	-0.04	+0.02	+0.12	+0.22	+0.32
	1200°C, 5h	+0.16	+0.53	+0.79	+0.96	+1.18
	1350°C, 5h	+0.36	+0.71	+0.91	+1.10	+1.19
	1500°C, 5h	+0.32	+0.71	+0.95	+1.19	+1.35
Water addition (wt. %)		4.7	4.7	4.7	4.7	4.7
Vibration flow value (mm)		208	202	207	207	209
Workable time* (min)		30	30	30	30	30

* The time when the flow value falls below 160 mm.

6.3 Conclusions of Chapter 6

(1) Through optimization in matrix rheology, using appropriate deflocculant and controlling magnesia's size in the fine portion, a series of Al_2O_3-MgO castables with good flowability at 4.7% water addition and containing MgO up to 30% have been successfully developed. Their overall properties, in particular workability and thermal expansion, are well accepted. This makes it possible to elaborate Al_2O_3-MgO-C castables based on good starting castables.

(2) Castable flowability is governed by its matrix rheology. "Extracting matrix" method, using rotary coaxial double cylinder viscometer to measure rheological parameters of the matrix suspension, is a useful and efficient approach to characterize rheological behaviors of the castables and assess appropriate type and amount of deflocculant.

(3) In the Al_2O_3-MgO castables, ultrafine calcined alumina is the key constituent dominating the flow behavior of the castables. Deflocculation is actually made mainly on alumina ultrafines. Among the four deflocculants, sodium polyacrylate (SPA), sodium hexametaphosphate (SHP), polyethyleneglycol (PEG) and melamine polymer (MP), PEG works the best and is used as the only deflocculant in the Al_2O_3-MgO and Al_2O_3-MgO-C castables. Its proper addition is 0.6% or so based on the dry matrix portion (< 0.074 mm).

(4) In-situ spinel formation in the castable starts from about 1000°C, thermal expansion reaches its maximum between 1240-1300°C when the samples are under 0.2MPa load, but 1350°C or higher without loading. More MgO addition leads to bigger expansion and lower strength. By controlling magnesia's size in the fine portion, 8-9% under 0.3 mm, excessive expansion leading to structural destruction can be avoided.

(5) Slag penetration increases with increasing MgO, which makes the erosion under dynamic condition also increase. Under the conditions in this work, when MgO addition becomes more than 6%, visible residual penetration appears, more pronounced when MgO reaches 12% and plus.

CHAPTER 7. INVESTIGATION AND ELABORATION OF Al_2O_3-MgO-C CASTABLES

Through the work reported in Chapter 6, Al_2O_3-MgO castables with a wide range of MgO content can be contemplated as starting castables for graphite incorporation. After graphite insertion, properties of the castables with 6-24% MgO and up to 6% C have been investigated, along a similar route as in Chapter 5. The results and interpretations are documented in this chapter, comparing the effects of PG and BAG with FG, correlating the properties with graphite inserting method, carbon content, MgO content and antioxidants package in terms of type, amount, combination and incorporating method. Slag resistance, oxidation resistance and their interdependence are emphasized.

7.1 Water Demand and Flowability

With flow values being controlled in between 170 and 200 mm, the water demand as a function of graphite content and inserting method is shown in Figure 7.1. It tells the same story as in the section 5.1 of Chapter 5. In the case of straight addition of FG, the flow value is ranked as the lowest. Even so, it requires the highest water addition, compared with adding PG or BAG at an equivalent or higher graphite level.

The water demand in weight percentage and in volume percentage respectively is further compared in Table 7.1. The latter is more meaningful to access the real water demand on a volume basis to enable the castable to flow well under vibration. It can be seen that

inserting graphite by PG or BAG rather than FG can significantly reduce water addition. This is attributed to the agglomeration of the graphite, with much less exposed surface that is strongly hydrophobic, when otherwise well dispersed.

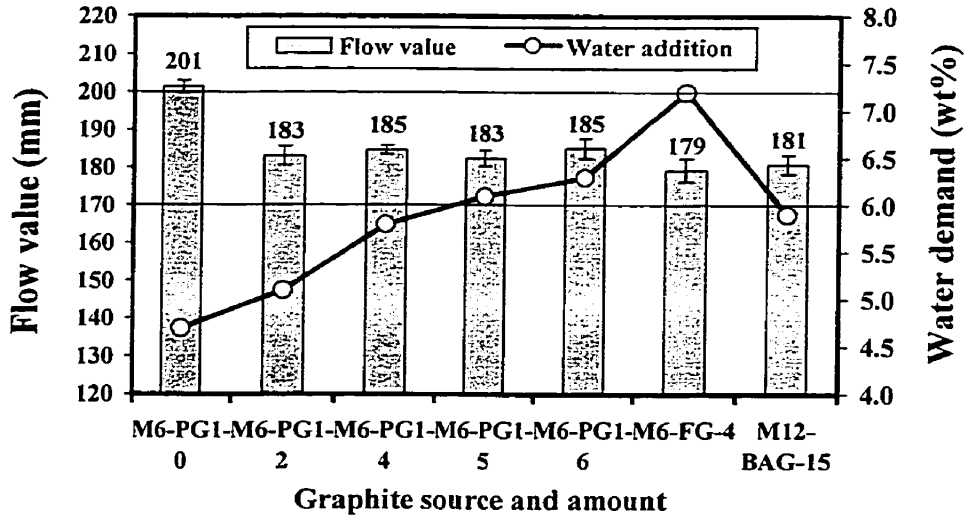

Figure 7.1 Water demand and flow value of the Al_2O_3-MgO- C castables vs. graphite content and inserting method.

Table 7.1 Water demand of the Al_2O_3-MgO- C castables to achieve a flow value of 170 –200 mm

	M6-PG1-0	M6-PG1-2	M6-PG1-4	M6-PG1-5	M6-PG1-6	M6-FG-4	M12-BAG-15
Wt. %	4.7	5.1	5.8	6.1	6.3	7.2	5.9
Index	100	109	123	128	134	153	126
Vol. %	14.7	15.2	16.5	17.0	17.2	20.3	16.8
Index	100	103	112	116	117	138	114

In one sense, making good castables is to strive to make compositions that can be placed under possibly minimum water addition to attain a possibly densest structure. Since the added water transforms to porosity upon heating, minimizing water addition becomes a challenge. The mechanism of the increase in water addition when adding FG powders can be schematically illustrated by Figure 7.2.

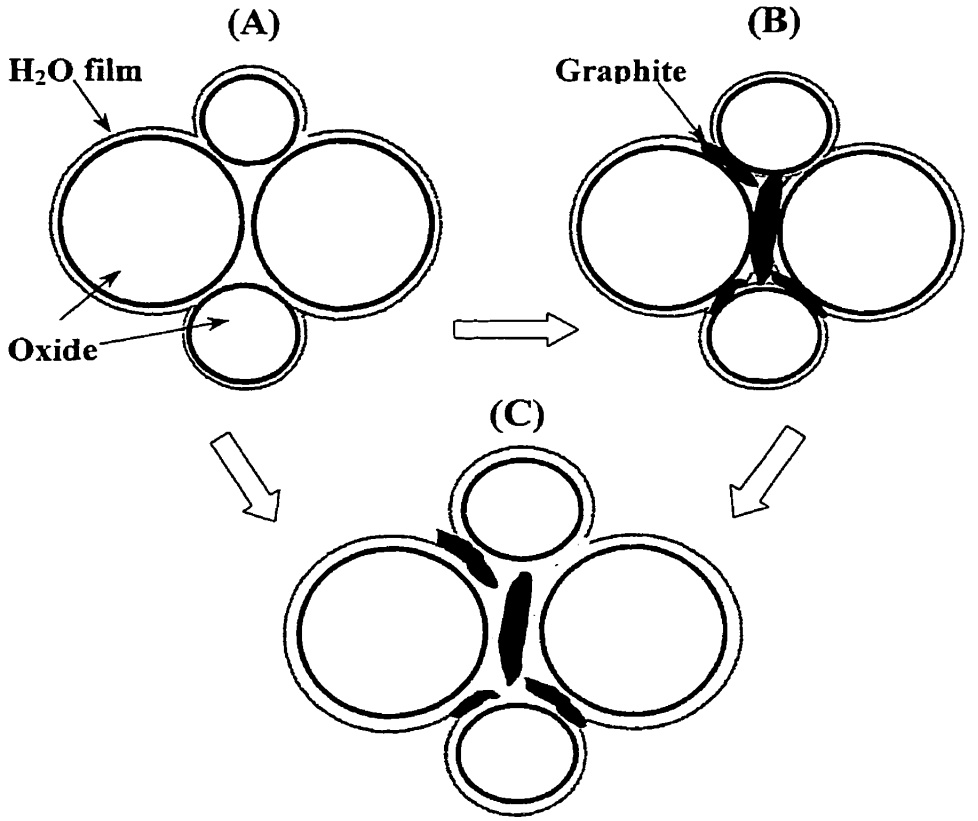

Figure 7.2 Schematic illustration of higher water demand due to FG dispersion.

To make a castable flow requires the particles being able to move relatively to one another, hence a water film on the particles or a flowable suspension of fine particles is needed. This can be established when the fine particles are well dispersed and the water

can thoroughly wet them, usually no problem in an oxide-water suspension system, as in the case of (A). In the presence of graphite, however, its non-wetting characteristic will disturb the water film-particle contact, when the oxide particles are in direct contact with graphite particles, as in the case of (B). To achieve an equal flow as without graphite, more water has to be used to force apart the oxide and graphite particles, as in the case of (C). This usually leads to water segregation during and after vibration and big pores in the castable.

7.2 Apparent Porosity and Bending Strength after Drying

By measuring AP and CMOR after drying at 110°C for 24h, we can access the compactness and the bonding strength of the castables. Figure 7.3 shows a very good linear relationship of both AP and CMOR with graphite content in M6-PG1-0~6 and in M6-FG-0~4 castables. Logically, increased graphite amount requires more water (see a detected proportional increase of water addition with graphite content in Figure 7.4), which consequently engenders higher porosity and decreased CMOR. By comparing PG with FG in Figure 7.3, it can be seen that at about 4% graphite content, the strength of M6-FG-4's is only about half of M6-PG1-4~5's, also significantly lower than M6-PG1-6's, which brings about 5% net FG in the castable! This fact indicates once again that highly dispersed graphite powders would impede the bonding of the matrix. Higher water addition, consequently more and bigger pores, accounts of course also for the significantly lower strength.

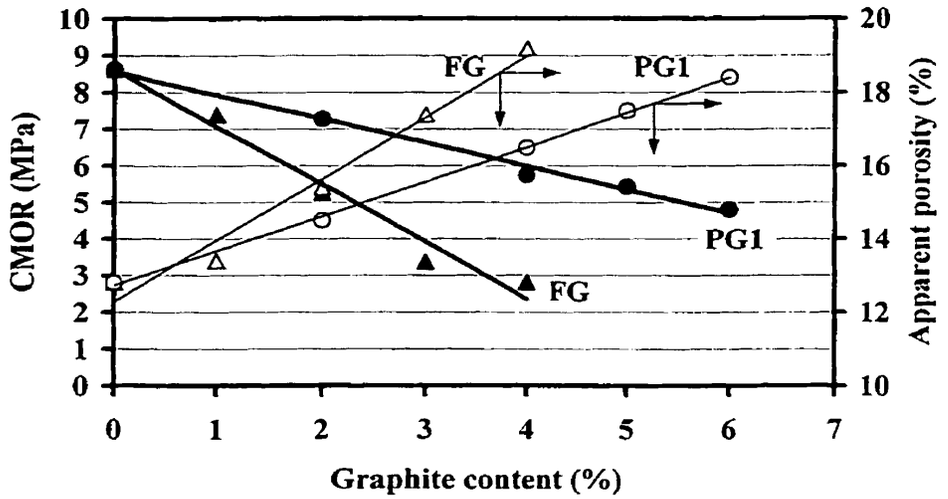

Figure 7.3 CMOR and AP as a function of graphite content by FG or PG1.

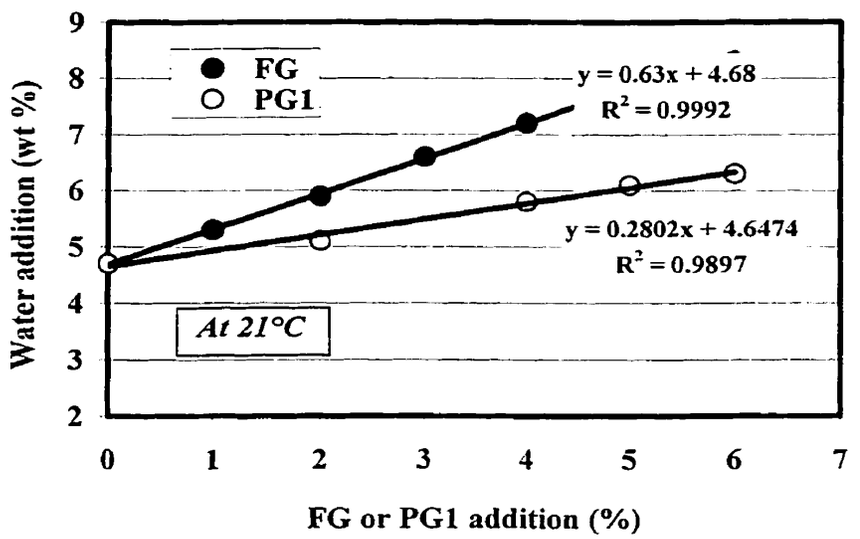

Figure 7.4 Water addition as a function of FG or PG1 content in the Al_2O_3-MgO-C castables.

7.3 CMOR and HMOR

Two series of castable samples have been prepared for CMOR testing, i.e., samples without adding extra antioxidant except for that encapsulated in PG or BAG, and samples with addition of the four antioxidants individually or in a combination, as coded in Table 7.2. For any specific sample, the used notation tells its composition, as explained in 4.3.2 of Chapter 4, p.74-76.

Table 7.2 Four types of antioxidants directly added into the castables

Antioxidant	Addition (%)	Code
Silicon (Si)	1 or 3	A1 or A3
Silicon carbide (SiC)	3	B3
Boron carbide (B_4C)	1	C1
Zirconium diboride (ZrB_2)	1	D1

CMOR data for the samples after drying at 110°C for 24h, firing at 1000°C for 5h and 1500°C for 5h with coke protection respectively are presented in Figure 7.5, Figure 7.6 and Table 7.3. As for the Al_2O_3-SiC-C castables, Figure 7.5 clearly indicates that inserting graphite in Al_2O_3-MgO-C castables by PG or BAG confers also higher strength than by FG. Figure 7.6 manifests that CMOR after 1000°C and 1500°C decreases as MgO increases, following the same tendency as in Al_2O_3-MgO castables, as a result of increased spinel formation, see 6.2 of Chapter 6.

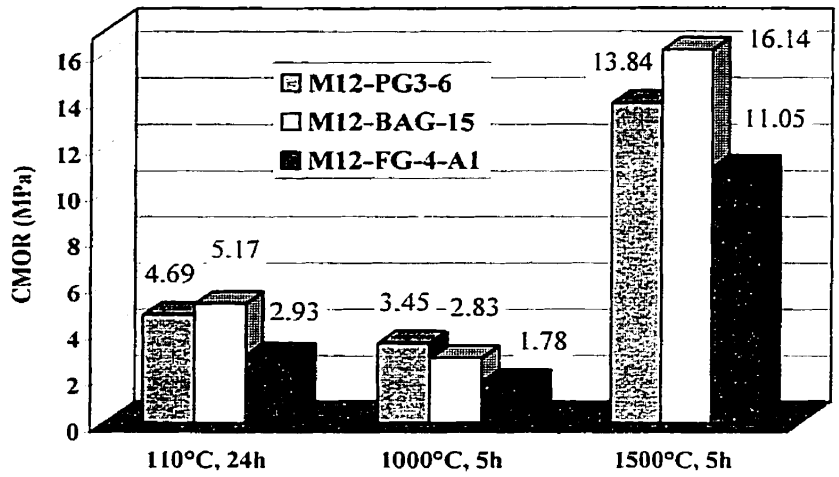

Figure 7.5 CMOR vs. the method of incorporating graphite (with constant MgO at 12%, 4-5% graphite is introduced via 3 methods respectively).

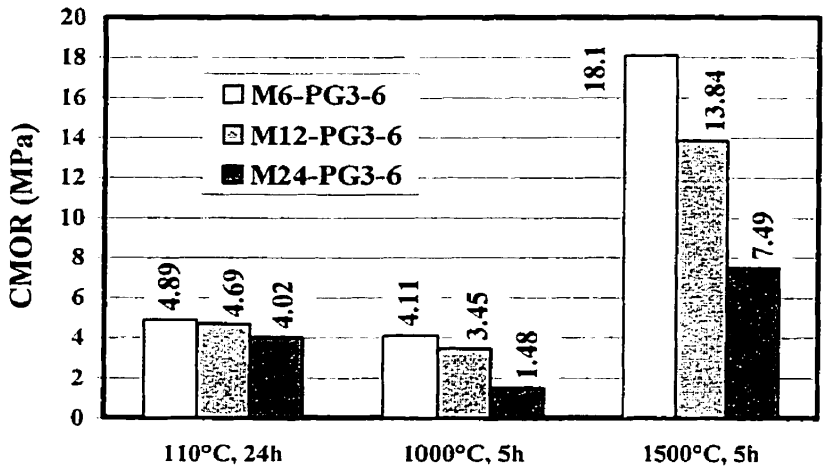

Figure 7.6 CMOR vs. MgO content in the castables (with constant PG3 addition at 6%, MgO varies from 6 to 24%).

The effects of antioxidants on oxidation resistance will be covered in 7.5 of this chapter, but they have also impact on strength. From Table 7.3 it can be seen that boron bearing additives, added either directly in the castable or in PG, help increase the

intermediate temperature(1000°C) strength, but not that after firing at high temperature(1500°C), comparing (3) ~ (6) with (1) ~ (2). Higher level of metallic additive, either in PG or directly in the castable, help enhance the strength fired at both intermediate and high temperatures, comparing (2) with (7), and (1) itself with two levels of Si addition. These phenomena will be interpreted later when oxidation resistance is dealt with.

Table 7.3 CMOR data of the samples added with extra antioxidant(s)

Specimen	110°C, 24h	1000°C, 5h	1500°C, 5h
(1) M12-PG2-5.5-A1(3)	4.80 (4.76)	2.11(3.52)	14.80 (17.91)
(2) M12-PG2-5.5-B3	4.66	1.98	13.71
(3) M12-PG2-5.5-C1	4.29	8.40	13.10
(4) M12-PG2-5.5-D1	4.28	5.25	11.05
(5) M12-PG5-6	4.65	7.89	9.83
(6) M12-PG6-6	4.20	4.92	9.76
(7) M12-PG3-6-B3	5.59	2.60	16.37
(8) M12-PG3-5-AG1-A1B3	4.56	2.71	12.85
(9) M12-FG4-A1	2.93	1.78	11.05

HMOR is tested on limited samples with 12% MgO and 4-5% graphite at 1400°C, when the in-situ spinel formation is still intensive. It is not out of the expectation that the HMOR values at this temperature are not so high. Nevertheless, the influence of graphite inserting method is pronounced, see Figure 7.7, the value of the sample with FG being only one third of those with PG3 or BAG. As contrasted to the effect on CMOR, adding

SiC in M12-PG3-6 castable appears unfavorable to HMOR. While adding Si has been found beneficial to HMOR.

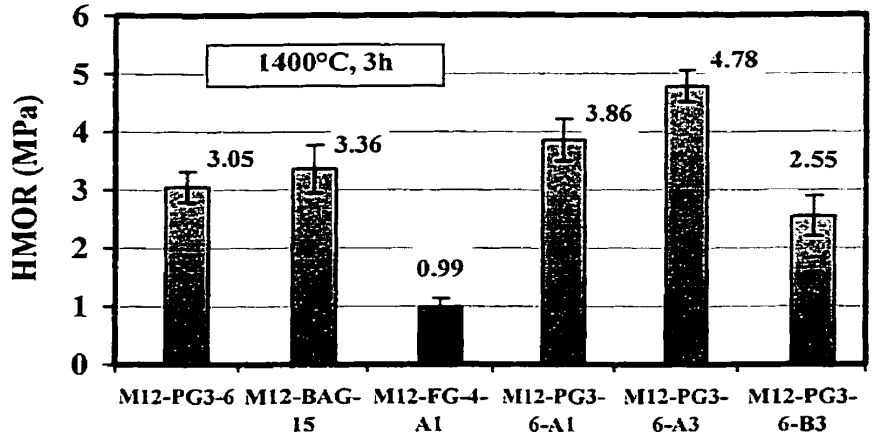

Figure 7.7 HMOR vs. incorporating graphite method and antioxidant addition.

7.4 Permanent Linear Change

PLC data of the measured samples after 1000°C for 5h and 1500°C for 5h are listed in Table 7.4. After drying at 110°C, the linear change of all the samples is around – 0.05%, excluded in the table.

As shown in Table 7.4, for all the graphite containing samples fired at 1500°C, the expansion is dramatically larger than that of M6-24 samples, especially with the presence of the boron bearing additives, see (8) ~ (11) in Table 7.4. This phenomenon, to be also interpreted later by microscopic analysis, is because:

1) To some extent, the graphite obstruct the contact between Al_2O_3 and MgO and their mass transition during solid reaction, thus intensive spinel formation has to occur at a

higher temperature; otherwise sintering, which is also obstructed in some way by graphite, would have led to some shrinkage to compensate expansion;

2) With the presence of liquid derived from the boron bearing additives, the mass transition is promoted, and the CA_6 and spinel crystals are more developed at higher temperature; and

3) MgO, even coarse grains, is reduced by carbon to Mg vapor which spreads and reacts with Al_2O_3 to form spinel, wherever the Mg vapor condenses.

Table 7.4 PLC of the measured Al_2O_3-MgO-C castables

Specimen	1000°C, 5h	1500°C, 5h
(1) M6-PG3-6	-0.03	+ 2.42
(2) M12-PG3-6	-0.02	+ 3.28
(3) M24-PG3-6	+0.19	+ 4.08
(4) M12-BAG-15	- 0.01	+ 2.38
(5) M12-FG4-A1	+ 0.01	+ 2.17
(6) M12-PG2-5.5-A1	- 0.01	+ 2.27
(7) M12-PG2-5.5-B3	+ 0.03	+ 2.88
(8) M12-PG2-5.5-C1	+ 0.31	+ 3.80
(9) M12-PG2-5.5-D1	+ 0.25	+4.24
(10) M12-PG5-6	+ 0.33	+ 3.83
(11) M12-PG6-6	+ 0.22	+ 3.71
(10) M12-PG3-6-B3	-0.03	+ 2.57
(11) M12-PG3-5-AG1-A1B3	+ 0.04	+ 2.48

Synergistically, these factors have resulted in a big PLC after 1500°C. This engenders an important issue deserving scrutiny into what a PLC would be tolerable for practical use.

According to literature[17-20,28,47,52], PLC for ladle castables varied from less than +0.5% to more than +2%, depending on different materials and specific application circumstances. In this work, PLC after firing at 1500°C for the developed Al_2O_3-MgO-C castables is provisionally controlled under +2.5%.

7.5 Oxidation Resistance

For oxidation test, the carbon content is controlled at 5% in all the samples except for M6-FG-4, by carefully adjusting PG and BAG additions, which are not anymore to be specified in the denotations.

By simply a visual observation, as shown in Figure 7.8, it is clear that inserting anti-oxidants into PG is definitely necessary to protect the graphite from oxidation. Mixing the antioxidants in close vicinity of the graphite, as in the case with pelletized graphite, confers a measurable advantage.

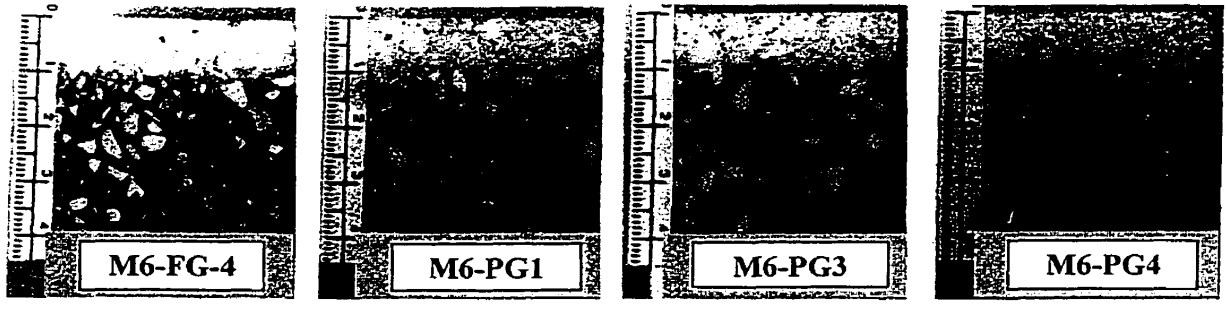

Figure 7.8 Oxidation resistance comparison between FG and PG added samples (1400°C for 3h in flowing air).

At a constant addition of 6% PG3, varying in MgO content from 6 to 24% doesn't show detectable influence on oxidation degree by visual observation, see Figure 7.9.

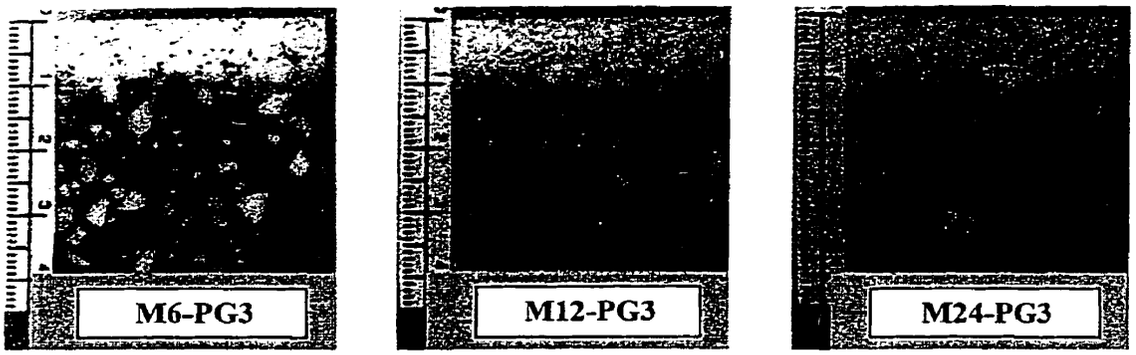

Figure 7.9 Oxidation resistance comparison among 3 levels of MgO addition (1400°C, 3h in flowing air).

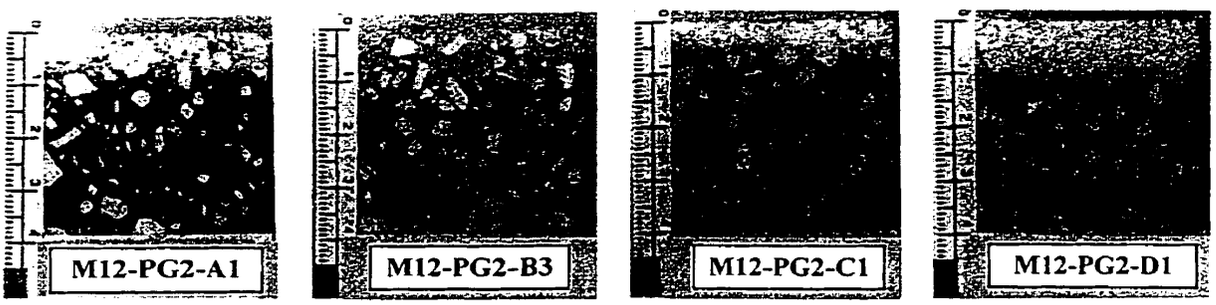

(1200°C, 3h in flowing air)

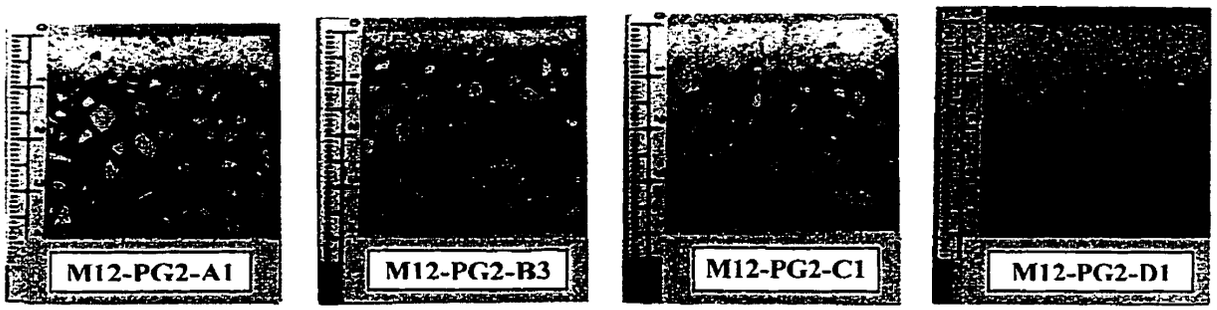

(1400°C, 3h in flowing air)

Figure 7.10 Oxidation resistance comparison among four types of antioxidants.

With respect to antioxidant type, they don't follow a same merit of order at different temperature, as compared in Figure 7.10. At 1200°C, B_4C is the best, followed by Si > SiC > ZrB_2; whereas at 1400°C, SiC becomes the best, followed by Si > B_4C > ZrB_2. Note, SiC addition is greater than the others, 3% vs. 1%. In both cases, ZrB_2 is the worst.

Inserting B_4C and ZrB_2 respectively into the micropellets, as PG5 and PG6 respectively, to replace silicon powders doesn't show any positive effect, as manifested by Figure 7.11. The mechanism remains unclear.

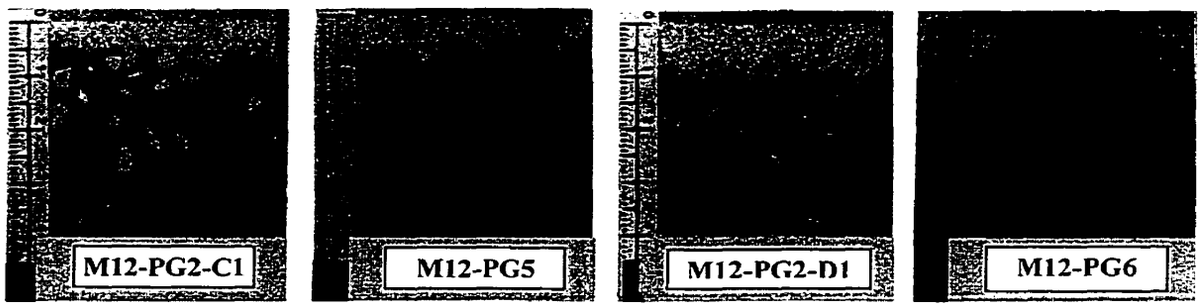

(1200°C, 3h in flowing air)

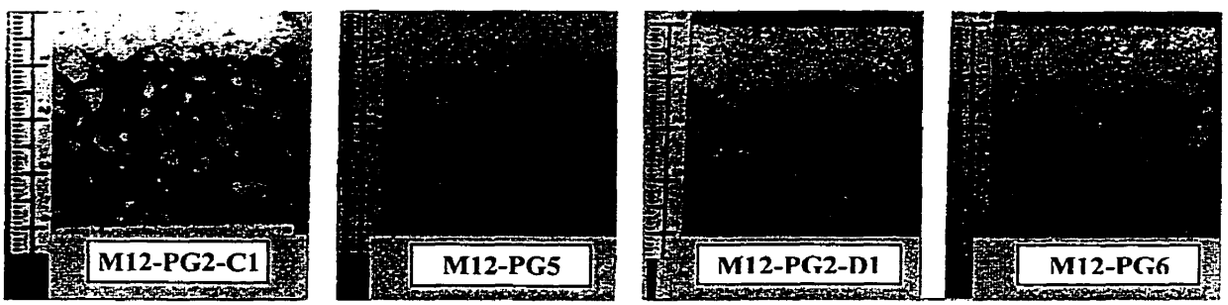

(1400°C, 3h in flowing air)

Figure 7.11 Oxidation resistance comparison between B_4C and ZrB_2 bearing samples.

To achieve good anti-oxidation effect, incorporating suitable antioxidants (so far Al, Si

and SiC; the boron compounds as dominant antioxidants have to be avoided) both into PG or BAG and into the castable is necessary. This has been shown to be effective by oxidation test at 1600°C and by rotary slag test, referring to sample M12-PG3-5-AG1-A1B3 in next section. The sectioned samples after the oxidation test are shown in Figure 7.12. Numerically they are compared by decarbonized area and depth in Figure 7.13.

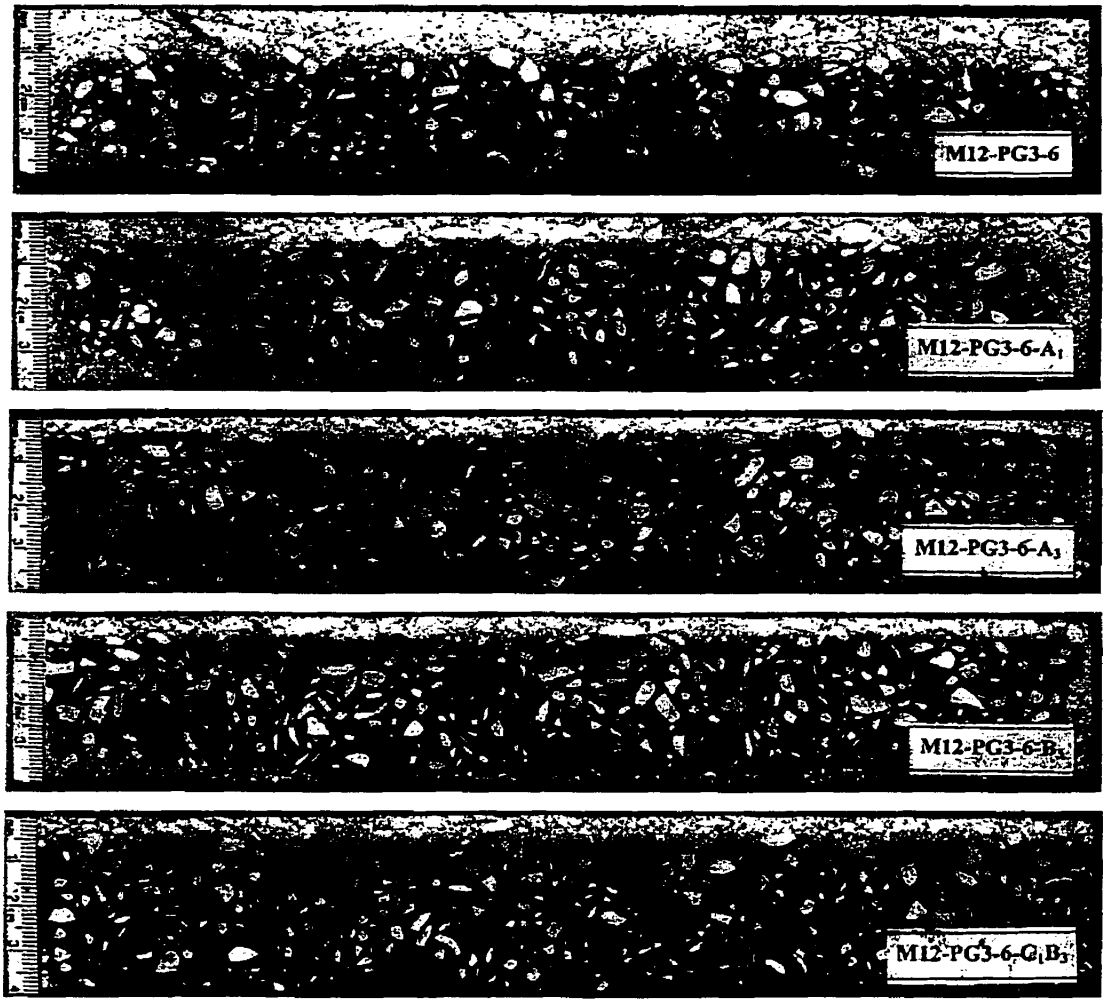

Figure 7.12 Oxidation resistance vs. antioxidant type and addition in the samples with 12% MgO and 6% PG3, at 1600°C for 5h by rotary furnace method.

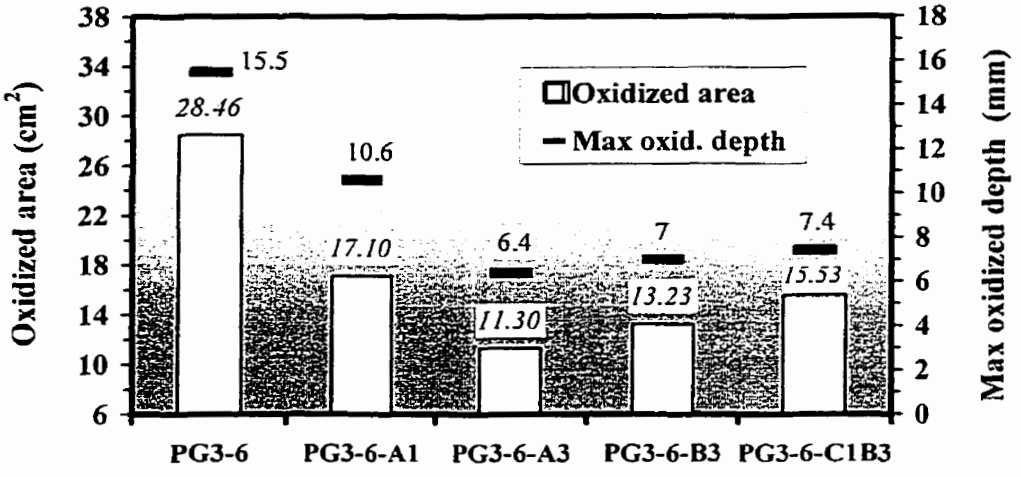

Figure 7.13 Oxidation resistance comparison by decarbonized area and depth (1600°C, 5h, rotary furnace method).

As revealed by Figure 7.12 and Figure 7.13, the level of Al and Si antioxidants encapsulated in PG3 is not enough to well inhibit the oxidation; by adding 3% Si or SiC into the castable, a noticeably improved anti-oxidation has been attained. But at lower temperature (1200°C) Si and SiC do not work as effective as at high temperature (above 1400°C). That is why on the back face, oxidation at lower temperature does have been observed, whereas in M12-PG3-6-C1B3 sample, this phenomenon does not appear at all, though the decarburization on the hot face is slightly higher than M12-PG3-6-A3's and M12-PG3-6-B3's, indicating that B_4C contributes to lower temperature anti-oxidation.

In order to prevent oxidation of carbon containing shaped refractories, metallic additives (such as Al, Si, Mg and their alloys), carbide (e.g., SiC) and boron based compounds (such as B_4C, ZrB_2 etc.) have been used[101-107]. A lot of research work has been done mainly on carbon bonded bricks, MgO based basic bricks in particular. The evolution of

these additives to be effective follows different paths to protect the carbon. Metallic and carbide additives act as CO(g)-reducing agent, reducing CO(g) to C(s), thus compensating carbon loss. The formed oxides bring about a densification effect due to volume expansion. They can also improve hot strength by forming whiskers and high-temperature ceramic bonds[101-103]. The roles of metal additives in Al_2O_3-C refractories are similar to those in MgO-C ones, acting to retard carbon oxidation and increase hot strength[106]. Boron bearing compounds act to block or seal open pores to reduce carbon oxidation by forming protective liquid layer of B_2O_3 or B_2O_3-metal oxide, which, however, lowers hot strength[104,105,107].

Boron carbide as an antioxidant is the most thoroughly studied of all boron compounds. B_4C, often in combination with metal powders or SiC, has been proven particularly effective for anti-oxidation in a variety of graphitic bricks. However, this work has shown some disparity in this aspect, referring to Figures 7.10 and 7.11. This is believed to relate to a different internal environment inside the castable, featured by more porous, non-carbon bonded and lower levels of carbon and MgO, for them to play their role in association with particular surroundings, when compared with carbon bonded bricks. Being wrapped in the pellets, they have poor accessibility of oxygen and MgO, and can less possibly be converted to B_2O_3(l) and MgO-B_2O_3 liquid via oxidation at low temperature under 1000°C and reacting with MgO[104,105]; even formed liquid, as have been reflected by higher intermediate temperature strength, it would be not enough to block the relatively more and bigger pores than in bricks. Another cause may be that

the derived $B_2O_3(l)$ is highly volatile, it may easily vaporize along the micro- or even macro-channels at elevated temperatures.

No published work has been found performed on the anti-oxidation mechanism in such Al_2O_3-MgO-C castables, using such antioxidants, nor can this work itself at this stage bring an insight into the real mechanism. It deserves to be an another research subject.

The work so far performed reveals that to improve oxidation resistance and strength, there is a big space to play with the antioxidant package in terms of their type, quantity, combination and incorporation mode. For graphitic castables, some related mechanisms and understandings do need to be established by in-depth work.

7.6 Slag Resistance

Slag resistance of the castables is compared by eroded area and depth from the original surface of the specimen after rotary slag test. Advantages of this particular method include that multiple specimens can be tested in one run, temperature gradient in the specimens, constantly renewed slag and mechanical wear, all interacting synergistically, help simulate practical working conditions when the castables are in service.

As reviewed in 2.2 of Chapter 2, slag penetration in the Al_2O_3-spinel (MgO) castables is a big issue. For the purpose to obtain very significant results, a highly ferrous steel-making basic slag (CaO/SiO_2 = 3.14 wt. ratio) has been chosen for the rotary slag test. Its chemical analysis is given in Table 7.5.

Table 7.5 Chemical composition(%)of the slag for rotary slag test

CaO	SiO_2	Fe_2O_3*	MgO	Al_2O_3	MnO	TiO_2	Na_2O	P_2O_5	Cr_2O_3
41.40	13.20	25.90	9.80	2.90	6.50	1.00	< 0.10	0.61	0.34

* Total Fe calculated as Fe_2O_3. 13.1% FeO and slight amount of metallic iron have been detected.

Three runs of rotary slag test, each consisting of 6 samples, have been conducted to investigate the following items:

In the 1st run:

1) The effect of carbon content from 0 to 6% PG3 additions in M6 series of castables.

2) The influence of MgO addition in the castables with constant 6% PG3 addition.

In the 2nd run:

3) Slag resistance vs. graphite incorporating method, comparing M12-PG3-6-A1 and M12-BAG-15 with M12-FG-4-A1.

4) The interdependence between oxidation resistance and slag resistance. Improved oxidation resistance should lead to better slag resistance, for which Si and/or SiC antioxidants are added in the samples with 12% MgO and equivalent carbon content from PG3 or BAG, which gives at least 4% net flake graphite to compare with straight addition of 4% FG in M12-FG-4-A1. For the purpose of preventing pre-oxidation during heating up before slag charging, samples in the 2nd run are painted on the hot face with a protective coating (its composition is given in Annex 7.6), 0.3-0.4 mm in thickness, to

inhibit the decarburization during the heating up process. It may otherwise facilitate the initial oxidation to form a porous decarbonized layer, thus less comparable to the carbon free samples.

In the 3rd run:

5) The contribution of improved oxidation resistance to the slag resistance, using the relatively optimized samples selected from the oxidation test.

6) The performance of the castables using the PG3/a~c micropellets, containing 7, 17 and 26% Al_2O_3 respectively and accordingly less graphite in the pellets, in comparison with PG3, under same volume based addition, equivalent to 5 wt.% PG3, other things being equal: 12% MgO, 1% AG, 1% Si, 3% SiC and 6.1% water addition. The samples are also painted on the working face with the above mentioned anti-oxidation coating.

As shown in Figure 7.14 for series 1, with the presence of graphite, almost no penetration trace is visible to the naked eyes. The erosion, however, is unexpectedly rather high, being reduced a little by increased PG3 addition, or higher level of carbon content. MgO addition between 6% and 12% makes little difference, but a big difference appears when it is as high as 24%. This is reasonably in connection with the less volume stability due to in-situ spinel formation at higher level of MgO, as reduced strength has been observed.

Under some magnification at the hot face, it is found that the attacked face of the graphitic samples is saw-like, not uniformly torn off by the slag like in the case of M6's.

This implies that some aggregates have been washed away, instead of being evenly eroded. In addition, the role in preventing slag intrusion by the graphite exhibits itself insignificantly. The results from the 1st run of slag test seem to be less encouraging.

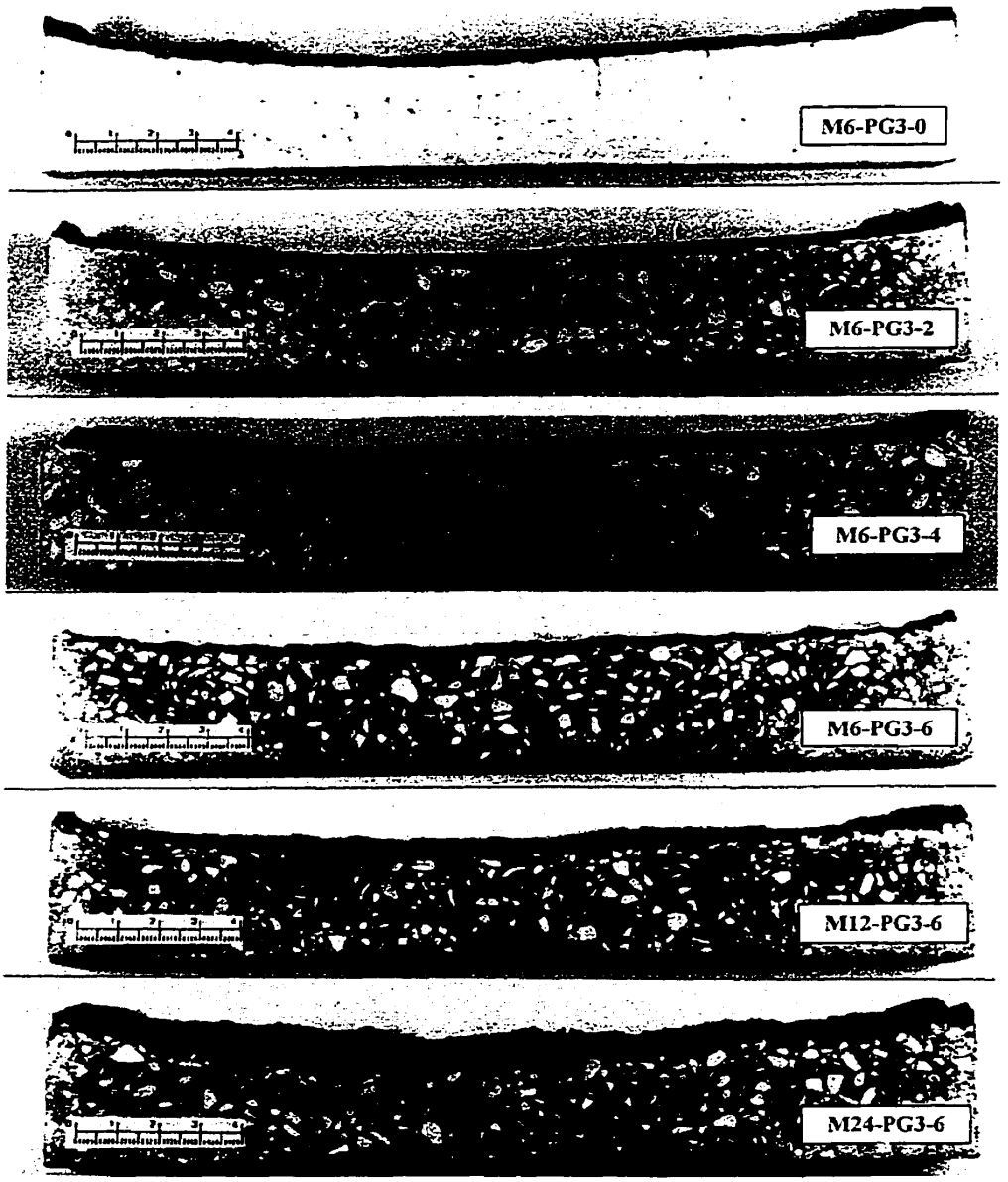

Figure 7.14 Sections of the samples in series 1 after rotary slag test at 1600°C for 8h.

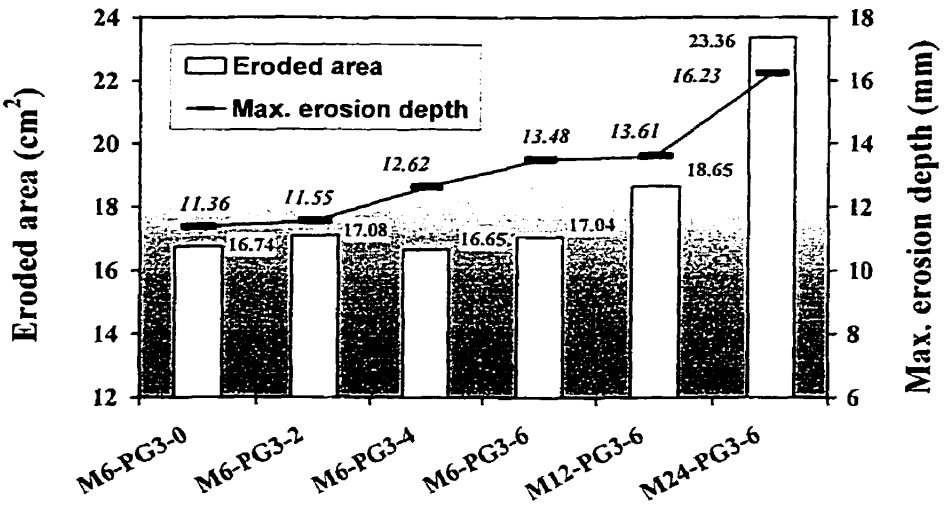

Figure 7.15 Eroded area and maximum erosion depth of the samples in the 1st run of rotary slag test at 1600°C for 8h.

It is believed that these rather discouraging results are attributed to the oxidation during heating up and slag attack process, leading to aggregates pulling-out in the decarbonized zone. The key is to prevent the carbon from oxidation as much as possible. Indeed, this is clearly shown in series 2 test.

Much improved slag resistance have been achieved, comparing Figure 7.16 with Figure7.14, by taking the anti-oxidation measure as aforementioned. There is a measurable difference with the same M12-PG3-6 sample, between the 1st run and the 2nd run, 18.65 cm^2 vs. 17.13 cm^2 in eroded area, and 13.61 vs. 10.30 mm in the maximum eroded depth, thanks to the protective coating on the hot surface and the antioxidants. By using simultaneously A and B, and substituting 1% of PG3 by AG, much better slag resistance has been attained, as indicated by Figure 7.17.

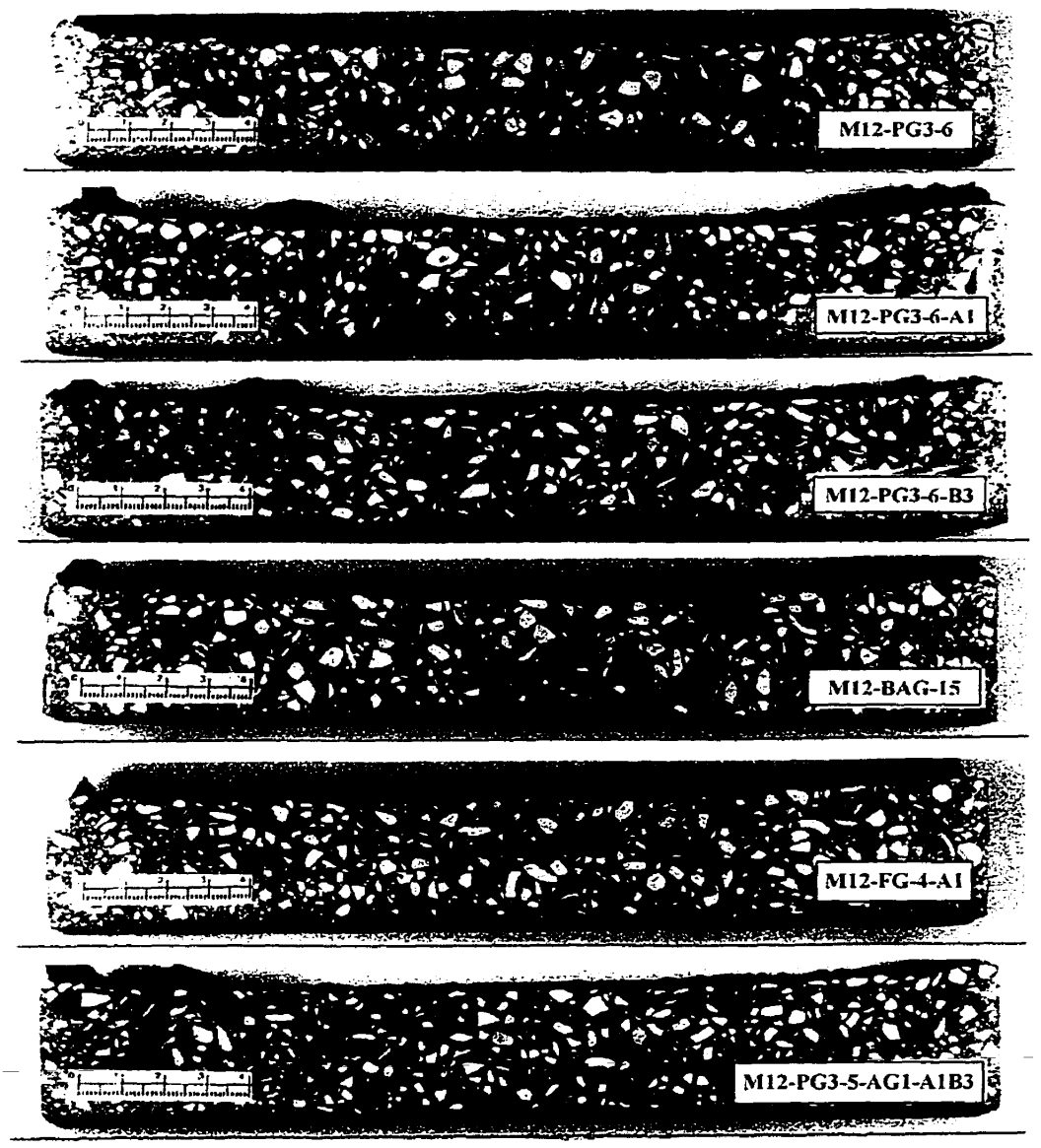

Figure 7.16 Sections of the samples in series 2 after rotary slag test at 1600°C for 8h.

As can be seen, M12-FG-4-A1 is not that bad in slag resistance, though its density and strength are being the lowest. This implies that oxidation resistance seems to be more vital to the slag resistance, in other words, slag resistance depends strongly on oxidation

resistance. So long as the graphite is retained in the castable, a good slag resistance can be ensured, a big issue worth a scrutiny for graphitic castables!

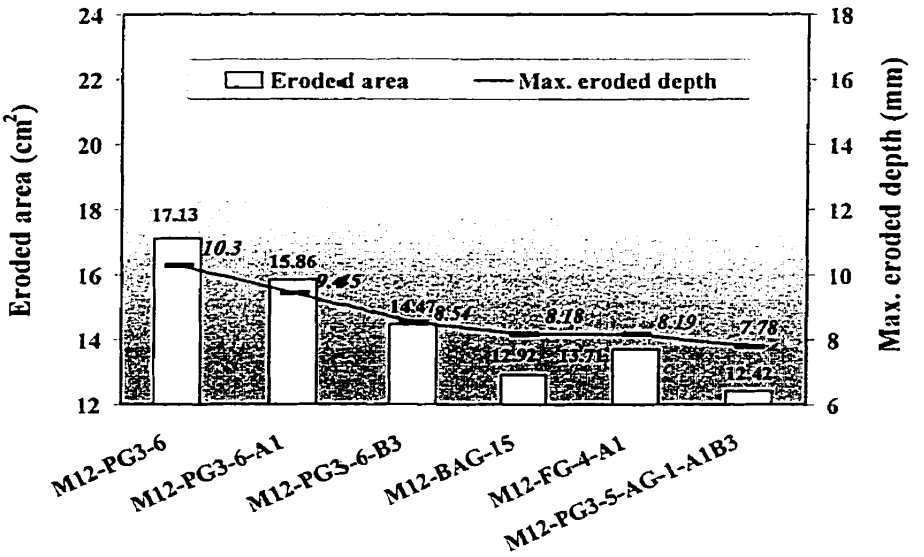

Figure 7.17 Eroded area and maximum erosion depth of the samples in the 2nd run of rotary slag test at 1600 °C for 8h.

The sections of the samples after the 3rd run of rotary slag test are shown in Figure 7.18, and their numerical comparison in eroded area and depth is presented in Figure 7.19. As seen, all, except for the PG3/c containing sample, show good slag resistance. Their difference is less than 10%, ascribing to their good oxidation resistance.

Interestingly, PG3/a and PG3/b are competitive with PG3 in slag resistance. From the inhibiting slag penetration point of view, the amount of carbon in castables is not necessarily to be the higher, the better, against the previously accepted belief. Even in

the graphite based micropellets, the graphite can be replaced to some extent by alumina powders to show an equal resistance to slag attack.

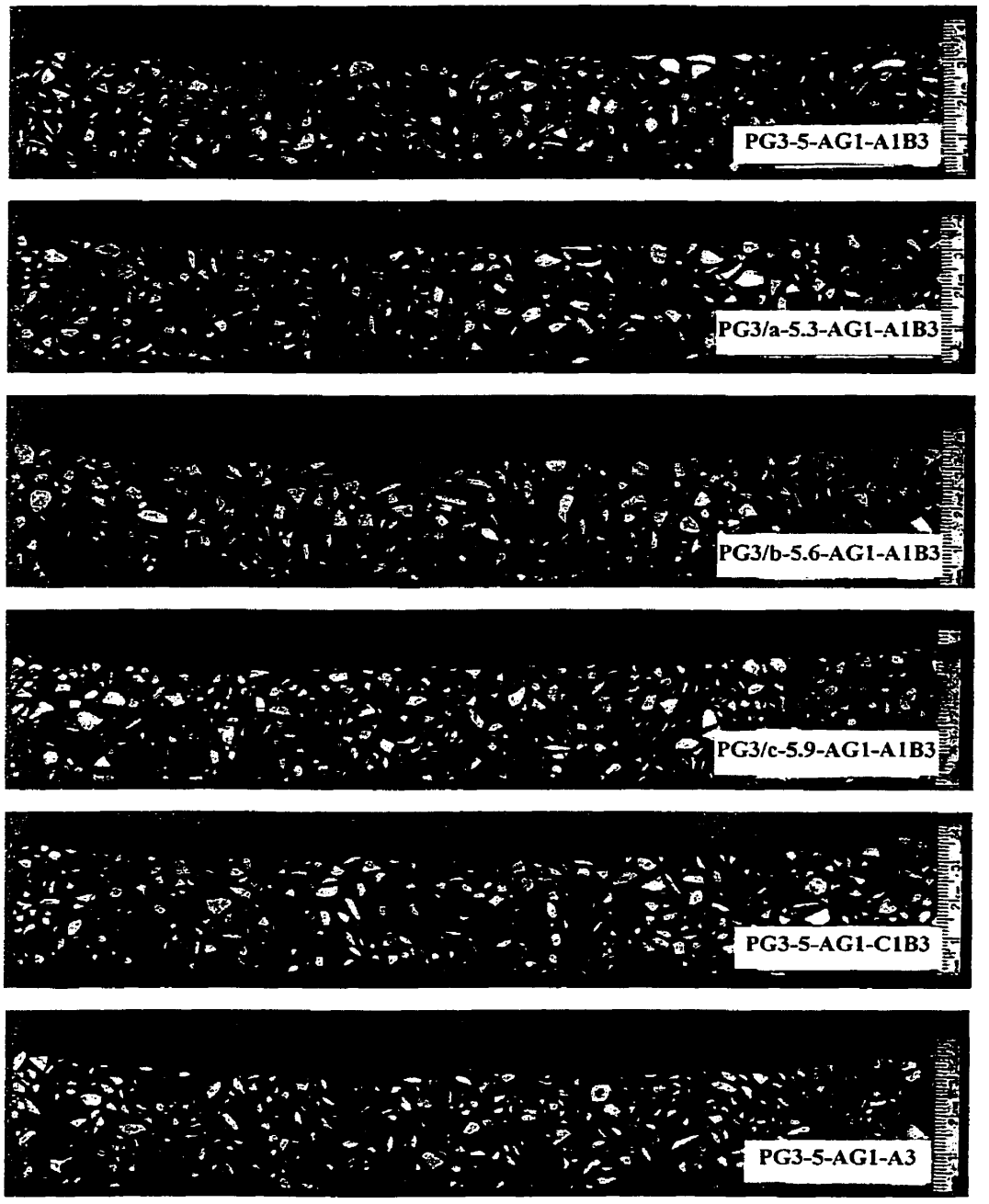

Figure 7.18 Sections of the samples in series 3 after rotary slag test at 1600°C for 8h.

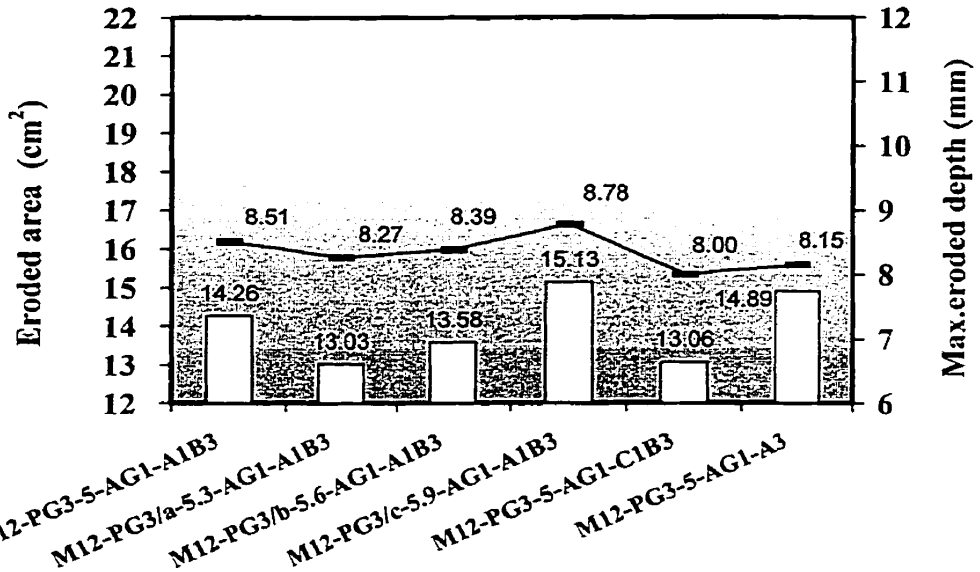

Figure 7.19 Eroded area and maximum erosion depth of the samples in the 3rd run of rotary slag test at 1600°C for 8h.

Another phenomenon worth attention is that in some carbon free samples the test vertical or parallel cracks have appeared, see Figure 6.22 and Figure 7.14, while none appeared for the graphite containing samples, see Figures 7.14, 7.16 and 7.18, a good sign of improved resistance to thermal and structural spalling brought about by graphite addition.

7.7 Microscopic Examination

Microstructural analysis by means of SEM and EDAX have been pursued on selected samples after heat treatment, oxidation test and rotary slag test to help reveal some mechanisms relating to anti-oxidation and slag resistance.

7.7.1 Analysis on the Heat Treated Castables

Figure 7.20 shows the microstructure of M12 sample fired at 1350 and 1500°C respectively. At 1350°C, in-situ spinel has been massively formed in the matrix, but not yet well developed, and the matrix texture looks loose, see (a), corresponding to the maximum expansion around this temperature. Extensive needle-like calcium hexaluminate (CA_6) phases mixed with some CA_2 are seen, especially on the boundary of corundum grains, see (b). CA_6 is known to form at temperatures above 1300°C in CA

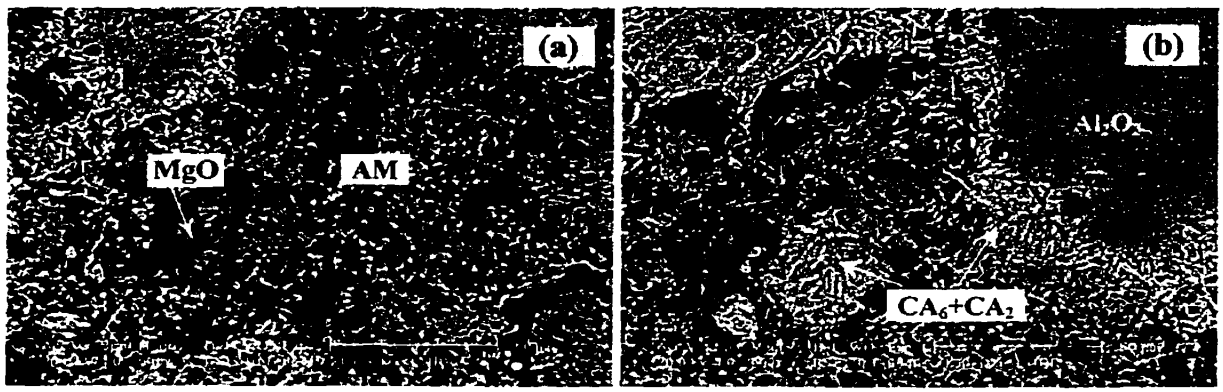

(1350°C, 5h in air)

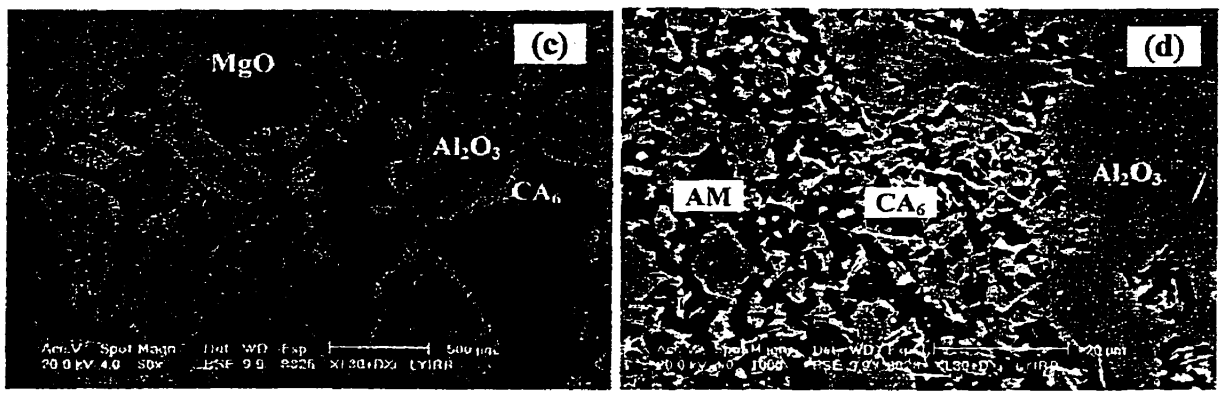

(1500C, 5h in air)

Figure 7. 20 SEM micrograph of M12 specimen after 1350°C and 1500°C.

bonded system[108]. At 1500°C, the significant difference is the progress of CA_6 penetration into Al_2O_3 grains. At lower magnification, CA_6 rims can clearly been seen, as shown in (c). Most of the CA_6 is close to the alumina surface, forming a network structure, see (d). Meanwhile spinel is more developed, forming a continuous net structure of spinel-rich matrix. Such a texture imparts the castable with a high strength.

The microstructure of M12-PG2-5.5-C1 specimen heated at 1500°C, for 5h in graphite breeze is shown in Figure 7.21 (a)~(e). Compared with Figure 7.20 (c) and (d), the CA_6 and spinel developed more thoroughly, see (b). It shows evidence that liquid derived from B_4C has promoted the crystal growth.

An interesting finding is that some big vacancies that take the shape of magnesia grains remain in the sample, see (a) and (c). It is deduced that MgO under such circumstances was reduced to Mg(g) by the carbon. The Mg(g) was later oxidized to MgO (g) and deposit preferably where alumina was available to react with it to form spinel, featured by uniform and dense texture. Pictures (d) and (e) provide an evidence for such mechanism. The dense spinel rim on the CA_6 rim around a alumina grain should be the reaction product between the deposited Mg(g) and Al_2O_3. In other samples, to be shown later, it is also found where there is such a cavity, nearby there is such a dense spinel rim. Within the micropellets, many fine spinel grains are included, confirmed by EDAX analysis, see (f). They can impossibly be formed through solid or liquid reaction. Only gaseous Mg can get inside of the PG. Such a featured microstructure may explain the high PLC due to strong expansion at this temperature.

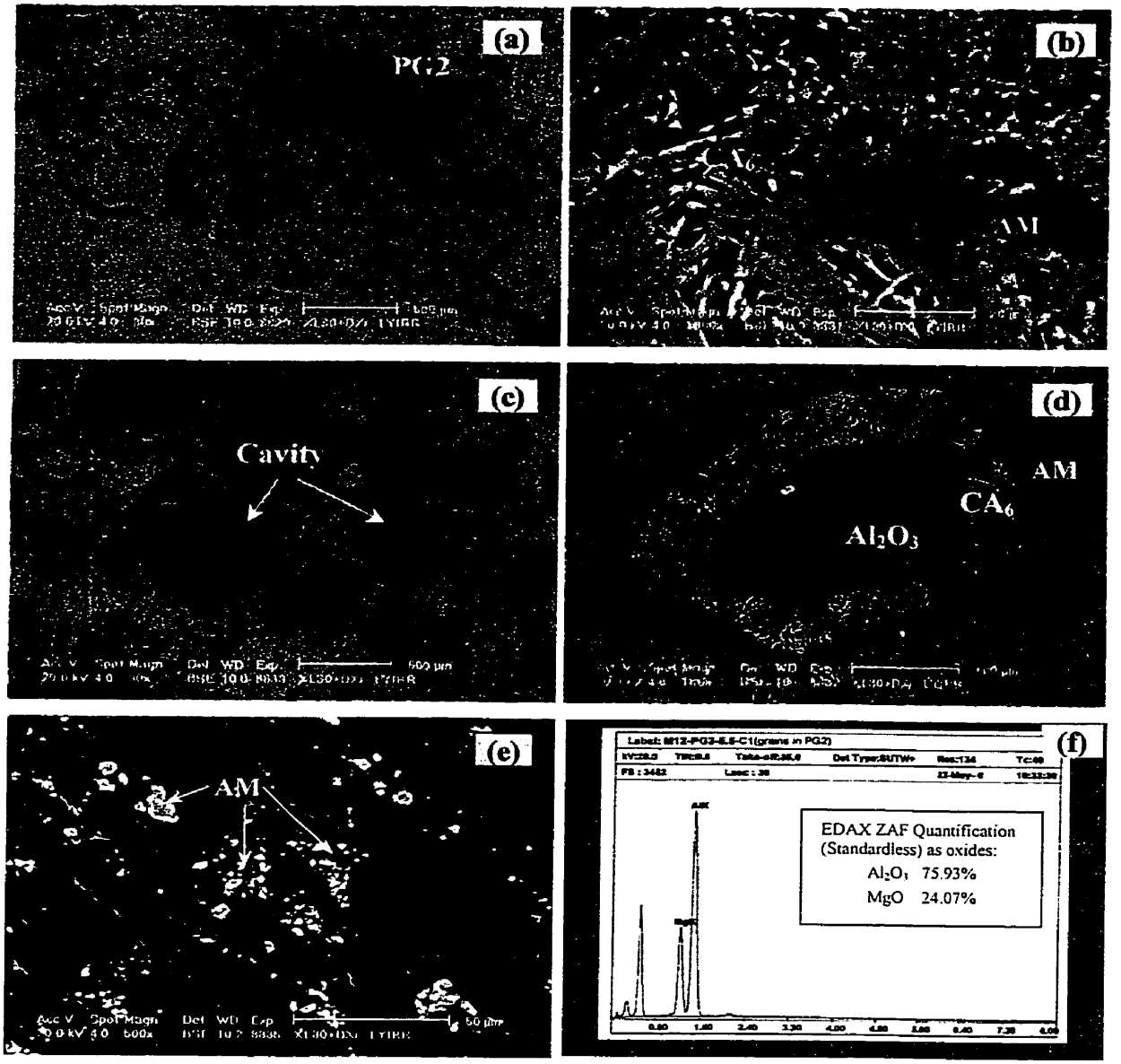

Figure 7.21 SEM micrograph of M12-PG2-5.5-C1 specimen heated at 1500°C for 5h in graphite breeze.

7.7.2 Analysis on the Castables after Oxidation Test

In Figure 7.22 (a) ~ (d), the microstructure of the M12-PG2-5.5-A1 sample, after the unidirectional oxidation test at 1400°C for 3h, is characterized.

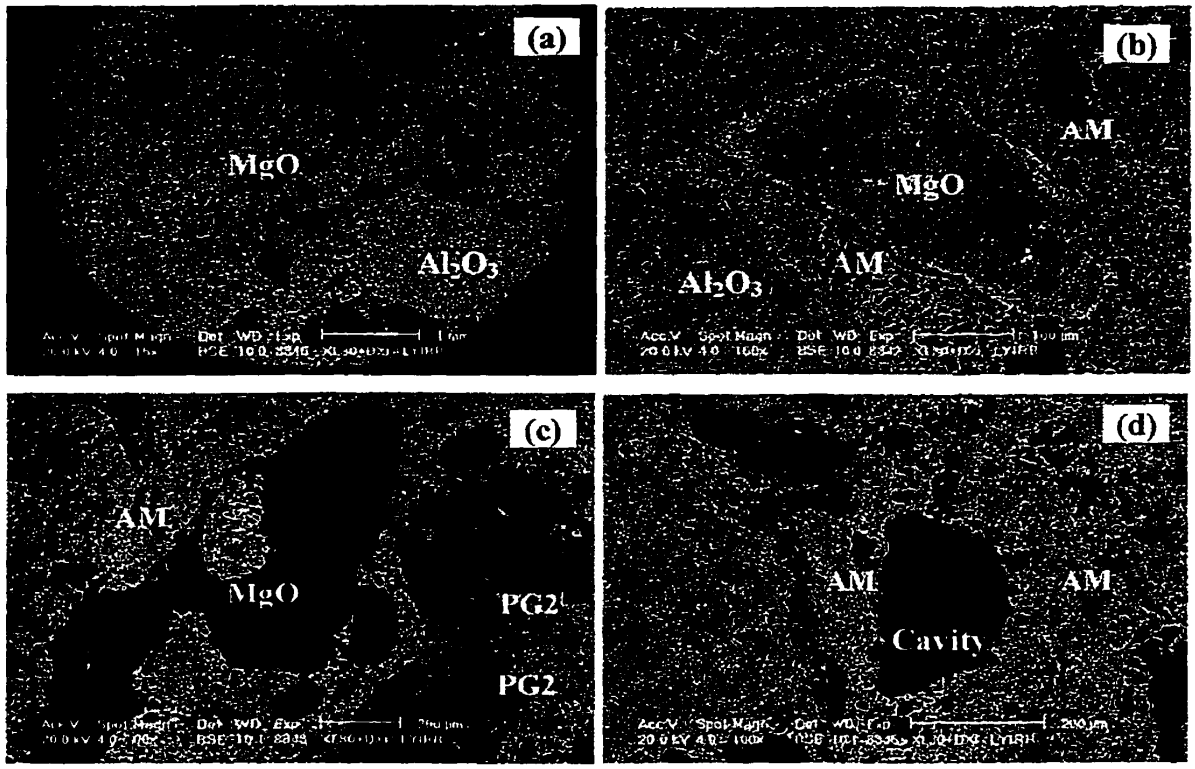

Figure 7.22 SEM micrograph of M12-PG2-5.5-A1 specimen after the unidirectional oxidation test at 1400°C for 3h in flowing air.

In the decarbonized zone, Figure 7.22 (a) and (b), PG2 pellets have been burnt out and left cavities with PG2's shapes; the unreacted MgO grains are detectable, see (a). On the surface of MgO grain, a silicate ring is formed, as shown in (b). Outwards, the brighter rim is CaO enriched. This indicates that CaO derived from cement and SiO_2 derived from Si together with MgO have formed silicate liquid. Indeed, no CA_6 phase can be found. All the CaO has entered into the liquid, which promotes sintering and spinel growth, forming a densified spinel-rich matrix, which is beneficial to anti-oxidation. Inside the unoxidized zone, most of the coarse MgO grains have gone, with cavities left, see (c) and (d), as a result of the above mentioned MgO reduction reaction with

carbon. Close to the cavities, dense spinel zone can be seen. In the residual MgO gain, as marked in (c), silicate components of MgO, CaO and SiO_2 have also been detected by EDAX, see Annex 7.7.2.

What have been observed and deduced here seems to fit well with what was reported by M. C. Flemings et al [109] and B. H. Baker et al [110]. When Si is added to the MgO-carbon system, the following reactions occur (with 10 mmHg vapor pressure shown in the reaction formulas), and a significant vapor pressure of Mg forms at above 1100°C.

$$MgO(s) + Si(s) + C(s) \rightarrow Mg(g) + SiO\ (g) \qquad @\ 1100°C$$

$$MgO(s) + C(s) \leftrightarrow Mg(g) + CO\ (g) \qquad @\ 1460°C$$

Figure 7.23 and Figure 7.24 show respectively the microstructure of the M12-PG2-5.5-B3 and M12-PG2-5.5-C1 samples after the oxidation test at 1400°C for 3h.

As seen in Figure 7.23 (a), the decarbonized zone is sintered well with the aid of silicate liquid (the bright parts are CaO rich) and many pores are isolated, which helps impede the air infiltration. In uncarbonized zone, (b), MgO's loss can also be found. Some SiC particles have been converted to SiO_2 through the reaction with CO(g). On the surface of MgO grains, silicate film is also seen, outwards it is richer in CaO. No CA_6 rims around Al_2O_3 grains can be found. In reviewing, this texture is similar to M12-PG2-5.5-A1's.

Different with M12-PG2-5.5-A1's and M12-PG2-5.5-B3's, the decarbonized zone of M12-PG2-5.5-C1's is quite porous, see Figure 7.24 (a). Inside, MgO grains have

reacted. Near the MgO cavities, dense spinel rim can be clearly seen. As shown in the center of picture (b), only semi-rim of spinel is formed towards to the MgO cavities' side, another proof of MgO's reduction, Mg(g) deposits preferably onto the nearest and easily accessible Al_2O_3 bearing surface. Another big difference is that CA_6 rims do exist inside, indicating that in the absence of SiO_2, CaO can only react with Al_2O_3, and no

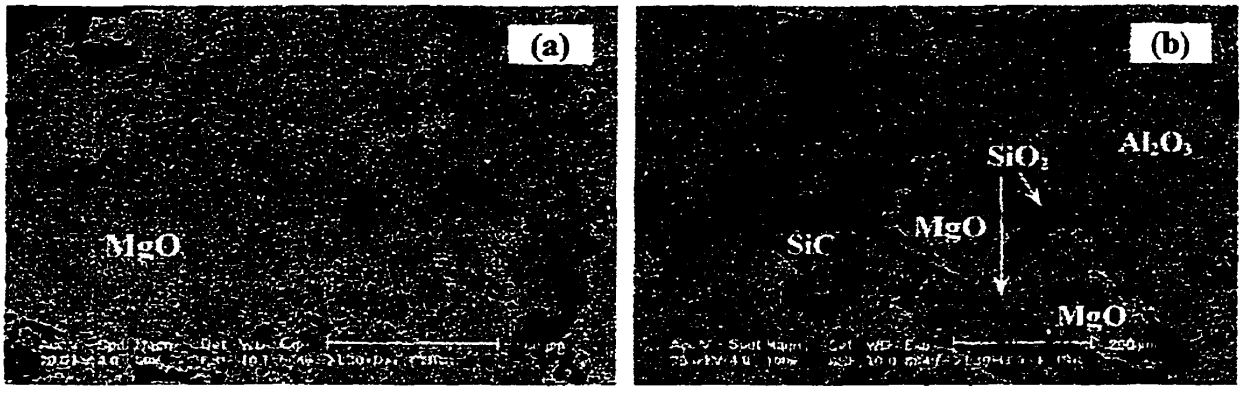

Figure 7.23 SEM micrograph of M12-PG2-5.5-B3 specimen after the unidirectional oxidation test at 1400°C for 3h in flowing air.

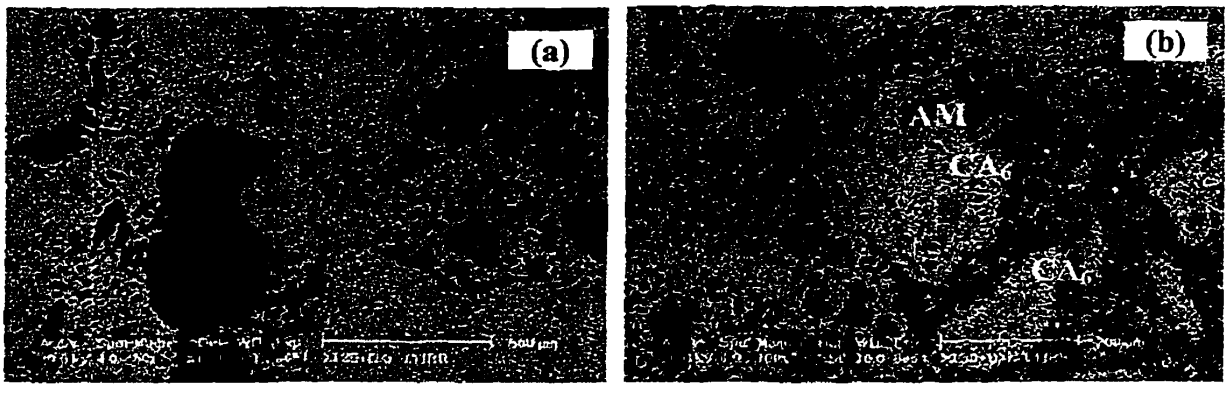

Figure 7.24 SEM micrograph of M12-PG2-5.5-C1 specimen after the unidirectional oxidation test at 1400°C for 3h in flowing air.

liquid can be formed. This may explain the poor anti-oxidation effect when boron compound is used alone as antioxidant in such castable system.

By now, it seems clear that anti-oxidation by a liquid protection mechanism in such graphitic castables is more effective. However, strength, oxidation and slag resistance must be compromised.

7.7.3 Analysis on the Castables after Rotary Slag Test

In this part, only the issue of penetration inhibition by graphite is stressed, based on evidence by microscopic analysis. Graphite-free and graphitic samples after the rotary slag test are thus compared below.

Figure 7.25 is the section of M12 sample. Slag intrusion into the castable can be clearly seen. From the slag-castable interface downwards, three areas at 1.5mm intervals, as schematically marked, denoted as 1#, 2# and 3# respectively, have been examined. As amplified in Figure 7.26. The element evolution is analyzed by EDAX, plotted in Figure 7.27. In the hot face zone there exists a lot of CA_6 phase, forming continuous net structure up to 3mm from the hot face, due to the intrusion of CaO from the slag. Fe_2O_3 is captured by spinel within the hot face zone.

In graphite containing samples, however, regardless whether the graphite is continuously or discontinuously distributed, there is no penetration at all, as shown in Figure 7.28 (a), (b), (c) and (d) for M12-FG-4-A1, M12-PG3-6-B3, M12-BAG-15 and M12-PG3-5-

AG1-A1B3 respectively. No CA_6 has been detected inside these samples, nor Fe_2O_3, even just behind the hot face by EDAX.

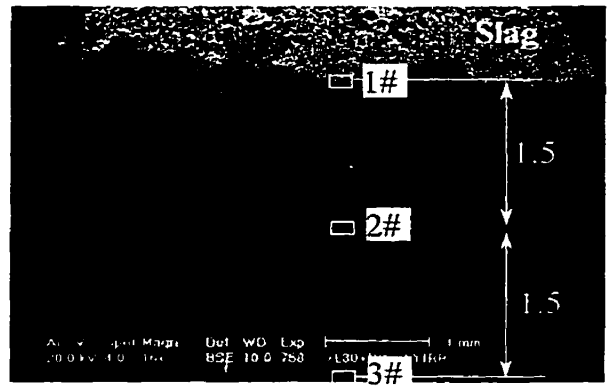

Figure 7.25 SEM micrograph of the section of M12 sample after rotary slag test.

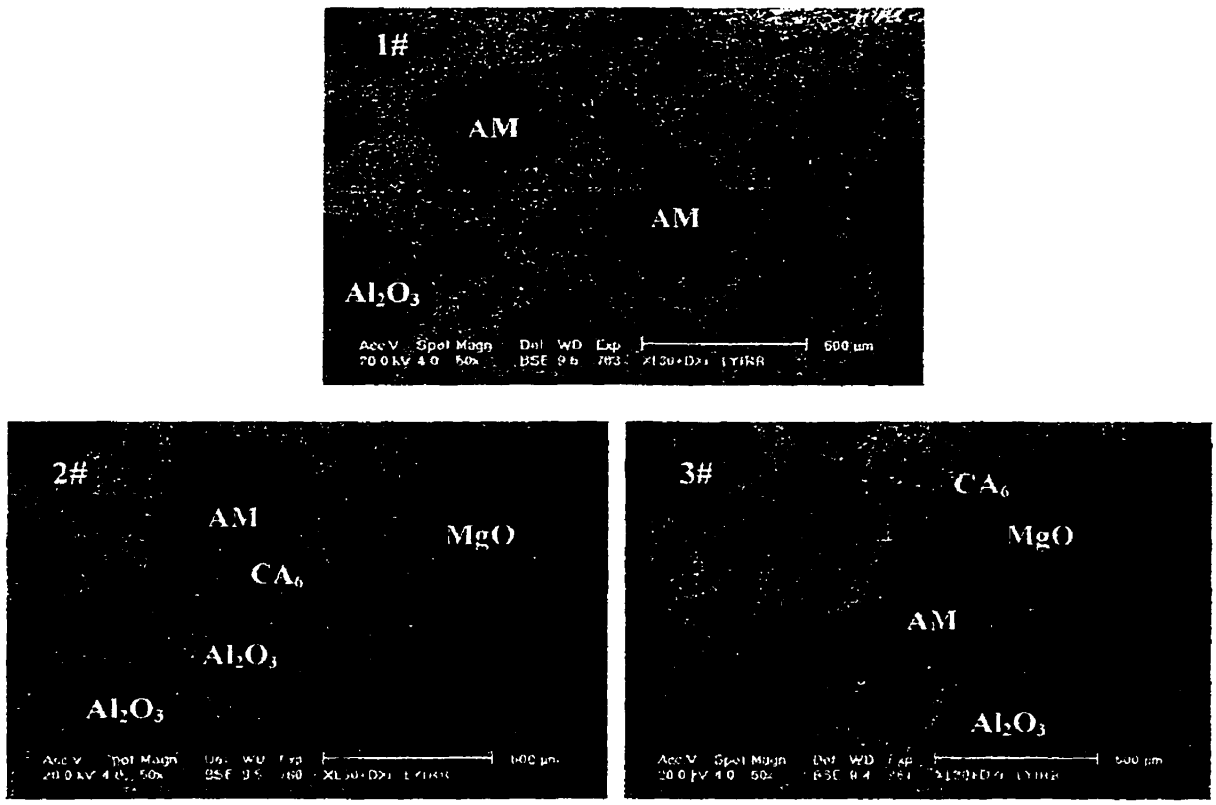

Figure 7.26 SEM micrograph of 1#, 2# and 3# zones in Figure 7.25 of M12 sample.

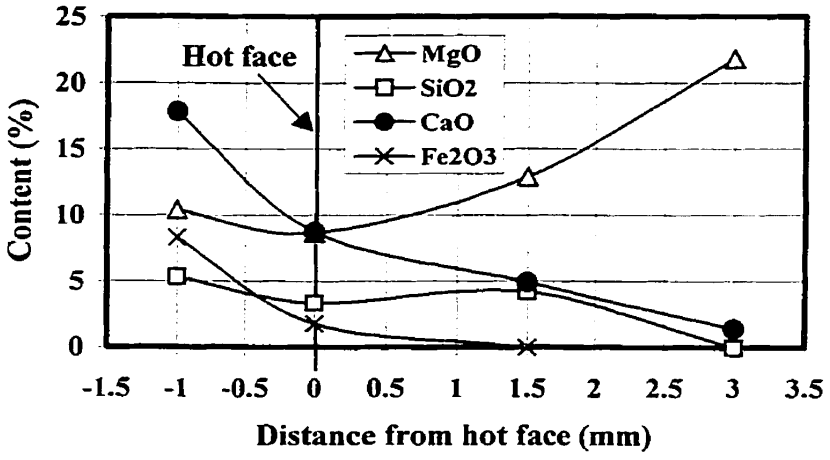

Figure 7.27 Chemical composition distribution in slag attached M12 sample.

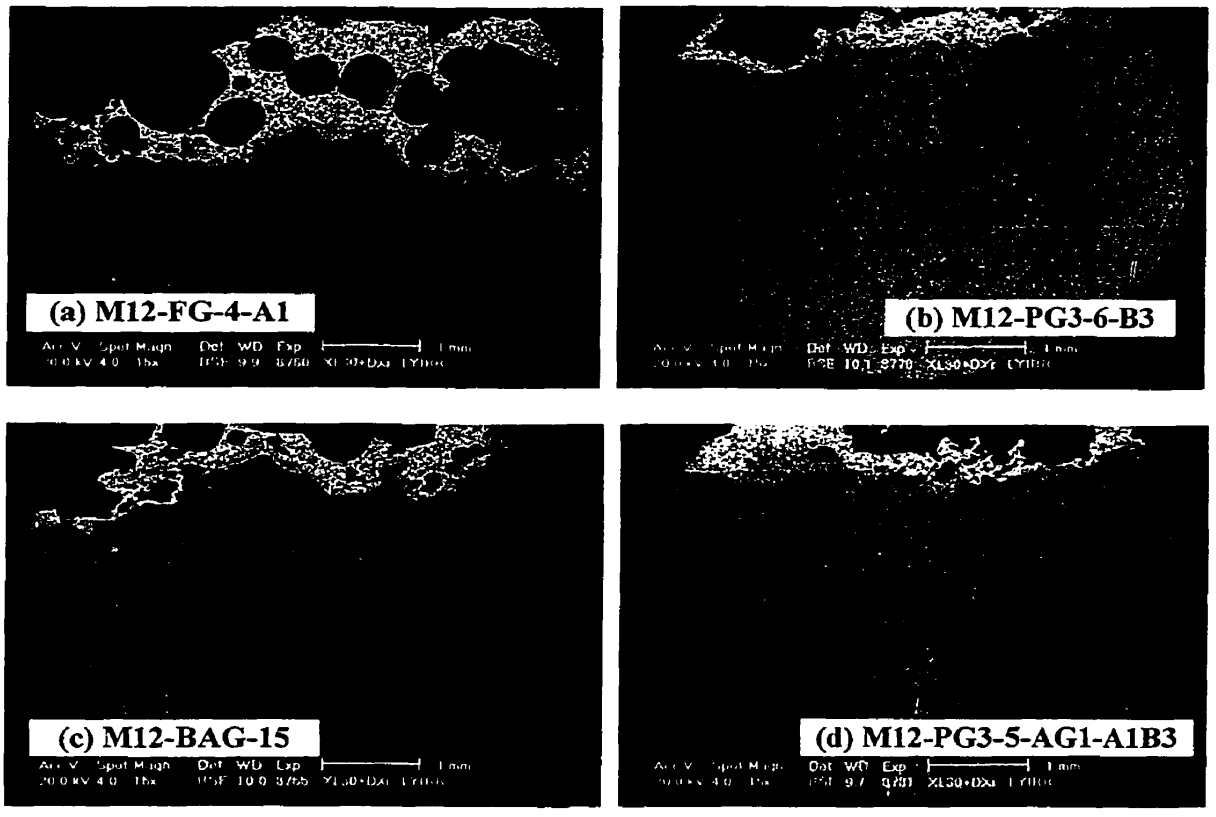

Figure 7.28 SEM micrograph of four graphite containing samples after rotary slag test.

The role of the graphite incorporated by FG, PG or BAG in inhibiting slag intrusion is well demonstrated by Figure 7.29. Where there is graphite, there is no way for the slag to intrude into the castable, typically in (b) and (c) in Figure 7.29. One concern would now be raised: whether a discontinuous distribution of the graphite introduced by PG or BAG will do harm to penetration resistance or becomes less effective. To reveal the truth, EDAX is adopted to make micro-area analysis, centered on the interface area, the upper part represents the slag composition and the lower part (just underneath the boundary) represents the composition in the castable. The results are summarized in Table 7.6, and the EDAX spectra are attached in Annex 7.7. The results can release the

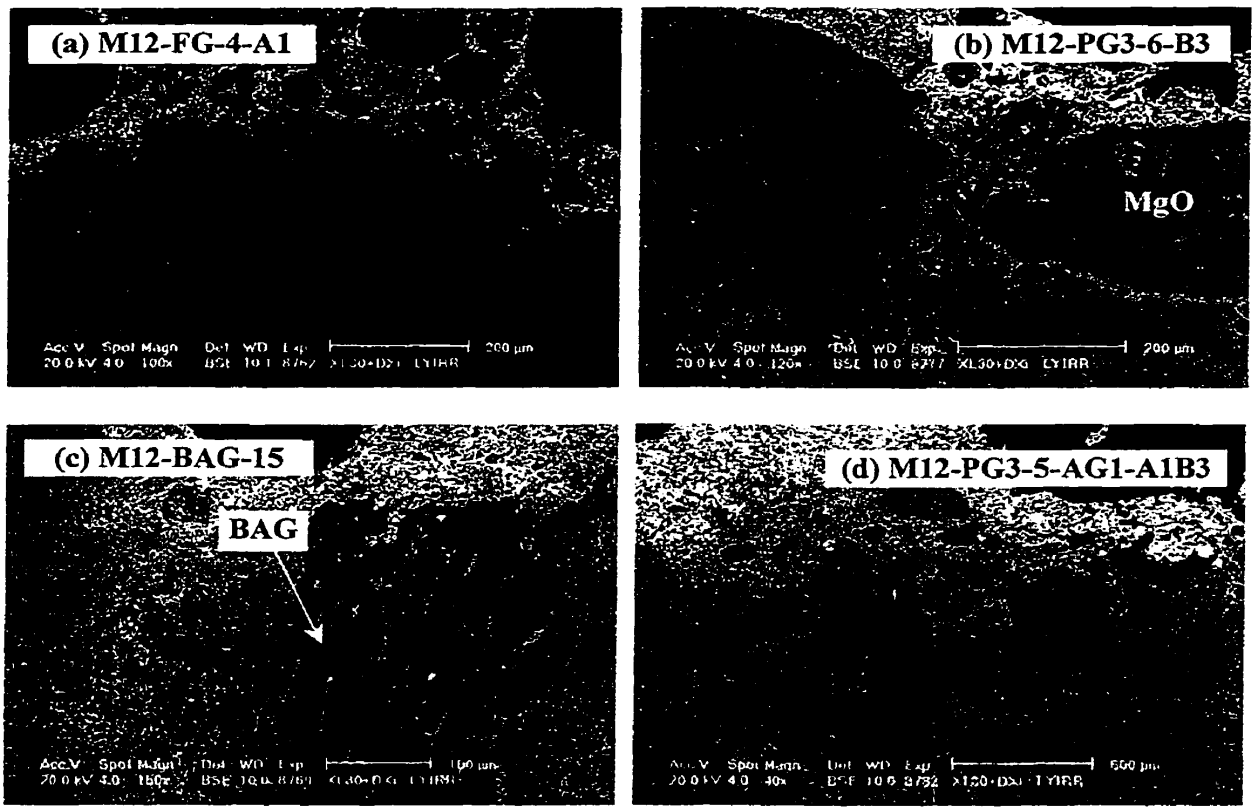

Figure 7.29 The role of graphite in inhibiting slag intrusion, observed by SEM.

concern. Of course such an analysis contains error and fluctuation, in particular for the lower part, as it is heterogeneous. But qualitatively, it is convincing. Actually the discontinuity of graphite distribution is just microscopically true. This seems not to affect the penetration characteristic of the molten slag.

Table 7.6 EDAX quantitative area analysis on 5 samples after rotary slag test

Castable notation	Location	Chemical composition (%)						
		MgO	Al_2O_3	SiO_2	CaO	TiO_2	MnO	Fe_2O_3
M12-FG-4-A1	Upper	5.12	27.77	10.00	30.78	0.97	5.16	20.19
	Lower	23.86	64.72	7.90	3.52			
M12-PG3-6-A1	Upper	7.27	26.44	8.42	29.94	0.99	5.30	21.63
	Upper	11.64	80.40	5.11	2.84			
M12-PG3-6-B3	Lower	8.25	28.22	7.02	27.00	0.95	5.76	22.80
	Upper	21.78	62.24	13.33	2.65			
M12-BAG-15	Lower	7.68	25.43	7.90	29.89	1.12	5.63	22.35
	Upper	19.39	76.55	1.39	2.67			
M12-PG3-5-AG1-A1B3	Lower	7.20	27.58	8.99	27.89	1.01	5.27	22.06
	Lower	12.31	66.13	19.43	2.12			

7.8 Conclusions of Chapter 7

The so far achieved results bring about the following conclusions:

(1) Incorporating natural flake graphite into Al_2O_3-MgO-C castables by micro-pelletized graphite (PG) or crushed briquette of alumina-graphite (BAG) does hold a net advantage

over straight addition of flake graphite in terms of water demand, flowability, density, cold and hot strengths.

(2) Impeding or retarding slag intrusion and in consequence enhancing slag resistance by incorporating graphite into the Al_2O_3-MgO castables have been proven very effective and meaningful. The key to maintain a good slag resistance is to protect the carbon from oxidation at elevated temperatures. So long as the incorporated graphite is retained in the castable, regardless of whether continuous or discontinuous distribution, no penetration, even micro-structurally, is observed.

(3) Incorporating aluminium, silicon and silicon carbide anti-oxidants, in a good combination, both in PG or BAG and in the castables plays a big role in minimizing carbon oxidation. Boron carbide additive helps improve oxidation resistance at intermediate temperature (1200°C), while silicon and silicon carbide are helpful in enhancing higher temperature oxidation(above 1400°C). For this particular kind of castable system, boron compounds are not suggested to be used as dominant antioxidants.

(4) At a microscopic scale, a discontinuous distribution of graphite in castables does not do harm to the slag penetration resistance. Only 1% amorphous graphite as dispersed carbon has been used in this work. Contrary to the "accepted truth", the ability of preventing slag penetration is not strongly dependant on the uniform distribution of graphite in the matrix.

(5) For inhibiting slag penetration only, the amount of carbon in castables is not necessarily to be the higher, the better. Even in the graphite based micropellets, the graphite can also be replaced to a considerable extent by alumina to show an equal resistance to slag attack.

(6) At least two kinds of advantageous Al_2O_3-MgO-C castables have been developed by this work, and the following properties have been achieved, as shown in Table 7.7.

Table 7.7 The achieved properties of the Al_2O_3-MgO-C castables developed by this work

		M12-PG3-5-AG1-A1B3	M12-BAG-15
Chemical composition (%)	Al_2O_3	77	81
	MgO	12	12
	CaO	1.1	1.1
	F.C.	5	5
Bulk density (g/cm^3)	110°C, 24h	2.85	2.93
	1000°C, 5h	2.76	2.88
	1500°C, 5h	2.55	2.61
C.M.O.R. (MPa)	110°C, 24h	4.56	5.17
	1000°C, 5h	2.71	2.83
	1500°C, 5h	12.85	16.14
H.M.O.R. (MPa)	1400°C, 3h	N. A.	3.36
P.L.C. (%)	1000°C, 5h	+ 0.04	- 0.01
	1500°C, 5h	+ 2.48	+ 2.38
Water addition (%)		6.1	5.9

CHAPTER 8. COMPREHENSIVE DISCUSSIONS, CONCLUSIONS AND RECOMMENDATIONS

This work has shown the effectiveness of the five adopted countermeasures against the problems associated with the hydrophobicity, low density and oxidation of natural flake graphite (FG): 1) to agglomerate the FG powders so as to decrease the specific surface area; 2) to diminish the density difference by using crushed carbon bonded compact of oxide-FG mixture; 3) to modify the surface of the flake graphite by forming hydrophilic coating; 4) to control the dispersion state of the graphite in the castable to maintain bonding strength; and 5) to use appropriate antioxidants to impede FG oxidation. Among them, however, the TiO_2 coated graphite (CFG) appeared less effective in reducing water addition and maintaining strength, also more costly and less practicable, when compared to micro-pelletized graphite (PG) and briquette of Al_2O_3-graphite (BAG).

From the measured overall properties of the various castables, it may be said that the preset objectives for this work have been met. The two purposely developed methods to incorporate FG into castables, PG and BAG, have been proven to be effective and feasible; they can truly minimize the problems encountered with straight addition of FG. The advantages of PG and BAG are ascribed to the reduced specific surface area, reduced density difference and microscopically discontinuous dispersion of the graphite in the castables. Such a graphite encapsulated heterogeneous structure is favorable for compromising properties of the castables, water demand and strength in particular.

Optimization on the Al_2O_3-SiC-C and Al_2O_3-MgO-C castables has been fulfilled to achieve the properties as summarized in Table 8.1. According to literature survey, properties of the Al_2O_3-SiC-C castables in this thesis are superior to the published ones; and most probably, this work has, for the first time, brought into being the Al_2O_3-MgO-C castables.

Table 8.1 The achieved properties of the graphitic castables developed by this work

		Al_2O_3-SiC-C		Al_2O_3-MgO-C	
		PG3-6	BAG-13	M12-PG3-5-AG1-A1B3	M12-BAG-15
Chemical composition (%)	Al_2O_3	82	81	77	81
	SiO_2	4	4	0	0
	SiC	7	7	12 (MgO)	12(MgO)
	F.C.	5	6	5	5
Bulk density (g/cm^3)	110°C, 24h	2.94	2.84	2.85	2.93
	1000°C, 5h	2.86	2.75	2.76	2.88
	1450°C, 5h	2.92	2.82	2.55 *	2.61*
Apparent porosity (%)	110°C, 24h	14.0	17.3	4.56	5.17
	1000°C, 5h	19.2	22.4	2.71	2.83
	1450°C, 5h	15.4	18.3	12.85*	16.14*
CMOR (MPa)	110°C, 24h	5.28	7.40	4.56	5.17
	1000°C, 5h	8.04	16.60	2.71	2.83
	1450°C, 5h	11.17	14.85	12.85*	16.14*
HMOR (MPa)	1450°C, 1h	5.23	7.43	N.A.	3.36**
P.L.C. (%)	1000°C, 5h	− 0.06	− 0.11	+ 0.04	− 0.01
	1450°C, 5h	− 0.09	0.00	+ 2.48*	+ 2.38*
Water addition (%)		5.70	5.05	6.1	5.9

* 1500°C, 5h; ** 1400°C, 3h, with coke protection

Castable's workability is governed by its matrix rheology. "Extracting matrix" method, using rotary coaxial double cylinder viscometer to measure rheological parameters of the matrix suspension, is a useful and efficient approach to characterize rheological behaviors of the castables and assess appropriate type and amount of deflocculant. In the Al_2O_3-MgO castables, ultrafine calcined alumina is the key constituent dominating the flow behavior of the castables. Deflocculation is actually made mainly on alumina ultrafines. Among the four investigated deflocculants, sodium polyacrylate (SPA), sodium hexametaphosphate (SHP), polyethyleneglycol (PEG) and melamine polymer (MP), PEG works the best and has been used as the only deflocculant in the Al_2O_3-MgO-C castables. By now, there still lacks of an effective and commercially available dispersant for FG powders. In this sense, straight addition of FG is not adaptable. When graphite is encapsulated, it affects less the matrix rheology.

In this work, 12% MgO, instead of 5-7.5% MgO as in the commercial Al_2O_3-MgO castables, has been successfully introduced into the Al_2O_3-MgO-C castables. This amount accounts for 42% stoichiometric spinel, when fully in-situ formed, almost doubled the spinel amount in the Al_2O_3-AM(MgO) castables. This is only possible when carbon is present to inhibit slag penetration. Higher MgO is not impossible, but firstly structural destruction due to in-situ spinel formation has to be avoided. Using pre-formed spinel to replace partially the alumina in aggregate portion is expected to be a way to increase MgO without volume stability problem.

Comparing the effect of BAG with PG, it can be seen that BAG performs better than

PG. This is thought to be due to the much wider size distribution of BAG grains, from 0.074 to 3.36 mm, higher volume fraction and geometrically more isotropic, instead of being elongated as in the case of PG. This inspires the idea of making spherical graphite based micro-pellets by spraying-drying process.

In regard to oxidation, the relative high level of SiC and microsilica additions impart, by forming protective liquid layer on the exposed surface, the Al_2O_3-SiC-C castables good anti-oxidation property, whereas for Al_2O_3-MgO-C castables, it is difficult to achieve as good oxidation resistance. Using anti-oxidation mortar to form a protective coating on the hot surface is an effective approach, which is already a practice in in-plant pre-heating the carbon containing brick linings. A good compatibility between the coating and the castable is requested. This, though beyond the scope of this work, should be further studied.

The achieved results bring to the following conclusions:

(1) The mode of incorporating graphite plays a big role in minimizing the problems caused by FG and has pronounced influence on overall properties of graphitic castables. In both Al_2O_3-SiC-C and Al_2O_3-MgO-C castables, incorporating graphite via micro-pelletized graphite (PG) or crushed briquette of Al_2O_3-graphite (BAG) have shown net advantages over straight addition of flake graphite (FG) and TiO_2 coated flake graphite (CFG), in terms of water addition, flowability, porosity, cold and hot strengths, thermal shock resistance, oxidation resistance and slag resistance. CFG doesn't show positive

effects on strength and slag resistance of the Al_2O_3-SiC-C castables, though it imparts lower water demand and better oxidation resistance than natural flake graphite.

(2) The role of the inserted graphite in precluding slag intrusion and also improving thermal shock resistance reveals itself dramatically. Slag resistance is strongly dependent on oxidation resistance. The key to maintain a good slag resistance is to protect the carbon from oxidation at elevated temperatures. So long as the incorporated graphite is retained in the castable, regardless of whether continuous or discontinuous distribution, no penetration, even micro-structurally, has been observed.

(3) At a microscopic scale, a discontinuous distribution of graphite in the castables is as good as a continuous carbon distribution to achieve good slag penetration resistance. This is contrary to the belief that resistance to slag penetration is strongly dependent upon the uniform distribution of graphite in the matrix.

(4) For the purpose of inhibiting slag penetration, the amount of carbon in castables is not necessarily to be the higher the better, 4-5% being sufficient. Even in the graphite based micropellets, the graphite can also be replaced to a considerable extent by alumina to reach an equal resistance to slag attack.

(5) Incorporating aluminium, silicon and silicon carbide as antioxidants both in PG or BAG and in the castables plays a big role in minimizing carbon oxidation. The oxidation resistance is attributed to liquid phase protection. For the Al_2O_3-MgO-C castable, boron

carbide additive helps improve the oxidation resistance at intermediate temperature (1200°C), while silicon and silicon carbide are more effective in enhancing oxidation resistance at higher temperatures (above 1400°C). Zirconium diboride additive does not show a positive effect on anti-oxidation at both 1200°C and 1400°C. For this particular Al_2O_3-MgO-C castable system, boron bearing compounds are not suggested to be added as dominant antioxidants.

(6) This work has met the preset objectives to develop Al_2O_3-SiC-C and Al_2O_3-MgO-C castables containing 4-5% flake graphite with such targeted properties: water addition: < 6.5%; flow value: >170mm; CMOR (after drying): >4MPa; HMOR(at 1400 or 1450°C): >2MPa; PLC (after 1000-1500°C): ± 0.5% for Al_2O_3-SiC-C castables and <+2.5% for Al_2O_3-MgO-C castables; good oxidation resistance and slag resistance. Nevertheless, the CMOR of the Al_2O_3-MgO-C castables after 1000°C heating is not high enough, only around 3 MPa at present. Oxidation resistance of the Al_2O_3-MgO-C castables under 1200°C needs also to be further improved.

This work is to be taken as the initial stage of a long term endeavor. Some recommendations for further improvements and studies are as follows:

(1) As shown microscopically, the made graphite based micropellets are still porous. It is unfavorable to the strength and the graphite fraction. By optimization in particle size distribution, binding system and using vacuum mixing and forming process, denser micropellets with higher graphite content are expected. On the other hand, other micro-

pelletization approach is also considerable, e.g. by spraying process to get spherical pellets.

(2) Straight addition of magnesia into the Al_2O_3-MgO-(C) castables encounters a limitation, when volume stability is concerned, not to mention the hydration risk during curing or pre-heating. As an alternative, MgO enriched spinel can replace partially the free MgO. Commercially, MgO rich spinels with MgO 30-50%, sintered or fused, are available and worth trying in the Al_2O_3-MgO-C castables.

(3) So far, aluminium powder as well known highly effective antioxidant can not be directly added into the graphitic castables, due to violent reaction with water leading to swelling. By special coating technology to make the surface inert, it could be possible to introduce Al or even Al-Mg alloy powders to improve the oxidation resistance.

(4) Oxidation resistance remains to be a very critical issue. Since inherently castables are more porous than bricks, further work in this field needs to be done to improve oxidation resistance of graphitic castables in a wide range of temperature, to reveal the anti-oxidation mechanisms and their impacts on other properties like hot strength and slag resistance. The concept of liquid and gaseous phase protection should receive some emphasis.

(5) Field trials with the so far developed graphitic castables are worth while to pursue.

REFERENCES

1. BROWN, A.J. and WHITE, J. (1986). New generation refractory materials: ceramic-carbon composites. Met. Mater. (Inst. Met.), Vol. 2(10), 632-639.

2. LI, N. and ZHANG, W. J. (1990). Carbon Containing Refractories, published by Science Press, China, 1-3.

3. TABATA, K. (1992). Recent progress and future trend of carbon bearing refractories in Japan. Proceedings of the 2nd International Symposium on Refractories, Oct. 30-Nov. 2, Beijing, China, 22-33.

4. LEE, W.E. and MOORE, R.E. (1998). Evolution of in situ refractories in the 20th century. Journal of the American Ceramic Society, Vol. 81(6), 1385-1410.

5. HENRY, F.W. Jr. and STENDERA, J.W. (1998). Recent development in spinel forming castable use in steel plants. 1998 Electric Furnace Conference Proceedings, Nov. 15-18, New Orleans, USA, Vol. 56, 221- 228.

6. RIGAUD, M. (1999). Magnesia-carbon castables: a review. 1999 Steelmaking Conference Proceedings, March 21-24, Chicago, USA, 251- 254.

7. SAKAMOTO, S., ONO, Y. and ONO, T. (1995). Graphite containing unshaped refractories. UNITECR'95 Proceedings, Nov. 19-22, Kyoto, Japan, Vol.2, 189-196.

8. ZHU, B.Q. (2000). The present progress and problems of carbon-containing castables. China's Refractories, Vol. 9, No. 1, 8-11.

9. RIGAUD, M., KOVAC, V., XING, C., PALCO, S. and RYBAR, A. (1998). Spinel and forsterite bonded magnesia castables for steelmaking applications. 81st Steelmaking Conference Proceedings, Toronto, Canada, March 22-25, 477-486.

10. TERANISHI, H., KAWAMURA, T., YASUI, K. and IMAI, I. (1998). Application of MgO-C castable to ladle furnace slag line. Taikabutsu Overseas, Vol. 18, No. 1, 38-42.

11. ISOMURA, K., KUMAGAI, M., TAKAGI, M., GOTO, S., NOMURA, M., JONO, K, TIRITANI, Y. and TANAKA, S. (1998). Development of graphite containing alumina castable and its application to BF trough. Proceedings of the 3rd International Symposium on Refractories, Nov. 3-6, Beijing, China, 51-56.

12. ZHOU, N.S. and RIGAUD, M. (1998). Different approaches to incorporating natural flake graphite into Al_2O_3-SiC-C castables. China's Refractories, Vol. 7, No. 4, 3-10.

13. ZHOU, N.S. and RIGAUD, M. (1998). Al_2O_3-MgO-C castables for steelmaking ladles. Proceedings of the 57th Electric Furnace Conference, Nov. 14-16, Pittsburgh, USA, 131-142.

14. NISHI, M. and MIYAMOTO, A. (1981). Lining materials and installation methods for blast furnace troughs. Taikabutsu Overseas, Vol. 1, No. 1, 26-39.

15. MIWA, T. and NISHI, M. (1992). Application of castable refractories for iron-making process at NKK. Stahl und Eisen Special - The 35th International Colloquium on Refractories, Oct. 1-2, Aachen, Germany, 39-46.

16. WANG, S.Y., WANG, Z.M., ZHOU, N.S., LI, Z.G., HE, X. and CUI, T.H. (1995). Development and application of Al_2O_3-SiO_2-SiC-C refractories for different types of BF troughs and runners. Proceedings of UNITECR'95, Nov. 19-22, Kyoto, Japan, Vol.1, 159-166.

17. KURATA, H., MATSUO, S. and EGUCHI, T. (1988). Development of alumina-spinel castable refractories for teeming ladle. Taikabutsu, Vol. 40 (10), 621-624.

18. OHISHI, I. and EBIZAWA, R. (1991). Application of alumina-spinel castable refractories to steel ladle. Proceedings of UNITECR'91, 2nd Ed., Sep. 23-26, Aachen, Germany, 148--151.

19. FURUTA, K., FURUSATO, I. and TAKITA, I. (1992). Development of castables for teeming ladle in Japan. Proceedings of the 2nd International Symposium on Refractories, Oct. 30-Nov. 2, Beijing, China, 334-348.

20. KOBAYASHI, M., KATAOKA, K., SAKAMOTO, Y. and KIFUNE, I. (1997). Use of alumina-magnesia castables in steel ladle sidewalls. Taikabutsu Overseas, Vol. 17(3), 39-44.

21. WANG, X.Z., LI, Y.Q., LI, Q.H., ZHANG, Y.M. and LIN Y.L. (1992). The use of Al_2O_3-MgO-C bricks for 300 ton steel ladle. Proceedings of the 2nd International Symposium on Refractories, Oct. 30-Nov. 2, Beijing, China, 349-355.

22. ZHONG, X.C. (1995). Refractories developments for iron and steel making in China. Proceedings of UNITECR'95, Nov. 19-22, Kyoto, Japan, Vol. 1, 75-85.

23. YORITA, E. (1999). Monolithic refractories in Japan--history and recent trend. Taikabutsu Overseas, Vol. 19 (3), 3-6.

24. LANKARD, D.R. (1985). Evolution of monolithic refractory technology in the United States. Advances in Ceramics, Vol. 13 (New Developments in Monolithic Refractories), edited by R.E. Fisher, published by The American Ceramic Society, Columbus, OH, USA, 46-66.

25. "Cutting Furnace Cost", Plibrico Jointless Firebrick Co., Chicago, USA, 1930, 1-39.

26. KREBS, K. (1999). Modern solution of refractory problems with unshaped refractories. Proceedings of UNITECR'99, Sep. 6-9, Berlin, Germany, 1-5.

27. CLAVAUD, B., KEIHL, J.P., and SCHMIDT-WHITELEY, R.D. (1983). 15 years of low cement castables in steelmaking. Proceedings of the 1st International Conference on Refractories, Nov. 15-18, Tokyo, Japan, 589-606.

28. KATAOKA, S. (1995). Refractories for Steelmaking in Japan. Proceedings of UNITECR'95, Nov. 19-22, Kyoto, Japan, Vol. 1, 1-27.

29. NAKAGAWA, H. (1999). Monolithic refractories for the iron and steel industry. Taikabutsu Overseas, Vol. 19 (3), 56-57.

30. "Statistics", Taikabutsu Overseas, Vol. 19 (3), 1999, 78.

31. FRANKLIN, S.A. and WARMAN, M.O. (2000). Where have all the bricks gone? The Refractories Engineer, No. 1, 2000, 2-11.

32. "Statistics on Refractories", The Yearbook of Iron and Steel Industry of China, ed. by the Chinese Society for Metals, 1999.

33. ISHIKAWA, M. (1999). Refractory castables. Taikabutsu Overseas, Vol. 19 (3), 7-13.

34. CLAVAUD, B., KEIHL, J.P. and RADAL, J.P. (1985). A new generation of low-cement castables. Advances in Ceramics, Vol. 13 (New Developments in Monolithic Refractories), edited by R. E. Fisher, published by the American Ceramic Society, Columbus, OH, USA, 274-284.

35. YE, G.T. and LI, Z.G. (1999). Trend in monolithic refractories technology. China's Refractories, Vol. 8, No. 3, 15-18.

36. HITTANDA, H., KATO, A. and MORIMOTO, S. (1999). Advanced precast blocks. Taikabutsu Overseas, Vol. 19 (3), 39-43.

37. HUNDERE, A.M., MYHRE, B. and SANDBERG, B. (1996). Mullite Bonded Castables. Proceedings of the 1996 International Symposium on Refractories, Nov. 12-15, Haikou, China, 624-628.

38. XING, C. (1999). Optimization of magnesia based, cement-free, spinel bonded castables. Ph. D. Dissertation, Ecole Polytechnique de Montreal, Canada, November 1999.

39. KAMEI, S. (1989). Progress of monolithic refractories for recent 10 years in Japan. Proceedings of UNITECR'89, Nov. 1- 4, Anaheim, USA, Vol.1, 46-86.

40. FLETCHER, N.C. and BRYDE, G.J.M. (1989). The development of blast furnace trough castables. Proceedings of UNITECR'89, Nov. 1-4, Anaheim, USA, Vol.1, 719-730.

41. KITANI, F., TAKAHASHI, T., HANMYO, M., OGURA, E., YOSHINO, S. and FUJIWARA, T. (1983). Refractories of molten ladle for pre-treatment. Taikabutsu Overseas, Vol. 3 (2), 30-37.

42. NISHITANI, T., MATSUO, S. and GENBA, T. (1989). Application of the alumina-spinel castable for BOF ladle lining. Proceedings of UNITECR'89, Nov. 1-4, Anaheim, USA, Vol.1, 529-540.

43. MORI, J., WATANABE, N., YOSHIMURA, M., OGUCHI, Y. and KAWAKAMI, T. (1990). Material design of monolithic refractories for steel ladle. The American Ceramic Society Bulletin, Vol. 69(7), 1172-1176.

44. NAGAI, B., MATSUMOTO, O. and ISOBE, T. (1991). Development of monolithic refractory linings for B.O.F. ladle in Japan mainly for the last decade. Proceedings of UNITECR'91, 2nd Ed., Sep. 23-26, Aachen, Germany, 116-122.

45. NAGAI, B., MATSUMOTO, O., ISOBE, T. and NISHIUMI, Y. (1992). Wear mechanism of castable for steel ladle by slag. Taikabutsu Overseas, Vol. 12 (1), 15-20.

46. OGUCHI, Y. and MORI, J. (1993). Wear mechanism of castable for steel ladle. Taikabutsu Overseas, Vol. 13 (4), 43-46.

47. NAKAMURA, R. and KANESHIGE, T. (1999). The current status of casting steel ladles in Japan. 1999 Steelmaking Conference Proceedings, March 21-24, Chicago, USA, 267- 278.

48. FUJII, K., ISAO, F. and TAKITA, I. (1992). Composition of spinel clinker for teeming ladle casting materials. Taikabutsu Overseas Vol. 12 (1), 4-9.

49. YAMAMURA, T., KUBOTA, Y., KANESHIGE, T. and NANBA, M. (1993). Effect of spinel clinker composition on properties of alumina-spinel castable. Taikabutsu Overseas, Vol. 13 (2). 39-45.

50. SUMIMURA, H., YAMAMURA, T., KUBOTA, Y. and KANESHIGE, T. (1991). Study on slag penetration of alumina-spinel castable. Proceedings of UNITECR'91, 2nd Ed., Sep. 23-26, Aachen, Germany, 138-144.

51. TAWARA, M., FUJII, K., TANIGUCHI, T., HAGIWARA, M., KIBAYASHI, T. and TANAKA, M. (1996). Application of alumina-magnesia castable in high temperature steel ladles. Taikabutsu Overseas, Vol.16 (2), 17-19.

52. ITOSE, S., ISOBE, T. and FURUKAWA, K. (1997). Optimum castable lining for steel ladle in Japan. Proceedings of UNITECR'97, Nov 4-7, New Orleans, USA, Vol.1, 165-174.

53. BIER, T.A., PARR, C., REVAIS, C. and FRYDA, H. (1997). Chemical interactions in calcium aluminate cement based castables containing magnesia. Proceedings of UNITECR'97, Nov. 4-7, New Orleans, USA, Vol.1, 15-21.

54. VERT, T.A. (1999). A comparison of precast bottom materials/designs at Dofasco Inc.. 1999 Steelmaking Conference Proceedings, March 21-24, Chicago, USA, 287- 297.

55. RIGAUD, M. and XING, C. (1997). Basic castables for ladle's steel making applications: a review. Journal of Canadian Ceramic Society, Vol. 66 (3), 206-209.

56. KENAN, W.M. (1989). Hidden properties of graphite. Proceedings of UNITECR'89, Nov. 1- 4, Anaheim, USA, Vol.2, 1463-1470.

57. KENAN, W.M. and ALLERA, E. (1994). Graphite. Ceramic Bulletin, Vol. 73(6), 101-104.

58. COOPER, C.F. (1985). Refractory applications of carbon. British Ceramic Transaction Journal, Vol. 84 (2), 48-53.

59. COOPER, C.F., ALEXANDER, I.C. and HAMPSON, C.J. (1985). The role of graphite in the thermal shock resistance of refractories. British Ceramic Transaction Journal, Vol. 84 (2), 57-62.

60. BROWN, A. and STEIN, G.R. (1983). The properties of ceramic graphite bodies. Refractories Journal, Vol. 58(2), 7-10.

61. COOPER, C.F. (1980). Graphite containing refractories. Refractories Journal, Vol. 55(6), 11-21.

62. BONNIN, G. (1769), British Patent. No. 919, 1769.

63. PERCY, J. (1875), Metallurgy, John Murray, London, p. 115

64. URE, A. (1843). Manufactures and mines. Dictionary of Arts. Longmens, Brown and Longmens, London, p. 1004.

65. KAWASAKI, H., YOSHITOMI, J., SHIKANO, H. and HAYASHI, T. (1991). Surface treatment of graphite for monolithic refractories. Taikabutsu Overseas, Vol. 11 (4), 46-47.

66. YOSHIMATSU, H., FUJIWARA, S., KONISHI, R., MIYAWAKI, M. and MIURA, T. (1995). The water wettability and oxidation resistance of Al_2O_3-coated graphite. Journal of the Ceramic Society of Japan, Vol. 103 (6), 929-934.

67. YU, J., UENO, S. and HIRAGUSHI, K. (1996). Improvement in flowability, oxidation resistance and water wettability of graphite powders by TiO_2 coating. Journal of the Ceramic Society of Japan, Vol. 104 (6), 481-485.

68. GUINEBRETIERE, R., MASSON, O., RUIN, P., TROLLIARD, G. and DAUGER, A. (1994). Sol-gel coating of ceramic powders. Philosophical Magazine Letters, Vol. 70 (6), 389-396.

69. Chemistry of Organotitanium Compound and Its Application. Technical Bulletin, ed. by Matsumoto Trading Co., Ltd., 1980, 6-7.

70. FUHRER, M., HEY, A. and LEE, W.E. (1998). Microstructural evolution in self-forming spinel/calcium aluminate-bonded castable refractories. Journal of the European Ceramic Society, Vol. 18, 813-820.

71. KOGA, Y., SATO, M., SEKIGUCHI, K. and IWAMOTO, S. (1998). Effects of alumina cement grade and additives on alumina-magnesia castables containing aluminum lactate. Taikabutsu Overseas, Vol. 18 (1), 43-48.

72. Alcoa Industrial Chemicals (1996). Chemicals Product Data (CHE 932 & CHE 934): T-64 Tabular Alumina; Product Catalogue: Calcined aluminas for Ceramics and Refractories.

73. Alcan Chemicals (1998). Data Sheet No. 461: BACO Low soda milled alumina RMA325 grade.

74. Alcan Chemicals (1996). Product Data: Aluminas (XA-45, C-70 series).

75. Exolon-ESK Co.(1997), Products Data Sheet: Silicon carbide.

76. Elkem Materials (1997), Data Sheet: Elkem Microsilica 971 U.

77. Lafarge Cement (1996), Data Sheet: Calcium aluminate cements (Secar series).

78. MYHRE, B. (1994). The Effect of particle-size distribution on flow of refractory castables. Paper presented at the 30th Annual Refractories Symposium of the American Ceramic Society, St. Louis, USA, March 25, 1994.

79. MYHRE, B. and SUNDE, K. (1995). Alumina based castables with very low contents of hydraulic compounds. Part I: The effect of binder and particle size distribution on flow and set. Proceedings of UNITECR'95, Kyoto, Japan, Nov. 19-22, 309-316.

80. CHAN, C.F. and KO, Y.C. (1998). Effect of CaO content on the hot strength of alumina-spinel castables in the temperature range of 1000° to 1500°C. J. Am. Ceram. Soc., Vol. 81(11), 2957-2960.

81. KRIECHBAUM, G.W., GNAUCK, V. and ROUTSCHKA, G. (1994). The Influence of SiO_2 and Spinel on the Properties of High Alumina Low Cement Castables. Stahl und Eisen Special - The 37th International Colloquium on Refractories, Oct 6-7, Aachen, Germany, 150-159.

82. EBATA, A., KANATANI, S., MORI, J., TORITANI, Y., OKAMOTO, T. and TANAKA, S. (1996). A consideration on wear mechanism of castable for steel ladle. Taikabutsu, Vol. 48(9), 490-491.

83. ASTM C860-91: Practices for determining and measuring consistency of refractory concretes. Annual Book of ASTM Standards, Vol.15.01, 1999.

84. ASTM C830-93: Test methods for apparent porosity, liquid absorption, apparent specific gravity, and bulk density of refractory shapes by vacuum pressure. Annual Book of ASTM Standards, Vol.15.01, 1999.

85. ASTM C1407-98: Practice for calculating areas, volume and linear change of refractory shapes. Annual Book of ASTM Standards, Vol.15.01, 1999.

86. ASTM C133-97: Test methods for cold crushing strength and modulus of rupture of refractories. Annual Book of ASTM Standards, Vol.15.01, 1999.

87. ICHIKAWA, K., NISHIO, H. and HOSHIYAMA, Y. (1994). Oxidation test of MgO-C bricks. Taikabutsu Overseas, Vol. 14 (1), 13-19.

88. ISO R 1893-70: Refractory products – Determination of refractoriness under load (Differential-with rising temperature).

89. FUNK, J.E., and DINGER, D.R. (1994). Particle Size Control for High-Solids Castable Refractories. Am. Ceram. Soc. Bull., Vol. 73(10), 1994, 66-69.

90. MYHRE, B. and HUNDERE, A. M. (1996). The use of particle size distribution in development of refractory castables. Presented at the 25th ALAFAR Congress, San Carlos de Bariloche, Argentina, Dec. 1-4, 1996.

91. MYHRE, B. and HUNDERE, A. M. (1996). On the influence of superfines in high alumina castables. Presented at the 39th International Colloquium on Refractories, Aachen, Germany, Sept. 25-26, 1996.

92. MYHRE, B. and HUNDERE, A. M. (1997). Substitution of reactive alumina with microsilica in low cement and ultralow cement castables. Proceedings of UNITECR'97, New Orleans, USA, Nov. 4-8,1997.

93. WATANABE, K., ISHIKAWA, M. and WAKAMATSU, M. (1989). Rheology of Castable Refractories. Taikabutsu Overseas, 1989, Vol. 9, No.1, 41-53.

94. BRINKER, C. J., and SCHERE, G.W. (1990). Sol-gel science: the physics and chemistry of sol-gel processing. Academic Press, Inc., New York, 239-250.

95. SHANEFIELD, D.J. (1996). Organic Additives and Ceramic Processing, 2nd Ed., Kluwer Academic Publishers, Boston, 142-153.

96. LI, Z.G., ZHANG, S.H., ZHOU, N.S. and YE, G.T. (1997). Difference in dispersing effect between organic and inorganic deflocculants in castables. Proceedings of UNITECR'97, Nov 4-7, New Orleans, USA, Vol. 3, 1355-1361.

97. NAKAGAWA, Z., ENOMOTO, N., YI, I.K. and ASANO, K. (1995). Effect of corundum/periclase sizes on expansion behavior during synthesis of spinel. Proceedings of UNITECR'95, Nov. 19-22, Kyoto, Japan, Vol. 1, 379-386.

98. NAKAGAWA, Z., ITOH, T. and ENOMOTO, N. (1996). Effect of compositional variation on expansion behavior of MgO/Al_2O_3 compact during spinel formation. Proceedings of 35th annual Conference of Metallurgists, Aug. 24-29, Montreal, Canada, 257-268.

99. HWANG, K.H., OH, K.D. and BRADT, R. C. (1997). In-situ bond formation (expansion/contraction) during firing. Proceedings of UNITECR'97, Nov 4-7, New Orleans, USA, Vol.3, 1575-1580.

100. BI, Z.Y., ZHOU, N.S. and ZHONG, X.C. (1997). Relationship between composition and properties of MgO-spinel castables. Proceedings of UNITECR'97, Nov. 4-7, New Orleans, USA, Vol. 1, 33-39.

101. YAMAGUCHI, A. (1984). Behavior of Si and Al added to carbon-containing refractories. Taikabutsu Overseas, Vol. 4 (3), 14-18.

102. LIPINSKI, T.R. (1988). Oxidations inhibiting effect of metal additives in refractory carbonaceous materials. Stahl und Eisen, Vol. 108(1988) Nv25, 61-65.

103. YAMAGUCHI, A. and TANAKA, H. (1991). Role and Behavior of non-oxide compounds added to carbon-containing refractories. Proceedings of UNITECR'91, 2nd Ed., Sep. 23-26, Aachen, Germany, 32-38.

104. RIGAUD, M., RICHMOND, C. and BOMBARD, P. (1991). Oxidation kinetics of graphite in basic refractory compositions. Proceedings of UNITECR'91, 2nd Ed., Sep. 23-26, Aachen, Germany, 383-388.

105. LIPINSKI, T.R. and FICHTNER, R. (1992). Study of the oxidation protection of MgO-C refractories by means of boron carbide. Steel Research, Vol. 63(11), 493-495.

106. TAFFIN, C. and POIRIER, J. (1994). The behaviour of metal additives in MgO-C and Al_2O_3-C refractories. Interceram. Vol. 43, 354-360.

107. YE, F.B. (1997). Effects of boron bearing additives on high temperature properties of doloma-based carbon bonded refractories. M. Sc. A. Dissertation, Ecole Polytechnique de Montreal, Canada, October 1997.

108. GIVAN, G.V., HART, R.D., HEILICH, R.P and MACZURA, G. (1975). Curing and firing high purity calcium aluminate-bonded tabular alumina castables. Am. Ceram. Soc. Bull., Vol. 54(8), 710-713.

109. FLEMINGS, M.C., KENNEY, G.B., SADAWAY, D.R., CLARK, J.P. and SZEKELY, J. (1981). An assessment of the magnesium primary production technology. Report to U.S. dept. of Energy (1981), 82-114.

110. BAKER, H.B. and BREZNY, B. (1991). Dense zone formation in magnesia-graphite refractories. Proceedings of UNITECR'91, 2nd Ed., Sep. 23-26, Aachen, Germany, 242-247.

Annex 3.3.1 A TGA Curves of $Ti(C_4H_9OH)_4$ and $Al(C_4H_9O)_3$

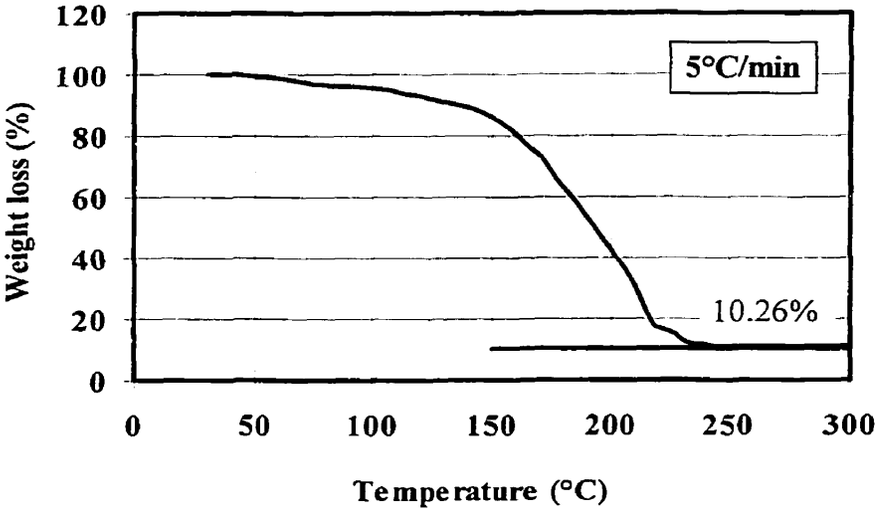

Figure A.3.3.1A-1 TGA curve of $Ti(C_4H_9OH)_4$.

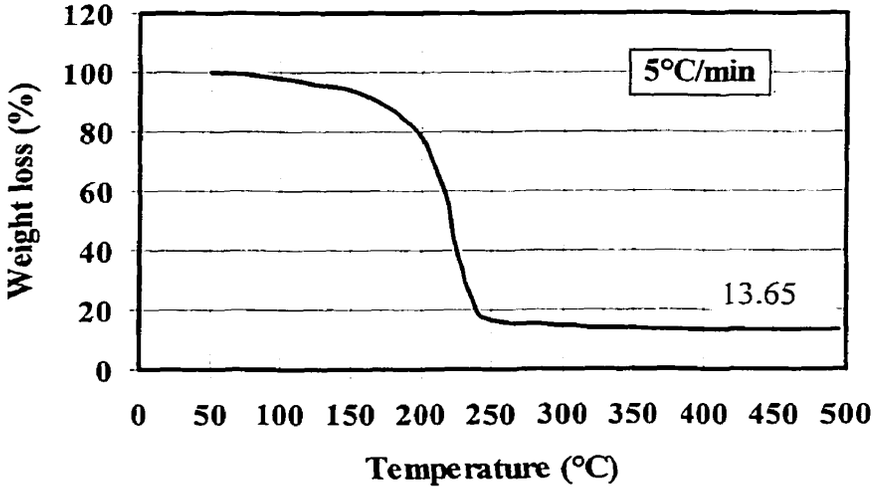

Figure A.3.3.1A-2 TGA curve of $Al(C_4H_9O)_3$.

Annex 3.3.1 B TGA on $Ti(C_4H_9OH)_4$ Gel

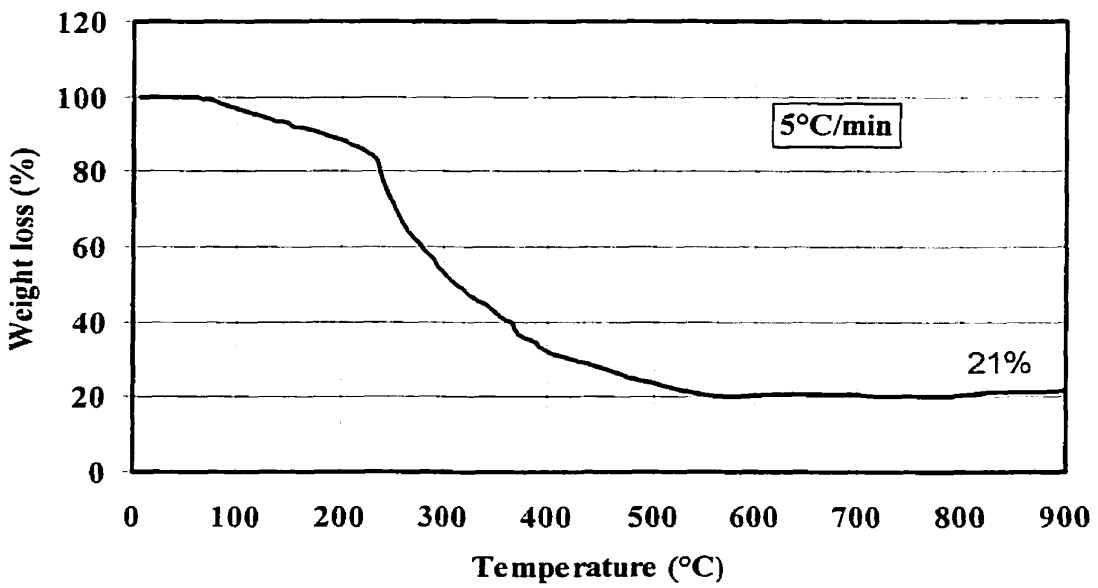

Figure A.3.3.1 B TGA curve of $Ti(C_4H_9OH)_4$ gel

ANNEX 3.3.1 C PARAMETERS FOR PRODUCTION OF TiO_2 COATED GRAPHITE (1)

Compound	D (g/cm^3)	M (g/mol.)	C (mol./L)	Vol. (mL)	Mass (g)	% Mol in sol	% Mass in sol
n-butoxyde titanium	0.95	340.4	2.79	265	251.75	4.22	21.85
acetic acid	0.9742	60.05	16.22	32	31.17	2.97	2.71
Propanol 2	0.784	60.1	13.04	1050	823.20	78.21	71.45
water	1	18	55.56	46	46.00	14.60	3.99
Sol	-	-	-	1393	1152.12	100.00	100.00
Graphite	2.2	12	-	-	508.612	-	-
TOTAL mixing					1660.74		

Ratios	Data	Calculated	Description	% Mass of coating after firing
R	0.6	0.702	aa/ti	10.41
W	3	3.455	H_2O/Ti	Volume of coating after firing
C (mol./L)	0.3	0.531	Ti	13.8678

Graphite (200 mesh) Saturation Solubility (g/mL)		
Solvant : water		0.00
Solvant : propanol 2		0.52
Solvant : ethanol		0.54
Solvant : butanol		0.40

Safety factor 0.5	Safety factor 0.7
0	0
0.2608	0.36512
0.27	0.378

ANNEX 3.3.1 C PARAMETERS FOR PRODUCTION OF TiO2 COATED GRAPHITE (2)

DRYING AND CALCINING

Step	Mass (g)	Mass %	Theoretical Mass	Theoretical mass %
Before drying at 110C	1650	100	1660.74	100
After drying at 110C	600	36.4	-	-
After calcining at 500C	540	32.7	567.69	34.18

TiO_2 (g/mol.)	79.88
Density (g/cm3)	4.26

ANNEX 6.1 DEFLOCCULATION MECHANISM (BY DLVO THEORY)

To understand the mechanism of improving flowability by deflocculant, a short review on the DLVO theory, then an interpretation is necessary.

To some extent, we can treat a system containing ultrafine powders and water as a suspension close to a colloidal dispersing system. As the dispersed phase possesses big specific surface area that makes the free energy of the system rather high, and the system thermodynamically unstable. The agglomeration of the dispersed phase to reduce the free energy is a spontaneous tendency.

DLVO theory (named after its principal creators, Derjaguin and Landau in 1941 and Verwey and Overbeek in 1948) is helpful to understand the stability and coagulation of colloids by the, which can be summarized as the following points[94,95]:

(1) There co-exist an attractive force (V_A), known as van der Waals attraction, and a repulsive force (V_R), known as electrostatic repulsion, between colloidal particles.

(2) The stability of a colloidal system depends on the interaction between the two forces. When $V_R > V_A$, so enough that it can prevent the particles stick due to the collisions by Brownian motion, the system stays at a relative stable state. When $V_A > V_R$, the particles will approach closely and cause flocculation or coagulation.

(3) V_A, V_R and the net force between the particles are all of the function of the separating distance between the particles, but their dependence on the distance is in a different relationship. As a result, at some separations, the predominant force is attractive, while at others, repulsive.

(4) Addition of electrolyte can have a significant effect on V_R , though little on V_A. This can also affect the sum of the forces, thus the stability of the system.

The van der Waals forces result from three types of interactions of fluctuating dipoles of atoms: permanent dipole-permanent dipole (Keesom forces), permanent dipole-induced dipole (Debye forces) and transitory dipole-transitory dipole (London forces). The van der Waals attraction between atoms is a short-range attraction, which is proportional to the polarizabilities of the atoms and inversely proportional to the sixth power of their separation. It is the London forces that produce the long-range attraction between colloidal particles. According to Hamaker's assumption, the interacting force between particles is the sum of those between atoms. In this case, however, the dependence of force on distance has changed from $V_A \propto -1/h^6$ to $V_A \propto -1/h^{1\sim2}$. It is proportional to Hamaker constant (it has a magnitude on the order of 10^{-19} to 10^{-20}) which depends on property of the material itself.

The electrostatic repulsion occurs due to the overlap of the double layers. The double layer is illustrated schematically in Figure A.6.1-1, using Stern's model. According to the standard theory, the potential drops linearly through the tightly bound layer of

counterions and water, called Stern layer. Beyond the Helmholtz plane, in the Gouy layer, the counterions diffuse freely; in that region the repulsive electrostatic potential of the double layer varies with the distance (h) from the particle, approximately according to

$$V_R \propto \exp[-\kappa(h-H)] \quad (h \geq H)$$

where $1/\kappa$ is called Debye-Hückel screening length and κ is proportional to the concentration and valence of the counterions. When κ is small, the repulsive potential extends far from the particles; this is the case when the counterion concentration is small. When counterions are present, the potential drops more rapidly with h. Since the repulsive force is proportional to the slope of the potential,

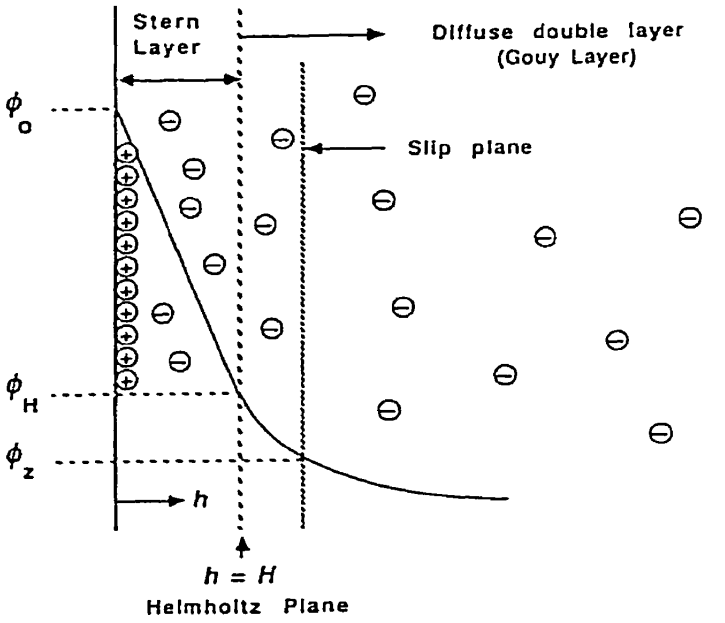

Figure A.6.1-1 Schematic of double electric layers, Stern model
(Surface charge on particle is assumed to be positive)

$$F_R = d\,V_R/dh \propto \kappa \cdot \exp[-\kappa(h-H)]$$

the repulsive force increases with small additions of electrolyte (i.e., F_R increases with κ). Of course, large amount of counterions will collapse the double layer (i.e., the exponential term in the above equation takes over), eliminating the repulsion.

The slip plane separates the region of fluid that moves together with the particle from the region that flows freely. The rate of movement of the particle depends on the potential at the slip plane, known as Zeta potential ϕ_ξ. The pH at which ϕ_ξ is zero is called the isoelectric point (IEP). The stability of the colloid correlates closely with the magnitude of ϕ_ξ, roughly speaking, stability requires a repulsive potential ϕ_ξ 30-50 mV.

Figure A.6.1-2 shows the net effect of adding V_A and V_R, as required by DLVO theory. Near the particle is a deep minimum in the potential energy produced by van der Waals attraction; farther away is a maximum produced by the electrostatic double layer. If the repulsive barrier is greater than ~10 kT, where k is Boltzmann's constant, the collisions produced by Brownian motion will generally not overcome it to cause aggregation. As the counterion concentration increases, the double layer is compressed, because the same number of charges are required to balance the surface charge and they are now available in a smaller volume surrounding the particle. Since the attractive force is unchanged, while the repulsive barrier is reduced, a secondary minimum appears, but it is not deep enough to bind the particles together. As the counterion concentration is increased

further, the double layer repulsion is reduced to the point where the net interparticle potential is attractive and the colloids will coagulate immediately.

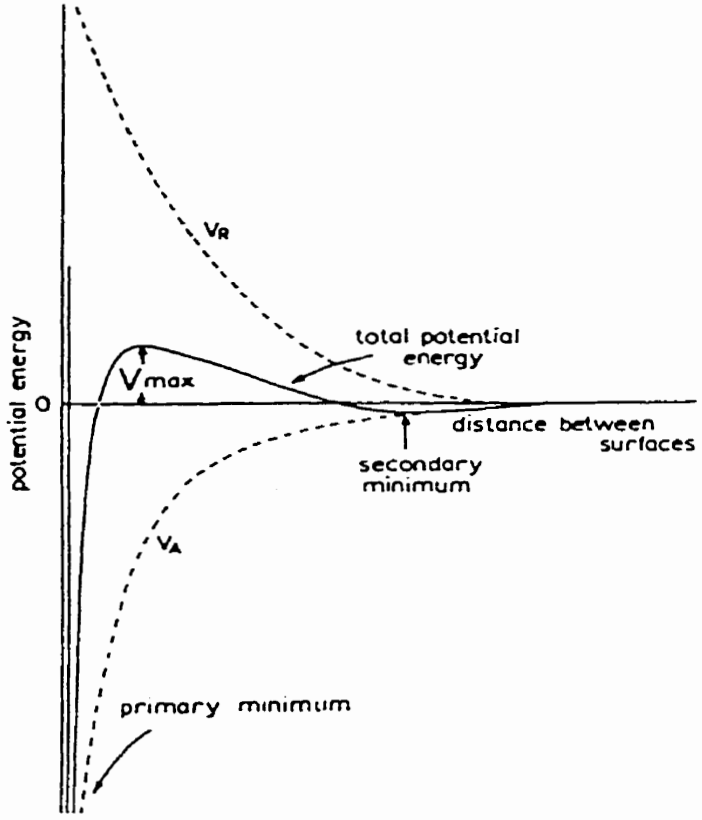

Figure A6.1-2 Schematic of DLVO potential.

The repulsive barrier depends on two types of ions that make up the double layer: charge-determining ions that control the charge on the particle surface and counterions that are in solution in the vicinity of the particle and act to screen the charges of the potential determining ions. For hydrous oxides, the charge-determining ions are H^+ and OH^-, which establish the charge on the particles by protonating or deprotonating the

MOH bonds on the surfaces of the particles:

$$M\text{-}OH + H^+ \rightarrow M\text{-}OH_2^+ \qquad (A)$$

or

$$M\text{-}OH + OH^- \rightarrow M\text{-}O^- + H_2O \qquad (B)$$

The pH at which the particle is neutrally charged is called the point of zero charge (PZC). At pH > PZC, equation (A) predominates, and the particle is negatively charged, whereas at pH < PZC, equation (B) gives the particle a positive charge.

So far, it is understandable that to maintain stability, it is necessary to raise the repulsive barrier. This can be done by increasing electrostatic repulsion between particles or by adsorbing a thick organic layer (called a steric barrier) on the particles to prevent close approach. Flocculation results from reduction in the double layer repulsion, which results from decreasing the surface potential (by changing pH) or from increasing the concentration of electrolyte (counterions) to lower ϕ_ξ. The effectiveness of a counterion in reducing the repulsion depends strongly on the valence of the ion. The Schulze-Hardy rule indicates that the concentration of electrolyte (C_f) required to cause flocculation is inversely proportional to the sixth power of the charge of the ion. This reflects the ability of highly charged ions to screen the surface potential.

If a uniform adsorption of a non-polar organic compound is made around each of two particles, and they then move toward each other until the coatings meet, the particles will not stick but will bounce away from each other. Two reasons are: 1) the non polar

materials have much less van der Waals attraction than the highly polar oxide powder surfaces do; 2) the coatings are weak and will break easily even if they do adhere. This phenomenon is called steric hindrance. In order to be adsorbed onto the particles, the molecules of the additives often have one polar end for van der Waals or other bonding to the particle, and one non-polar end to prevent sticking to the other particle's coating. If the molecule is too small, it is easily pushed out of the way and is therefore ineffective. If too big, it can tangle up with the adsorbate on another powder particle and may cause flocculation.

A great deal of fundamental work on steric hindrance has been published in literatures of colloids, ceramics and castables, along with experimental support[96].

ANNEX 7.6 ANTI-OXIDATION COATING MIX

To protect the hot surface of the Al_2O_3-MgO-C castable samples from oxidation during heating up process of rotary slag test, a protective layer with the formulation as given below in the table was coated on the samples, by painting the wet mix, using a brush.

Table A. 7.6 Formulation of the Anti-oxidation Coating Mix

Material	Size (mm)	Percentage (wt%)
Silicon carbide	- 0.074	16.0
	- 0.044	16.0
J99 Silicon	- 0.074	6.0
A101 Aluminium	- 0.044	1.0
Microsilica 971 U	- 0.001	10.0
Secar 80 CA cement	- 0.074	15.0
Calcine alumina RMA 325	- 0.020	9.0
Calcine alumina AF3000FL	- 0.010	14.0
Calcine alumina AX-45B	-0.001	13.0
Dispersant Darvan 811D	(In addition)	0.18
Water addition	(In addition)	20.0

ANNEX 7.7 EDAX SPECTRA

Totally, 11 EDAX spectra are included in Annex 7.7 in the next 6 pages.

Spectrum-1 is the analysis on the residual MgO gain, marked in Figure 7.22(c). Silicate components of MgO, CaO and SiO_2 have been detected. This indicates that CaO derived from cement and SiO_2 derived from Si together with MgO have formed silicate liquid, and no CA_6 phase can be found.

Spectra 2-11 are of the micro-area chemical composition analyses on 5 Al_2O_3-MgO-C samples, as indicated by the label in the spectra, after the rotary slag test. The analyses were centered on the slag-castable interface area. The upper part represents the slag composition (though with dissolved Al_2O_3 in it) and the lower part (just underneath the boundary) represents the composition in the castable. The compositions as oxides have been summarized in Table 7.6.

EDAX Spectrum 1

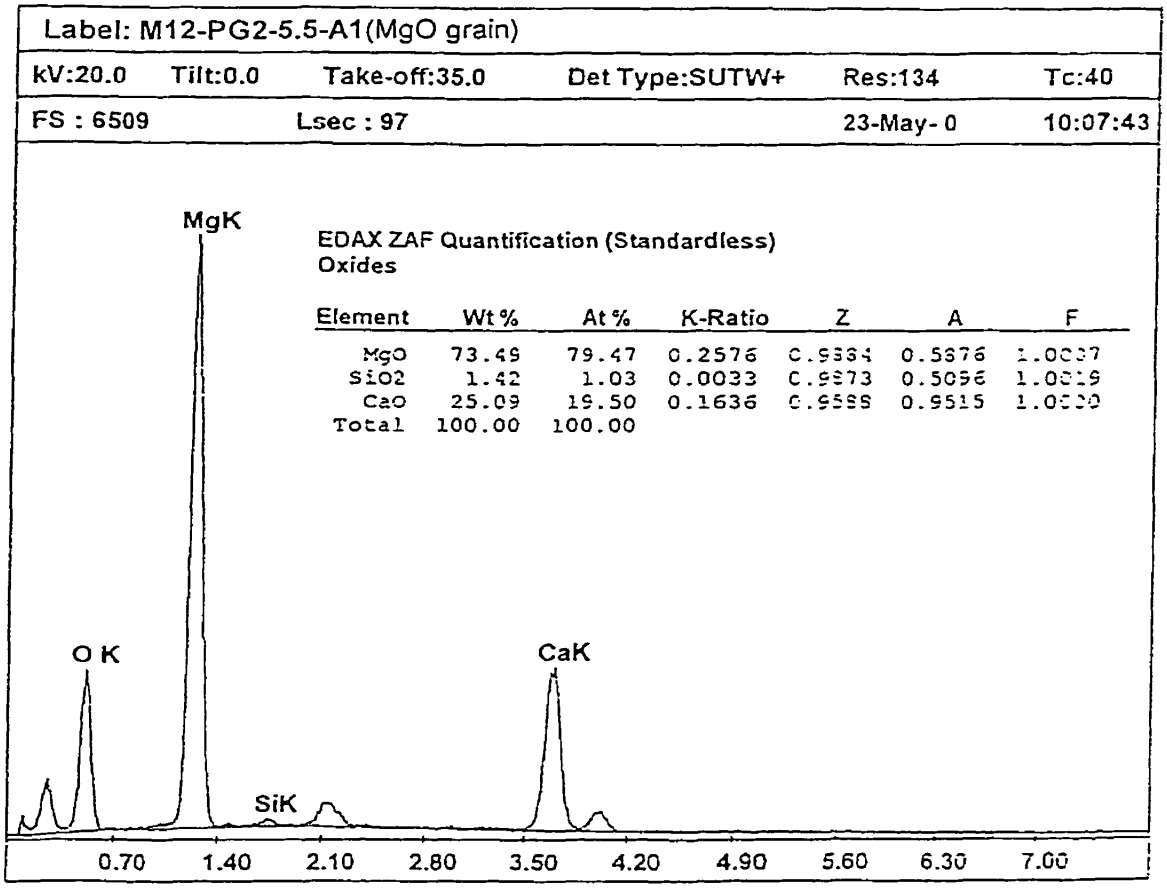

EDAX Spectra 2 and 3

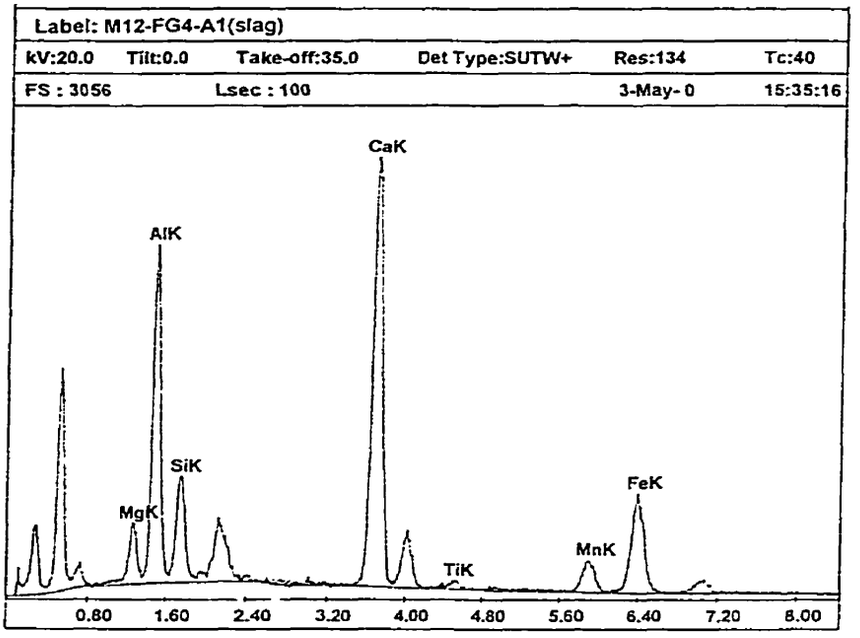

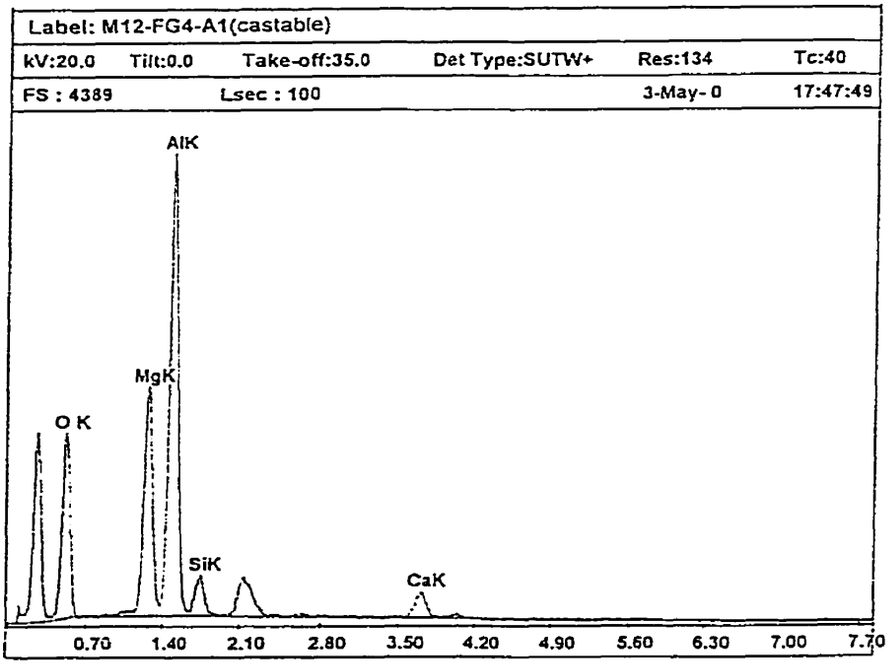

EDAX Spectra 4 and 5

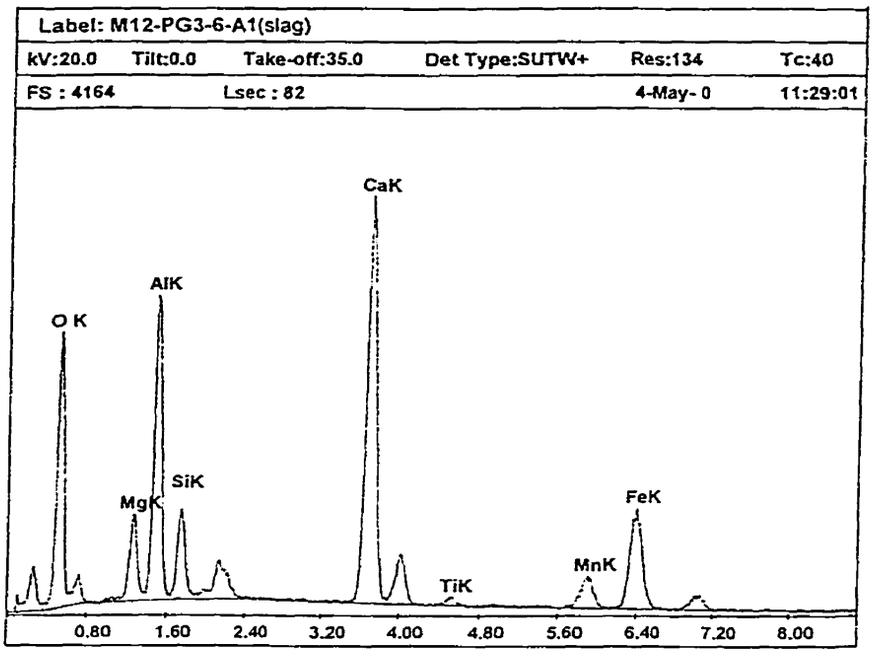

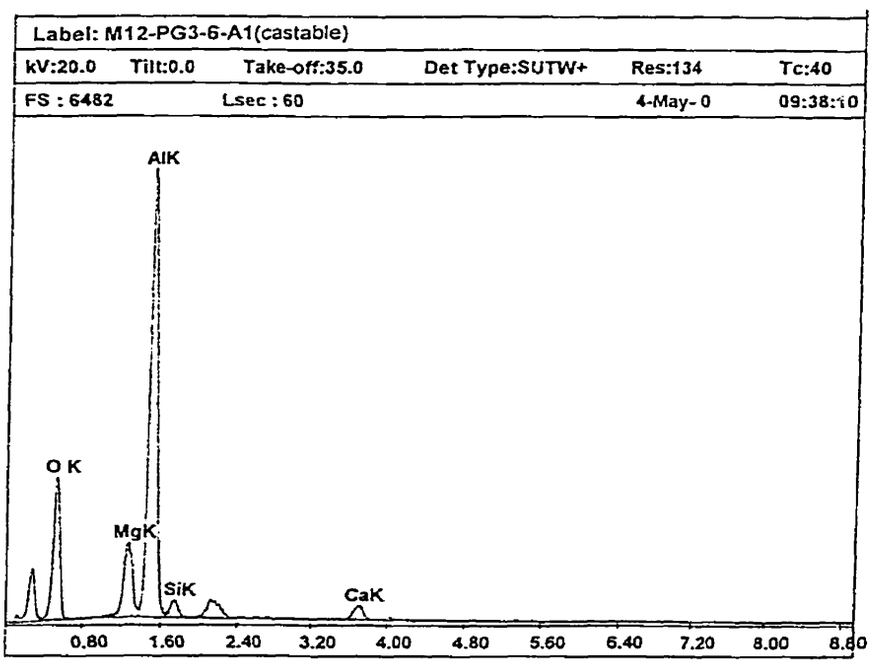

EDAX Spectra 6 and 7

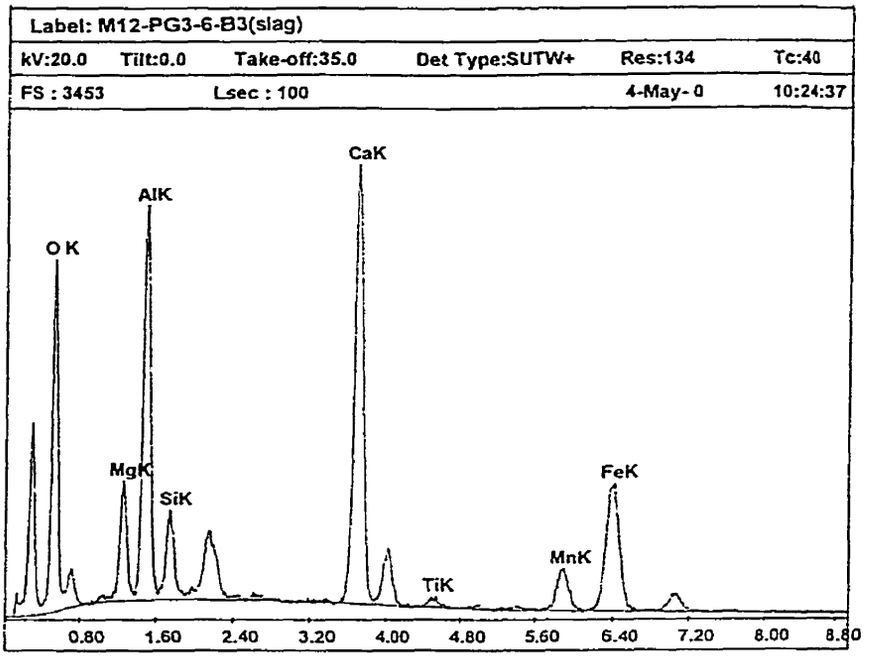

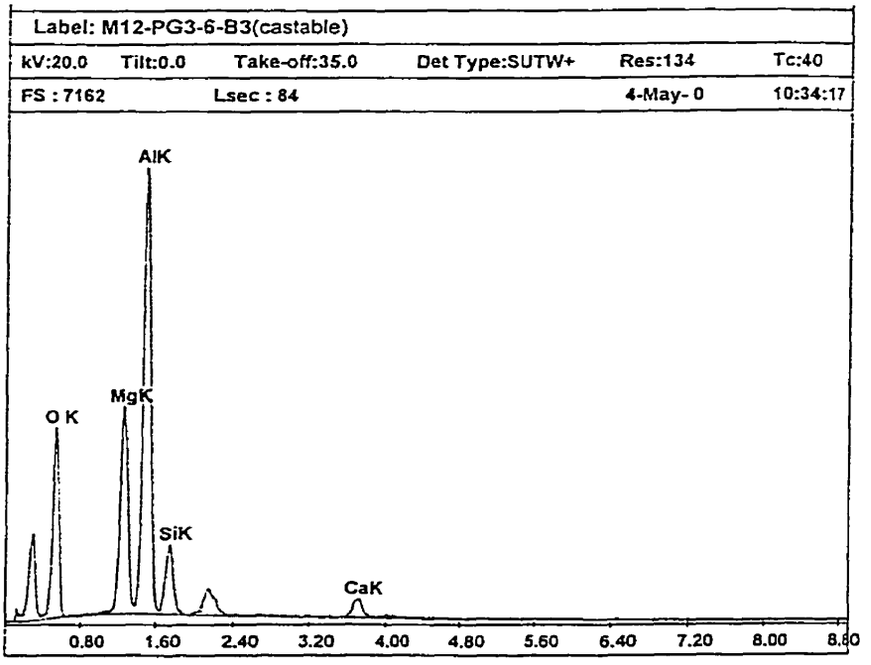

EDAX Spectra 8 and 9

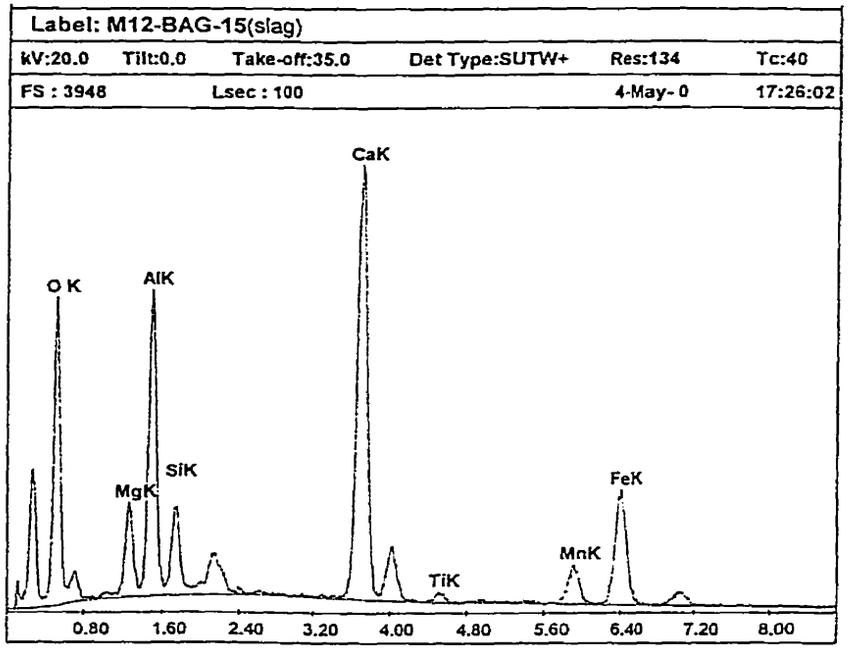

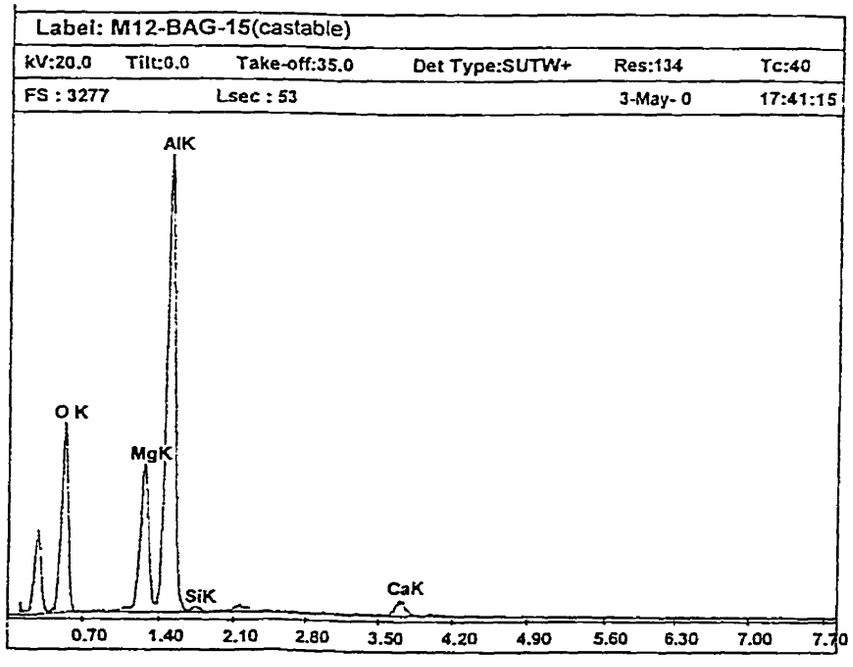

EDAX Spectra 10 and 11